Chromatin remodelling in *Saccharomyces cerevisiae* by RSC

Samuel Charles Durley

Thesis submitted for the degree of Doctor of Philosophy

School of Biosciences, Cardiff University

2013

Chromatin remodelling in *Saccharomyces cerevisiae* by RSC

Abstract

RSC is a member of the multi-subunit SWI/SNF family of ATPase-dependent chromatin remodelers and it is implicated in transcriptional regulation and DNA repair in *Saccharomyces cerevisiae*. The central ATPase subunit, Sth1, translocates nucleosomes *in vitro* and mutations in human RSC sub-unit orthologues are implicated in human disease. RSC is found in two isoforms, defined by the presence of either the Rsc1 or Rsc2 subunits, and these appear to confer distinct remodelling functions in different genomic contexts. At the *MAT* locus, Rsc1 and Rsc2 appear to mediate different forms of nucleosome positioning which are required for efficient mating type switching. Elsewhere in the genome, it has been suggested that RSC can create partially un-wrapped nucleosomes in order to facilitate transcription factor binding. This thesis uses indirect-end-label analysis and chromatin-sequencing technologies to dissect the chromatin remodelling functions of RSC and to determine the roles of Rsc1, Rsc2 and their subdomains.

The work presented here suggests that four chromatin-remodelling outcomes arise from RSC activity. Firstly, RSC alters the positions of a tract of nucleosomes abutting HO endonuclease-induced double-strand DNA breaks both at *MAT* and non-*MAT* loci in a Rsc1-dependent manner. This activity can be transferred from Rsc1 to Rsc2 by swapping BAH domains. Secondly, RSC can aggregate nucleosomes into a large nuclease-resistant structure, termed an alphasome, in a Rsc2- and Rsc7-dependent manner. Thirdly, RSC positions nucleosomes at tRNA genes in a manner that requires both Rsc1 and Rsc2. Finally, chromatin particles consistent with previously described un-wound nucleosomes are confirmed to be present in specific promoter regions. Although Rsc1- and Rsc2- dependent subsets of these promoters could be identified, and associations with binding motifs for particular transcriptions factors were discovered, it was ultimately not possible to unambiguously define why some gene promoters depend on one RSC sub-unit rather than the other.

DECLARATION

This work has not been submitted in substance for any other degree or award at this or any other university or place of learning, nor is being submitted concurrently in candidature for any degree or other award.

Signed …… (candidate)

Date ……

STATEMENT 1

This thesis is being submitted in partial fulfillment of the requirements for the degree of ……(insert MCh, MD, MPhil, PhD etc, as appropriate)

Signed …… (candidate)

Date ……

STATEMENT 2

This thesis is the result of my own independent work/investigation, except where otherwise stated.

Other sources are acknowledged by explicit references. The views expressed are my own.

Signed …… (candidate)

Date ……

STATEMENT 3

I hereby give consent for my thesis, if accepted, to be available for photocopying and for inter-library loan, and for the title and summary to be made available to outside organisations.

Signed …… (candidate)

Date ……

Acknowledgements

This work was funded by a BBSRC studentship for which I am grateful. I am indebted to my supervisor, Dr Nick Kent, for his unwavering patience, guidance, support, and comments on the work presented in this thesis. I am grateful for the freedom to pursue my own scientific interests and to entertain my need to take part in scientific engagement. I am grateful to Jessica Downs, and the members of her laboratory at the University of Sussex, for various materials used in this thesis and the collaborative effort in publishing the results of our endeavours. I would like to thank Tracey Beacham and Janet Harwood, both members of the Kent laboratory past and present, they have taught me everything I know and, most importantly, that I cannot boldly go anywhere.

I would like to thank my Mum and Dad, and various Grandparents, biological or otherwise, for, in spite of a total lack of understanding of why yeast can cure cancer, their support throughout the last 20 odd years of my education. Finally, I am especially grateful to Kirsty for getting me here and going onwards with me.

Publications arising from this work

Chambers AL, Brownlee PM, Durley SC, Beacham T, Kent NA, Downs JA. (2012) The two different isoforms of the RSC chromatin remodeling complex play distinct roles in DNA damage responses. *PLoS One; 7(2):e32016*

Chambers AL, Ormerod G, Durley SC, Sing TL, Brown GW, Kent NA, Downs JA. (2012) The INO80 chromatin remodeling complex prevents polyploidy and maintains normal chromatin structure at centromeres. *Genes Dev; 26(23):2590-603*

Maruyama H, Harwood JC, Moore KM, Paszkiewicz K, Durley SC, Fukushima H, Atomi H, Takeyasu K, Kent NA. (2013) An alternative beads-on-a-string chromatin architecture in *Thermococcus kodakarensis*. *EMBO Rep; 14(8):711-717*

Contents

1 Introduction

1.1 An overview of chromatin structure and function

DNA is a long, charged molecule thus it has to be packaged within cells by proteins in order to compact it into the relatively small space of the nucleus. Packaging of DNA in eukaryotic cells is achieved by interactions with proteins called histones, which form an octamer consisting of two of each of the canonical histone forms; H2A, H2B, H3 and H4. 147bp of DNA wraps around the histone scaffold in two left handed superhelical turns to form a structure called the nucleosome (Chakravarthy et al., 2005; Luger et al., 1997). DNA repeatedly wraps around histone cores to form chains of nucleosomes with intervening lengths of DNA between each nucleosome termed linker DNA (Kornberg, 1977). The nucleosomal DNA makes contact with the residues with the histone-fold α-helices to form the core nucleosome particle (Luger et al., 1997). The structure of DNA wrapped around sequential nucleosomes is often referred to as a "beads-on-a-string" structure or the "10nm" fibre and chains of nucleosomes are able to fold into a number of higher order superhelical structures to further condense DNA (Figure 1.1) (Li and Reinberg, 2011; Luger et al., 2012).

The complex of DNA and proteins is termed chromatin and due to the nature of the close interactions of DNA and protein, chromatin consequently has the potential to regulate the access of DNA to factors, including those catalysing and regulating process such as transcription, replication, segregation and repair (Kouzarides, 2007; Rando and Winston, 2012). An area of intense research interest therefore surrounds processes in the eukaryotic nucleus that serve to remodel chromatin.

The subject of this thesis concerns the RSC (Remodels the Structure of Chromatin) complex of the budding yeast *Saccharomyces cerevisiae* that in many ways epitomises the complexity of chromatin remodelling processes. RSC is a large multi-subunit complex that is recruited to specific regions of chromatin; it brings to bear a catalytic activity that acts at the level of individual nucleosomes. Its activity is utilised to facilitate several distinct processes, in this case both transcriptional regulation and DNA repair (Cairns

et al., 1996; Floer et al., 2010; Kent et al., 2007; Ng et al., 2002). The broad aims of this thesis are to understand how the various subunits of RSC direct its chromatin remodelling activity to achieve specific mechanistic and functional outcomes. Human cells contain a RSC-like complex called PBAF, defects in which have recently been implicated in the progression of cancer (Brownlee et al., 2012; Goodwin and Nicolas, 2001; Varela et al., 2011). By working in the yeast model system, with its tractable reverse genetics and genome analysis methodologies, this thesis also aims to shed light on chromatin mis-regulation in oncogenesis.

The remainder of this Chapter will introduce the yeast model system, the processes of DNA repair, chromatin structure, chromatin remodelling and the current state of knowledge concerning RSC.

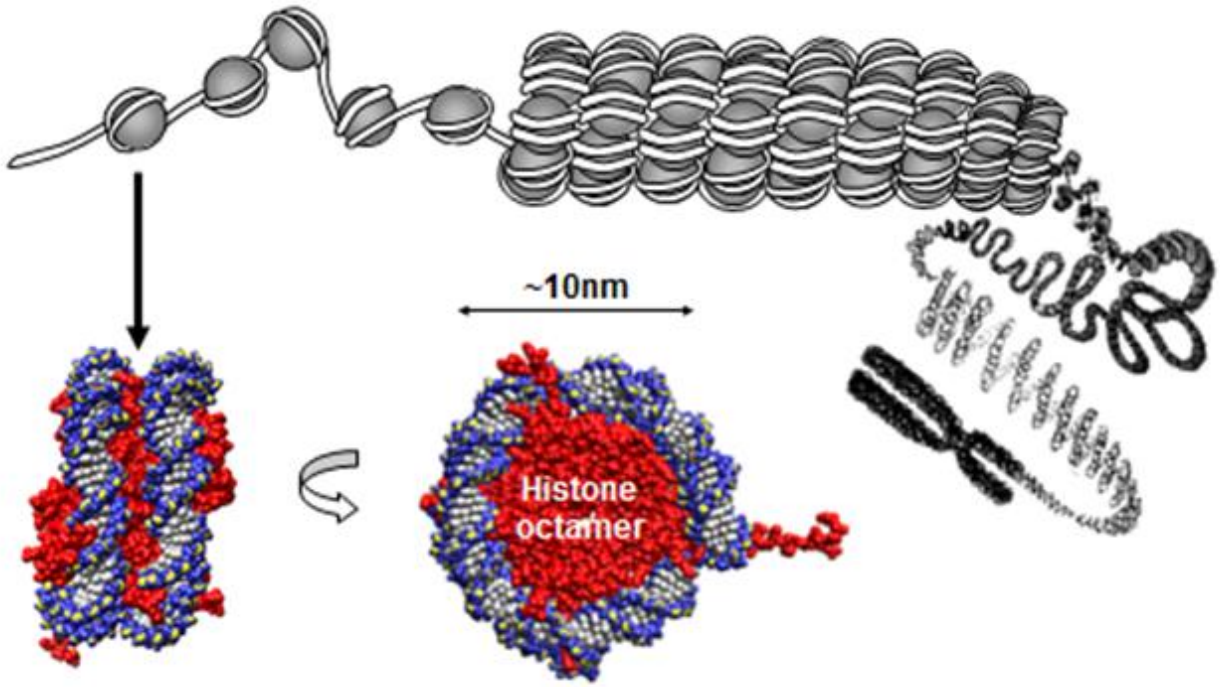

Figure 1.1 – Chromatin Structure: Beads-on-a-string to chromosomes
Sequential nucleosomes separated by linker DNA, referred to as the 'beads-on-a-string' structure further condenses to the 10nm fibre. This fibre can be folded in higher order superhelical structures to form a chromosome, a highly ordered chromatin structure. The individual nucleosome comprises of a core histone octamer bound by 147bp of DNA. (Nucleosome structure as rendered from PDB ID: 1AOI)

1.2 Experimental model system: *Saccharomyces cerevisiae*

1.2.1 Basic characteristics, genetic manipulation and analysis

S. cerevisiae, often referred to as budding yeast, is a highly versatile and well studied eukaryotic organism, well suited for use as a model organism (Botstein and Fink, 2011). Each cell is approximately 3-4 micrometres in diameter and surrounded by a cell wall composed of chitin. *S. cerevisiae* can exist in either a haploid form, with sixteen chromosomes or as a diploid (Herskowitz, 1988). As with other eukaryotic cells, yeast contains mitochondria with their own genetic information. Most yeast strains also contain the 2µm plasmid, with about 25 to 100 copies of the cell constituting approximately 4% of the entire DNA content of the cell (Futcher, 1988; Zakian et al., 1979).

As budding yeast can be maintained stably as a haploid and has an extensively characterised and annotated genome (http://www.yeastgenome.org/), it is an ideal organism for genetic manipulation. Complete knock-outs of non-essential genes are easily engineered by replacing the targeted coding region with a selectable marker using homologous recombination. A nearly complete deletion set exists for every non-essential open reading frame (C. Guthrie, 1991; Giaever et al., 2002; Oliver et al., 1998; Winzeler et al., 1999). An example of a selectable marker is the *kanMX* gene, which was obtained from the Tn903 transposon and confers resistance to the aminoglycoside antibiotic G418, also known as Geneticin (Guldener et al., 1996). Short-flanking homology for the targeted coding region is cloned alongside the selectable marker, normally using PCR, and the cassette is transformed into yeast. The cassette can integrate into the genome by homologous recombination. Integration events can be selected by growing on media containing the appropriate antibiotic and integration into the appropriate locus can be checked via PCR (Section 2.2.8.4) (Kelly et al., 2001; Oliver et al., 1998; Winzeler et al., 1999)

Temperature sensitive mutants also play an important part in yeast biology and have been used in the analysis of essential genes (Hartwell, 1967). Temperature sensitive mutants are obtained in one of two ways:

firstly, they can be obtained by engineering a mutagenized version of the gene of interest into a plasmid with a selectable marker and transforming the plasmid into a heterozygous diploid deletion mutant for the gene of interest. These cells then undergo sporulation to form four haploid daughter cells. Haploid cells that contain the plasmid but are null mutants for the gene of interest can be obtained by growing on appropriate selective media for the plasmid and mutant markers. Secondly, a mutagenized version of the gene of interest can be directly integrated into the endogenous locus using flanking homology regions to the *kanMX* cassette. A selectable marker is cloned alongside the mutagenized gene within the *kanMX* flanking homology. This construct can be transformed into a diploid strain that is heterozygous for the gene of interest with one allele replaced by the *kanMX* cassette. The mutagenized version can then integrate into the null allele locus by HR with via homology with the *kanMX* cassette and transformants can be obtained by selective media for the selectable marker in the construct. Temperature sensitive mutants are then selected by growing at the permissive and non-permissive temperature and selecting those colonies that fail to grow at the non-permissive temperature (Ben-Aroya et al., 2010).

The plasmid shuffle technique is used to analyse protein function by reintroducing the endogenous gene, borne on a plasmid, to a strain with a mutant allele for the gene of interest. Plasmids carry a marker that is selectable in auxotrophic strains such as *URA3* or *LEU2* which can be selected for in the appropriate media (Brachmann et al., 1998; Forsburg, 2001).

1.2.2 The *MAT* locus and mating-type switching

Budding yeast, with sufficient nutrients, have a doubling time of approximately one hundred minutes. The mother cell replicates the 16 chromosomes which are separated into two cells and the mother cell gives rise to an ellipsoidal daughter cell. In growth media poor in nutrients yeast will arrest in the unbudded G1 phase in which they survive well. Haploid cells undergo simple mitosis and divide by budding; however the diploid cells are also able to undergo meiosis and sporulate to form four haploid cells (Figure 1.2). Homothallic yeast strains have life cycles which, via mating type switching, allow a single haploid cell to become a diploid cell capable of meiosis and spore formation (Haber, 2012; Herskowitz, 1988). Heterothallic strains in contrast do not switch mating types and consequently they can stably propagate as haploid cells that are unable to give rise to diploid cells (Herskowitz, 1988). The central control element for programming these mating-type specific cellular processes differences is the mating type (*MAT*) locus (Haber, 1998; Haber, 2012).

The presence of yeast of the opposite mating type in close vicinity allows mating, and mating partners can transiently arrest each other's cell cycle in in G1 phase to undergo cell fusion (Nasmyth, 1982). The haploids can exist in two specialised mating types, *a* or *alpha*, which result in primitive sexual differentiation, and can mate efficiently with each other to form an a/alpha diploid cell. The diploid cell is unable to mate but can undergo meiotic division to form four haploid daughter cells. Each mating type produces a distinct signalling pheromone to induce mating and mating-type specific genes (Haber, 1998; Haber, 2012; Herskowitz, 1988).

The *MAT* locus is found on chromosome III of the *S. cerevisiae* genome and can encode two allelic variations for the mating type, the *MAT* locus is therefore transcriptionally active (Haber, 2012; Nasmyth, 1982). The two mating type alleles vary by 700bp, known as Yα and Ya respectively, and encoded within are promoters and open reading frames that, when transcribed, will regulate the cell's sexual activity (Haber, 1998; Herskowitz, 1988). The *MAT* locus can interconvert between the two mating types using

homologous recombination and the switching of genetic information from one genomic position to another (Figure 1.3) (reviewed by (Haber, 2012))

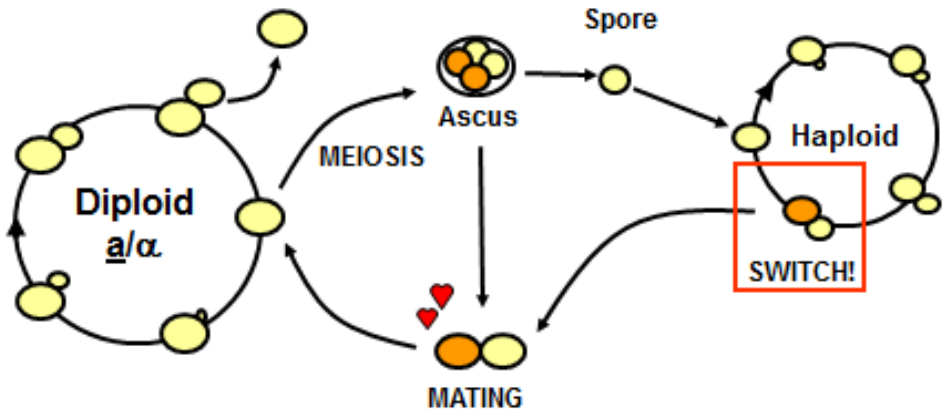

Figure 1.2 – The budding yeast life cycle
Haploid yeast undergo simple mitosis and can exist in one of two Mating types. Mating type switching allows for two haploid cells to fuse, or 'mate', and form a diploid. This diploid is able to undergo meiotic division to form four haploid daughter cells.

1.2.2.1 Silencing of *HMR* and *HML*

Both complete mating type alleles are also found in silent mating type cassettes at *HMLα* (*MATalpha*) and *HMRa* (*MATa*) respectively (though opposite variants do exist naturally) and are silenced by the *SIR* (Silent Information Regulator) genes (Herskowitz, 1988). Silencing is enforced by flanking sequences at *HMR* (*HMR* –E and *HMR* –L) and at *HML* (*HML* –E and *HML* –L), which are all *cis*-acting elements (Brand et al., 1985). There are a number of *trans*-acting factors that interact with the *cis*-elements which induce silencing by formation of heterochromatin across a 3kb region including the silent loci (Ravindra et al., 1999; Weiss and Simpson, 1998). Sir proteins are recruited to *HMR-E/HMR-E* via ORC proteins, Rap1 and Abf1, which bind to elements of *HMR-E/HML-E* (Moretti et al., 1994) Sir1 recruits the Sir2-Sir3-Sir4 complex (Moazed et al., 1997) which deacetylates lysines on histone H3 and H4 via Sir2 NAD^+-dependent HDAC activity (Imai et al., 2000). Sir3-Sir4 bind and stabilise the position of the nucleosome and the process is repeated on the downstream neighbouring nucleosome and progresses in one direction to the second silencing element (Haber, 2012; Hecht et al., 1995). These heterochromatin regions are transcriptionally silent for both RNA Pol II and RNA Pol III transcribed genes (Brand et al., 1985). The spreading of silencing at *HMR-I* is blocked by the presence of a tRNA gene (Donze et al., 1999) but boundary elements at *HML-I and HMR-E* are yet to be fully characterised (Haber, 2012). Transition of the genetic information from one position to another does not alter the information found at the silent locus; therefore interconversion of mating types from the *MAT* locus with the opposite silent mating type is a nonreciprocal event known as gene conversion (Haber, 1998; Haber, 2012). Gene conversion is initiated by the formation of a double-strand DNA break at *MAT* by HO endonuclease (Haber, 2012)

1.2.2.2 HO endonuclease

The difference between homothallic and heterothallic strains is the presence or absence of a single gene *HO* (homothallic) (Herskowitz, 1988). Homothallic strains have a functional version of the gene *HO* whereas heterothallic strains have a defective version *ho*, useful for laboratory strains to prevent mating type switching (Haber, 2012). The expression of *HO* is tightly regulated; expression only occurs at the G1 phase of a haploid mother cell (Nasmyth et al., 1987). The *HO* gene encodes a sight specific endonuclease that initiates mating-type switching by making a double-strand DNA break (DSB) at the *MAT* locus resulting in both strands having a four nucleotide long 3' overhang (Nickoloff et al., 1990; Russell et al., 1986). The HO endonuclease requires a minimum of 24 base pairs of a degenerative recognition site *in vitro,* and cleaves at the MAT locus across the Y/Z boundary (Nickoloff et al., 1986). However, HO cannot cleave the sequence found in the silent *HML* or *HMR* due to the occlusion by nucleosomes (Connolly et al., 1988). The HO protein is rapidly degraded by the ubiquitin-mediated SCF protein degradation complex (Kaplun et al., 2006) so the mother cell is only briefly exposed to HO activity.

1.2.2.3 *MAT* Switching

The HO-induced DSB at the *MAT* locus is subsequently processed by 5’ to 3’ exonucleases that create long 3’-ended tails. A complex of Mre11, Rad50 and Xrs2 (the MRX complex), Sae2 and Exo1 is responsible for this 5’ to 3’ processing (Nicolette et al., 2010; Tsukuda et al., 2009). Rad51 recombinase protein displaces the ssDNA-binding protein RPA, and assembles around the 3’ ended ssDNA to form a filament (Haber, 2012; Wang and Haber, 2004). Loading of Rad51 is dependent on Rad52 (Sugawara et al., 2003) and the Rad51 filament will search for homology in the silent mating type loci (Haber, 2012; Kostriken et al., 1983)

The Y region is not homologous between the cassette and its donor in the silent locus, so this is not involved in the early stages of recombination. In contrast there is extensive homology between the W/X sides but this is not used in the initiation of the copying of the donor sequence, rather, it is the

smaller Z region (Figure 1.3 and Figure 1.4) (Coic et al., 2011). New DNA synthesis is primed by the 3' end of the strand invading the Z-region of the silent locus which will copy the Y region of the donor DNA (White and Haber, 1990). The strand invasion creates a replication fork in which leading and lagging strand synthesis occurs as the newly synthesised strand will anneal back with the second broken end, a process known as synthesis-dependent strand-annealing (SDSA) (Ira et al., 2006). The second strand is then synthesised by lagging strand replication after the original Y region is removed (Lyndaker et al., 2008). The region switched is substantially longer than just the Y-region; both X and Z regions are replaced during *MAT* switching (Figure 1.4) (Mcgill et al., 1989).

Gene conversion requires a number of accessory proteins; Rad54 is required for the opening up of silent chromatin at the donor locus (Jaskelioff et al., 2003) a flap endonuclease of Rad1/Rad10, Msh2/Msh3 and Srs2 is required for the removal of the non-homologous Y region in the *MAT* locus before the second strand can be synthesised (Lyndaker et al., 2008) . Only a fraction of the proteins normally associated with origin-dependent DNA replication are required for the copying of donor sequences; RPA, PCNA, and DNA polymerases *Δ* and ε. (Lydeard et al., 2010). Due to DNA synthesis not using all the factors involved in normal DNA replication, gene conversion is more susceptible to mutation (Hicks et al., 2010).

MAT switching is a conservative gene conversion process as the newly synthesised strand is displaced from the template and used as a template by the second end resulting in an unaltered donor (Haber, 2012). The SDSA mechanism is not expected to produce crossovers as there is no stable Holliday junction though *MAT* switching ensures avoidance of a crossing-over event by the action of the Sgs1 helicase complex. The complex acts as a disolvase to remove any double Holliday junctions that would become crossovers (Ira et al., 2003).

1.2.2.4 Donor preference

The donor preference of the recombination event is highly accurate with *MATα* cells choosing *HMRa* and *MATa* cells choosing *HMLα* in up to 90% of events. Selection of the donor is not dependent on the Y region, rather, it is the chromosomal location of the donor that leads to its selection (Weiler and Broach, 1992). Preferential donor selection is mediated by a recombination enhancer (RE) (Haber, 1998; Weiss and Simpson, 1997). In *MATa* cells the recombination enhancer activates the left arm of chromosome III to make *HML* the preferred donor, though *HMR* is still available as an emergency backup to repair the DSB. In *MATalpha* cells the recombination enhancer is absent and the left arm of chromosome III is inaccessible due to highly positioned nucleosomes so *HMR* becomes the preferred donor (Weiss and Simpson, 1997). This change is mediated by the *MATα2* gene which forms a Matα2-Mcm1 complex that represses all *MATa* specific genes and binds and turns off the RE (Szeto and Broach, 1997)

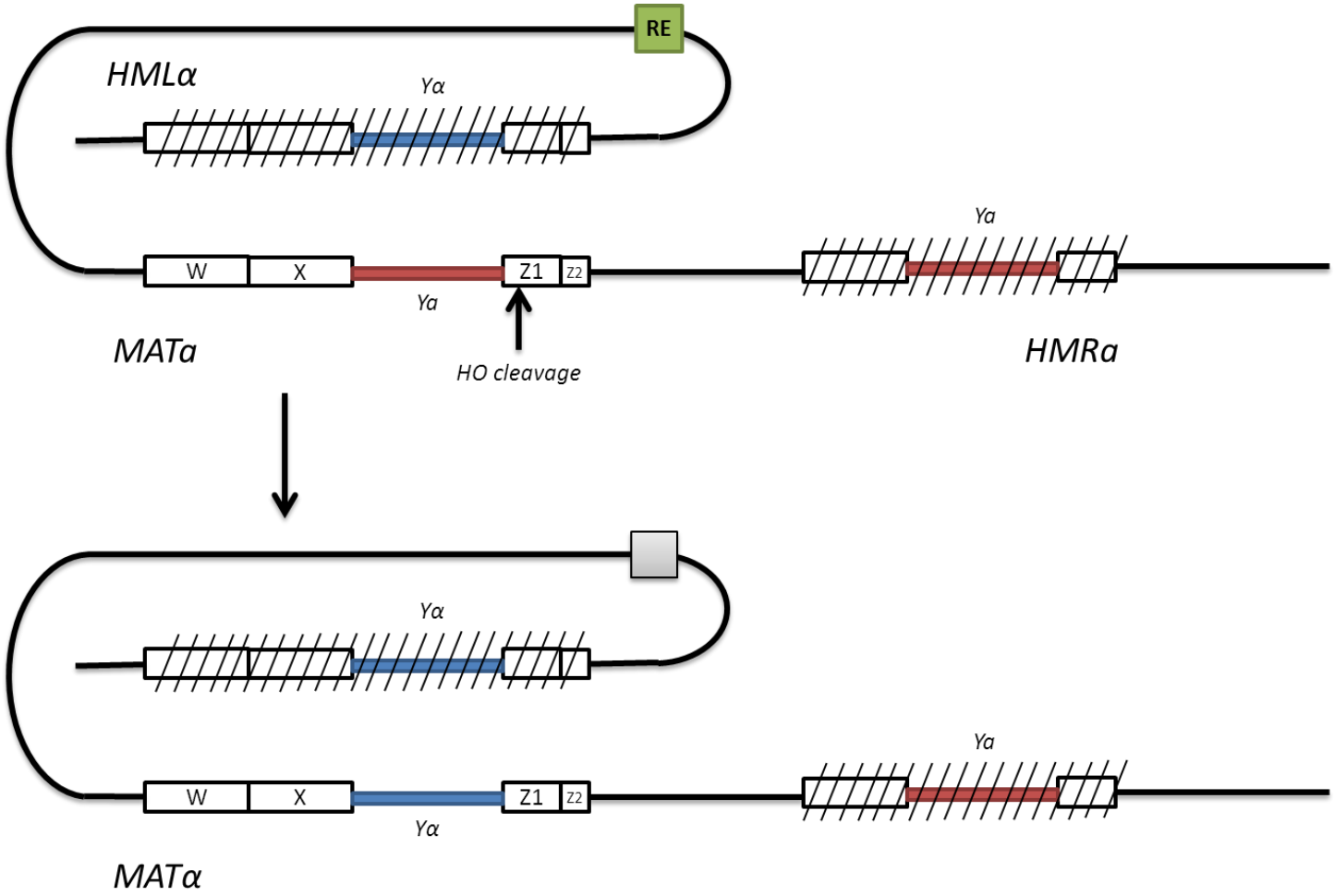

Figure 1.3 – The structure of the Mating type locus
The basic structure of MATα and MATa are identical with the exception of the Y region. Regions X and Z1 share homology with HMRa and W and Z2 share homology with HMLα. Both silent loci have closed chromatin states (hashed lines). Cleavage by HO endonuclease at the Y/Z boundary (indicated by arrow) initiates mating type switching by gene conversion which is directed by the recombinational enhancer (green box). Here Ya information(red box)is swapped for Yα information (blue box)

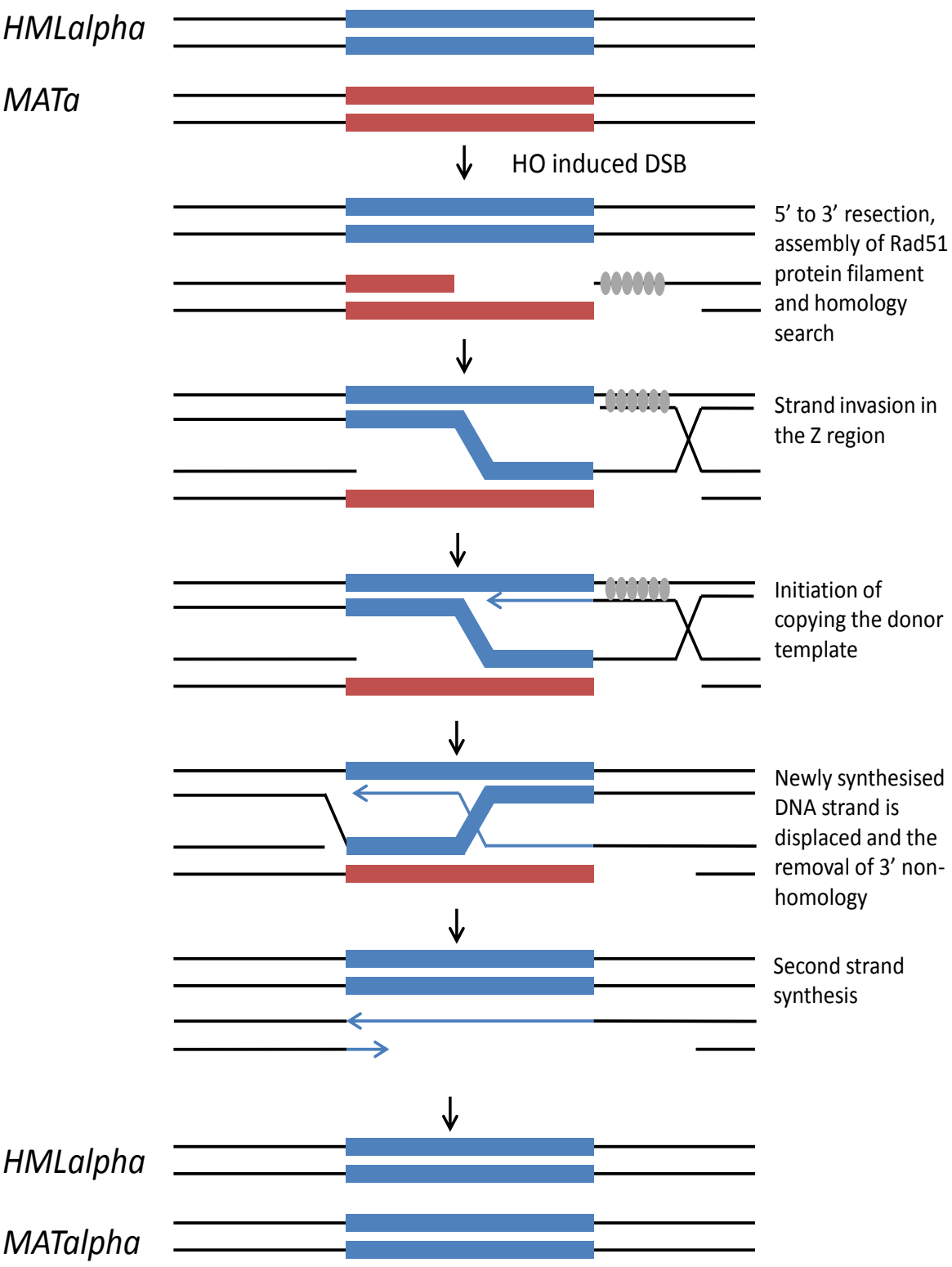

Figure 1.4 –Mating type switching
The key steps in mating type switching – The Rad51 filament forms around the 3'ended ssDNA from the 5' to 3' resected HO-induced DSB. The Rad51 filament searches for homology in the Z region and synthesis is initiated to copy the donor sequence. The newly copied strand anneals with the second end. The non-homologous sequence is clipped off and the new 3' end is a primer to extend and copy the second strand.

1.3 DNA damage and repair

Environmental exposure, intracellular metabolites, and clinical therapies all have the potential to damage the DNA strand by either breaking the DNA backbone or chemically changing a DNA base (Lindahl, 1993b; Nyberg et al., 2002). These sites of DNA damage must be repaired with high efficiency and fidelity to ensure the maintenance and stability of the genome (Kolodner et al., 2002). There are many different types of DNA damage that can alter the structure of the DNA strand or the underlying sequence. Consequently there are a number of specific pathways of detection and repair employed by organisms to ensure the health of their genomes (Boiteux and Jinks-Robertson, 2013; Wood, 1996). The sections below will highlight the key types of DNA damage and the repair processes to ensure genomic stability.

1.3.1 Types of DNA damage

There are multiple different DNA damage types (Figure 1.5) and each has distinct mechanisms of recognition and repair. The types of DNA damage are highlighted below.

1.3.1.1 Altered base

Base modifications, particularly of guanine to 8-oxo-7,8-dihydroguanine, are caused by endogenous oxidants such as free radicals and hydrogen peroxide reacting with the nucleotide base (Figure 1.5) (Grollman and Moriya, 1993). An oxidised guanine is mutagenic resulting in the GC to TA transversion (Boiteux et al., 2002; van der Kemp et al., 2009). Alkylating agents such as methyl methanesulfonate (MMS), result in the methylation of guanine to 7-methyl guanine or 1-methyladenine (Beranek, 1990). Altered bases often lead to error prone replication and lead to a change in the DNA sequence, as altered bases change the interaction with DNA-binding proteins (Lindahl, 1993a; Sancar et al., 2004).

1.3.1.2 Abasic site

An abasic site is a location in the DNA strand which has neither a purine or pyrimidine base associated with the sugar backbone as a result

from hydrolytic cleavage of the N-glycosylic bond (Lhomme et al., 1999). This can be caused by reactive oxygen species, ionizing radiation, alkylating agents, and can happen spontaneously at a rate of approximately 10,000 abasic sites per day. (Lindahl, 1993a). Guanine and adenine bases are cleaved most efficiently and lead to a loss of genetic information (Obeid et al., 2010) Unrepaired abasic sites can cause a stall in the replication fork and the insertion of a random base (Hubscher et al., 2002). In *E. coli,* adenine is preferentially inserted into an abasic site leading to a change in the underlying sequence, this preference for the adenine at abasic sites is termed the "A-rule" and most DNA polymerases comply with the A-rule. (Boiteux and Guillet, 2004; Obeid et al., 2010).

1.3.1.3 Single strand break

A single strand break (SSB) is the most common form of DNA damage and occurs at a frequency of tens of thousands per day. Reactive oxygen species endogenous to the cell such as hydrogen peroxide and ionizing radiation can result in DNA strand breaks of one of the strands by direct disintegration of oxidised sugars or indirectly during the DNA base excision repair pathway (Caldecott, 2008). Abortive activity of DNA topoisomerase 1 (Top1) can occur if Top1 collides with RNA or DNA polymerases and can result in TOP1-linked SSBs (Caldecott, 2008; Pommier et al., 2003). The consequence of SSBs is the blockage or collapse of DNA replication forks (Zhou and Doetsch, 1993) which may lead to the formation of DSBs leading to genetic instability and cell death if repair pathways become saturated (Caldecott, 2008)

1.3.1.4 Intrastrand cross links

Neighbouring bases in the DNA strand may undergo attack by reactive oxygen species which result in purine base-centred secondary radicals which can attack neighbouring pyrimidine bases. Exposure to gamma-radiation can result in C8 of a guanine residue with the 5-methyl group of an adjacent thymine (Colis et al., 2008). A typical UVB induced DNA damage is a cyclobutane pyrimidine dimer (Figure 1.5) (Mouret et al., 2006). The DNA double helix becomes destabilised as a result of oxidative intrastrand cross-

link lesions (Hong et al., 2007). Platinum containing compounds also causes intrastrand cross links by mediating the crosslinking of two adjacent guanine bases (Poklar et al., 1996). This type of damage radically changes the three dimensional structure of the DNA strand and will antagonise DNA processes such as replication and transcription (Poklar et al., 1996).

1.3.1.5 Bulky DNA adducts

There are many compounds which bind reversible and irreversible to DNA but the most studied intercalating agents are acridine and its derivatives (Ferguson and Denny, 2007). Intercalating agents which can bind non-covalently and covalently to DNA prevent proper replication by stalling replication forks (Minca and Kowalski, 2011). For example the commonly used laboratory DNA stain ethidium bromide is a well known carcinogen as it intercalates into the DNA helix and antagonises normal DNA processes (Cariello et al., 1988). The large class of planar polycyclic aromatic molecules that acridine belongs too can intercalate between two adjacent base pairs. Local structural changes to the DNA, including unwinding of the double helix and lengthening of the DNA strand all result from the act of intercalation (Ferguson and Denny, 1991). Intercalating agents such as acridine result in frame-shift mutagenesis due to the local structural changes in DNA increasing the propensity of DNA slippage during DNA replication (Denny et al., 1990; Ferguson and Denny, 2007)

1.3.1.6 Base Mismatches, small insertions and deletions

Cells have developed DNA polymerases that can replicate DNA with astonishingly high fidelity, for example studies of *E. coli* show that in vivo the rate of base substitution error is 10^{-7}, with eukaryotic polymerases with a similarly low error rate (Iyer et al., 2006; Kunkel, 2004) . In *E. coli* single base mismatches are more often base transitions rather than base transversions, and base deletions often occur in runs of adjacent identical bases (Schaaper and Dunn, 1987). However, even though the rate of error during replication is very low, base nucleotide mis-incorporations result in a change in the DNA sequence causing dysfunction and disease (Li, 2008; Lindahl, 1993a).

1.3.1.7 Interstrand cross links

It has been estimated that as few as 20 interstrand crosslinks in the bacterial or mammalian genome can lead to cell death (Lawley and Phillips, 1996). This highly toxic DNA damage prevents DNA strand separation and results in an absolute block of DNA replication and transcription (Noll et al., 2006; Sancar et al., 2004). Platinum compounds such as cis-platin, and alkylating agents, such as nitrogen mustard (Figure 1.5), can produce covalent adducts with bases on both strands resulting in an interstrand cross link (Noll et al., 2006). Nitrogen mustard reacts with guanine residues to form an alkylated guanine derivative (Falnes et al., 2002) which can react with a second guanine and result in an interstrand crosslink. As suggested by the example of cis-platin, this type of DNA damage is the mechanistic basic for a number of anti-cancer drugs as it prevents DNA replication and therefore cell proliferation (Noll et al., 2006; Poklar et al., 1996).

1.3.1.8 Double strand break

Double-strand DNA breaks (DSBs) occur three fold less than single stranded breaks but are likely the most dangerous type of DNA damage (Caldecott, 2008; Hefferin and Tomkinson, 2005; Jackson, 2002). They are caused by reactive oxygen species generated by normal cell metabolism or by exogenous and environmental agents such as ionizing radiation and UV light exposure. DSBs can also be caused if a replication fork encounters a single stranded break or other types of DNA lesions (Khanna and Jackson, 2001; Polo and Jackson, 2011). DNA DSBs occur when two complementary strands of the DNA are simultaneously broken at sites that are sufficiently close to one another that base-pairing and chromatin is insufficient to keep the two DNA ends juxtaposed (Jackson, 2002) These lesions can compromise the integrity of the genome unless they are efficiently repaired by mechanisms highly specialised to contend with different types of break (Polo and Jackson, 2011). Joining of two previously non-continuous DNA ends can result in chromosomal translocations with tumorigenic potential (Jackson, 2002).

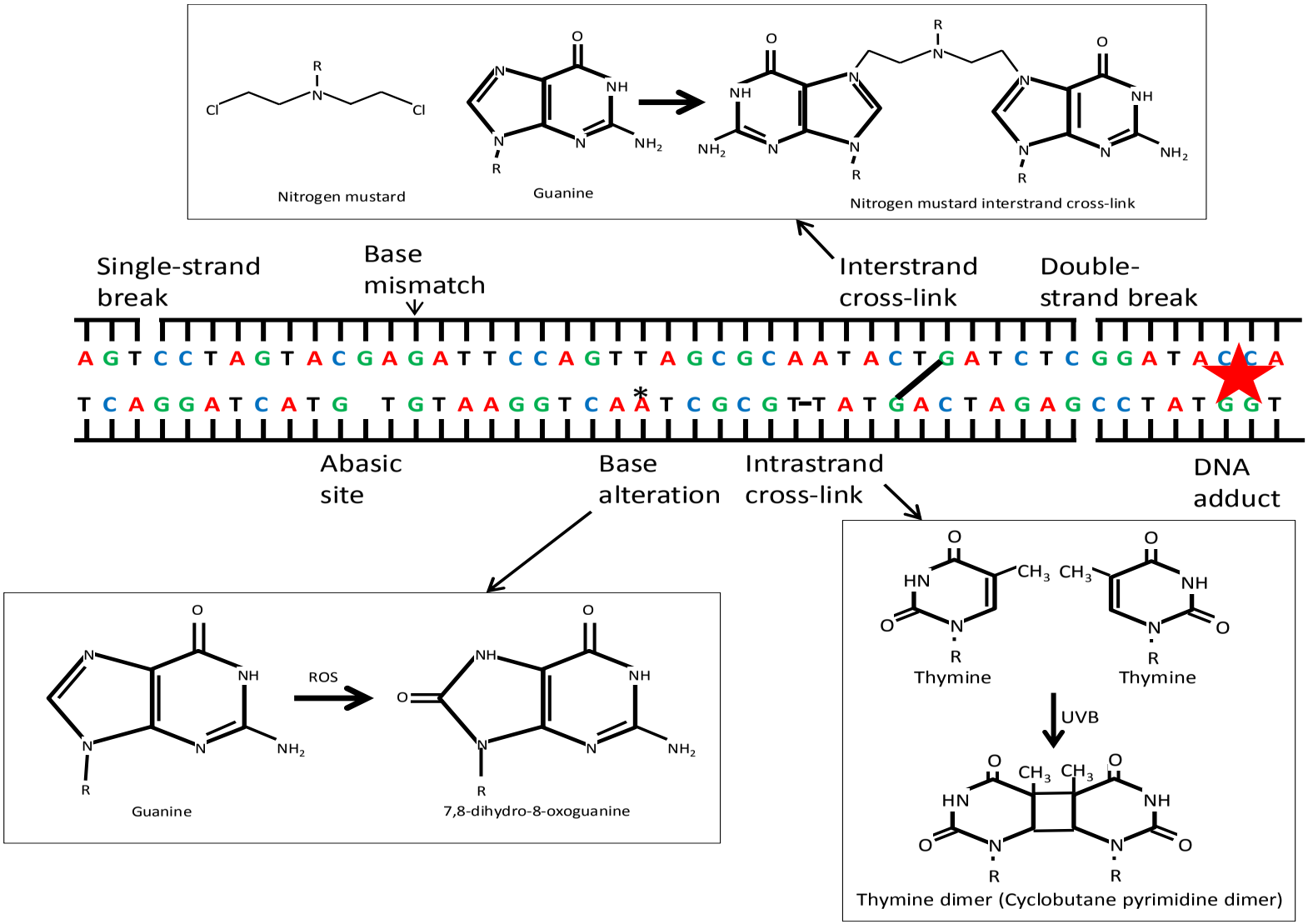

Figure 1.5 – Types of DNA Damage
The DNA strand can undergo physical and chemical damage which, if left unrepaired, can impair normal DNA processes such as replication and transcription.

1.3.2 Repair mechanisms

Mechanisms exist to detect DNA damage in bacterial and eukaryotic cells by epigenetic marks and specific signals at cell cycle stage progression checkpoints. There are four distinct responses elicited by DNA damage; DNA repair, transcriptional response, DNA damage checkpoints and apoptosis (Sancar et al., 2004; Wood, 1996). Recognition of damaged DNA is a complex process as the quantity of undamaged DNA in the cell far exceeds that which is damaged, therefore several strategies are employed the cell in the recognition process (Wood, 1996). Erroneous repair of DNA can lead to loss or amplification of chromosomal material or chromosomal rearrangement leading to an oncogenic protein (Khanna and Jackson, 2001). Different types of lesions are repaired by different pathways which are highlighted below:

1.3.2.1 Direct repair

Damage can be directly recognised by repair proteins that have an affinity for their repair substrate, for example the *E*. *coli* photolyase repairs cyclobutane pyrimidine dimers. The enzyme first interacts with the phosphate backbone and then will make specific contacts between the distorted DNA backbones. The enzyme, in a light dependent reaction, flips the dimer out of the DNA duplex into its active site and uses the energy of an absorbed proton to split the dimer back to two canonical pyrimidines (Sancar et al., 2004).

A second example of an enzyme that is able to directly repair the methylation of guanine by an alkylating agent is the yeast protein Mgt1, a methylguanine DNA methyltransferase (Boiteux and Jinks-Robertson, 2013). The enzyme can flip out the O^6MeGua base into the active site where the methyl is transferred to a cysteine residue which inactivates the active site thus this enzyme is referred to as a suicide enzyme. Mice lacking methylguanine methyltransferase are highly susceptible to tumorigenesis by alkylating agents demonstrating the necessity of the enzyme in maintaining genomic stability (Boiteux and Jinks-Robertson, 2013; Sancar et al., 2004).

1.3.2.2 Base excision repair

Bases damaged chemically by oxidation or alkylation are removed by base excision repair (BER) and is initiated by a DNA glycosylase that releases the modified base from the DNA strand to leave an abasic site; therefore BER is also the mechanism of repair for abasic sites (Boiteux and Jinks-Robertson, 2013). Individual DNA glycosylases can recognise and catalyse the removal of alkylated (methylated) bases, deaminated bases, and base mismatches (McCullough et al., 1999). DNA glycosylases are similar to DNA photolyase as they recognise small distortions in the DNA backbone which allows low affinity binding. This is followed by base flipping into the enzyme which results in a high affinity complex where multiple proof-reading mechanisms ensure high specificity (McCullough et al., 1999).

Glycosylases can simply cleave the base to leave an abasic site or catalyse an AP (apurinic/apyrimidinic site) lyase reaction that results in a 5'-phosphomonoester and a 3'-unsaturated sugar phosphate leaving a nick in the DNA strand. The 3' sugar residue is then cleaved by an endonuclease 5' to the abasic sugar resulting in a gap. This gap can then be filled by DNA polymerase β and ligated by DNA ligase III a process known as short patch, where the one nucleotide gap is replaced. Alternatively, after the 5' incision to the AP site, 2-10 nucleotides 3' to the nick are displaced and a patch of the same size is synthesised by DNA pol*Δ*/ε with the aid of PCNA and ligated by DNA ligase I (Boiteux and Jinks-Robertson, 2013; Memisoglu and Samson, 2000).

1.3.2.3 Nucleotide excision repair

Bulky DNA lesions that distort the DNA helix are often caused by UV radiation producing 6-4 photoproducts or protein addition to the DNA (Boiteux and Jinks-Robertson, 2013) however the most common product of UV radiation is a cyclobutane pyrimidine dimer (Mouret et al., 2006). NER is subdivided into two classes depending on the recognition step; global-genome NER is dependent on Rad7 and Rad16, in contrast transcription coupled NER is dependent on Rad26 and Rpb9. Following recognition the two pathways converge (Boiteux and Jinks-Robertson, 2013). Rad7 and

Rad16 form a stable complex with Abf1 and the binding of Abf1 to its DNA recognition sites promotes efficient GG-NER (Yu et al., 2009). Following recognition, a multi-subunit excision nuclease removes the damaged base or bases by making dual incisions in the DNA strand. After the recognition and excision of the damaged region the excised oligomer is released. In prokaryotes this oligomer is 12-13 nucleotides, in eukaryotes it is 24-32 nucleotides. The resulting gap is then filled in by DNA synthesis and the newly synthesised strand is ligated by DNA ligases (Boiteux and Jinks-Robertson, 2013). Recognition of the damaged region is ATP-independent; however the unwinding of the DNA duplex prior to nuclease excision is ATP-dependent. (Prakash and Prakash, 2000; Sancar et al., 2004; Wood, 1996). Defects in the excision repair pathway cause a photosensitivity syndrome called xeroderma pigmentosum, characterised by a high incidence of light induced skin cancer.(Cleaver and Bootsma, 1975; Wood, 1996)

1.3.2.4 Mismatch repair

Mismatch repair (MMR) targets mismatched bases that occur in DNA synthesis or non-identical duplexes are exchanged during recombination (reviewed in (Boiteux and Jinks-Robertson, 2013). In *E. coli*, three dedicated proteins function to repair mismatches; MutS homodimer binds mismatches, MutL coordinates detection and downstream processes, and MutH nicks the nascent strand to initiate the removal of damaged bases. MutH nicks the new, unmethylated DNA strand which is then degraded via a helicase (UvrC) and a single strand exonuclease. The gap is then filled by DNA polymerase and a DNA ligase seals the remaining nick (Boiteux and Jinks-Robertson, 2013).

Two families of proteins, MutS homologs (MSHs) and MutL homologs (MLHs), form multi-protein heterodimers in yeast, MutH-like proteins are absent from eukaryotes. MSH1 is unique to yeast and functions exclusively in the mitochondria whereas MSH2 to MH6 are conserved from yeast to mammals (Boiteux and Jinks-Robertson, 2013). The heterodimer of MSH2/MSH6, known as MutSa plays a major role in the recognition of mismatched bases whereas the heterodimer of MSH2/MSH3, known as MutSb, primarily functions in the repair of insertion/deletion loops (Fleck and

Nielsen, 2004; Modrich and Lahue, 1996). MutS complexes are ATPases which require ADP-ATP exchange to convert a mismatch-bound complex into a sliding clamp (Hargreaves et al., 2010).

The four MutL homolog in yeast, *MLH1-MHL3* and *PMS1*, form three MutL-like dimeric complexes with Mhl1 being the common component: Mhl1-Pms1, Mhl1-Mhl2, and Mhl1-Mhl3, referred to as MutLα, MutLβ, and MutLγ respectively. MutLα physically interacts with MutSa and MutSb to coordinate MMR as well as a exonuclease (Exo1), a DNA *N*-glycosylase/lyase (Ntg2), and a helicase (Sgs1) (Boiteux and Jinks-Robertson, 2013). MutSa, MutSb and Mlh1 are all associated with the proliferating cell nuclear antigen (PCNA) which aids the detection and affinity to newly synthesised mismatched DNA bases. In yeast, ExoI, a 5' to 3' exonuclease, is physically associated with MSH2 and MLH1. Like prokaryotes, the eukaryotic yeast cell uses 3' to 5' and 5' to 3' exonuclease activity for base correction however the discrimination of the nascent strand for the initial DNA nick has yet to be elucidated. PCNA and RFC (Replication Factor C) can regulate 3' to 5' excision activity of ExoI. Once the damaged strand is removed surrounding a mismatched base, DNA synthesis occurs by DNA polymerase d, in the presence of PCNA and RPA. The remaining nick is then repaired by a DNA ligase. (Boiteux and Jinks-Robertson, 2013; Jun et al., 2006; Modrich and Lahue, 1996)

1.3.2.5 Recombinational repair and Double-Strand Break Repair

Double strand breaks can be the result of ionizing radiation or reactive oxygen species (Hefferin and Tomkinson, 2005; Karpenshif and Bernstein, 2012), and also the normal result of Mating Type switching in budding yeast or in the V(D)J immunoglobulin class-switching process (Haber, 2012). DSBs may also be formed as a consequence of replication fork arrest. There are however two key mechanisms of repair pathway that are utilised in repairing DSBs; homologous recombination (HR) and non-homologous end-joining (NHEJ) are the principle mechanisms used interstrand crosslinks and double-strand DNA breaks (Hefferin and Tomkinson, 2005; Peterson and Cote, 2004)

HR can be further sub divided into single strand annealing, gene conversion or break-induced replication, with the *MAT* locus being a model for homologous recombination in yeast (Haber, 2012). The initial step of HR requires 5' to 3' strand resection by the Mre11/Rad50/Xrs2 (MRX) complex and the Sae2 endonuclease to leave long 3' tails. Invasion of the ssDNA into a homologous duplex requires binding by RPA which is then displaced by Rad52-dependent loading of Rad51 which displaces RPA (Haber, 2012; Sugiyama et al., 1997). The Rad51 filaments are essential for all subsequent homology searching; 16bp of homology are required for pairing and 80bp are required for strand exchange (Karpenshif and Bernstein, 2012). Once homologous double-stranded DNA is found, the Rad51 filament facilitates the invasion of the ssDNA displacing one strand of the duplex DNA leaving the complementary strand to serve as a template for repair. This recombination structure is known as the displacement-loop (D-loop); the invading strand of the D-loop can be extended to repair any missing information. (Karpenshif and Bernstein, 2012). Resolution of the D-loop structure can be resolved by two different mechanisms; synthesis dependent strand annealing (SDSA) and resolution of double-Holliday junctions. In SDSA the invading strand is displaced and re-anneal to the other broken chromosome end. Alternatively the second end of the DSB can be captured resulting in the two recombining duplexes being covalently joined by single strand crossovers. These junctions are resolved by a family of enzymes termed resolvases to separate the two duplexes. Resolution can result in a crossover or non-crossover product (Agmon et al., 2011; Karpenshif and Bernstein, 2012).

Non-homologous end joining (NHEJ) binds the two ends of a double strand break back together and is a repair mechanism is conserved during evolution (Hefferin and Tomkinson, 2005). In *S. cerevisiae* the Ku70/Ku80 (Hdf1/Hdf2) heterodimer binds to the two ends of the breaks and recruits the Mre11/Rad50/Xrs2 complex to form an end bridging complex between the two ends. The NHEJ-specific ligase, Dnl4, associates to the break with the associated factor Lif1 which promote Rad27 endonuclease and Pol4-dependent processing and gap-filling (Hefferin and Tomkinson, 2005). Because of this non-specific nature of NHEJ previously unlinked DNA

molecules mat be joined resulting in gross chromosomal rearrangements (Hefferin and Tomkinson, 2005). Therefore, HR is the more error free mechanism for repairing physical breaks in the DNA strand, however NHEJ is more common in human cells (Daley et al., 2005).

1.3.3 DNA damage cell cycle checkpoints

Cell cycle progression can be delayed or arrested at a number of DNA damage checkpoints when the integrity of the DNA is 'checked' before progression is permitted (Hartwell and Weinert, 1989). Eukaryotic cells have four distinct phases within the cell cycle, G1, S, G2, and M, with one outside the cell cycle G_0 (Longhese et al., 1998). DNA damage checkpoints are not activated by DNA damage, rather the checkpoint pathways operate under normal growth conditions and they are upregulated in response to DNA damage to prevent cell cycle progression The proteins that are involved in the DNA checkpoint pathways are therefore the same as those that regulate the tightly controlled transition between G1/S, G2/M and S phase progression. (Nyberg et al., 2002). The checkpoint pathway has four conceptual stages, DNA damage sensing, signal mediators, signal transducers, and effectors. Many of the proteins involved are shared at each checkpoint and may have more than one role in the signalling pathway (Houtgraaf et al., 2006).

Sensors of DNA damage are required to initiate subsequent steps and in *S. cerevisiae* these are Rad9, Rad17, Rad24, Mec3 and Ddc1 (Durocher and Jackson, 2001; Paulovich et al., 1998). These proteins recognise or modify DNA damage and activate signal transducers (Paulovich et al., 1998). The transducers can be can be split into two checkpoint-specific damage sensors: the phosphoinositide 3-kinase-like kinase (PIKK) family members; Mec1 and Tel1 in budding yeast (ATR and ATM in mammals), and the RFC/PCNA-like proteins; Rad24 in budding yeast (Houtgraaf et al., 2006; Longhese et al., 1998). Mec1 is essential whereas the loss of Tel1 does not result in a checkpoint phenotype however overexpression of Tel1 can suppress the phenotype of Mec1 suggesting some functional overlap (Carr, 1997). Mec1 has significant sequence homology to phosphoinositide kinase

and upon sensing of DNA damage Mec1 hyperphosphorylates the signal transducer Rad9 (Emili, 1998)

Mec1, with the aid of Rad9, phosphorylates proteins such as Chk1 and Rad53 and these effectors regulate the transcription of cyclins that are required for cell cycle progression (Carr, 1997). The G1/S checkpoint recognizes the presence of damaged DNA during G1 and will delay the onset of S phase and DNA replication and the intra-S phase checkpoint will stall ongoing replication and initiation of late firing replication origins (Siede et al., 1994). Detection of DNA damage at the G2/M cell cycle checkpoint will delay mitosis to prevent segregation of chromosomes (Weinert et al., 1994).

1.4 Eukaryotic transcription

The basic mechanism of transcription, not taking account chromatin, is similar between prokaryotes and eukaryotes; the RNA polymerase binds a specific promoter region with specificity provided by accessory DNA binding factors (the basal transcription factors in eukaryotes and the sigma factor in prokaryotes). In eukaryotic protein-coding genes RNA polymerase II (Pol II) will bind upstream of the transcriptional start site of the open reading frame (ORF) mediated through recruitment by general transcription factors (GTFs) TFIID, TFIIA, and TFIIB that place Pol II at the core promoter, to form a molecular aggregate termed the preinitiation complex (PIC). RNA synthesis is initiated by TFIIH, a helicase, which denatures approximately 15bp of DNA that can be bound by Pol II. Phosphorylation of the Pol II C-terminal domain (CTD) by TFIIH results in the dissociation of the PIC as it proceeds into the elongation stage of synthesis (Li et al., 2007). This process is complicated upon addition of nucleosomes and other chromatin particles as these antagonise the binding of the transcriptional machinery (Figure 1.6) (Li et al., 2007; Rando and Winston, 2012).

Generally, histone modifications that are associated with active transcription are termed euchromatin modifications whereas those associated with inactivation of genes or regions of DNA are termed heterochromatin modifications (Berger, 2007; Kouzarides, 2007). The

location of the modification (5’ and 3’ of the ORF, the core promoter and the upstream region) is tightly regulated as to ensure the desired effect on transcription, (Li et al., 2007). These modifications are driven by highly specific enzymes that add or remove moieties to change the interaction between DNA and histone proteins (Rando and Winston, 2012).

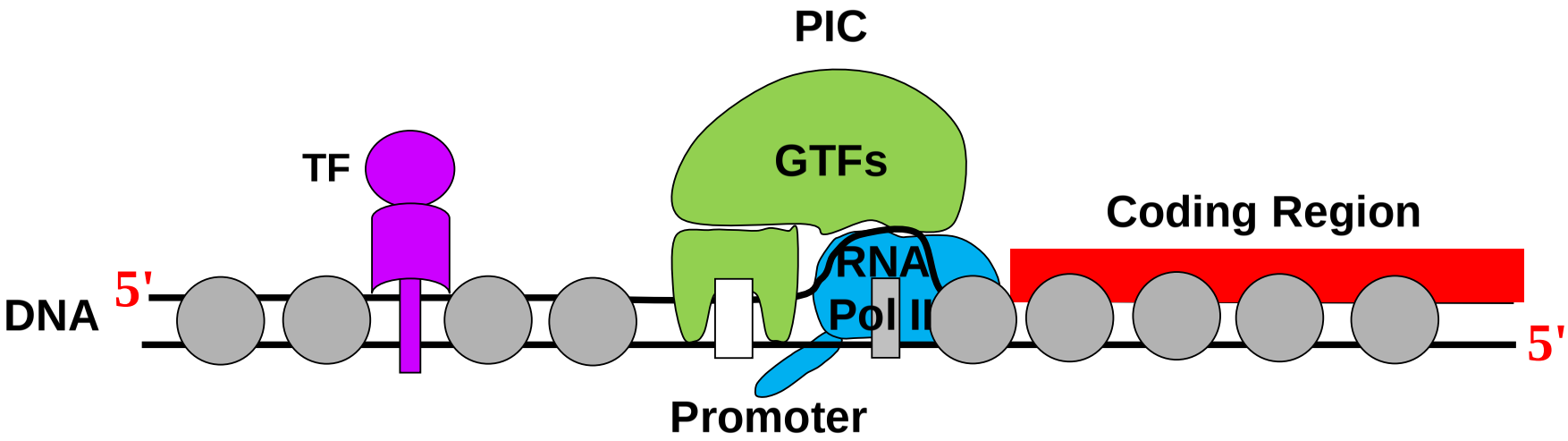

Figure 1.6 – Initiation of eukaryotic transcription in the context of chromatin
Chromatin is a potential barrier to binding of transcription factors and the progress of RNA polymerase through the coding region (Li *et al* 2007).

1.5 Chromatin structure

The repeating unit of chromatin is the nucleosome, 147 base pairs of DNA wrapped 1.65 times around a histone octamer formed by two dimers of H3-H4 that form a stable tetramer, and flanked by two separate H2A-H2B dimers Histone proteins interact through a hydrophobic core termed the globular domain and histone fold domain (Figure 1.7) (Luger et al., 1997)..

Nucleosomes interfere with access to DNA of other proteins in the nucleus, for example transcription factors, as the histones tightly bind DNA to their surface (Chodaparambil et al., 2006). Protein-DNA interactions occur through salt links and hydrogen bonds. The bulk of the DNA-protein interactions are between basic and hydroxyl side groups of histones and phosphates in the DNA backbone (Richmond and Davey, 2003). The 14 histone/DNA interactions that are present in the nucleosome form a highly stable protein-DNA structure that is well suited for the packaging function of chromatin (Peterson and Laniel, 2004; Richmond and Davey, 2003).

Chromatin structure has to be dynamic to allow protein-DNA interactions to occur and to allow nuclear processes such as transcription and repair to proceed (Chodaparambil et al., 2006). Each histone protein has an approximately 35 amino acid tail protruding from the nucleosome core of globular domains. These tails are rich in basic residues and are key targets for post-translational modifications that may alter histone/DNA interactions (Peterson and Laniel, 2004). The histone scaffold can also be altered by the exchange of histone proteins in the nucleosome core. In general the dimer of H2A and H2B is easily exchanged in and out of the nucleosome core and under certain conditions the entire histone octamer can be exchanged (Sarma and Reinberg, 2005). There are two basic modes of chromatin regulation; residues on the histone proteins can be modified to alter DNA/protein interactions or ATPase dependent complexes can evict, reposition, slide or exchange histones to regulate access to chromatin. Each mode of chromatin modification requires its own subset of enzymes, however many of the pathways overlap and in reality most modifications require a combination of the two (Zentner and Henikoff, 2013).

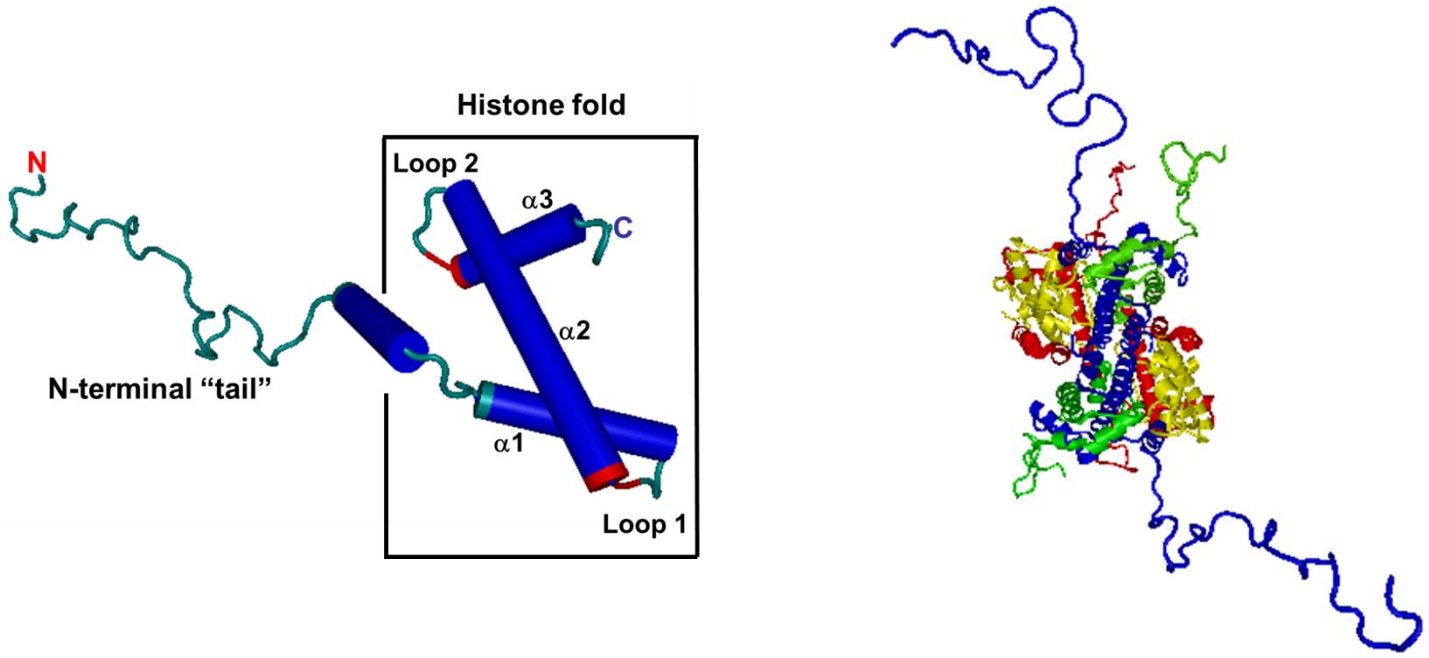

Figure 1.7 – Histone structure allows for modifications that alter the interaction with DNA
Histone proteins have core histone folds that interact with DNA and long N-terminal tails which can be modified to alter histone/DNA interactions.

1.5.1 Covalent histone modification

Histone proteins form direct interactions with the DNA strand which can be reversibly modified as to alter the local chromatin environment and to result in a biological function. With one exception (histone methylation) histone modifications result in a change in the net charge of the nucleosome, this may strengthen or weaken the histones interaction with the negatively charged DNA (Strahl and Allis, 2000). Histone modifications also alter the interaction between the histone proteins which facilitates histone protein displacement (Peterson and Laniel, 2004). Histone modifications imprint the chromatin code which influences chromatin structure, such as further condensation, for example the acetylation of H4K16 that antagonises the formation of a 30nm fibre. Modifications also recruit other nonhistone proteins that modify chromatin dynamics and function such as ATP-dependent remodelling enzymes. (Shogren-Knaak et al., 2006; Strahl and Allis, 2000).

At least 11 types of post-translational modification have been identified on 60 different residues of histone proteins and the modifications are dynamic so both enzymes that add and remove the modification have been identified (Bannister and Kouzarides, 2011; Tan et al., 2011; Zentner and Henikoff, 2013). There are functionally distinct chromatin environments, however modifications are context dependent and their effect on DNA processes vary (Berger, 2007) The full spectrum of modifications that occur in budding yeast and mammals vary. Because this thesis concerns work in budding yeast, only those modifications found in this organism are discussed in detail below (Figure 1.8):

1.5.1.1 Acetylation

Histone acetyltransferases (HATs) are divided into three main families, GNAT (including yeast Gcn5 (Sternglanz and Schindelin, 1999)), MYST (including yeast Sas2 (Sutton et al., 2003)), and CBP/p300 (including yeast Rtt109 (Bazan, 2008)). Gcn5, like all those in the GNAT (Gcn5-like N-acetyltransferases) acetylates conserved amino acids by transferring an acetyl group from a bound acetyl CoA onto a primary amino group, for example the ε-amino group of lysine which neutralises the lysines positive charge (Sternglanz and Schindelin, 1999). The MYST protein lysine

acetyltransferases are conserved throughout eukaryotes and include Sas2, the catalytic subunit of the SAS complex and Esa1, the catalytic subunit of the NuA4 complex (Shia et al., 2005).

Acetyltransferases are invariably associated with the activation of transcription, and most acetylation occurs in the N-terminal tail of histones and generally acetyltransferases modify more than one lysine residue (Tan et al., 2011). In yeast the NuA4 histone acetyltransferase (HAT) is responsible for the acetylation of H4 and H2A. The catalytic subunit of NuA4, Esa1, is the only essential HAT in yeast, and is required for cell cycle control and transcriptional regulation (Allard et al., 1999) The SAS complex however specifically acetylates H4 lysine 16 to antagonize the spreading of a repressive chromatin structure at silent loci (Shia et al., 2005)

Acetylation of lysine residues of H3K9, and H3K14 and histone H4 by the transcriptional coactivator NuA4 histone acetylase (HAT) are found in nucleosomes surrounding transcriptional start sites (Doyon and Cote, 2004; Liu et al., 2005; Roh et al., 2004; Zentner and Henikoff, 2013). Phosphorylation of H3S10 by the kinase Snf1 regulates gene activation by the recruitment of the histone acetylase complex, SAGA, which acetylates H3K14 through its catalytic subunit Gcn5 (Lo et al., 2001). In yeast, the level of acetylation of H3 and H4 are proportional to the level of transcription (Pokholok et al., 2005) and this acetylation is provided by the histone acetyl transferases (HATs) Gcn5 and Esa1 which are generally recruited to promoters (Robert et al., 2004).

1.5.1.2 Deacetylation

Opposing transcriptional activation by acetylation, histone deacetylases (HDACs) remove acetyl groups from amino acids restoring the positive charge. HDACs are generally non-specific and are present in numerous repressive chromatin complexes. HDACs fall into four distinct classes of enzymes, with yeast Rpd3 and Hda1 defining classes I and II respectively. Class III HDACs are homologous to yeast Sir2 and require a coactivator for activity, NAD^+ (Bannister and Kouzarides, 2011). HDAC11 is the unique member of class IV HDACs suggesting it has an non-redundant function however it is found all eukaryotes with the exception of fungi

suggesting other HDACs perform these functions in yeast (Minucci and Pelicci, 2006).

1.5.1.3 Phosphorylation

Histone phosphorylation takes place on serine and threonine residues predominantly in the N-terminus of histone tails. The level of phosphorylation is a dynamic balance between kinases and phosphatases that are responsible for the modifications (Zentner and Henikoff, 2013). ATP is required for the reaction as inorganic phosphate from the ATP molecule is added to the hydroxyl side group of a targeted amino acid and addition of a phosphate group adds a significant negative charge to the histone (Bannister and Kouzarides, 2011). Snf1 is a threonine/serine specific kinase activated by AMP, and is required for the regulation of glucose-repressible genes by phosphorylating histone protein H3. Snf1 belongs to a highly conserved family of threonine/serine kinases, AMP-activated protein kinases (AMPK) (Amodeo et al., 2010).

In *S. cerevisiae* phosphorylation of histone protein H2A occurs on Ser129 in response to a double-strand DNA break in order for efficient repair of the chromosomal lesion. (Harvey et al., 2005; Zentner and Henikoff, 2013). A similar modification can also be seen in mammalian cells where histone protein H2A.X is phosphorylated at the C-terminus on Ser139 and the phosphorylation of the mammalian histone protein is dependent upon the DNA-dependent protein kinases (DNA-PK), ataxia-telangiectasia mutated (ATM) and AT-related (ATR) kinases (Zentner and Henikoff, 2013). Yeast contains ATR/ATM homologues Mec1 and Tel1 which phosphorylate yeast H2A which is required for repair of DSBs by non-homologous end joining (NHEJ) (Cheung et al., 2005).

An early signal of DNA damage is the extensive phosphorylation of the histone variant γ-H2AX (mammalian cells) or H2AX (yeast) and histone phosphorylation is extensive and covers many kilobases surrounding the site of damage. Double-strand DNA breaks can be repaired via two mechanisms, non-homologous end joining (NHEJ) and homologous recombination. Mec1-dependent phosphorylation of H2AS129 and Casein kinase II

phosphorylation of H4S1 play a role in NHEJ of DSBs (Cheung et al., 2005; Downs et al., 2000).

1.5.1.4 Lysine and arginine methylation

Lysine methyltransferases have enormous specificity compared to acetyltransferases, having just a single target residue on a single histone however this modification does not alter the charge of the histone protein (Zentner and Henikoff, 2013). This is a more complex modification as the amino group of lysine can be mono-, di- or tri methylated. In yeast lysine methylation is found on histone H3 and histone H4 which suppresses histone exchange and is mediated by the methyltransferase Set2. Set2 actively methylates lysine residues in the wake of transcribing RNA Pol II to recruit histone deacetylases in order to restore normal chromatin after transcription and to inhibit inappropriate initiation within coding regions (Lee and Shilatifard, 2007).

Protein arginine methyltransferases (PRMTs) are recruited to promoters by transcription factors and can fall into four classes depending on their action. Asymmetric- and symmetric-dimethylation are catalysed by the type-I or type-II class respectively whereas the type III class catalyses mono-methylation. To date class IV is unique to *S. cerevisiae* and catalyses the methylation of the *Δ*-nitrogen atom of the guanidine group. Methylation of arginine involves the addition of one or two methyl groups to the guanidine group by the transfer of a methyl group from SAM (S-Adenosyl methionine). In budding yeast the enzyme Hmt1 is a type I PRMT and catalyses the formation of mono- and asymmetric di-methylarginine and is conserved throughout eukaryotes though there are differences in biological function. In budding yeast arginine methylation of histone proteins is associated with transcriptional repression however in higher eukaryotes the converse is true (Low and Wilkins, 2012).

Methylation of lysine residues have different effects transcription, histone 3 lysine 4 (H3K4) by the methylase Set1 functions to activate transcription (Zentner and Henikoff, 2013). Methylation of H3K4 occurs on a gradient across the gene with the 5’ being tri-methylated which shifts to mono and di methylated when moving towards the 3’ (Liu et al., 2005). Methylation

H3K36 by Set2 also correlates with active gene expression (Krogan et al., 2003b). In fission yeast (*S. pombe*) and higher eukaryotes variable levels of methylation of H4K20 lead to different downstream responses; mono- and di-methylation is required for the recruitment of repair factors in response to DNA damage (Sanders et al., 2004; Southall et al., 2014) whereas tri-methylation is a mark of heterochromatin (Schotta et al., 2004). Methylation of arginine residues on H3 occurs in mammalian cells to activate transcription (Li et al., 2007).

1.5.1.5 Demethylation

It was originally believed that histone methylation is a stable and static modification however a number of pathways have been discovered that can reverse the modification. There are two distinct demethylase domains with distinct catalytic reactions; the LSD1 (lysine-specific demethylase 1) domain which uses FAD as a co-factor, and the JmjC (Jumonji) domain found in the yeast protein JmjD2. Demethylases have a high level of substrate specificity and are sensitive to the level of methylation (Bannister and Kouzarides, 2011).

1.5.1.6 Ubiquitylation

This is a large covalent modification in which ubiquitin, a 76-amino acid polypeptide, is attached to lysines of the histone proteins (Zentner and Henikoff, 2013). Ubiquitylation occurs in three steps by distinct enzymes, activation, conjugation and ligation. The complexes have substrate specificity and catalyse varying degrees of ubiquitylation, either mono- or poly-ubiquitylated (Hershko and Ciechanover, 1998). In yeast the enzyme Ubp8 is responsible for the process of deubiquitylation and falls into the family of isopeptidases which are important in gene activity and silencing.

Ubiquitination is a modification that is more extensively observed in mammalian systems however this modification is facilitated in budding yeast by the Rad6 ubiquitin ligase of H2B K123 (Robzyk et al., 2000) and can result directly in gene repression (Turner et al., 2002). It must be noted however that Rad6 can also indirectly result in gene activation through its

ubiquitinating activity on proteins involved in the DNA damage response pathway (Fu et al., 2008).

1.5.1.7 Sumoylation

In a mechanistically similar process to ubiquitylation, modifier enzymes covalently attach ubiquitin-like small molecules, SUMO, to histone proteins (Seeler and Dejean, 2003). Specific sites for sumoylation have been identified on histones H4, H2A, and H2B and it is known to take place on H3. Sumoylation antagonises acetylation and ubiquitylation modifications as these occur on the same residues (Nathan et al., 2006).

1.5.1.8 Deimination (citrullination)

This modification involves the conversion of an arginine residue to a cirtulline; this reaction removes the positive arginine as it is replaced by the neutral citrulline (Takahara et al., 1985). This modification antagonises the effect of arginine methylation as citrulline cannot be methylated (Cuthbert et al., 2004).

1.5.1.9 ADP Ribosylation

Arginine and glutamate residues can be mono- and poly- ADP ribosylated by the poly-ADP-ribose polymerase (PARP) family of enzymes. This reaction can be reversed by the poly-ADP glycohydrolase family of enzymes. Histone mono-ADP-ribosylation is performed by mono-ADP-ribosyltransferases and the modification increases the negative charge of the histone changing the chromatin structure (Zentner and Henikoff, 2013). This modification significantly increases upon DNA damage and poly-ADP ribosylation is greatly increased over heat shock genes and is linked with nucleosome eviction (Hassa et al., 2006; Zentner and Henikoff, 2013).

1.5.1.10 Proline Isomerization

Prolines in the tail of H3 can undergo a conformational change from a *cis* to *trans* conformation changing the dihedral angle of the peptidyl peptide bond by 180º. Proline isomerases catalyse this interconversion and a conformational change in the proline will severely distort the polypeptide

backbone (Schmid, 1995). The budding yeast proline isomerase Fpr4 belongs to the family of FK506-binding protein (FKBP) family of peptidyl prolyl iosomerases (Gothel and Marahiel, 1999; Monneau et al., 2013). Fpr4 was identified as a histone chaperone protein (Xiao et al., 2006) and further investigation has shown that Fpr4 isomerises histone protein H3 P38 in order to inhibit the methylation of H3K36 by Set2 in order to regulate transcription (Nelson et al., 2006)

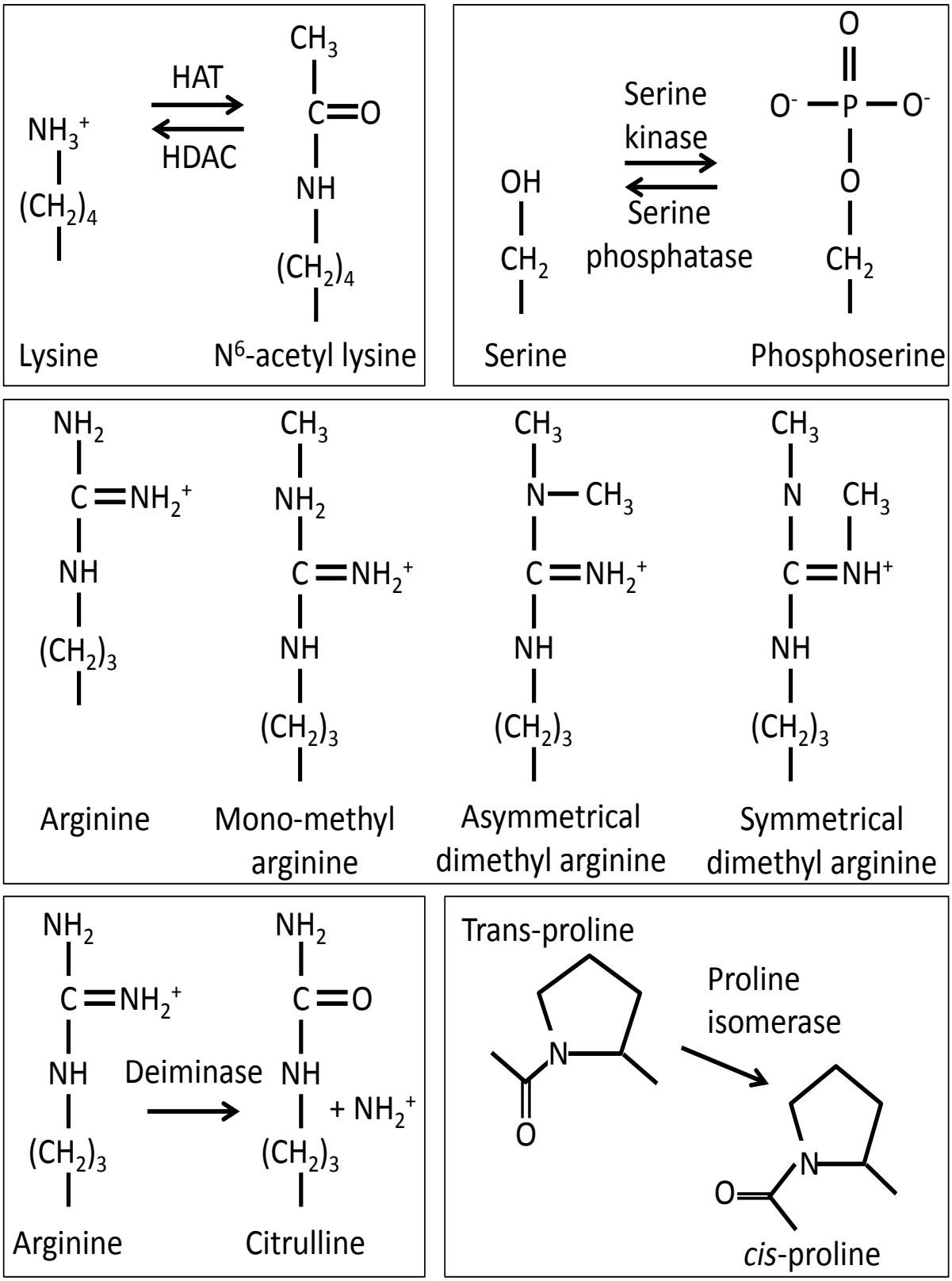

Figure 1.8 – Histone modifications occur on amino acids of histone tails
Shown are the examples of acetylation, phosphorylation, methylation, deimination and isomerisation modifications of amino acids that occur can occur in histone protein tails.

1.5.2 Histone variants

Another method for altering the direct physical structure of the nucleosome is by incorporation of histone variants (Sarma and Reinberg, 2005). The genes expressing canonical histones H2A, H2B, H3 and H4 are normally present in multiple copies in eukaryotic genomes and are expressed in a highly regulated process during S phase (Gunjan et al., 2005). However, single copy histone variant genes are also present in many eukaryotes and are expressed, and incorporated into chromatin in a DNA-replication independent manner (Linger and Tyler, 2006). Differences between the canonical histone proteins and the variants are found in the histone tails and the histone fold domains though sites of modification are often conserved suggesting that variants are readily interchangeable with the canonical proteins and chromatin regulatory proteins with equal affinity (Eriksson et al., 2012; Linger and Tyler, 2006). ATPase-dependent reactions are required to catalyse the exchange of histone proteins in the histone core (Bruno et al., 2003). Mammalian systems have a variety of histone variants such as that of H3, H3.3 which activates transcription by incorporation into the transcribing region that allows elongation during RNA synthesis (Ahmad and Henikoff, 2002). Similarly H2A has four variants each with a distinct function that prevent nucleosome sliding, repress initiation and transcription, and used to inactivate the X chromosome (Kamakaka and Biggins, 2005). Interestingly however the canonical H2A protein in *S. cerevisiae* is more similar to the mammalian H2A.X variant and instead has a variant that is more similar to H2AZ called Htz1 (Malik and Henikoff, 2003). High resolution maps of the yeast genome reveal that Htz1-containing nucleosomes flank the NFR and are resistant to elongation modifications and remodelling. However, upon transcriptional activation it is readily evicted from the promoter which either allows for the mobilization of other nucleosomes or to make the DNA sequence completely accessible (Zhang et al., 2005). Incorporation of Htz1 is required to prevent the spreading of silent chromatin in telomeric regions (Krogan et al., 2003a)

1.5.3 ATP-dependent chromatin remodelers

The second class of enzymes require an ATPase subunit to disrupt nucleosome/DNA contacts, reposition nucleosomes or exchange histone proteins forming DNA loops that alter the accessibility of transcription factors to DNA (Li et al., 2007; Narlikar et al., 2013). Many of these complexes are essential for viability in both yeast and mammalian cells highlighting their essential role on cellular processes (Flaus and Owen-Hughes, 2011; Narlikar et al., 2013). The first of these ATP-dependent chromatin remodelers was identified in mutant yeast strains defective in mating-type switching and defective in growth on sucrose media. As a result they were named SWI (SWItching deficient) and SNF (Sucrose NonFermenting) and were shown to alter chromatin structure (Hargreaves and Crabtree, 2011; Narlikar et al., 2013). The genes containing these mutations were identified to be *SWI2* and *SNF2*, part of the multi-subunit complex named SWI/SNF. SWI/SNF is required for transcription by sequence-specific transcription factors such as GAL4. Therefore SWI/SNF is a general activator of transcription in coordination with sequence specific *trans*-activating factors (TFs) and the histone acetylase Gcn5 (Rando and Winston, 2012). The SWI/SNF family has now been shown to be evolutionary conserved in flies, plants and mammals and all of the complexes contain an ATPase subunit that belongs to the SNF2 superfamily. Since then 17 ATPases have been added to the Snf2 superfamily with 4 separate complex families of ATP-dependent chromatin remodelers have been identified (Clapier and Cairns, 2009; Flaus and Owen-Hughes, 2011; Narlikar et al., 2013)

In yeast there are defined nucleosome free regions (NFR) of approximately 200bp at promoter regions of coding regions. These regions are flanked by positioned nucleosomes and the maintenance of the NFR by ATP-dependent remodelers is essential for transcriptional regulation, as highlighted at a number of yeast promoters (Burns and Peterson, 1997; Kent et al., 2001; Moreira and Holmberg, 1999) Nucleosomes antagonise the passage of RNA Pol II along the DNA strand and evidence is emerging that ATP-dependent chromatin complexes help RNA Pol II pass through nucleosomes (Li et al., 2007). For example it has been demonstrated that the

ATPase dependent chromatin remodeler RSC (Remodels the Structure of Chromatin) helps RNA Pol II continue after stalling at a nucleosome (Carey et al., 2006). Interestingly this reaction is promoted by histone acetylation, a noteworthy observation as the RSC complex contains multiple bromodomains in a number of subunits as detailed later in this chapter.

1.5.3.1 Mechanism of ATP-dependent chromatin remodelling

The structure of the RSC-nucleosome complex shows that the nucleosome binds into a central cavity within the RSC complex. The nucleosomal DNA appears to bulge out away from the complex whereas the RSC-nucleosome complex appears stable (Chaban et al., 2008). This is consistent with the hypothesis that RSC translocates DNA around the histone octamer rather than displacing the histone octamer (Chaban et al., 2008; Saha et al., 2005). It has since been shown that, in an ATP-dependent manner, DNA is uncoupled from the histone forming small DNA loops which can propagate around the surface of the octamer leading to repositioning (Liu et al., 2011; Lorch et al., 2010).

1.5.4 ATP-dependent chromatin remodeler families

1.5.4.1 SWI/SNF Family

The SWI/SNF family has two complexes in yeast; SWI/SNF and RSC. Both are multi-subunit complexes containing a highly conserved ATPase subunit belonging to the Snf2 superfamily; Swi2/Snf2, and Sth1 (Flaus and Owen-Hughes, 2011). Yeast SWI/SNF complex contains 11 subunits and has been shown to be involved in transcriptional regulation (Rando and Winston, 2012). RSC (Remodels the Structure of Chromatin) is a highly related complex, and many subunits are homologues of SWI/SNF complex and indeed the complexes share two subunits. RSC is far more abundant than SWI/SNF and is essential for viability (Mohrmann and Verrijzer, 2005). In general, SWI/SNF complexes appear to destabilise histone/protein interactions (Clapier and Cairns, 2009). RSC is described in further detail later in this section (Section 1.6). Humans contain two highly similar SWI/SNF-like multisubunit complexes defined by unique subunit composition

and the DNA-dependent ATPase/helicase subunits, hBRG1 or hBRM, both highly homologous to Swi2/Snf2 (Wang, 2003). Both complexes share at least 7 subunits, though SWI/SNF-A, also known as BAF contains either BRG1 or hBRM and BAF250 whereas SWI/SNF-B, also known as PBAF contains only BRG1 and three unique subunits, BAF200, BAF180 and BRD7. The complex PBAF is also known as polybromo due to the six bromodomains found in the subunit BAF180. (Mohrmann and Verrijzer, 2005). This single subunit has surprising homology to three of the yeast RSC complex subunits, Rsc1, Rsc2, and Rsc4, which between them contain 6 highly homologous bromodomains and two bromo-adjacent homology domains (Brownlee et al., 2012; Mohrmann and Verrijzer, 2005).

In yeast, RSC is essential and highly abundant in contrast to the non-essential SWI/SNF complex. The two complexes have distinct targets in transcriptional regulation and are involved in cell cycle progression; the functions of RSC are described in extensive detail below (Section 1.6) (Mohrmann and Verrijzer, 2005). Origins of DNA replication in *S. cerevisiae* are characterised by short (approximately 11bp) essential DNA sequences called autonomously replicating sequences or ARS elements. DNA replication is initiated by the recruitment of the origin replication complex (ORC) and the chromatin structure around ARS elements is dependent on SWI/SNF (Brown et al., 1991; Flanagan and Peterson, 1999). SWI/SNF is recruited to acetylated histones through bromodomains and is important for histone eviction in transcriptional activation and in transcriptional elongation (Chatterjee et al., 2011; Schwabish and Struhl, 2007)

1.5.4.2 INO80/SWR1 Family

The INO80 subfamily, including INO80, SWR1 and Fun30 complexes, is characterized by a split ATPase domain in the core ATPase subunit and the presence of two RuvB-like proteins (Bao and Shen, 2007b). The INO80 complex consists of 15 principal subunits including Rvb1 and Rvb2, proteins conserved from yeast to mammals, Ino80 is the ATPase/helicase domain of the complex and is the largest subunit (Bao and Shen, 2007b; Udugama et al., 2011). INO80 is important for transcriptional activation of a number of genes and was originally identified by mutants that affect inositol biosynthesis

(Ebbert et al., 1999; Shen et al., 2000). The chromatin remodelling activity of INO80 can mobilise nucleosomes in an ATP-dependent manner (Shen et al., 2003) and is recruited to double-strand breaks sites by phosphorylated H2AX and for nucleosome eviction prior to DNA repair by homologous recombination (Morrison et al., 2004; van Attikum et al., 2004) INO80 is also required to maintain proper chromatin structure at centromeres in order to maintain proper ploidy within cells (Chambers et al., 2012b). In yeast, H2A.Z nucleosomes are mislocalized in the absence of INO80 as INO80 has a histone exchange activity to which replaces nucleosomal H2A.Z/H2B with free H2A/H2B dimers in order to promote genomic stability (Papamichos-Chronakis et al., 2011).

The SWR1 complex contains 14 proteins and four of these subunits are also found In INO80, the ATPase subunit is the Swi2/Snf2-related ATPase Swr1 (Mizuguchi et al., 2004). Budding yeast has two main histone variants Htz1 and centromeric H3 (Cse4); Htz1-H2B dimer is a exchanged for the H2A-H2B dimer by the SWR1 complex in order to promote transcription by preventing chromatin silencing (Mizuguchi et al., 2004; Raisner and Madhani, 2006) Htz1 is enriched in promoter regions of chromatin, in a replication independent manner, to mark promoters for proper activation (Bao and Shen, 2007b; Li et al., 2005; Meneghini et al., 2003).

Fun30 is closely related to SWR1 and INO80, Fun30 also genetically interacts with four subunits of the SWR1 complex suggesting a functional connection (Durr et al., 2006; Krogan et al., 2003a). Fun30, like INO80, can promote non-specific histone dimer exchange and therefore contributes to the global distribution of H2A.Z in the genome (Papamichos-Chronakis et al., 2011). Fun30 is also enriched over centromeres and positions nucleosomes flanking centromeres and the core centromere nucleosome (Durand-Dubief et al., 2012). Fun30 also has an ATP-dependent nucleosome sliding activity that has a role in specific gene repression of functionally grouped genes by positioning the -1, +2, and +3 nucleosomes (Byeon et al., 2013). Fun30 also has a redundant role in promoting resection of DNA double-strand break ends by remodelling nucleosomes to facilitate Exo1-mediated strand resection (Chen et al., 2012)

1.5.4.3 ISWI family

The ATPase subunit of these related complexes is the ISWI proteins Isw1 and Isw2 (Imitation SWI) (Mellor and Morillon, 2004). Remodelers are further characterised by C-terminal SANT domains and SLIDE domains: putative DNA and nucleosome binding motifs (Corona and Tamkun, 2004; Eberharter and Becker, 2004). In flies there are three complexes in this family, ACF (ATP-utilising chromatin assembly and remodelling factor), NURF (nucleosome remodelling factor) and CHRAC (chromatin accessibility complex) (Vignali et al., 2000). *S. cerevisiae* has two non-essential homologs, Isw1 and Isw2, which appear in distinct complexes (Corona and Tamkun, 2004). Isw1 either forms a complex with loc3 (Isw1a complex) or loc2 and loc4 (Isw1b complex). Isw2 interacts with ltc1 to form the Isw2 complex (Mellor and Morillon, 2004).

The Isw1 and Isw2 complexes interact with DNA and nucleosomal arrays to space nucleosomes in an ATP-dependent manner (Mellor and Morillon, 2004). Mutations in Isw1 result in the derepression of a number of genes, ISWI can repress transcription through spacing and sliding activity (Hughes et al., 2000; Kassabov et al., 2002). Isw1 represses transcription by remodelling chromatin in the mid-coding region whereas Isw2 maintains repressive chromatin at gene ends (Goldmark et al., 2000; Tirosh et al., 2010). Isw1 remodelling complex may be involved in silencing gene expression involving the Sir2 deacetylase by binding over coding regions and preventing histone exchange (Mellor and Morillon, 2004; Smolle et al., 2012).

1.5.4.4 CHD (Mi-2) family

The CHD (Chromodomain Helicase DNA-binding) family is characterised by the presence of tandem chromodomains in the N-terminal region and the SNF2-like ATPase domain in the central region of the protein structure (Marfella and Imbalzano, 2007). The CHD family has three subfamilies; Chd1-Chd2, Chd3-Chd4 and Chd5-Chd9 families however budding yeast contains a single CHD family remodeler, the monomeric Chd1 remodeler and belongs to the Chd1-Chd2 subfamily (Marfella and Imbalzano, 2007).

The chromodomain (chromatin organisation domain) serves to mediate interactions between the complex and DNA, RNA and methylated histone H3 (Marfella and Imbalzano, 2007). CHD1 in budding yeast functions, in a similar way to the Isw1a and Iswb complexes, to slide nucleosomes along DNA in a highly directional manner (McKnight et al., 2011; Stockdale et al., 2006). The CHD1 complex is required to space nucleosomes within coding regions and deletion of Chd1 results in the loss of regular spacing between nucleosomes in coding regions (Gkikopoulos et al., 2011; Narlikar et al., 2013). Chd1 interacts with transcription elongation factors suggesting it has a role in mediating the passage of RNA polymerases through the coding region (Simic et al., 2003). Similar to ISWI, the loss of Chd1 results in an increase of histone exchange, an increase in histone acetylation over the coding region, and an increase in transcription (Smolle et al., 2012)

1.6 The RSC complex

The RSC (Remodels the Structure of Chromatin) complex is an essential ATPase dependent chromatin remodeler in *S. cerevisiae* and is part of the SWI/SNF family, initially discovered in 1996 (Cairns et al., 1996). The SWI/SNF (SWItch deficient/Sucrose Non Fermenting) family is defined by the presence of a Snf2 superfamily ATPase subunit, in RSC this is Sth1. RSC shares subunits with the SWI/SNF complex, a second SWI/SNF family chromatin complex in yeast but RSC is much more abundant in the cell (Cairns et al., 1996).

RSC is a 17 subunit protein complex that exists in two functionally different isoforms defined by the presence of either the Rsc1 or Rsc2 protein (Chambers et al., 2012a; Kent et al., 2007). As shown in Figure 1.9 RSC contains a core structure with Sth1, Rsc8, Rsc6, Rsc4, Rsc1 or Rsc2, Sfh1, Arp7, Arp9, Rsc58, and Rsc9 (Cairns et al., 1999; Chambers et al., 2012a). RSC also contains a fungal specific module containing Rsc7/Npl6, Ldb7/Rsc14, Rsc3, Rsc30 and Htl1 (Wilson et al., 2006). Some evidence suggests that approximately 10-20% of the RSC complexes found in yeast exist without the Rsc3/Rsc30 heterodimer termed RSCa (Cairns et al., 1996; Chambers et al., 2012a)

1.6.1 RSC subunits and function

The subunits of the RSC complex have been studied in isolation, though two subunits (Arp7 and Arp9) are shared between RSC and SWI/SNF complex (Tang et al., 2010). Each of the subunits and their functions are reviewed below:

Sth1

Each RSC complex contains a single Sth1 molecule; Sth1 (Snf Two Homolog) is the essential ATPase dependent subunit of RSC and is part of the Snf2 superfamily of ATPases and is essential for mitotic growth in yeast. (Du et al., 1998; Laurent et al., 1992; Tsuchiya et al., 1998). Both Sth1 and Snf2 have nucleoside triphosphate-binding sites and helicase motif sequences that are conserved amongst other eukaryotic proteins (Laurent et

al., 1992). Sth1 contains a 75 amino acid C-terminal bromodomain which is essential for the interaction with histones and is distinct from the bromodomain of Snf2 (Du et al., 1998). Temperature sensitive mutants of Sth1 have been extensively used to interrogate the local and global function of RSC in budding yeast. At restrictive temperatures there are changes in chromatin structure surrounding the centromere and the expression profile of meiotic genes suggesting that RSC has essential functions distinct from SWI/SNF (Du et al., 1998; Tsuchiya et al., 1998; Yukawa et al., 1999).

Through the hydrolysis of ATP via the Sth1 subunit, RSC remains bound to a histone octamer and translocates the DNA strand around the octamer (Saha et al., 2002). Models of RSC-dependent translocation suggest that RSC forms an intranucleosomal DNA loop which allows the nucleosome to translocate approximately 20bp along the DNA strand (Fischer et al., 2007; Zhang et al., 2006)

Rsc1/Rsc2

Rsc1 and Rsc2 are likely to have occurred through a genome duplication event thus are highly similar in amino acid sequence and they share the same domain organisation but they exist in two separate isoforms of the RSC complex and have distinct functions. Loss of either Rsc1 or Rsc2 does not affect cell growth but loss of both causes lethality suggesting Rsc1 and Rsc2 have related but non-identical function. (Cairns et al., 1999; Chambers et al., 2012a). Both have two bromodomains, a bromo-adjacent homology domain, an AT hook. Both also have a C terminal tail which is required for recruitment of Rsc1 and Rsc2 into the RSC complex (Cairns et al., 1999). Homologous complexes such as PBAF in humans contain an AT hook in the ATPase subunit but the ATPase subunit of RSC, Sth1, does not. It is therefore suggested that the AT hook in Rsc1 and Rsc2 may perform the function of the AT hook, normally found in the ATPase subunit (Cairns et al., 1999). The AT-hook is associated with transcription factors and proteins that affect chromatin structure and is a short DNA-binding motif and prefers to bind with the minor groove of DNA (Huth et al., 1997)

One of the bromodomain-2 (BD2) is essential for the survival of yeast, this may be BD2 of either Rsc1 or Rsc2, whereas bromodomain-1 (BD1) is non-essential (Cairns et al., 1999). Little evidence exists of Rsc1/Rsc2 BDs binding preference but some research suggests that they have a binding preference for H3K14ac (Zhang et al., 2010). The approximate 130 amino acid bromo-adjacent homology (BAH) domain was named because it was originally discovered adjacent to bromodomains through the vertebrate protein PBAF (polybromo) and the yeast protein Rsc2 (Callebaut et al., 1999; Goodwin and Nicolas, 2001). Searches then revealed the presence of the BAH domains in a number of chromatin-associated complexes and can be subdivided into two categories by amino acid sequence analysis; the RSC-like BAH domains including Rsc1, Rsc2 and the higher eukaryote homologue BAF180, and the Sir3-like class comprising of Orc1 homologues and the budding yeast protein Sir3 (Chambers et al., 2013; Goodwin and Nicolas, 2001; Hickman and Rusche, 2010). The BAH domain of Orc1 and Sir3 are essential for Orc1 and Sir3-mediated silencing at telomeres and *HML/HMR* (Norris and Boeke, 2010). Orc1 and Sir3 bind directly to nucleosomes with interactions with dimethylated histone H4K20 (Kuo et al., 2012b) and the LRS region (from histone H3 and H4) respectively (Armache et al., 2011; Norris et al., 2008). Rsc2-BAH binds specifically to histone H3 and has a distinct structure to the Sir3-like BAH domains suggesting a distinct mechanism of binding to chromatin (Chambers et al., 2013).

Conflicting data has shown that Rsc1 (Kent et al., 2007) or Rsc2 (Shim et al., 2007) is required for remodelling of chromatin in response to a double-strand DNA break at the *MAT* locus to ensure efficient repair. Rsc2 is also required to set the chromatin structure at *MATalpha* prior to mating-type switching to ensure efficient cleavage by HO (Kent et al., 2007). Rsc1 and Rsc2 have functional differences controlling the expression of sporulation specific genes (Bungard et al., 2004; Yukawa et al., 2002) though chromatin immunoprecipitation analysis has shown that Rsc1 and Rsc2 equally bind to the same genes (Ng et al., 2002). Rsc2 is also required to maintain silencing of rDNA on chromosome XII by interacting with chromatin along the length of the rDNA repeats (Chambers et al., 2013)

Rsc4

Rsc4 has two adjacent bromodomains (BD) that have been extensively studied. BD2 has a strong binding affinity of H3K14ac, the product of histone acetylase Gcn5 (Kasten et al., 2004). RSC also binds directly to all three of the DNA polymerases found in yeast through Rsc4 which interacts through its C terminus with Rpb5, a subunit common to all three nuclear RNA polymerases (Soutourina et al., 2006). Rsc4 is acetylated at K25 in the second BD by Gcn5 which inhibits binding to H3K14ac as BD1 of Rsc4 binds acetylated K25 in BD2 (VanDemark et al., 2007). As Rsc4 binds to DNA polymerases and Rsc4 BD mutations results in a genome wide decrease in transcription, it is suggested RSC translocates along the DNA with RNA polymerases remodelling nucleosomes by interacting with acetylated histone H3 through the Rsc4 subunit (Choi et al., 2008; Soutourina et al., 2006).

Rsc6/Rsc8

Both Rsc6 and Rsc8 are essential subunits of the RSC complex but both subunits share homology with subunits of the SWI/SNF complex; Rsc8 shares homology with Swi3 and Rsc6 is homologous to Swp73. Rsc6 and Rsc8 have a direct interaction and together interact with Sth1 to form a structural core for the RSC remodelling complex and the homologous subunits performing a similar function in the SWI/SNF complex (Treich and Carlson, 1997; Treich et al., 1998b).

Sfh1

Sfh1 (Snf 5 homology 1) is essential for viability and directly interacts with Sth1 within the RSC complex (Treich et al., 1998a). A temperature sensitive *sfh1* allele arrests cells in the G1 phase (Cao et al., 1997). Sfh1 contains a 200 amino acid homology to the human hSNF5/INI1 tumour suppressor gene, however this SNF5 homology domain is thought to confer species specific function (Bonazzi et al., 2005).

Rsc9

Rsc9 is an essential DNA-binding protein with genome-wide localisation at rRNAs and genes regulated by the stress-inhibited TOR pathway suggesting a role in transcriptional control in stress-activated pathways. This suggests a role for RSC in remodelling chromatin in signalling cascades from environmental stimuli to result in changes in transcriptional control (Damelin et al., 2002)

Arp7/Arp9/Rtt102

Arp7 and Arp9 (Actin Related Proteins) form an essential dimeric module found in both yeast SWI/SNF and RSC complexes (Szerlong et al., 2003). Similarly Rtt102 is present in both complexes but little is known about its function (Lee et al., 2004). The actin-related regions are used for heterodimerisation and the C-terminal domains are essential for incorporation into RSC. Evidence suggests that the Arp7/9 dimer function with DNA bending proteins to facilitate chromatin remodelling functions (Szerlong et al., 2003).

Rsc58

Rsc58 is also an essential component of the complex but with the exception of the C-terminus required for assembly into the complex it seems to have limited function. Interactions between Rsc58 and the transcription cofactor Swi6 suggest that it may have a role in recruiting the complex to sites of transcriptional initiation (Taneda and Kikuchi, 2004).

The following subunits form a fungal specific module of the RSC complex (Wilson et al., 2006):

Rsc3/Rsc30

RSC contains two paralogous zinc cluster domain proteins Rsc3 and Rsc30, with both proteins also containing leucine zipper domains. The zinc cluster domain of Rsc3 and Rsc30 have shown to be essential for function and the C-terminus of Rsc3 is essential for assembly into the RSC complex

(Angus-Hill et al., 2001). When Rsc3 and Rsc30 occur in RSC they occur concurrently, however some evidence suggests that another isoform of RSC exists without either Rsc3 or Rsc30, termed RSCa (Cairns et al., 1999).

Even though the proteins are highly similar, the *RSC3* gene is essential whereas the *Δrsc30* null mutant shows few phenotypic defects. To study Rsc3, temperature sensitive mutants of *RSC3* were identified. Temperature sensitive *rsc3* mutants display G2/M arrest due to activation of the spindle checkpoint pathway. Overexpression of *RSC30* is sufficient to suppress temperature sensitive *rsc3* mutants but *Δrsc30* mutants with a Rsc3 Ts^- mutant are not viable whereas overexpression of *RSC3* mostly suppresses *Δrsc30* null mutants. Taken together, this suggests that Rsc3 can perform most Rsc30 functions and Rsc30 interacts with Rsc3 but is not required for all its functions (Angus-Hill et al., 2001). Rsc3 and Rsc30 have been shown to be involved in the transcriptional control of a number of genes by excluding nucleosomes from promoters and are potentially recruited through their respective zinc-binger DNA binding domains (Badis et al., 2008; van Bakel et al., 2013); this is discussed in detail in Section 1.6.2.

Rsc7 (Npl6)/Rsc14 (Ldb7)

Rsc7 is a paralog to Swp82 of the SWI/SNF complex, both containing a central conserved region which are conserved in fungi but not found in higher eukaryotes Similarly Rsc14 is conserved in yeast species but is not present in higher eukaryotes. (Wilson et al., 2006). Rsc7 and Rsc14 form a heterodimer in RSC and null mutants are lethal in combination suggesting both have an essential role in the RSC complex. Rsc7 contributes to the general assembly of RSC and taken together Rsc7/Rsc14 are required for proper assembly of Rsc3/Rsc30 into the RSC complex, though Rsc7 and Rsc14 bind to RSC independently of each other (Wilson et al., 2006).

Evidence shows that Rsc7 confers a highly specific chromatin remodelling function of the RSC complex at the *MAT* locus when in the *MATalpha* conformation only (Kent et al., 2007) Null mutants of *Δrsc7* and *Δrsc14* show increased sensitivity to genotoxic agents and some evidence

has suggested that Rsc14 has a role in controlling transcription at a subset of genes (Conde et al., 2007).

Htl1

Htl1 (High Temperature Lethal 1) is a factor that interacts with the yeast complex through interactions with the scaffold protein Rsc8 (Florio et al., 2007; Romeo et al., 2002) Deletion of *HTL1* leads to the derepression of the RSC target *CHA1* indicating that Htl1 influences RSC function. Evidence also shows that *Δhtl1* mutants also display cell wall defects, temperature sensitivity and ploidy maintenance defects, mediated by the change in expression of a MAP kinase signalling pathway intermediate (Wang and Cheng, 2012).

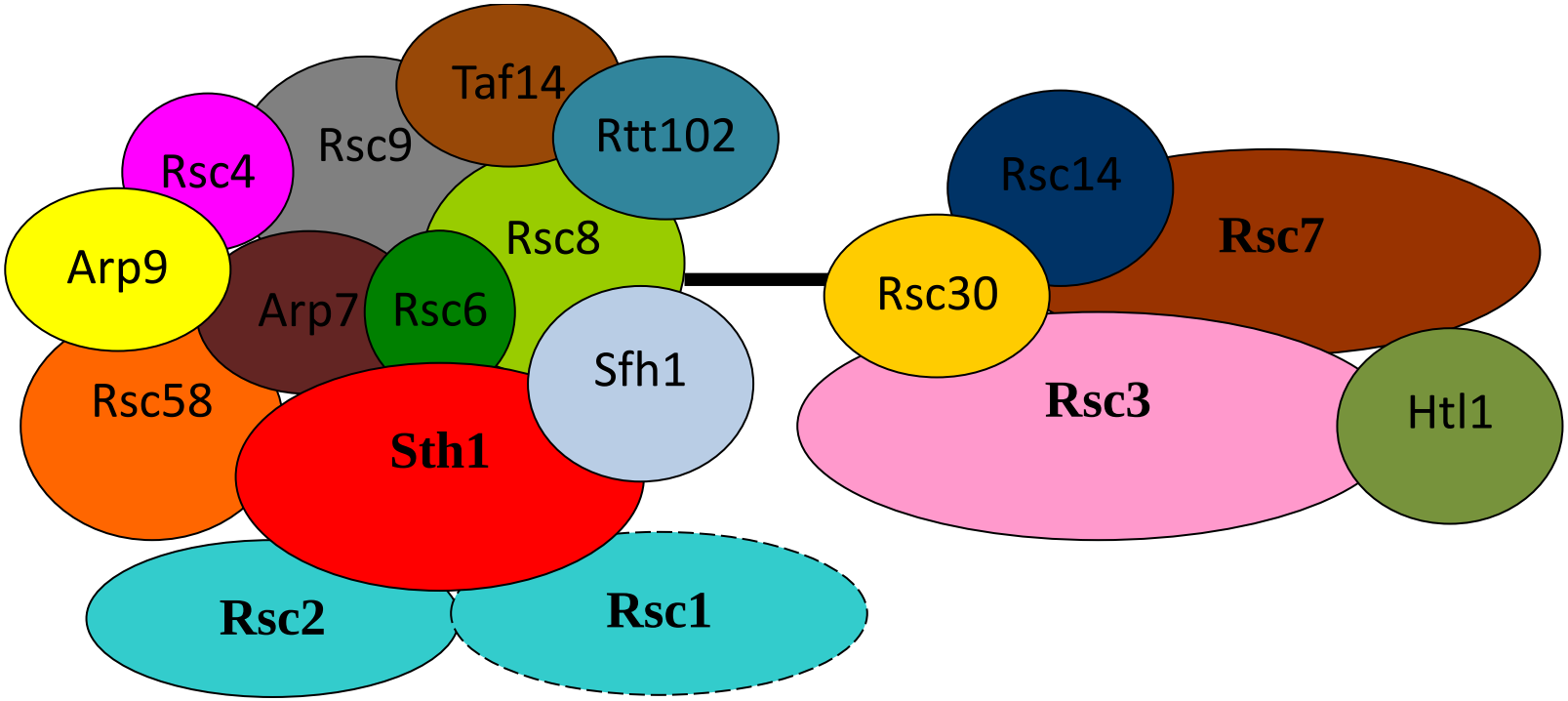

Figure 1.9 – The RSC complex has a core structure with a fungal-specific set of subunits
The cartoon representation of the RSC complex shows that it is made up of 17 subunits but exists in two subunits defined by the presence of either Rsc1 or Rsc2. The complex also has a fungal-specific component made up of Rsc7, Rsc14, Rsc3, Rsc30 and Htl1.

1.6.2 RSC and transcription

The loss of the ATPase subunit of RSC, Sth1, results in the loss of nucleosome positioning at RNA Pol II genes and loss of nucleosome density at RNA Pol III genes suggesting a role in transcriptional control (Parnell et al., 2008). Previous work has identified the setting of the chromatin pattern in the upstream region of the open reading frame of a number of genes dependent on RSC, for example *CHA1* and *PHO8* (Moreira and Holmberg, 1999; Wippo et al., 2011). Other work has shown that the loss of RSC subunits results in a change in transcriptional activity of a small subset of genes but does not suggest a mechanism (Conde et al., 2007; Wang and Cheng, 2012) As described above RSC contains two zinc finger binding proteins, Rsc3 and Rsc30. Microarray analyses of *rsc3* and *rsc30* mutants show variable effects on the expression levels of ribosomal and cell wall genes. (Angus-Hill et al., 2001). The consensus binding motif of Rsc3 and Rsc30 has been determined by systematic microarray analysis and there are potentially over 700 binding sites for Rsc3 at RNA Pol II and RNA Pol III dependent genes (Badis et al., 2008; Parnell et al., 2008). At many RNA polymerase II promoters, RSC is required to maintain a nucleosome free region (NFR) and RSC prevents nucleosomes encroaching over the NFR by remodelling nucleosomes away from the predicted thermodynamically stable histone/DNA site (Badis et al., 2008; Hartley and Madhani, 2009). Genome wide location analysis (ChIP-chip) has also confirmed that RSC binds to RNA pol III- dependent genes, and loss of RSC function results in increased nucleosome occupancy and decreased transcription (Ng et al., 2002; Parnell et al., 2008). RSC is also required to maintain a non-canonical histone structure, most likely a partially unwound nucleosome, over the *GAL1/10* divergent regulatory region. This structure is required to facilitate the binding of the transcription factor Gal4 (Floer et al., 2010).

RSC also controls transcription elongation; RSC is directly connected to all three RNA polymerases in the cell through the Rsc4 subunit (Soutourina et al., 2006). RSC is required for the passage of RNA Pol II through positioned nucleosomes, likely as a result of Rsc4 bromodomains interacting with acetylated histone H3, acetylated by Gcn5, and RSC

remodels nucleosomes to allow passage of RNA Pol II (Carey et al., 2006; Choi et al., 2008; Ginsburg et al., 2009). Gcn5 regulates the binding of Rsc4 to acetylated histone H3 by acetylating the bromodomain of Rsc4 (VanDemark et al., 2007)

For this thesis it was necessary to define genomic sites to which RSC is likely to bind; Ng *et al.* (2002) used chromatin immunoprecipitation with DNA microarray technology to identify 429 intergenic regions that significantly bind Rsc1, Rsc2, Rsc3, Rsc8 and Sth1 ($p<0.001$) (Ng et al., 2002). The authors however concede that the cross-linking efficiency of RSC subunits is 5- to 10-fold less than that of specific DNA-binding proteins and therefore this analysis may not reveal all RSC physiological targets. Badis *et al.* (2008) have identified the binding motif of the zinc-finger-containing Rsc3 subunit of the RSC complex using microarray based analysis. These binding sites are 16-fold more likely to occur in the NFR (-130 to -75 from TSS) rather than in genic regions, approximately 708 genes have a significant motif threshold. At the most liberal P-value cut-off ($p=0.003$), of the 5171 yeast genes with well-defined TSSs, 2325 have a match to the Rsc3 motif. Of the RSC 667 targets with a P-value of <0.01 defined by Ng *et al* (2002), 416 are found in the Rsc3-motif list. Therefore, due to the likelihood of RSC not being defined at all targets due to poor cross-linking efficiency, the list of 2325 genes with a Rsc3 binding motif was used in this study as list of genes that potentially bind RSC upstream of the TSS (Badis et al., 2008).

1.6.3 RSC and DNA damage

RSC is implicated in the initial processing of DNA damage and the consequent repair pathways: RSC has an early role at the processing of the HO induced double-strand DNA break and facilitates Rad59-dependent homologous recombination (Oum et al., 2011; Shim et al., 2007). Analysis shows that RSC remodels nucleosomes at double-strand DNA breaks formed as part of mating-type switching (Kent et al., 2007; Shim et al., 2007). Using a budding yeast strain with an inducible HO endonuclease, the chromatin surrounding a double-strand DNA break (DSB) was analysed prior to and after a DNA lesion event at the *MAT* locus (Connolly et al., 1988; Kent

et al., 2007; Shim et al., 2007). Nucleosomes are rapidly repositioned (within 30 minutes) in response to the DNA damage, as shown in Figure 1.3. These sliding events occur prior to the histone eviction event mediated by the INO80 complex which occurs 60-180 minutes after lesion formation (Tsukuda et al., 2005). Insertion of HO cleavage sequences into non-*MAT* loci show that nucleosome remodelling occurs outside of the highly specialised *MAT* locus suggesting RSC has a genome wide role in responding to DNA damage (Kent et al., 2007). Using isogenic null mutants of RSC subunits, conflicting studies have identified Rsc1 or Rsc2 as being essential for the sliding of nucleosomes in response to DNA damage (Kent et al., 2007; Liang et al., 2007; Shim et al., 2007).

RSC-dependent nucleosome remodelling is required for the efficient phosphorylation of H2A on Ser129 by Mec1, this histone mark is essential for strand resection during homologous recombination (Downs et al., 2004; Harvey et al., 2005). However, blocking H2AX phosphorylation by mutation of Ser129 does not abolish the recruitment of RSC, indicating the RSC complex is one of the first complexes to respond to this damage (Kent et al., 2007). Repair by homologous recombination and end joining is delayed in a *Δrsc1* mutant when nucleosome remodelling in response to the DSB is thought to be abolished (Kent et al., 2007).

Double-strand breaks are preferentially repaired via homologous recombination which uses a homologous chromosome or sister chromatid as a template for repair (Aylon and Kupiec, 2004). RSC interacts with the recombination protein Rad59 by a physical interaction with Rsc1 and Rsc2 subunits. RSC is essential for the maximum loading of cohesion at DNA breaks, a process that is required for sister chromatid cohesion and subsequent repair by recombination between sister chromatids (Oum et al., 2011)

1.6.4 Distinct Rsc2/Rsc7 function at the *MATalpha* locus

Kent *et al* (2007) have shown that there is a large MNase resistant structure immediately on the *MAT* locus side of the HO cleavage site in *MATalpha* (Figure 1.10). This structure is not remodelled in response to the formation of a DSB in contrast to the nucleosomes on the other side of the lesion. Analysis of isogenic null mutants of RSC complex subunits revealed that the large MNase resistant structure is both Rsc2- and Rsc7-dependent. In *Δrsc2* or *Δrsc7* null mutants this large structure has a MNase cleavage pattern that is suggestive of three individually positioned nucleosomes (Kent et al., 2007).

Taken together, previous investigations have determined that *S. cerevisiae* contains two isoforms of RSC which are distinct by the presence of either Rsc1 or Rsc2, and the two isoforms have similar but non-identical functions throughout the genome.

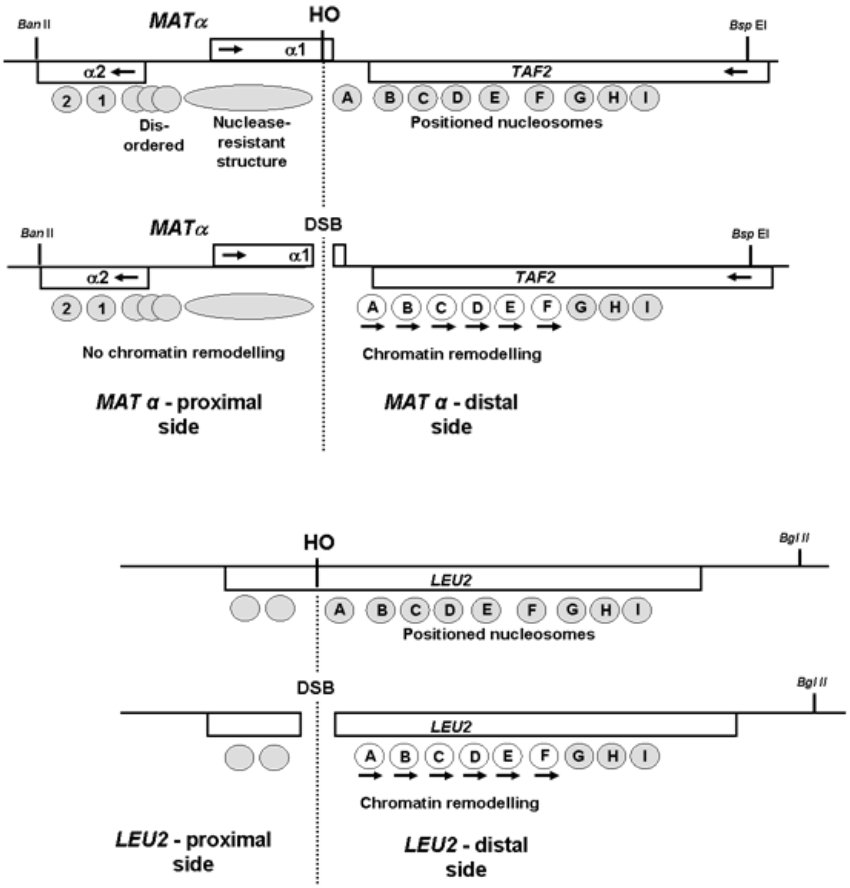

Figure 1.10 – Chromatin is remodelled in response to DSB formation by HO
Kent et al. (2007) have used MNase digestion and indirect end labelling to map nucleosomes before and 40 minutes after DSB formation by HO induction. At both *MAT α* and *LEU2* this remodelling is dependent on Rsc1, a subunit of the RSC complex. Six nucleosomes slide away from the break site allowing for efficient histone H2A phosphorylation to signal for DNA damage.

1.7 Thesis Aims

As described above, the RSC complex has been shown to remodel nucleosomes at the HO-induced double-strand break at the *MAT* locus in a manner required for efficient DNA processing and repair. However the model system utilised in these studies has exclusively used the *alpha* form of *MAT*. The first aim of this thesis (described in Chapters 3 and 4) is to use indirect-end-label type analysis to provide an in-depth characterisation of the chromatin structure at the alternate *MATa* form of the locus and HO cleavage sites engineered into non-*MAT* loci and to test whether or not the same RSC subunit dependencies apply.

Chromatin remodelling by RSC requires the presence of two homologous subunits, Rsc1 and Rsc2, which both contain bromo-, bromo-adjacent-homology (BAH) and AT-hook domains hypothesised to mediate chromatin binding. There is debate in the literature whether remodelling of nucleosomes at HO-induced double-strand DNA breaks is dependent on Rsc1 or Rsc2. The second aim of this thesis (Described in Chapter 3 and 5) is to test, using domain-swap experiments and isogenic null mutants, which components of Rsc1 and Rsc2 are required for specific RSC chromatin remodelling events during DSB formation and chromatin setting at *MATalpha.*

As described above, the RSC complex is also implicated in chromatin remodelling at a variety of gene regulatory locations. The final aim of this thesis (described in Chapter 6) is to test the chromatin remodelling roles of Rsc1 and Rsc2 in the wider genome by applying a chromatin-seq methodology to compare nucleosome positions and/or chromatin structure changes between wild-type cells and *Δrsc1* and *Δrsc2* mutants.

Taken together this work aims to define the modes of chromatin remodelling brought about by the RSC complex, the RSC subunits required to mediate them, and the biological roles that they play.

2 Materials and Methods

2.1 Materials

With the exceptions of those listed below, general chemicals used in the following methods were obtained from Fisher Scientific.

2.1.1 Growth media

Agar, peptone and yeast extract were purchased from Formedium. D-glucose was purchased from Fisher Scientific, glycerol and lactic acid was purchased from Sigma-Aldrich. Luria Broth Base and Luria Broth Base with agar were obtained from Formedium.

2.1.2 Antibiotics

Geneticin (G418) was purchased from Melford Laboratories and hygromycin was purchased from Formedium.

2.1.3 Restriction enzymes

Unless otherwise indicated restriction enzymes were purchased from New England Biolabs along with the enzyme specific digestion buffer. Micrococcal nuclease which was purchased from Affymetrix and stored at 15u/µl in 20µl aliquots at -20ºC in 10mM Tris-HCl pH7.5, 10mM NaCl, 100mg/ml BSA.

2.1.4 DNA molecular weight marker

All gels were run with 5µl of Full Ranger 100bp DNA Ladder, purchased from Geneflow. Purified marker DNA was obtained by phenol/chloroform extraction for random priming radiolabelling for use in the indirect end labelling experiments.

2.1.5 Haemocytometry and Microscopes

Yeast culture density was calculated by haemocytometry using a Neubauer Improved haemocytomer and Leitz-Wetzlar SM Lux microscope.

2.1.6 Oligonucleotides

All oligonucleotides were purchased from Sigma-Aldrich

2.1.7 PCR

All PCR amplification reactions were performed using a Techne – TC 312 thermocycler.

2.1.8 Plasmids

All plasmids were purchased from the European *Saccharo*myces *Cerevisiae* Archive for Functional analysis (EUROSCARF)

2.1.9 Yeast Strains

Yeast strains used in this thesis are described in Table 2.1

Name	Description	Genotype	Source
BY4741	A wild type reference strain	MATa his3Δ0 leu2Δ0 met15Δ0 ura3Δ0	Brachmann *et al* (1998)
YO4686	Isogenic to BY4741 except for *RSC1* replacement by KanMX	MATa his3Δ0 leu2Δ0 met15Δ0 ura3Δ0, *rsc1::KanMX*	EUROSCARF
YO5266	Isogenic to BY4741 except for *RSC2* replacement by KanMX	MATa his3Δ0 leu2Δ0 met15Δ0 ura3Δ0, *rsc2::KanMX*	EUROSCARF
JKM139	As JKM139 except *MAT a*	*MAT*a, ade1-100, leu2-3, 112, lys5, trp1::hisG, ura3-52, hoΔ, hmlΔ, hmrΔ, ade3::GAL1pro::HO	Moore and Haber (1996)
YTB38-9	Isogenic to JKM139 except for *RSC1* replacement by KanMX	*MAT*a, ade1-100, leu2-3, 112, lys5, trp1::hisG, ura3-52, hoΔ, hmlΔ, hmrΔ, ade3::GAL1pro::HO, *rsc1::KanMX*	Beacham, T. This laboratory
YTB65-34	Isogenic to JKM139 except for *RSC2* replacement by *Hph*	*MAT*a, ade1-100, leu2-3, 112, lys5, trp1::hisG, ura3-52, hoΔ, hmlΔ, hmrΔ, ade3::GAL1pro::HO, *rsc2::KanMX*	Beacham, T. This Laboratory
YSD139-141	Isogenic to JKM139 except for *RSC7* replacement by KanMX	*MAT*a, ade1-100, leu2-3, 112, lys5, trp1::hisG, ura3-52, hoΔ, hmlΔ, hmrΔ, ade3::GAL1pro::HO, *rsc7::KanMX*	This study
YFP17	A strain with a 117bp HO cleavage site in the open reading frame of *LEU2* and *HO* under a galactose-inducible promoter	mataΔ::hisG, ade1, lys5, trp1::hisG, ura3-52, leu2::HOcs, hoΔ, hmlΔ, hmrΔ, ade3::GAL1pro::HO	Paques *et al.* (1998)
YNKFP17-20	Isogenic to YFP17 except for *RSC7* replacement by KanMX	mataΔ::hisG, ade1, lys5, trp1::hisG, ura3-52, leu2::HOcs, hoΔ, hmlΔ, hmrΔ, ade3::GAL1pro::HO, *rsc1::KanMX*	Kent *et al* (2007
YNKFP17-25	Isogenic to YFP17 except for *RSC7* replacement by KanMX	mataΔ::hisG, ade1, lys5, trp1::hisG, ura3-52, leu2::HOcs, hoΔ, hmlΔ, hmrΔ, ade3::GAL1pro::HO, *rsc2::KanMX*	Kent *et al* (2007
YNKFP17-10	Isogenic to YFP17 except for *RSC7* replacement by KanMX	mataΔ::hisG, ade1, lys5, trp1::hisG, ura3-52, leu2::HOcs, hoΔ, hmlΔ, hmrΔ, ade3::GAL1pro::HO, *rsc7::KanMX*	Kent *et al* (2007
MK205a	A strain with a 39bp HO cleavage site in the open reading frame of *URA3* and *HO* under a galactose-inducible promoter	MATa-inc, ura3::HOcs, ade3::GALHO, ade2-1, leu2-3,112, his3-11,15, trp1-1, can1-100	Aylon *et al.* (2003)
YSD205-101	Isogenic to MK205a except for *RSC1* replacement by KanMX	MATa-inc, ura3::HOcs, ade3::GALHO, ade2-1, leu2-3,112, his3-11,15, trp1-1, can1-100, *rsc1::KanMX*	This study
YSD205-204	Isogenic to MK205a except for *RSC2* replacement by KanMX	MATa-inc, ura3::HOcs, ade3::GALHO, ade2-1, leu2-3,112, his3-11,15, trp1-1, can1-100, *rsc2::KanMX*	This study
YSD205-405	Isogenic to MK205a except for *RSC7* replacement by KanMX	MATa-inc, ura3::HOcs, ade3::GALHO, ade2-1, leu2-3,112, his3-11,15, trp1-1, can1-100, *rsc7::KanMX*	This study
JKM179	This strain allows for the inducible induction of *HO* and prevents the *MAT* locus from repairing by HR by removal of the silent mating loci	*MAT*α, ade1-100, leu2-3, 112, lys5, trp1::hisG, ura3-52, hoΔ, hmlΔ, hmrΔ, ade3::GAL1pro::HO	Moore and Haber (1996)
YNK179-177	Isogenic to JKM179 except for *RSC1* replacement by KanMX	*MAT*α, ade1-100, leu2-3, 112, lys5, trp1::hisG, ura3-52, hoΔ, hmlΔ, hmrΔ, ade3::GAL1pro::HO, *rsc1::KanMX*	Kent *et al* (2007)
YNK179-190	Isogenic to JKM179 except for *RSC2* replacement by KanMX	*MAT*α, ade1-100, leu2-3, 112, lys5, trp1::hisG, ura3-52, hoΔ, hmlΔ, hmrΔ, ade3::GAL1pro::HO, *rsc2::KanMX*	Kent *et al* (2007)
YNK179-101	Isogenic to JKM179 except for *RSC7* replacement by KanMX	*MAT*α, ade1-100, leu2-3, 112, lys5, trp1::hisG, ura3-52, hoΔ, hmlΔ, hmrΔ, ade3::GAL1pro::HO, *rsc7::KanMX*	Kent *et al* (2007)
YSD179-182	Isogenic to JKM179 except for *RSC14* replacement by KanMX	*MAT*α, ade1-100, leu2-3, 112, lys5, trp1::hisG, ura3-52, hoΔ, hmlΔ, hmrΔ, ade3::GAL1pro::HO, *rsc14::KanMX*	This study
YSD179-191	Isogenic to JKM179 except for *HTL1* replacement by KanMX	*MAT*α, ade1-100, leu2-3, 112, lys5, trp1::hisG, ura3-52, hoΔ, hmlΔ, hmrΔ, ade3::GAL1pro::HO, *htl1::KanMX*	This study
YLO-1	Isogenic to JKM179 except for *RSC30* disruption by KanMX	*MAT*α, ade1-100, leu2-3, 112, lys5, trp1::hisG, ura3-52, hoΔ, hmlΔ, hmrΔ, ade3::GAL1pro::HO, *rsc30::KanMX*	This study
The following strains are isogenic to JKM179 except for replacement of *RSC1* and *RSC2* by KanMX. The plasmid description and plasmid columns describes the plasmid construct used to rescue the otherwise inviable double mutant			
Name	*Plasmid description*	*Plasmid*	Source
JDY786	*RSC1*	p*RSC1*	Chambers *et al* (2012)
JDY768	*RSC2* with the BAH domain of *RSC1*	pRSC2 $^{BAH\text{-}RSC1}$	Chambers *et al* (2012)
JDY767	*RSC2* with the bromodomain-2 of *RSC1*	pRSC2 $^{BD2\text{-}RSC1}$	Chambers *et al* (2012)
JDY765	*RSC2*	pRSC2	Chambers *et al* (2012)
JDY793	*RSC2* with the bromodomain-1 of *RSC1*	pRSC2 $^{BD1\text{-}RSC1}$	Chambers *et al* (2012)
JDY794	*RSC1* with a bromodomain-1 mutation	pRSC1 N88A	Chambers *et al* (2012)
JDY801	*RSC2* with a bromodomain-1 mutation	pRSC2 N96A	Chambers *et al* (2012)
JDY803	*RSC2* with a bromodomain-2 mutation	pRSC2 Y315A	Chambers *et al* (2012)
JDY805	*RSC2* with the bromodomain-1 of *RSC1* and a bromodomain-2 mutation	pRSC2$^{BD1\text{-}RSC1}$ Y315A	Chambers *et al* (2012)
JDY807	*RSC2* with a mutated bromodomain-1 of *RSC1* and a bromodomain-2 mutation	pRSC2$^{BD1\ N88A\text{-}RSC1}$ Y315A	Chambers *et al* (2012)
JDY824	*RSC2* with a bromodomain-1 and bromodomain-2 mutation	pRSC2 N96A Y315A	Chambers *et al* (2012)

Table 2.1 – Yeast strains used in this study

2.2 General Methods

2.2.1 Yeast growth media

All strains were grown at 29ºC in either a static incubator for solid media growth, or a shaking incubator for liquid media growth. Media was made with analytical grade water (Fisher Scientific).

For solid agar media, all strains were grown on YPD or drop out media (synthetic complete media lacking one or more amino acid). YPD was 1% yeast extract, 1% bacto-peptone, and 2% D-glucose (YPD) media (all % are w/v). Drop out media was 0.67% yeast nitrogen base, 2% D-glucose (all% are w/v), and a mixture of all the amino acids, 10 mg/l adenine, 50 mg/l arginine. 80 mg/l aspartic acid, 20 mg/l histidine, 50 mg/l isoleucine, 100 mg/l leucine, 50 mg/l lysine, 20 mg/l methionine, 50 mg/l phenylalanine, 100 mg/l threonine, 50 mg/l tryptophan, 50 mg/l tyrosine, 20 mg/l uracil, 140 mg/l valine, less one or more indicated. For solid media 10g/l of agar was added and media was sterilised by autoclaving.

Kanamycin solid agar media plates (YPD_{G418}) were made by adding 200µg/µl of G418 and hygromycin solid media were made by adding 300µg/µl hygromycin, both antibiotics were added after autoclaving.

Yeast were stored on solid agar plates for up to 6 months. Longer term storage was achieved by suspending 500µl of an overnight 5ml culture in 500µl 100% glycerol (sterilised by autoclaving) and incubating at -80ºC indefinitely.

For liquid media, yeast strains were grown in YPD, YPGL, or YPD plus antibiotic. YPD was 1% yeast extract, 1% bacto-peptone and 2% D-glucose. YPGL was 1% yeast extract, 1% bacto-peptone (sterilized by autoclaving), 1% glycerol, and 1% D-lactic acid (sterilized by filter sterilization at 0.22µm). Media containing antibiotics was prepared by adding either 200µg/µl G418 or 300µg/µl hygromycin after autoclaving.

2.2.2 Bacterial media

Bacterial strains (*Escherichia coli)* were grown at 37ºC in either a stationary incubator (solid media) or in a shaking incubator (liquid media)

L-Broth (Luria Broth) is 10g/l tryptone, 5g/l yeast extract and 0.5g/l NaCl and was purchased as a pre-mix from Formedium. For solid plates a pre-mix was purchased from Formedium with the previous formula with the addition of 15g/l agar.

2.2.3 Gel electrophoresis

Standard agarose gel electrophoresis for the separation of chromatin particles ("check gels"), PCR products and restriction enzyme digestions was performed using 1.5% agarose gels in 1x TBE (89mM Tris-borate, 2.5mM EDTA) buffer stained with 0.01% (v/v) ethidium bromide. DNA for purification was separated on TAE (0.04M Tris- acetic acid, 1mM EDTA) buffered gels.

2.2.4 The Polymerase Chain Reaction

PCR reactions were all performed on 10-50ng of template DNA with 1mM dNTPs, *Taq* DNA Polymerase (New England Biolabs), and 1mM each of forward and reverse primers (Sigma-Aldrich) in 20µl reactions in 0.2ml thin walled tubes. Reactions were initially denatured at 95ºC for 5 minutes and the following cyclic conditions followed: 95ºC for 45 seconds, 52ºC for 45 seconds and 72ºC for 1 minute per kbp being amplified.

2.2.5 Restriction enzyme digestion

Restriction enzyme digestions were performed using enzymes supplied by New England Biolabs and the supplied digestion buffer and according to manufacturer's instructions.

2.2.6 Gel DNA purification using GeneClean Kit ® (Biogene)

To purify DNA fragments between 100bp and 10 kb, DNA was separated on a 1.5% agarose, 0.01% ethidium bromide, and TAE buffered agarose gel. The slice of gel containing the DNA of interest was cut from the TAE gel (after detection under UV light or Safeviewer) and transferred to a microfuge tube. 4 volumes (weight:volume) of 6M NaI were added to the slice, and incubated at 55°C with mixing every 20 seconds to dissolve the gel slice into the NaI solution. Once the gel slice had dissolved the tube was placed on ice for 1 minute to allow the DNA ends to re-anneal. GlassMilk

was resuspended by vortexing and 10µl added to the NaI/gel solution. After mixing the GlassMilk/gel solution was incubated for 10 seconds (~75% binding) – to 5 minutes (~99% binding) at room temperature. The GlassMilk/DNA was pelleted by centrifugation at 14500g for 1 minute and the NaI discarded. The pellet was then washed twice in 600µl NEW Wash (prepared according to manufacturer's instructions). After all the NEW wash buffer was removed the glass pellet was allowed to dry for 3 minutes at room temperate. The GlassMilk was resuspended in 10µl of AR water and incubated at room temperature for 30 minutes. The non-DNA bound glass milk was pelleted by centrifugation at 14500g for 1 minute and the supernatant containing the DNA fragment was collected.

2.2.7 Using *Escherichia coli* for plasmid manipulation

2.2.7.1 Preparation of transformation competent DH5α cells

lml of a stationary phase DH5α culture (5ml L-Broth, grown overnight at 37ºC with vigorous shaking) was added to 50ml L-broth that had been pre-warmed at 37ºC. The remaining 4ml of stationary phase culture was stored in glycerol (50% glycerol, 50% culture), at -80ºC. The 50ml culture was grown to mid-log phase at 37ºC in a shaking incubator (typically 1 hour of growth). Cells were cooled at on ice for 15 minutes and subsequently harvested by centrifugation at 3000g for 7 minutes at 4ºC. The cells were resuspended in 30ml cold 100mM $CaCl_2$ and incubated at 5ºC for 30 minutes. Cells were again harvested by centrifugation at 3000g for 7 minutes at 4ºC and cells resuspended in 1ml cold 100mM $CaCl_2$. Cells were then stored for 2-18 hours at 4ºC to achieve maximum competency.

2.2.7.2 Transformation of DH5α

100µl of transformation competent cells were placed on ice with 10ng of plasmid DNA. The reaction was incubated on ice for 10 minutes and then underwent heat shock at 42ºC for 2 minutes. The reaction was immediately placed back on ice for 2 minutes and then made up to 1ml with L-broth. Cells were then incubated at 37ºC in a shaking incubator for 1 hour.

10µl of transformed cells were plated onto L-broth agar as a non-selective control and the remaining cells were plated onto L-broth agar containing ampicillin for selection. Both were grown overnight at 37ºC.

2.2.7.3 Boil-lysis plasmid extraction

*E. coli c*olonies from transformation plates were picked using a sterile micro-pipette tip and grown in 2ml L-broth with ampicillin (100µg/ml) at 37ºC for 4 hours in a shaking incubator. Cells were harvested by micro-centrifugation at 12500g for 15 seconds and resuspended in 100µl sterile water. Cells were then boiled for 15 minutes. The lysed cells were centrifuged at 12500g for 5 minutes and the supernatant containing plasmid DNA was aspirated to a fresh microcentrifuge tube.

2.2.7.4 Alkaline-lysis plasmid extraction (Mini-Prep)

E.coli colonies from transformation plates were grown overnight in 5ml L-broth with ampicillin (100µg/ml) at 37ºC. 1.4ml of cells were harvested at 14500g for 2 minutes and resuspended in 100µl ice cold 50mM D-glucose, 25mM Tris-HCl (pH8), 10mM EDTA. Cells we lysed by addition of 200µl 0.2M NaOH, 1% SDS and mixed gently until the solution became transparent. The mixture was centrifuged at 12500g for 5 seconds and incubated at room temperature for a further 2 minutes. 150µl ice-cold potassium acetate was then added to form a precipitate. The reaction was incubated at 5ºC for 1 minute. The aqueous phase was collected by centrifugation at 14500g for 5 minutes and a volume of 400µl was collected. Plasmid DNA was extracted by addition of 1 volume of phenol (buffered in 10mM Tris-HCl pH 8.0 and 1mM EDTA)/chloroform (1:1 ratio), an emulsion formed by vortexing for 10 seconds, and the aqueous layer separated by centrifugation at 14500g for 5 minutes. The aqueous phase was collected and subjected to digestion by 5µl RNase A (10mg/ml) for 30 minutes at 37ºC. The resulting mixture underwent a second phenol/chloroform extract, 1 volume phenol/chloroform (1:1 ratio) and the aqueous layer separated by centrifugation at 14500g for 5 minutes. The plasmid DNA was precipitated by addition of 800µl 100% propan-2-ol and a pellet formed by centrifugation at 14500g for 10 minutes. The pellet

was washed in 70% ethanol, dried, and resuspended in 20µl TE buffer (10mM Tris [pH7.5], 1mM EDTA).

2.2.8 Creation of isogenic yeast knockout strains

All knockouts, unless otherwise stated, were created by the disruption of the coding region by replacement of the entire coding region with either: *kanMX4* gene from Tn903 that confers resistance to the aminoglycoside antibiotic Geneticin (G418) of transformed yeasts or the *hph* gene from *Klebsiella pneumoniae* encoding hygromycin B phosphotransferase and confers resistance to the antibiotic hygromycin B of transformed yeasts.

Unless indicated, the *kanMX* cassette with 200bp of flanking homology region was amplified by PCR from a strain containing the knockout mutant of interest purchased from the EUROSCARF deletion collection.

In the case of YTB66-34 (*MATa Δrsc2*) the coding sequence was replaced by the *hph* gene amplified from the plasmid pAG32 with flanking homology regions by PCR using overhanging primers with flanking *RSC2* homology.

In the case of *RSC30* the promoter region and first 500bp of the coding region were replaced using the *kanMX* cassette amplified by PCR from pUG6 using overhanging primers with *RSC30* homology. This variation was used due to the location of the ARS180-associated repetitive sequence close to the *RSC30* coding region which prevents total gene replacement by homologous recombination.

2.2.8.1 Integration cassette purification

kanMX based integration cassette constructs were amplified using standard PCR from purified genomic DNA of knockout strains purchased from EUROSCARF. The resulting product was separated by gel electrophoresis on a 1.5% agarose TAE and purified using the Gene Clean Kit ©. 5µl of the resuspended purified fragment was re-amplified by PCR using the same primers in order to create 10-20µg of DNA for transformation. To improve the efficiency of transformation, 10µl salmon sperm DNA (10mg/ml) was added as a carrier to the cassette fragment. The transformation cassette/salmon sperm DNA was purified by phenol-

chloroform extraction; 1 volume of phenol and chloroform were added in a 1:1 ratio and the emulsion centrifuged at 14500g for 5 minutes. The aqueous phase was aspirated to a new microfuge tube and the DNA precipitated with 40µl 7.5M ammonium acetate and 260µl 100% propan-2-ol. The precipitate was pelleted by centrifugation at 14500g for 10 minutes and the resulting pellet washed in 70% ethanol. The dried pellet was resuspended in 10µl AR water.

2.2.8.2 Yeast transformation

The general protocol was based on that described by Guthrie (1991) (C. Guthrie, 1991) Cells were grown overnight in 100ml YPD media in a conical flask at 29°C in a shaking incubator to a density of $2x10^7$ cells/ml. $2x10^8$ cells were harvested by centrifugation at 2500g for 3mins in a swing out rotor. The media was discarded and the cells were resuspended in 30ml sterile AR H_20 and centrifuged at 2500g for 3mins. The water was discarded and the cells were resuspended in 800µl LiAc/TE buffer (0.1M Lithium acetate, 10mM Tris-HCl [pH 7.5], 1mM EDTA) and transferred to a 1.5ml microfuge tube. Cells were centrifuged at 12500g for 15 seconds, the LiAc/TE buffer discarded and the cells resuspended in 100µl of LiAc/TE buffer. Aliquots of 50µl of cells were transferred to a microfuge tube containing only carrier DNA as a control and to microfuge tubes containing 5µl of vector/cassette/carrier DNA. A further 300ul of PEG/LiAc/TE buffer (40% PEG (v/v), 0.1M LiAc, 10mM Tris-HCl [pH 7.5], 1mM EDTA) was added and tubes were incubated at 29°C for thirty minutes in a stationary incubator. A further 35µl of 100% DMSO was added and carefully mixed and the cells incubated at 42°C for 15 minutes. Immediately afterwards the cells were incubated on ice for a further 2 minutes. The transformed cells were collected by centrifugation at 10500g for 15 seconds and plated onto non-selective YPD agar plates and incubated at 29°C for approximately 8 hours in a stationary incubator. Transformant micro-colonies were replica plated onto the appropriate selective media (YPD G418 or YPD Hyg) and then incubated at 29°C for 48 hours. Colonies on the selective media plate were picked and streaked on selective media to isolate cell clones as single colonies.

2.2.8.3 Yeast genomic DNA preparation

Yeast were grown overnight in 5ml YPD media at 29ºC in a shaking incubator, those containing the *kanMX* gene, were grown under selection in YPD with kanamycin (200µg/ml). 1.8ml of cells were harvested by centrifugation at 12500g for 30 seconds and the supernatant discarded. Cells were resuspended in 200µl yeast lysis buffer (2% Triton X-100, 1% SDS, 0.1M NaCl, 1mM EDTA, 10mM Tris-HCl [pH8.0]) as described previously (Hoffman and Winston, 1987), 200µl phenol (buffered in 10mM Tris-HCl pH8.0, 1mM EDTA, 200µl chloroform, and 0.3g acid-washed 0.22µm glass beads were added to the mixture and then vigorously vortexed for 3 minutes using a Disruptor Genie (Scientific Industries). 200µl of TE buffer (10mM Tris-HCl [pH 7.5], 1mM EDTA) was added and the solution vortexed again to reform an emulsion. The aqueous phase was separated by centrifugation at 14500g for 5 minutes and collected to a fresh microcentrifuge tube. Nucleic acid was precipitated by addition of 1ml of 100% ethanol, mixing, and then centrifugation at 14500g for 1 minute. The supernatant was discarded and the nucleic acid pellet was allowed to dry and then resuspended in 400µl TE buffer and digested with 7µl RNase A at 37ºC for 30 minutes. Following digestion the mixture was subjected to a second phenol/chloroform reaction and the resulting aqueous phase was collect. DNA was then precipitated with 40µl 7.5M ammonium acetate and 260µl 100% propan-2-ol and a pellet formed by centrifugation at 14500g for 10 minutes. The pellet was allowed to dry and resuspended in 50µl TE buffer (pH 7.5).

2.2.8.4 Confirmation of integration events after yeast transformation by PCR

Amplification of the region 700 base pairs outside the targeted reading frame and the inserted antibiotic resistance cassette by PCR was used to confirm a successful recombination event. Genomic DNA of yeast colonies that had grown on selective media was prepared as previously detailed (2.2.9.3).

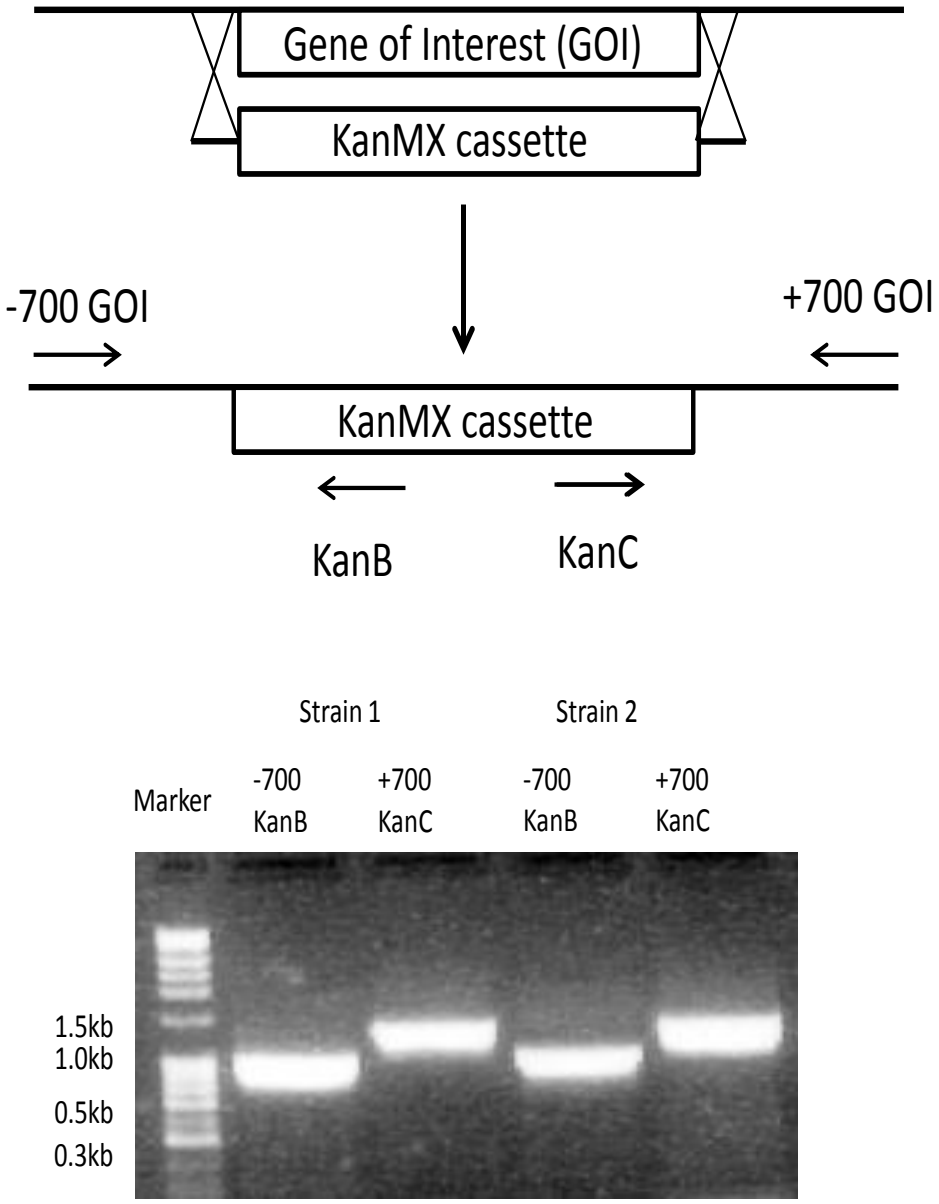

Figure 2.1 – Cassette insertion checked by PCR of cassette/locus junctions
To create knock-out null mutants the entire coding region was replaced using the *KanMX* cassette via homologous recombination and successful events were checked by production of a PCR production from primers downstream (-700 GOI) and upstream (+700 GOI) of the gene of interest locus with internal *KanMX* primers. PCR products were separated by gel electrophoresis to determine presence of the locus/junction DNA sequence in the strain,

2.3 Nucleosome mapping by indirect end labelling of micrococcal nuclease digested chromatin

Micrococcal nuclease (MNase) is a non-specific endo-exonuclease derived from *Staphylococcus aureus*. MNase is unique as it produces single stranded nicks on nucleosome bound DNA, whereas in the linker regions it produces double stranded cleavage with 3' phosphates. This means when MNase is incubated with chromatin bound DNA it will cleave in DNA in the linker regions, leaving relatively intact DNA-duplexes surrounding nucleosomes (Brogaard et al., 2012). Chromatin in yeast cells can be made accessible to MNase by the enzymatic removal of the yeast cell wall to form spheroplasts. Spheroplasts can be further permeabilised by the addition of buffer containing a small amount of detergent. These semi-permeabilised cells can then be incubated with increasing amounts of MNase which will diffuse into the nucleus and digest chromatin. This fast, *in vivo* approach allows snapshots of chromatin structure to be taken.

Semi-permeabilised yeast cells are briefly incubated with MNase and the resulting DNA fragments purified. The fragments are digested to completion by restriction enzyme digestion to produce a common end. These fragments can then be separated by gel electrophoresis and be blotted onto a nylon membrane in a process termed Southern Blotting. A radiolabeled probe specific to a gene or region in the genome is then hybridised to the Southern blot and a MNase chromatin footprint is produced. Deproteinized DNA is also digested and labelled so that nucleosome positions can be inferred where there are protected regions of DNA.

2.3.1 *In vivo c*hromatin digestion of semi-permeabilised budding yeast using micrococcal nuclease

The general method described by Kent *et al* (1993) and Kent and Mellor (1995) was used (Kent et al., 1993; Kent and Mellor, 1995). Yeast cells were grown overnight at 29ºC in a shaking incubator in 100ml YPGL in a conical flask to a density of $2x10^7$ cells/ml. $6x10^8$ cells were harvested by centrifugation at 3000g in a swing out rotor for 3 minutes and the cells transferred to a 2ml microcentrifuge tube in the remaining media. The cells

were pelleted by centrifugation at 12500g for 15 seconds and the remaining medium was discarded. The cells were spheroplasted (removal of cell wall) with *Athrobacter luteus* yeast lytic enzyme (MP-Bio at 10mg/ml in 1M sorbitol/5mM β-mercaptoethanol) for one to two minutes at RT. Spheroplasted cells were pelleted by centrifugation at 12500g for 15 seconds and the yeast lytic enzyme was discarded or recycled for reuse. Cells were washed in 800µl of 1M sorbitol and the cells re-pelleted. The cells were resuspended in 600µl spheroplast digestion buffer containing igepal (SDBI) – (10mM Tris-HCl [pH7.4], 50mM NaCl, 5mM $MgCl_2$, 1mM $CaCl_2$, 0.5mM spermidine, 1mM β-mercaptoethanol, 0.075% v/v igepal in 1M sorbitol). 200µl aliquots of semi-permeabilised cells were added immediately to microcentrifuge tubes containing either 1µl MNase, 2µl MNase (MNase concentrations 75units/ml and 150units/ml respectively), or 20µl STOP buffer (250mM EDTA, 5% SDS). Digestions were incubated at 37ºC for 2 minutes, immediately followed by the addition of 20µl STOP buffer (5% SDS, 250mM EDTA).

2.3.2 DNA purification

STOP lysed MNase digested and undigested chromatin was purified by phenol/chloroform DNA extraction. One volume of phenol (buffered in10mM Tris-HCl [pH 8.0], 1mM EDTA)::chloroform in a 50:50 ratio was added and mixed by vortexing to form an emulsion. The emulsion was separated by centrifugation at 14500g for 5 minutes and the aqueous phase was aspirated to a new 1.5ml centrifuge tube. 7µl of RNase A (10mg/ml) was added to the aqueous phase and incubated at 37ºC for 30 minutes. The resulting DNA was purified by phenol/chloroform extraction by the addition of 1 volume of phenol and chloroform (1:1 ratio) and an emulsion formed by vortexing. The aqueous phase was separated by centrifugation at 14500g for 5 minutes. The resulting aqueous phase was transferred to a new tube and the DNA precipitated by the addition of 40µl of 7.5M ammonium acetate and 260µl 100% propan-2-ol. The DNA was pelleted by centrifugation at 14500g for 10 minutes. The resulting pellet was washed in 70% ethanol, air dried, and resuspended in 18 or 20µl AR water

2.3.3 Deproteinized ("Naked") DNA digestion

Phenol/chloroform purified DNA from STOP lysed cells to which MNase had not been added was used as a deproteinized DNA control sample. This purified DNA was diluted in 300µl SDBI to maintain a common digestion buffer and the DNA digested for 10 seconds with 1.5units MNase in 1M sorbitol. One volume of phenol/chloroform (1:1 ratio) was immediately added to stop the reaction and an emulsion formed by vortexing. Phases were separated by centrifugation at 14500g for 5 minutes and the aqueous phase was transferred to a new centrifuge tube and the DNA precipitated with 60µl ammonium acetate and 520µl 100% propan-2-ol and pelleted by centrifugation at 14500g for 10 minutes. The DNA pellet was washed in 70% ethanol, dried, and resuspended in 18 or 20µl AR water.

2.3.4 Restriction Enzyme digestion for indirect-end-labelling analysis of chromatin particle position

Purified DNA samples (either from chromatin or deproteinized DNA MNase digests) was digested to completion with the appropriate restriction enzyme in a final volume of 25µl using the buffer and instructions supplied by the manufacturer.

2.3.5 Southern Blotting for indirect-end-label analysis

The resulting purified and digested chromatin and naked DNA were run on a 1.5% agarose/0.01% Ethidium bromide TBE buffered gel. The resulting gels were denatured by two incubations in 5 gel volumes of 1.5M NaCl, 0.5M NaOH for 15 minutes. The gels were twice further treated with 1.5M NaCl, 0.5 Tris-HCl, 1mM EDTA. The DNA was transferred overnight onto 0.45µm nylon membrane (Osmonics) against 20X SSC (3M NaCl, 300mM tri-sodium citrate [pH7.0]) by capillary blotting. Blots were briefly washed in 2X SSC before being baked at 80ºC for 2 hours.

2.3.6 Preparation of indirect end label probes

The Prime It II ® Random Priming Kit (Stratgene) was used to label PCR synthesised and gel purified DNA probes for indirect-end-label analysis. This was also used to label phenol/chloroform purified marker DNA (Norgen

FullRanger 100bp DNA Ladder). A mixture of 50-100ng of template DNA in a volume of 5µl and 2µl of random 9mers buffer was denatured at 95ºC for 2 minutes and allowed to anneal at room temperature for a further 2 minutes. 2µl of nucleotide mix lacking dCTP was added followed by the addition of dCTP [α-^{32}P] (Amersham) equating to an activity of 0.37MBq, and 2.5units DNA polymerase I – Klenow fragment (New England Biolabs). The reaction was incubated at 37ºC for 10 minutes. The reaction was stopped by the addition of TE buffer to a total volume of 100µl and the mixture was passed through a TE buffered Sephadex G-50 medium spin column to remove unincorporated nucleotides.

2.3.7 Hybridisation

Blots were placed in a hybridisation bottle (Hybaid) and soaked in 20ml hybridisation buffer (2x SSC, 5x Denharts reagent, 0.1% SDS) and pre warmed at 64ºC for 20 minutes in a rotisserie-oven system. 500µl of non-specific DNA blocking agent, (salmon sperm DNA – 2.5mg/ml) was added to the prepared radiolabelled probe and radiolabel marker DNA and the mixture boiled for 5 minutes and immediately quenched by placing on ice for two minutes. The denatured probe/DNA/marker was added to the hybridisation bottle and hybridised overnight at 64ºC.

2.3.8 Washing of blots

Blots were washed twice in 2x SSC, 0.1% SDS at 64ºC for 15 minutes and for a further 20 minutes in the same buffer but at 61ºC. Blots were heat sealed in thin plastic bags and autoradiographed using Fuji RX and a Chronex intensifying screen at -80ºC for 48 hours to 14 days. Films were processed by hand using Redichem Developer and Redichem Fixer (PLH Medical).

2.4 Chromatin-SEQ: Chromatin Particle Spectrum Analysis

The general method was as described by Kent *et al.* (2011) (Kent et al., 2011). A summary work flow chart for this analysis is shown in Figure 2.2. All PERL scripts used in this analysis and size-specific frequency distribution files (.sgr) are available on the supplied CD-ROM.

2.4.1 Chromatin digestion and size selection

Yeast cell cultures were grown overnight to an exact density of $2x10^7$ cells per ml in YPD at 29ºC. $1.2x10^9$ cells were harvested by centrifugation at 3000g for 3 minutes in a swing out rotor and the harvested cells transferred to a 2ml microcentrifuge tube. The cells were pelleted by centrifugation at 12500g for 15 seconds and the remaining media discarded. Cells were resuspended in 500µl *Arthrobacter luteus* yeast lytic enzyme (MP-Bio - 10mg/ml in 1M sorbitol, 5mM β-mercaptoethanol) for 1 minute 30 seconds at 22ºC. Cells were pelleted by centrifugation at 12500g for 15 seconds and washed in 800µl 1M sorbitol. Cells were pelleted by centrifugation at 12500g for 15 seconds and resuspended in 1.2ml SDBI (as described in Section 2.3.1). 400µl of spheroplasted yeast cells in SDBI were added to 150u/ml micrococcal nuclease for 2 minutes 15 seconds at 37ºC. After digestion the samples were immediately centrifuged at 14500g for 15 seconds to pellet cell debris and high-molecular weight genomic chromatin fragments and the supernatant was transferred quickly to a fresh microfuge tube containing 40µl STOP buffer (250mM EDTA, 5% SDS).

2.4.2 DNA purification

DNA was extracted by phenol/chloroform extraction as described previously (Section 2.3.2) with the following modifications: 400µl phenol/chloroform was added (1:1 ratio), the first aqueous phase was digested with 15µl RNase A for 30 minutes at 37ºC, DNA was precipitated with 60µl ammonium acetate (7.5M) and 520µl propan-2-ol (100%). Three replicate samples from each strain were pooled in a final volume of 84µl AR water.

2.4.3 End processing

To remove the 3' phosphates from the DNA fragments left by MNase (Johnson et al., 2006), 80µl of purified DNA was incubated with 100units of T4 polynucleotide kinase (New England Biolabs) at 37ºC for 30 minutes in a 100µl reaction volume. DNA was purified by phenol/chloroform extraction and precipitated with sodium acetate (7.5M) and propan-2-ol (100%). The resulting pellet was washed in 70% ethanol and the pellet was resuspended in TE (pH7.5).

2.4.4 Paired-end mode Next Generation Sequencing

All sequencing chemistry including library preparation was undertaken by the Exeter University Sequencing Service. Briefly, Illumina adapters were ligated to 4µg of DNA fragments using the NEBNext DNA sample prep master mix set 1 and size selected on polyacrylamide gels to preserve the size distribution of input DNA fragments. Ligated products were amplified using Phusion DNA polymerase and adaptor-specific primers (Illumina) for 12 cycles and then purified using AMPure XP beads (Agencourt). 7 pM DNA was hybridized to each lane of an Illumina flowcell (1 flow cell per yeast strain) resulting in a clusters density of ~700 K/mm^2. DNAs were sequenced using 100 nucleotide paired-end mode on an Illumina HiSeq 2000 using TruSeq SBS reagents version 3. The HiSeq pipeline software calculated a Q-score (quality score) for each base sequenced. The Q-score is derived using the Phred algorithm (Ewing and Green, 1998; Ewing et al., 1998) which defines the Q-score as being logarithmically related to the probability of the base being incorrectly called by the sequencer. Sequence was outputted with a Q-score of ≥30 i.e. a probability of 1 in 1000 bases being incorrectly called. Outputted sequence is therefore of high quality.

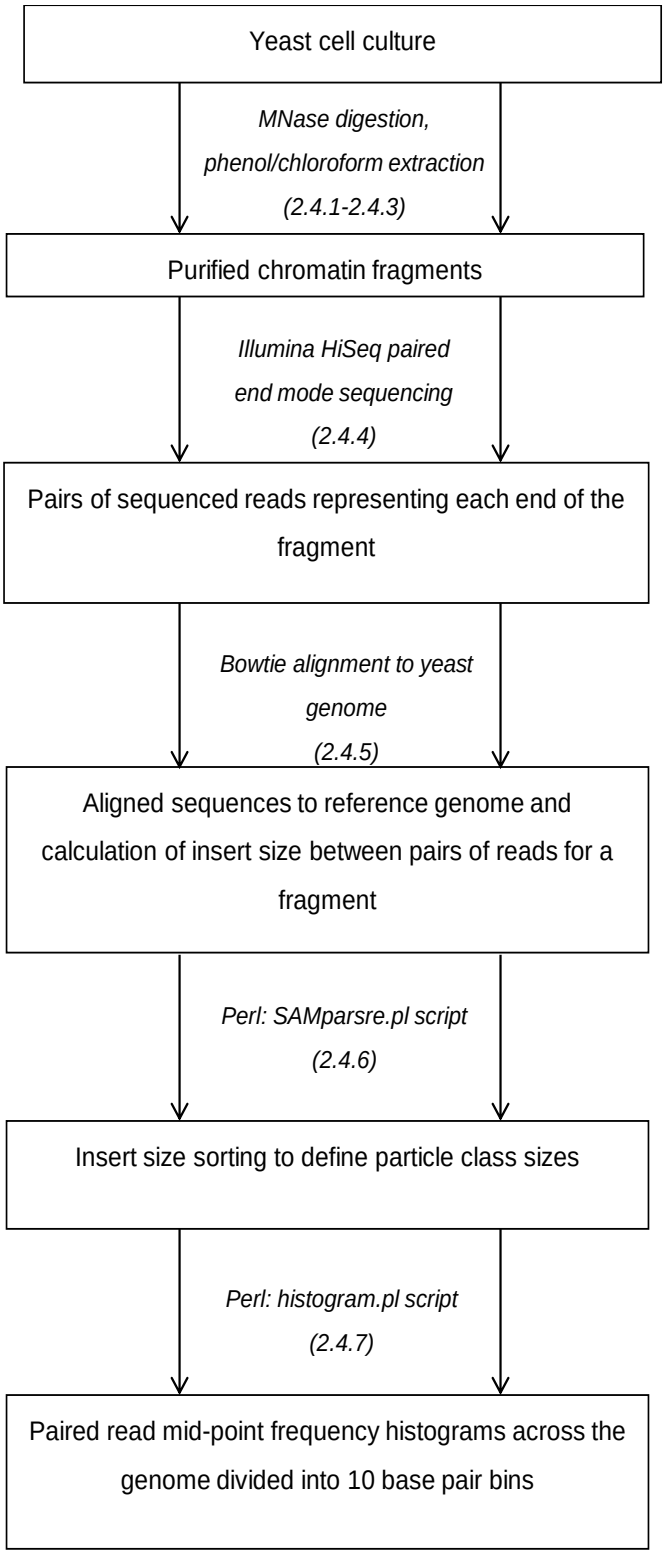

Figure 2.2 Chromatin Particle Spectrum Analysis Flow Chart
Five processes are required to obtain a chromatin landscape of the yeast genome from a growing yeast culture. Each input and output is contained within the closed boxes and the processes required are contained within the arrows with each number relating to the section in the text.

2.4.5 Sequence Alignment

Sequences were aligned to the *Saccharomyces cerevisiae* March 2012 NCBI RefSeq build genome using Bowtie v0.12.7. (Langmead et al., 2009) running under a UNIX operating system. An example of the command line flags is shown below:

./bowtie -v 2 --trim3 64 --maxins 5000 --fr -k 1 -p 1 --sam indexes/S_cer_full_refseq -1 NK-RSC2_ACAGTG_L003_R1_001.fastq -2 NK-RSC2_ACAGTG_L003_R2_001.fastq RSC2_6_full36bp.sam

./bowtie; directs the operating system to use the program “Bowtie” found in that directory
-v 2; allowed up to and including two mismatches in each alignment
--trim3 64; removes 64 base pairs from the 3’ end of each fragment to be aligned (i.e. only 36bp was aligned)
--maxins 5000; paired fragments that were more than 5000bp away from each other on the DNA strand were ignored,
--fr; paired fragments were paired on the same chromosome.
–k 1; only outputted one alignment for each read pair,
-p 1; the program used only 1 processing core of the CPU,
--sam; the outputted data should was in the .sam format (Li et al., 2009),
indexes/S_cer_full_refseq; the reference sequence called “S_cer_full_refseq” was used for the alignment,
- NK-RSC2_ACAGTG_L003_R1_001.fastq; the named file contained the first read of a pair,
-2 NK-RSC2_ACAGTG_L003_R2_001.fastq; the named file contained the second read of a pair,
RSC2_6_full36bp.sam; the name to call the output file.

The .sam file output contained a list of all the read pairs which Bowtie had aligned to the genome as shown in Figure 2.3 The important data values , with respect to the CPSA process, are those that refer to the NCBI (National Centre for Biotechnology Information) reference code to which

chromosome the read pairs have aligned [3], the base pair positioning of the 5’ end of the read on that chromosome [4], and the distance in base pairs to the 3’ end of its paired read i.e. the insert size (ISIZE) [9].

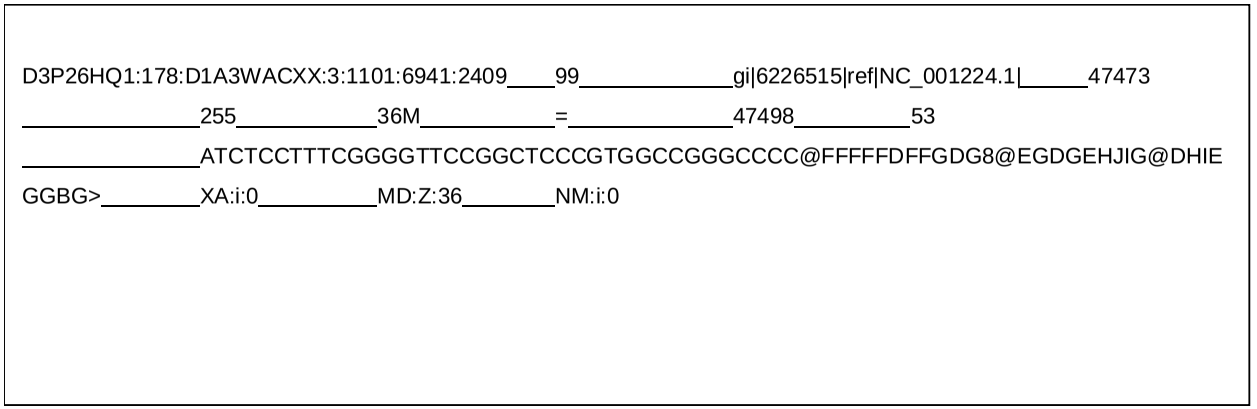

Figure 2.3 - Bowtie Output of a paired read
Each line in the .sam output contained 12 tab-delimited fields (for simplicity white space between tab-delimited fields is underlined in this figure): [1] – The name of the aligned read, [2] – the sum of flags (information about the read alignment), [3] – Name of the reference sequence, [4] – the leftmost character of the alignment base pair on the forward strand offset by 1 base pair, [5] – the quality of mapping, [6] – CIGAR string representation of the alignment, [7] – name of the reference sequence that the mate's aligns to, [8] – the leftmost character of the mate's alignment base pair on the forward strand offset by 1 base pair, [9] – inferred insert size, negative if the alignment is upstream, [10] – read sequence, [11] – ASCII-encoded read quality on Phred quality scale, [12] – optional fields

2.4.6 Chromatin particle definition, size selection and mid-point mapping

The SAM file from Bowtie was sorted into chromosome-specific reads (output in SAM format but without headers and with a .txt file end) using the UNIX “grep” command via the shell script; chgrep.sh. Mitochondrial DNA was designated chromosome 17 and the 2µ-plasmid was designated chromosome 18.

Each of the individual chromosome-specific .txt files were then processed using the Perl script SAMparser,plx which further sorts the paired reads into ISIZE classes representative of known and putative MNase-resistant chromatin species/particles. Particle size were defined as ISIZE values of 50, 75, 100, 125, 150, 175, 200, 225, 250, 275, 300 and 450bp plus/minus a particle window size ($pwind) of 0.2 (+/-20%). Thus reads deriving from nucleosomes (approximately 150bp MNase-resistant DNA fragments) would occur in the 150bp size class and this size class would contain reads with ISIZE values ranging from 120bp to 180bp. This window allows for discrimination of smaller particle size classes and prevents 50-, 100-, 150-, 300-, and 450bp size classes from overlapping.

To define a single and simple genomic position for each chromatin particle SAMparser calculates the mid-point of each paired read. For nucleosomes this position is equivalent to the DNA “dyad” position (Luger et al., 1997) .

chr1	179549	52	179575
chr1	69655	41	69675.5
chr1	20780	50	20805
chr1	23059	42	23080
chr1	197637	44	197659
chr1	119711	46	119734
chr1	120232	49	120256.5

Figure 2.4 - SAMparser output for chromosome of 50 base pair particle size
The output file contains four tab-delimited fields; [1] – chromosome name, [2] – start point of the base pair for that read in the genome, [3] – the insert size for the paired read, [4] – the genome base pair representing the mid-point of the paired read.

2.4.7 Calculation of paired-read mid-point frequency histograms

The Perl script histogram.pl was used to calculate frequency distributions for paired read insert size mid-points binned at 10 base pair intervals. The input files were the individual chromosome specific, particle size defined .txt files output by SAMparser. The histogram.pl script outputs the frequency distribution histogram in files of .sgr format for output into the Integrated Genome Browser (IGB) (Nicol et al., 2009). The file type contains three columns of information: chromosome identification, the base pair positions of each bin start, and the frequency of paired-read mid-point values falling within that bin, smoothed to a 3 bin moving average. Chromosome-specific .sgr files were finally concatenated to yield a series of histograms for the entire genome at each size class. This file was then rendered in the IGB to visualise particle class size distribution relative to genomic features such as open reading frames.

chr1	0	0
chr1	10	0
chr1	20	1
chr1	30	2
chr1	40	1
chr1	50	0
chr1	60	0

Figure 2.5 - Histogram output for chromosome 1 for read pairs with an ISIZE of 50
The output file contains three tab-delimited fields; [1] – the chromosome name, [2] – the base pair bin, [3] – the frequency of read pairs distributed in that bin.

2.4.8 Normalised cumulative frequency graphs of chromatin particle distribution surrounding specific genomic sites

To determine whether or not common patterns of chromatin organisation exist surrounding particular genomic feature sites (e.g. transcriptional start sites, *trans*-acting protein binding sites) the Perl script "SiteWriter" was used (Kent et al., 2011). This script calculates normalized cumulative frequency values for chromatin particle positions in a dataset in the bins surrounding a list of user-defined genomic feature sites. Sites were defined in a four column tab-delimited text file (chromosome name, site identification, string, chromosome position, and DNA strand i.e. forward or reverse) and chromatin particle information was provided by the .sgr format files described in Section 2.4.7.

The SiteWriter script produces four output files: the first contains the cumulative frequency values (outputted in a tab-delimited text file with the ending CFD.txt) which are normalised by dividing the cumulative frequency value in each bin by the average cumulative read frequency across the whole window for that feature list: the second file (with ending C3.txt) contains a matrix of all the individual bin values surrounding the sites rendered in a format that can be inputted into the Cluster 3.0 program (http://bonsai.hgc.jp/~mdehoon/software/cluster/software.htm): the final two files render the individual bin value data set in .sgr format for either the forward or reverse strand features so that the chromatin particle distributions at each site can be visualised using the IGB. The values in the .CFD.txt output files were rendered as graphs in either Excel or LibreOffice Calc.

2.4.9 Particle position marking, counting and comparison

To compare the number of chromatin particles of a particular size class present in two datasets the Perl script PeakMarkCompare.plx was used. This script marks peaks in the mid-point frequency histogram data for a particular particle size class in both datasets that pass a read frequency threshold. The threshold is set to filter out low level noise in the histogram data. The comparison dataset is scaled to the control dataset by an estimate in the difference in read depth and peaks which pass the same threshold in the comparator dataset are then marked. Marked peaks are then compared

between the two datasets to determine which match (in A AND B) and which are unique to one dataset (In A NOT B or In B NOT A). A boundary score is given to bins which fall within a defined percentage of the threshold for a peak in order that during peak comparison these bins are not marked as 'not' if they are over the threshold in one dataset but just under the threshold in the comparator. The script also identifies read frequency differences above a user defined fold-difference between matching peaks in the two datasets and can add these to the NOT output files.

2.5 Amino acid sequence alignments

Amino acid sequence alignments were performed using the ClustalW method in the GUI LaTeX based program 'Strap' (Gille and Frommel, 2001; Thompson et al., 2002). Secondary structures of amino acid sequences were predicted using the SOPMA method (Geourjon and Deleage, 1995) in the Strap interface. Graphical outputs of the alignments and secondary structures were generated using the LaTex extension TeXshade which exports the graphical results into a *.pdf format (Beitz, 2000)

3 Chromatin is remodelled by Rsc1 at *MAT* and non-*MAT* HO induced double-strand DNA breaks

3.1 Aims of the chapter

1. To validate indirect-end-label chromatin mapping technology to investigate nucleosome positions surrounding an HO-induced double-strand break.

2. To compare chromatin structure and DSB-dependent remodelling at *MATa* and *MATalpha* forms of the *MAT* locus

3. To characterise the RSC-dependency of chromatin structure and DSB-dependent remodelling at a HO-induced DSB in a non-*MAT* locus context

3.2 Chromatin is remodelled asymmetrically at *MATalpha* after DSB formation

In order to validate the use of indirect-end-label nucleosome mapping technology for the analysis of chromatin structure surrounding HO-induced DSBs used extensively in this thesis, the original observations of Kent et al., (2007) were repeated. The authors used the haploid yeast strain JKM179 (*MATα, ade1-100, leu2-3 112, lys5, trp1::hisG, ura3-52, hoΔ, hmlΔ, hmrΔ, ade3::GAL1pro::HO*), originally created in the Haber laboratory (Moore and Haber, 1996). In this strain the expression of the homothallic (*HO*) endonuclease gene is controlled by the *GAL* promoter allowing for rapid induction of expression by addition of galactose to the media. HO endonuclease creates a specific double strand DNA break (DSB) at the *MATalpha* locus and cleavage in more than 80% of the cell population is observed within 40 minutes of induction (by addition of galactose to the media). The DSB is sustained because this strain lacks the silent mating-type loci thus preventing the DSB from being repaired by homologous

recombination. Repair of the break is dependent upon NHEJ however HO endonuclease is continually produced which sustains the break. Figure 3.1 shows a map of the *MATalpha* locus indicating the HO cleavage site, the *TAF2* gene, downstream of the *MAT α1* open reading frame and the two unique restriction sites that allow the indirect-end-label mapping of chromatin on both sides of the HO cleavage site.

Figure 3.2 shows an indirect-end-label analysis of chromatin at the *TAF2* side of the *MATalpha* HO site in strain JKM179 before and after induction of the DSB by HO. Comparison of the MNase cleavage pattern of chromatin associated DNA to the MNase cleavage pattern of deproteinized DNA (compare lanes 3 and 4 with lane 1 respectively) reveals MNase protected regions at the *MATalpha* locus before HO cleavage suggestive of an organised chromatin structure. The sizes of these protected regions were calculated by plotting the distance migrated against log fragment size for bands indicated on the analysis shown in Figure 3.2 (calibration curve shown in Appendix A.1)

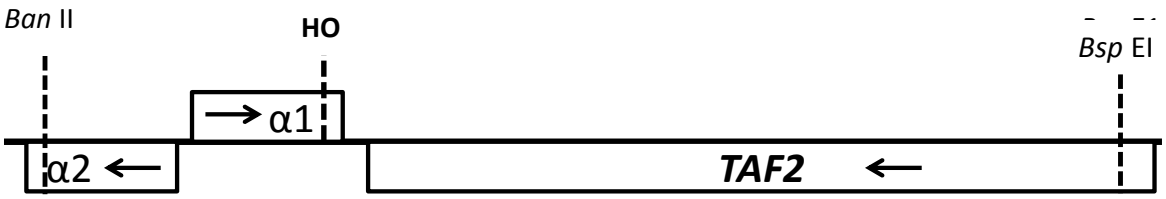

Figure 3.1 – Map of the *MATalpha* locus
The alpha form of the *MAT* locus (*MATalpha*) consists of two divergently transcribed genes *α1* and *α2* located next to the *TAF2* gene on chromosome III. The HO endonuclease cleavage site is located within the 3' end of the *MAT* α1 gene. Two unique restriction sites (*Ban* II and *Bsp* E1) occur within this region and allow indirect-end-label nucleosome mapping of both sides of the HO cleavage site.

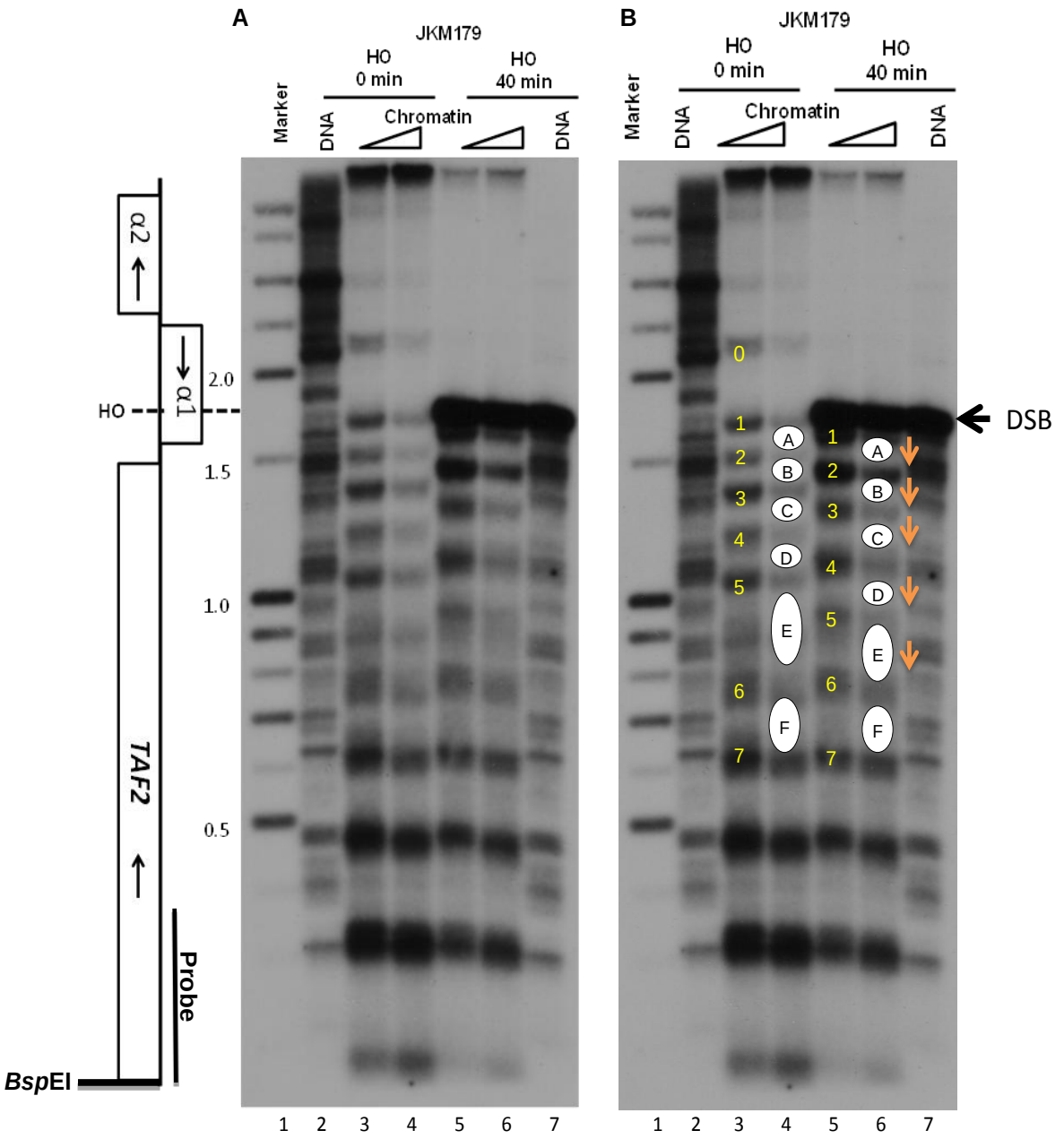

Figure 3.2 Chromatin is remodelled at an HO-induced DSB on the *TAF2* side of *MAT*alpha

$2x10^8$ cells were harvested before (*t*=0) and 40 minutes after HO induction (*t*=40). The cell wall was enzymatically removed, and spheroplasts were permeabilised and incubated with increasing amounts of MNase, 75u/ml or 150 u/ml (indicated by sloped triangle), for 2 minutes. DNA fragments were purified, separated by gel electrophoresis on a 1.5% agarose gel, transferred to a nylon membrane, and probed with the probe indicated. Deproteinized "naked" DNA was digested with MNase as a control (labelled as DNA) **A** – Chromatin associated DNA has protected regions when compared with deproteinized DNA (compare lanes 3 and 4 with lane 2). A strong band at approximately 1800bp indicates the formation of a DSB at *t*=40 (indicated by arrow). 40 minutes after induction of HO the pattern of protected regions has changed on the *TAF2* side of the DSB. **B** – Inferred nucleosome structure. Regions that are protected from MNase cleavage are approximately 150bp in size inferring positioned nucleosomes. Up to five inferred nucleosomes from the (open circles) move to new positions away from the HO cleavage site subsequent to the formation of the DSB at *MATalpha*. This is shown in the cleavage pattern as bands 1 – 6 migrate further whilst maintaining 150bp separation.

The MNase protected regions as demarcated by MNase cleavage sites 1-2, 2-3, 3-4, 4-5, 5-6, 6-7 in lanes 3 and 4 have an average size of 180bp which is consistent with the presence of an array of positioned nucleosomes labelled A-F abutting the HO cleavage site and stretching into the *TAF2* coding region (Figure 3.2B). A much larger region of MNase protected DNA is demarcated by band 0-1 with a size of approximately 500bp indicating that the *alpha1* coding region is apparently protected by a much larger particle than a single nucleosome. Both the tract of positioned nucleosomes on the *TAF2* side of the HO site and the large MNase resistant structure abutting the HO cleavage site on the *MAT* locus side are consistent with the analyses of *MATalpha* chromatin as previously described (Kent et al., 2007; Weiss and Simpson, 1997).

Figure 3.2 also confirms the presence of a DSB-dependent nucleosome remodelling event that occurs on the *TAF2* side of the HO-induced DSB as previously described (Kent et al., 2007). 40 minutes after the induction of HO in JKM179, the DSB is clearly visible as a strong band migrating at 1750bp in Lanes 4 – 6. The MNase cleavage fragments of chromatin-associated DNA on the *TAF2* side of the DSB have migrated further into the gel when compared to those prior to HO cleavage (compare lanes 4 and 5) but the deproteinized DNA pattern is not altered (compare lanes 2 and 7). This shows that new regions of DNA are protected from MNase digestion and is consistent with nucleosomes A – E remaining associated with the locus but having moved away from the DSB as indicated in Figure 3.2B.

In contrast, Figure 3.3 shows that, unlike the repositioning of nucleosomes observed on the *TAF2* side of the DSB, the large MNase resistant structure on the *MAT* side of the break is not altered in response to an HO-induced DSB. The cleavage pattern produced prior to induction of *HO* does not change when compared to the pattern produced 40 minutes after the addition of galactose to the growth media (compare lanes 3 and 4 with 5 and 6). This asymmetrical remodelling of nucleosomes in response to a DSB at the *MATalpha* locus is therefore consistent with previous observations

(Kent et al., 2007). Figure 3.4 summarises the inferred chromatin structure at *MATalpha* before and after cleavage by HO.

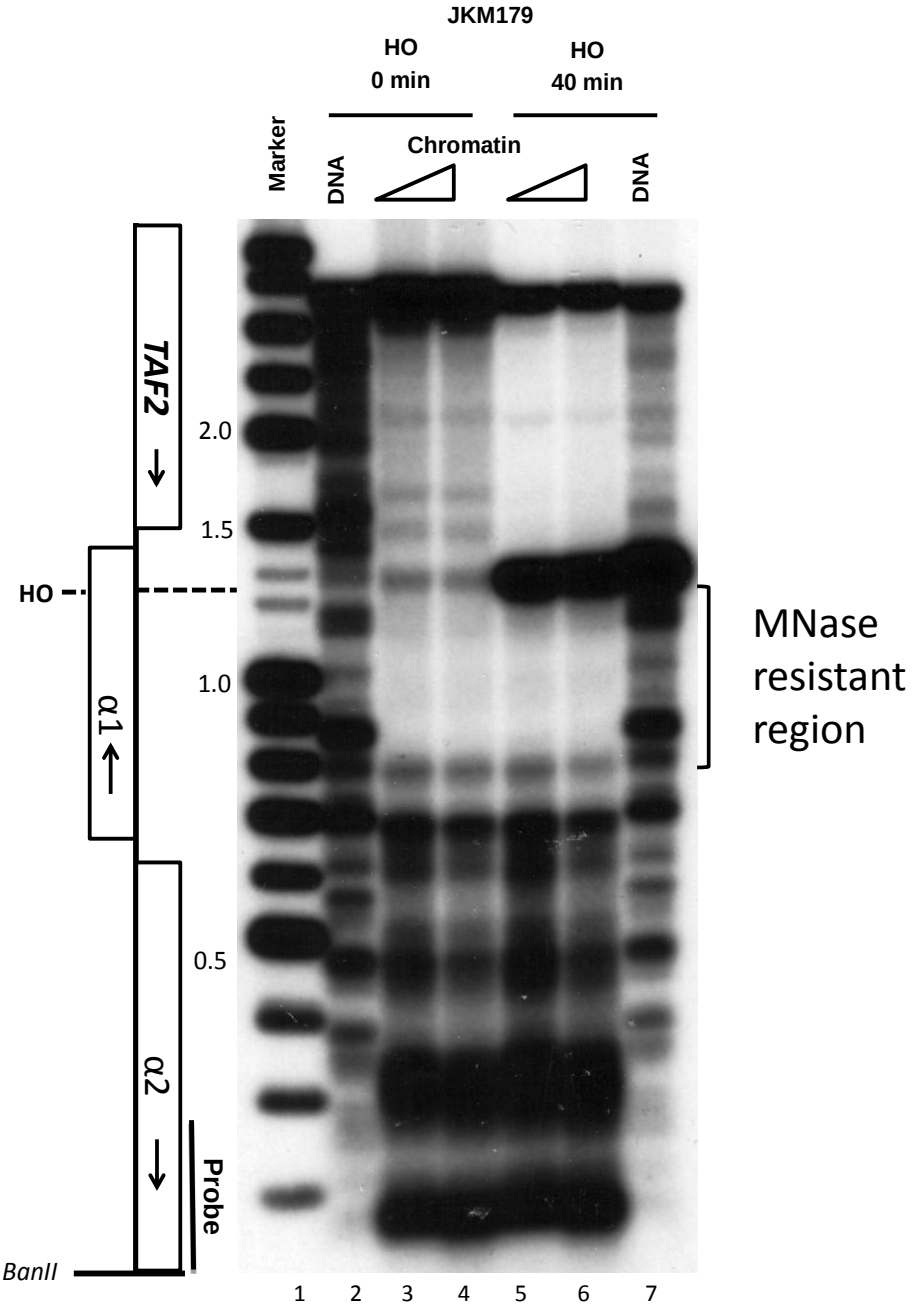

Figure 3.3 Chromatin is not remodelled on the *MAT* side of a HO-induced DSB at *MATalpha*
Similar analysis was performed as in Figure 3.2 with the exception of a different combination of restriction enzyme and probe (as indicated) to allow the investigation of the chromatin on the *MAT* locus side of a HO-induced DSB. As in Figure 3.2, comparison of chromatin-associated and deproteinized DNA reveals MNase protected regions inferring the positions of chromatin particles bound to the DNA (compare lanes 3 and 4 with lane 2). The MNase resistant region immediately neighbouring the HO cleavage site is approximately 450bp – 500bp indicating a non-canonical nucleosomal organisation (indicated by bracket). The MNase resistant region is followed by a disordered region of MNase cleavage indicating non-positioned nucleosomes but the pattern seen at *t*=0 is not altered at *t=40* by the formation of an HO-induced DSB (compare lanes 3 and 4 with lanes 5 and 6)

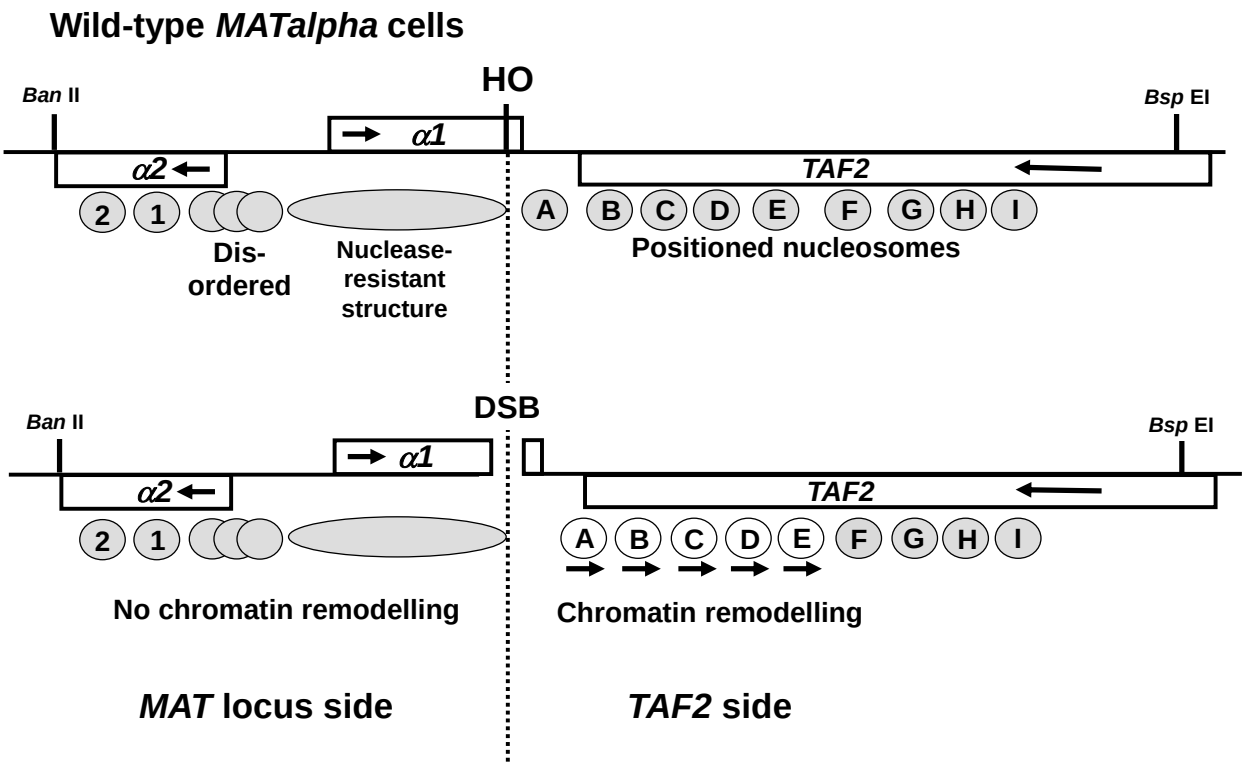

Figure 3.4 A summary of the response to an HO-induced DSB at *MATalpha*
Chromatin is remodelled asymmetrically in response to a HO induced DSB. *MATalpha* has a defined pattern of positioned nucleosomes on the *TAF2* side of the HO cleavage site and a large MNase resistant structure followed by a disordered region of nucleosomes on the *MAT* side of the HO cleavage site. Formation of a DSB by endonuclease HO results in extensive remodelling of five nucleosomes on the *TAF2* side away from the site of the DSB but the chromatin structure on the *MAT* locus side of the break is unchanged.

3.3 Chromatin structure at *MATalpha* is RSC dependent

Kent et al. (2007) previously reported that various components of RSC (Remodels the Structure of Chromatin), described in Section 1.6, are required for normal chromatin structure at *MATalpha* and for subsequent remodelling in response to a HO-induced DSB. To confirm that the *MATalpha* chromatin structure is dependent on RSC subunits, RSC subunit knock-out null mutants were created in the strain JKM179. Figure 3.5 shows the indirect-end-label analysis of *MATalpha* in *Δrsc1, Δrsc2* and *Δrsc7* strains before and after the induction of DSB by HO. Chromatin remodelling, similar to that seen in wild-type cells on the *TAF2* side of the DSB, is observed in *Δrsc2* and *Δrsc7* 40 minutes after the induction of HO (compare with Figure 3.2). Post-DSB remodelling however is almost completely abolished in *Δrsc1* (Figure 3.5C compare lanes 3 and 4 with 5 and 6). This result is identical to that previously obtained by Kent et al. (2007) and suggests that chromatin remodelling on the *TAF2* side of a HO-induced DSB at *MATalpha* is dependent on Rsc1.

3.4 *MATa* and *MATalpha* have different chromatin structures

The analysis presented above confirms the work of Kent *et al.* (2007) and shows that the chromatin environment surrounding the HO cleavage site at *MATalpha* consists of a large MNase resistant region on the *MAT* side of the locus and an array of positioned nucleosomes on the *TAF2* side of the locus. These data suggest that in response to the creation of a DSB by the HO endonuclease the array of nucleosomes on the *TAF2* side slide away from the DSB. This nucleosome remodelling event influences normal histone H2A phosphorylation and strand resection and is therefore required for efficient break repair (Kent et al., 2007; Shim et al., 2007). However the *MAT* locus can exist in two possible conformations, *MATalpha* and *MATa* (see Section 1.2.2). Hence chromatin structure was analysed in JKM139, a *MATa* strain otherwise isogenic to JKM179 (see Section 2.1.9), to determine whether similar RSC-dependent chromatin remodelling is observed at *MATa.*

Figure 3.6B shows indirect-end-label analysis of JMK139 before and after induction of HO. The analysis shows that prior to cleavage by HO the chromatin environment abutting the HO cleavage site on the *MAT* locus side is cleaved three times by MNase revealing three regions of MNase protection of approximately 150bp (lanes 3 and 4). This pattern is suggestive of three positioned nucleosomes occupying the *a1* region of the *MATa* locus in contrast to the large MNase resistant structure observed in the similar position in *MATalpha.* This analysis shows that the chromatin environments surrounding the HO cleavage site in *MATa* and M*ATalpha* are very different.

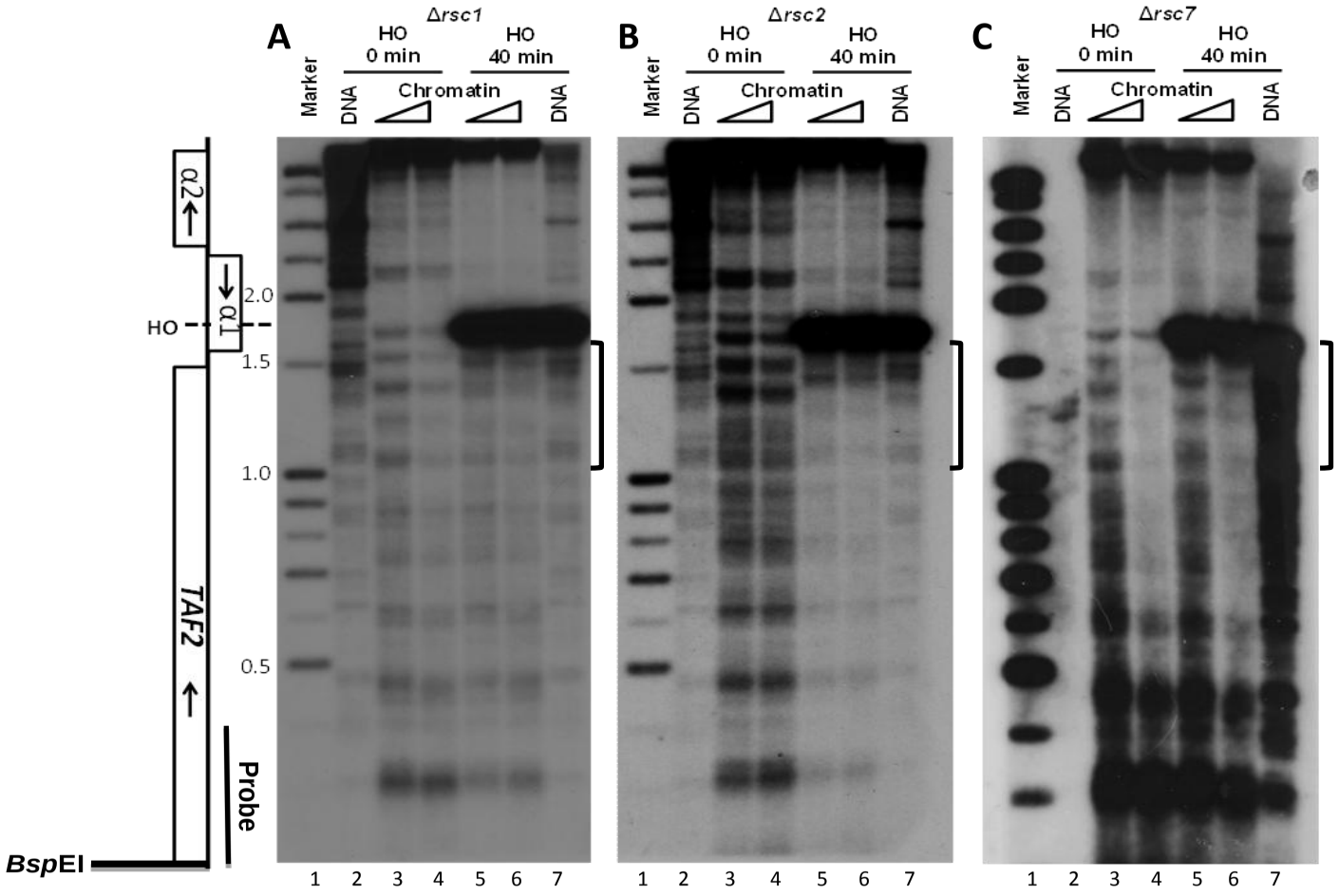

Figure 3.5 - Chromatin remodelling is Rsc1-dependent on the *TAF2* distal side of *MATalpha*
Analysis of HO-induced DSBs at *MATalpha*, similar to that in Figure 3.2, by indirect-end-label analysis of MNase digested chromatin and deproteinized DNA was performed in isogenic (yeast strain JKM179) *Δrsc1::KanMX*, *Δrsc2::KanMX* and *Δrsc7::KanMX* strains using the restriction enzyme and probe indicated. The loss of Rsc2 and Rsc7 does not alter the extensive nucleosome repositioning in response to a DSB as seen in the wild type (compare bracketed region in panels **B** and **C** with Figure 3.2). The loss of Rsc2 and Rsc7 does disrupt the large MNase resistant structure on the *MAT* side of the HO cleavage site that is seen in the wild type. Loss of Rsc1 mostly abolishes the extensive repositioning of nucleosomes that is observed in the wild type (compare bracket region of panel **A** with Figure 3.2) but the immediate area on the *MAT* locus side of the HO cleavage site resolves as one large MNase resistant structure as in the wild type.

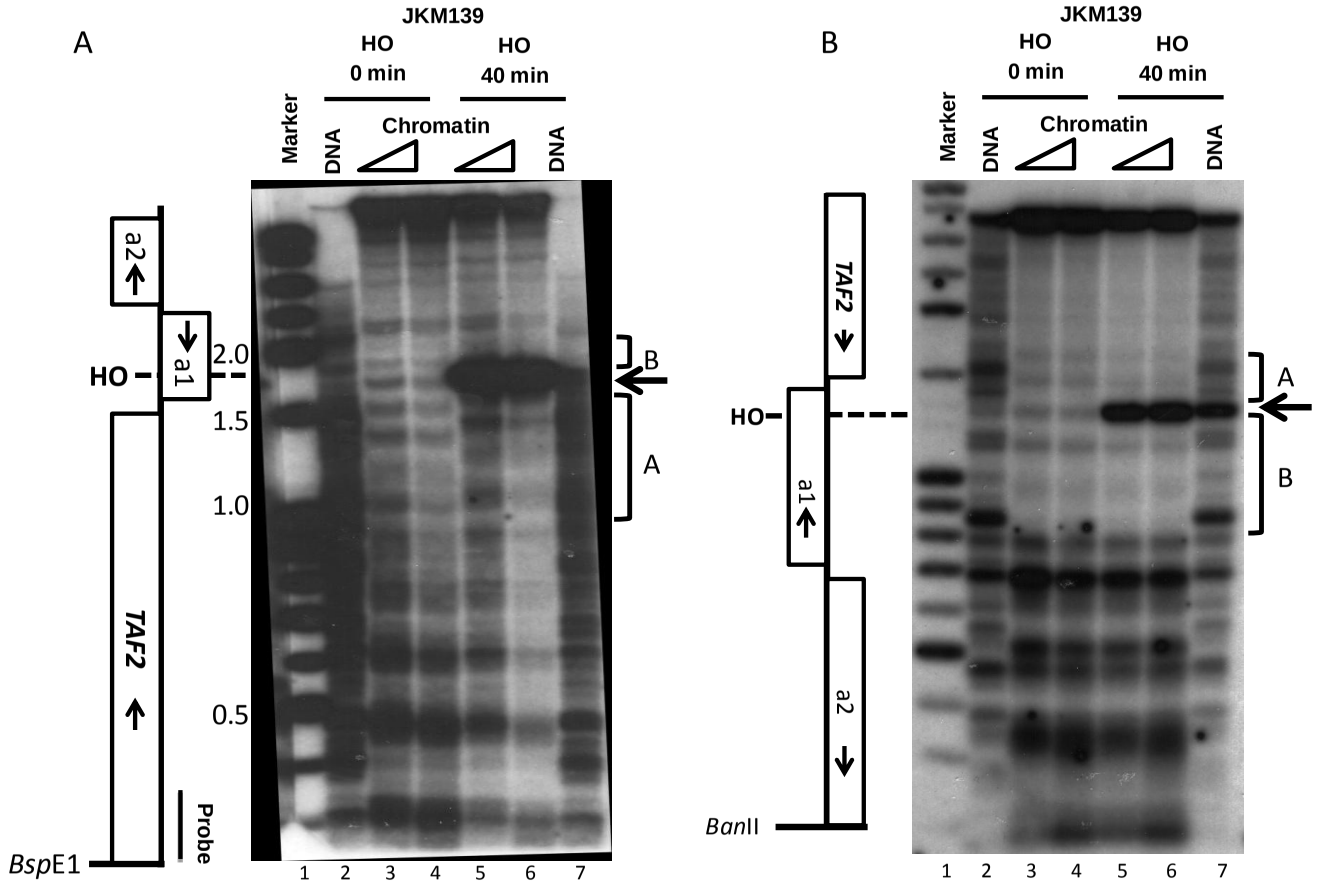

Figure 3.6- Chromatin is remodelled at *MATa* in response to a DSB
Similar analysis was performed in the strain JKM139 to analyse *MATa* using the restriction probes indicated. **A** - The MNase cleavage pattern shows that, like *MATalpha*, *MATa* has a defined chromatin environment with positioned nucleosomes on the *TAF2* side of the HO cleavage site. *MATa* behaves like *MATalpha* in response to an HO-induced DSB. The analysis shows that at *t*=40 the nucleosome pattern has been extensively remodelled when compared with *t=0* (compare bracket region A of lanes 2 and 3 with lanes 4 and 5). Like *MATalpha* five nucleosomes are repositioned in response to the formation of a DSB (indicated by arrow). **B** - The area immediately on the *MAT* locus side of the HO cleavage site (bracketed region B) has a different structure to *MATalpha* but similarly this region is not remodelled in response to a HO-induced DSB

3.5 Nucleosomes at *MATa* are remodelled in an identical manner to *MATalpha* on in response to an HO-induced DSB

Indirect-end-label analysis was performed on JKM139 before and after induction of HO as described above. Figure 3.6A shows that at 40 minutes after induction of HO some of the fragments produced by MNase cleavage of chromatin-associated DNA migrate further into the gel showing that nucleosomes are remodelled on the *TAF2* side of a HO induced DSB formed in *MATa* (compare lanes 3 and 4 with lanes 5 and 6). Figure 3.6B shows that chromatin on the *MAT* locus side of the HO-induced DSB remains unchanged. This shows that chromatin is remodelled at both *MATalpha* and *MATa* only on the *TAF2* side of the break in response to a HO-induced DSB

3.6 DSB-dependent nucleosome remodelling at *MATa* is Rsc1 dependent

As shown above, DSB-dependent nucleosome remodelling at *MATalpha* is dependent on Rsc1. In order to investigate the dependency on RSC subunits for remodelling at *MATa*, RSC subunit knock-out null mutants were created in JKM139. Figure 3.7 shows the indirect-end-label analysis of the chromatin on the *TAF2* side of a HO-induced DSB in *MATa*. Remodelling of nucleosomes similar to that found in wild-type cells is observed in the analysis of *Δrsc2* and *Δrsc7* (Panel B and C) however activity is almost abolished in *Δrsc1*. As previously observed at *MATalpha*, very little change is observed in the cleavage pattern of MNase after 40 minutes after induction of HO in the *Δrsc1* strain (Figure 3.7C). Together these two observations show that Rsc1 is generally required to remodel chromatin in response to the HO-induced DSB at the *MAT* locus.

In contrast to the chromatin structure at *MATalpha*, the chromatin structure immediately abutting the *MAT* side of the HO cleavage site of *MATa* is independent of RSC. Comparing the MNase cleavage patterns immediately flanking the HO cleavage sites before HO-induction in the three RSC-subunit mutants analysed here shows the same pattern of three

positioned nucleosomes as observed in the wild-type strain (compare Figures 3.6 and 3.7). Taken together the DSB-dependent nucleosome remodelling event at *MATa* requires Rsc1 but there is no detectable dependency on the Rsc1, Rsc2, or Rsc7 subunits of RSC for the normal (pre-DSB) chromatin structure.

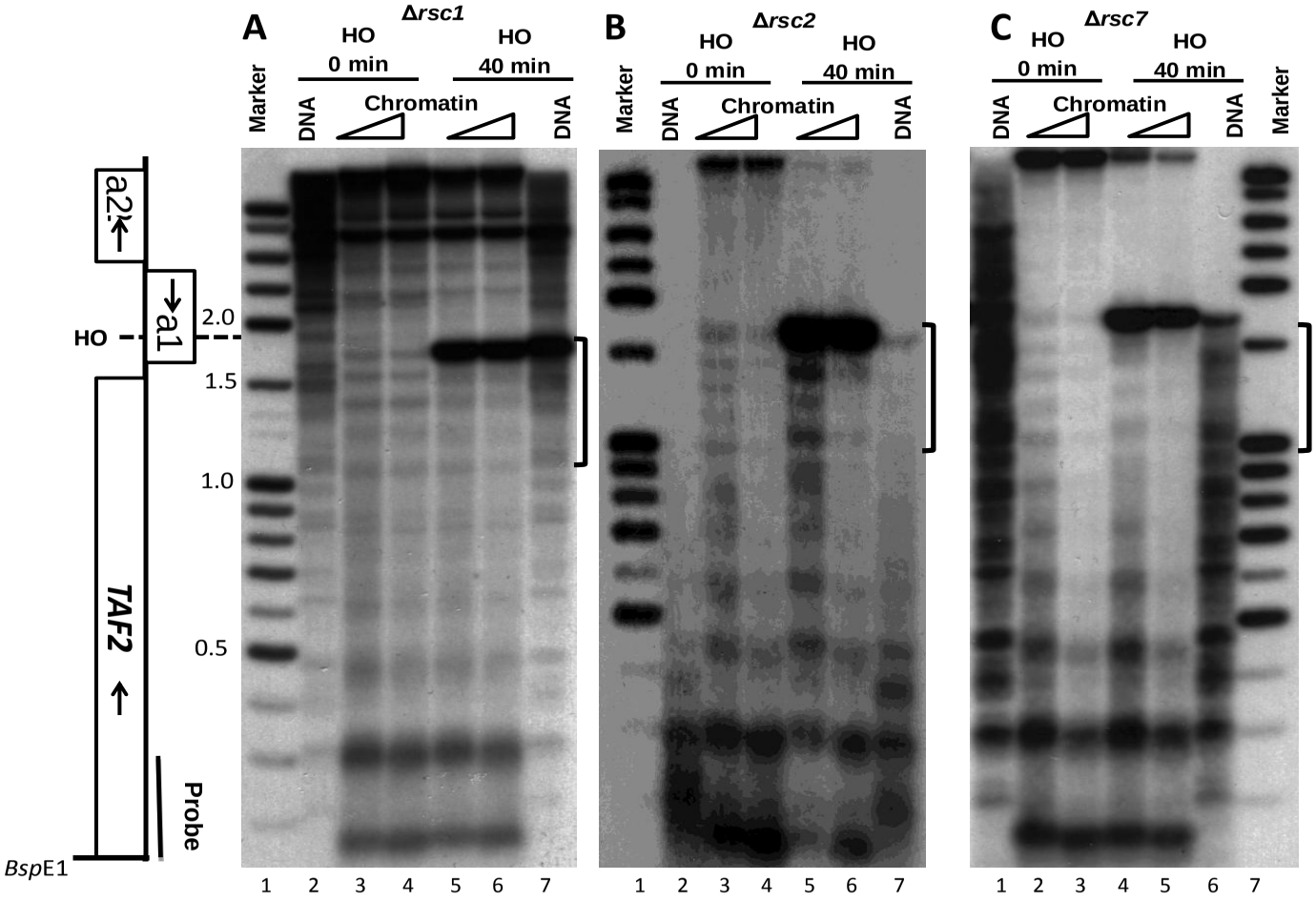

Figure 3.7 Rsc1 is required for nucleosome repositioning at the *TAF2* side of *MATa* after DSB induction
Analysis of HO-induced DSBs at *MATa* in RSC mutant strains. Indirect-end-label analysis was performed on chromatin and deproteinized digestion samples from isogenic null mutants in yeast strain JKM139 (*MATa*) of *Δrsc1::KanMX, Δrsc2::KanMX,* and *Δrsc7::KanMX* using the restriction enzyme and probe indicated. The loss of Rsc2 or Rsc7 does not alter nucleosome repositioning activity in response to the HO-induced DSB at *t=40* as seen in the wild type (compare Figure 5 with panels **B** and **C**). The loss of Rsc1 abolishes the remodelling activity in response to the DSB (panel **A**).

3.7 Chromatin is remodelled in response to an HO-induced DSB in a non-*MAT* locus

The *MAT* locus is a highly specialised region of the genome used for mating type switching. To study the effect of an HO-induced DSB on chromatin structure in a different chromosomal context *i.e.* outside the mating-type locus, chromatin was analysed in the strain YFP17. YFP17 has a 117bp HO cleavage site inserted at +251 in the open reading frame of *LEU2* on chromosome III (Paques et al., 1998). YFP17 was also derived from a background in which *HO* is placed under a galactose-inducible promoter and had been integrated into the *ADE3* locus (Moore and Haber, 1996).

Figure 3.8 shows the indirect-end-label analysis of YFP17 prior to and 40 minutes after the induction of the DSB. Comparing the MNase cleavage pattern of chromatin-associated DNA and of deproteinized DNA shows MNase resistant structures protecting regions of 150bp inferring that there is a tract of positioned nucleosomes in the reading frame of *LEU2* (compare lanes 2 with 3 and 4). After 40 minutes HO cleavage is observed as a distinct band at 1800bp. Comparing lanes 3 and 4 with lanes 5 and 6 shows a change in the MNase cleavage pattern of chromatin-associated DNA as the bands have migrated further into the gel. This is indicative of repositioning of nucleosomes after the formation of the DSB. The presence of a Ty element immediately 5' to *LEU2* prevents analysis of the nucleosomes on both sides of the DSB so it cannot be shown whether this is remodelling event is asymmetrical. These observations are again consistent with those of Kent et al., (2007) and suggest that DSB-dependent nucleosome sliding adjacent to an HO-induced DSB occurs independently of HO site chromosomal context.

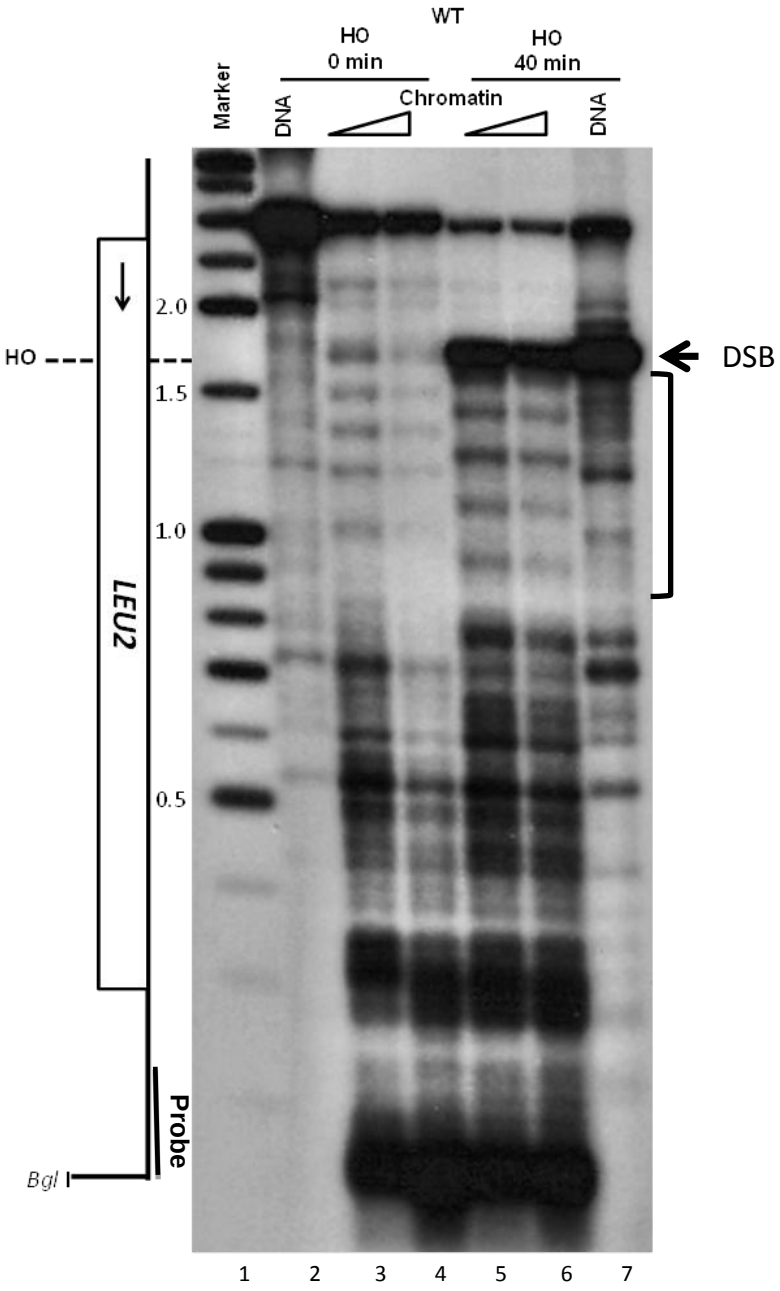

Figure 3.8 Chromatin is remodelled at a HO induced DSB in *LEU2*
Analysis of the chromatin surrounding a DSB in *LEU2*. Indirect end labelled analysis of MNase digested chromatin and deproteinized DNA using the restriction enzyme and probe indicated in the strain YFP17 which contains a HO cleavage sequence of *LEU2*. As in the JKM179/JKM139 strains, *HO* is induced by the addition of galactose to the media and subsequently HO forms a DSB in the *LEU2* protein coding region. An upstream Ty element precludes analysis of both sides of the DSB. Comparing digested chromatin with digested deproteinized DNA shows protected regions of 150bp indicating positioned nucleosomes. Lanes 3 and 4 show that the coding region of *LEU2* has highly positioned nucleosomes. Comparing lanes 3 and 4 at *t=0* with lanes 5 and 6 at *t=40* shows that after the formation of a HO-induced DSB (indicated by arrow) the nucleosomes on the protein coding region side are extensively repositioned (as indicated by the bracketed region).

3.8 DSB-dependent nucleosome remodelling at *LEU2* is Rsc1-dependent

It has been shown above that DSB-dependent nucleosome remodelling at both *MATalpha* and *MATa* is dependent on the RSC subunit Rsc1. To determine whether any of the RSC subunits were required for remodelling at an HO-induced DSB knock-out strain null mutants of RSC subunits were created in YFP17. Figure 3.9 shows the indirect-end-label analysis of the chromatin on the open reading frame side of the HO cleavage site in *Δrsc1, Δrsc2* and *Δrsc7* knock-out null mutants. Comparing lanes 3 and 4 with 5 and 6 in both panels B and C show that, 40 minutes after the induction of a DSB by HO, the MNase cleavage pattern from chromatin-associated DNA has significantly changed in both *Δrsc2* and *Δrsc7* strains showing nucleosome remodelling. In contrast, comparison of lanes 3-4 with 5-6 of Panel A shows that there is little change in the MNase cleavage patterns of chromatin-associated DNA 40 minutes after DSB induction. Therefore the positions of nucleosomes on the open reading frame side of the *LEU2* break are unchanged after the formation of a DSB. This shows that DSB-dependent nucleosome remodelling at an HO cleavage site in *LEU2* is also dependent on Rsc1.

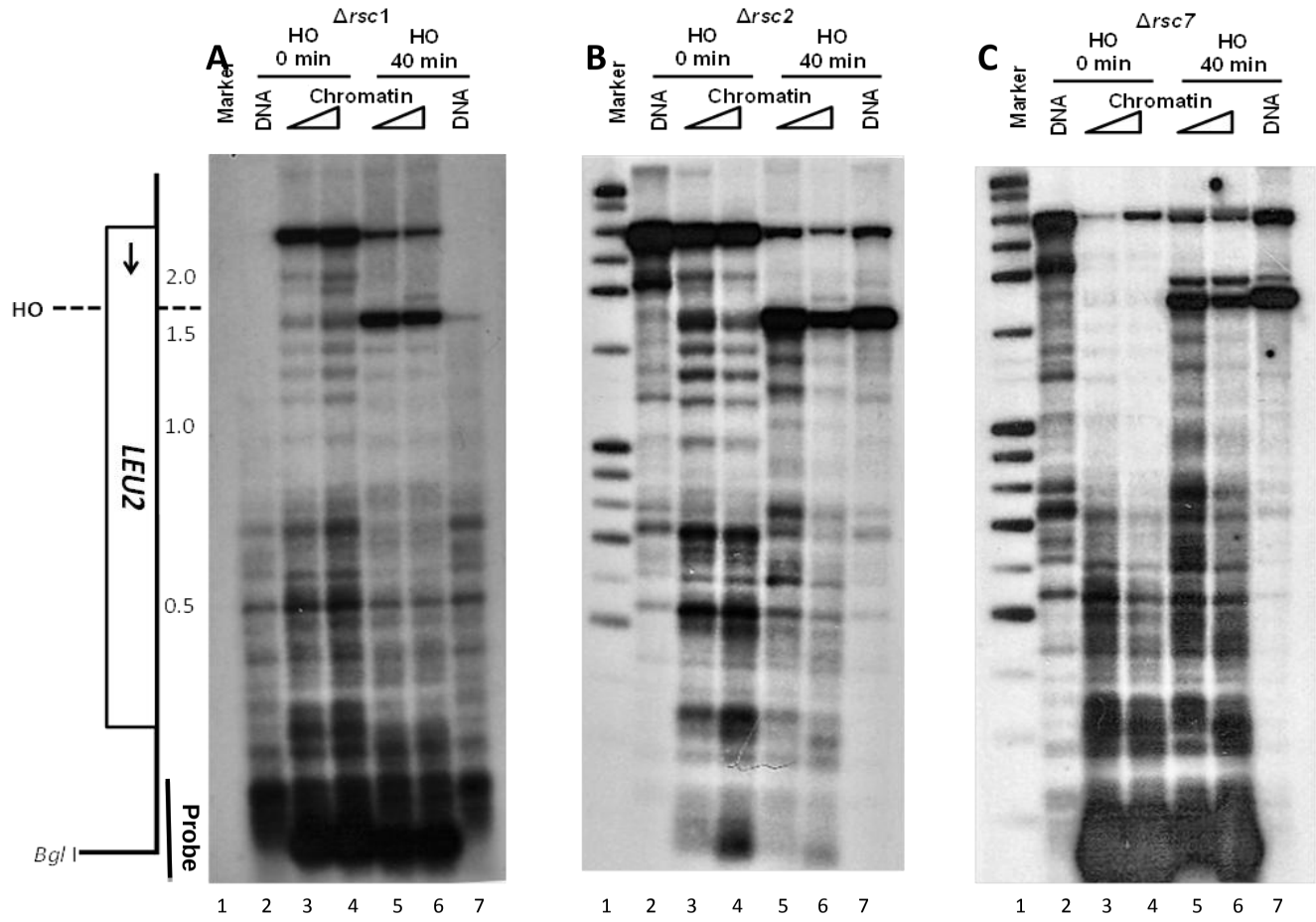

Figure 3.9 Chromatin is remodelled in a Rsc1-dependent manner at *LEU2* DSBs
Analysis of HO-induced DSBs in RSC mutant strains at *LEU2*. Indirect-end-label analysis was performed on chromatin and deproteinized digestion samples from isogenic null mutants in yeast strain YFP17 (*LEU2::HOcs*) of *Δrsc1::KanMX, Δrsc2::KanMX,* and *Δrsc7::KanMX* using the restriction enzyme and probe indicated. The loss of Rsc2 or Rsc7 does not alter nucleosome repositioning activity in response to the HO-induced DSB at *t=40* seen in the wild type (compare Figure 3.8 with panels **B** and **C**). Similar to previous observations the loss of Rsc1 abolishes the remodelling activity in response to the DSB (panel **A**). Like *MATa* the chromatin structure of *LEU2* prior to formation of the DSB is not disrupted in either *Δrsc1*, *Δrsc2*, and *Δrsc7.*

3.9 Summary

Using indirect end labelling of *in vivo* MNase digested chromatin in *HO* inducible strains, nucleosome remodelling has been confirmed to occur in response to a double-strand DNA break at *MATalpha.* Using isogenic null mutants of subunits of the ATPase-dependent complex RSC, it has been shown that this remodelling is dependent on Rsc1. These data are consistent with previous work by Kent et al*.,* (2007) but contrast that of Shim et al*.,* (2007) who suggest that remodelling is Rsc2-depedent (Kent et al., 2007; Shim et al., 2007).

This analysis has investigated this remodelling activity in the second conformation of the highly specialised *MAT* locus when in the *MATa* form and shows that remodelling of nucleosomes also occurs to the *TAF2* side of the HO induced double-strand DNA break. Using isogenic knock out null mutants it has been shown that this remodelling activity is also dependent on Rsc1.

The *MAT* locus is a highly specialised and regulated locus on the chromosome so it was important to investigate whether this Rsc1-dependent remodelling activity was unique to the *MAT* locus or whether it was a genome-wide function of RSC at sites of chromosomal lesions. The results presented above reveal that nucleosomes are remodelled in a Rsc1-dependent manner at a non-*MAT* HO induced DSB in *LEU2*. Interestingly there was no change in the chromatin structure surrounding the HO cleavage site in *LEU2* prior to cleavage in any of the RSC null mutants.

These observations, therefore, demonstrate that RSC generally remodels nucleosomes away from HO-induced double-strand DNA breaks in a Rsc1 dependent manner. However these results presented above also uncovered a difference between the two *MAT* locus conformations in terms of their chromatin structure prior to HO cleavage. The *MATalpha* locus exhibited a large MNase protected region on the *MAT* gene side of the HO site, whereas this region in *MATa* appeared to be associated with canonically-sized nucleosomes. The nature of this difference is explored in the next Chapter.

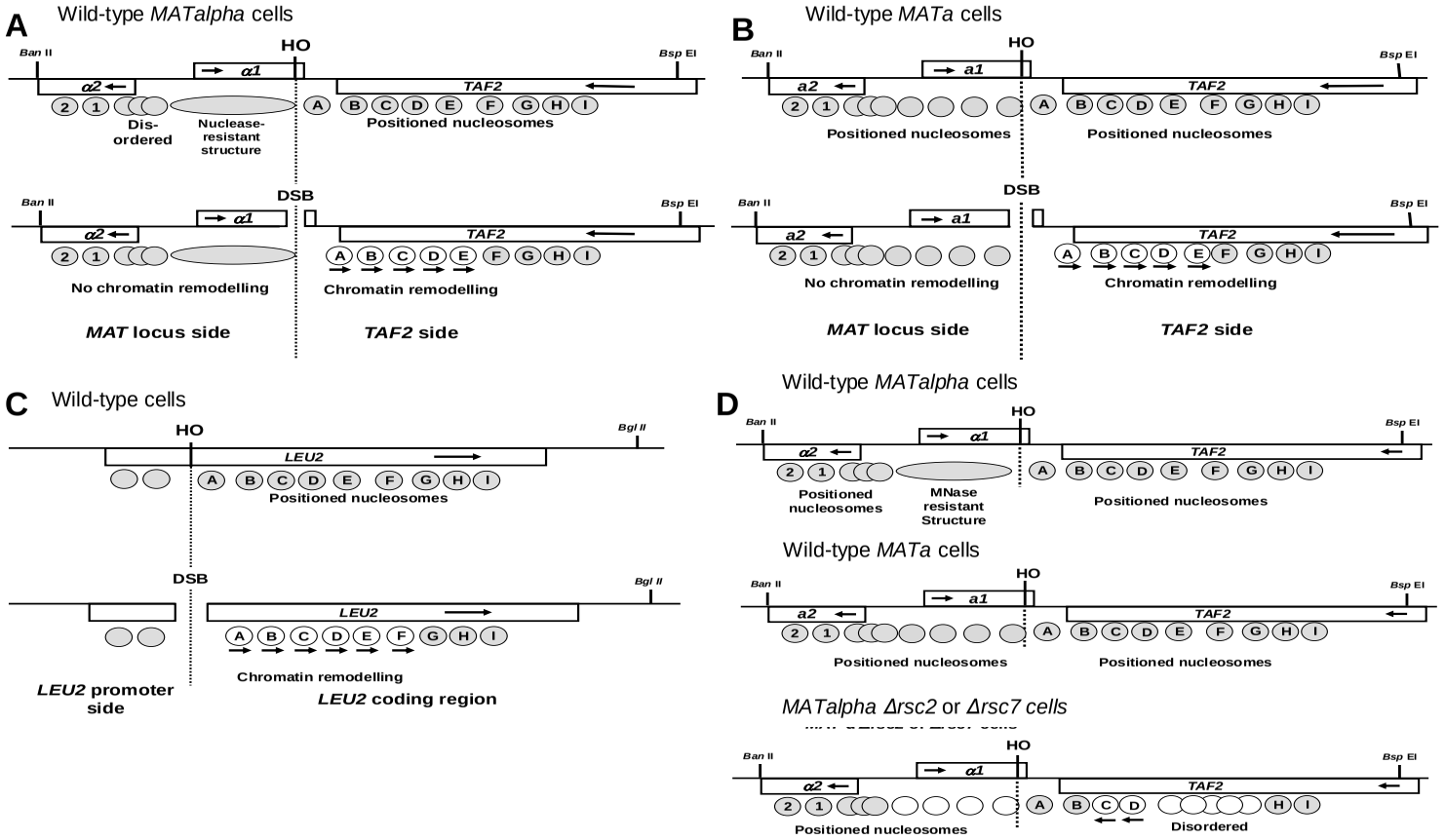

Figure 3.10 Summary of the functionally different isoforms of RSC at HO cleavage sites at the *MAT* locus at *LEU2*

A summary of the activity of RSC surrounding HO cleavage sites before and after formation of a DSB. **A** – Indirect-end-label analysis of MNase digested chromatin-associated and deproteinized DNA samples shows that nucleosomes have defined positions over the *MATalpha* locus by the pattern of 150bp regions MNase resistance which infer positioned nucleosomes. Nucleosomes on the *TAF2* side of the HO cleavage site are remodelled in an asymmetric fashion in response to an HO induced DSB with five nucleosomes repositioned away from the site of damage. This activity is dependent on Rsc1, a subunit of the RSC complex. **B –** Similar to *MATalpha, MATa* has positioned nucleosomes as shown by similar analysis. Nucleosomes are also remodelled on the *TAF2* side of a HO-induced DSB in a Rsc1-dependent manner. **C –** A HO-cleavage site has been inserted into the non-*MAT* locus, *LEU2*. Similar analysis shows that *LEU2* has a defined nucleosome pattern and similar to the activity at the *MAT* locus, these nucleosomes are remodelled in response to the formation of a DSB by HO. This activity is dependent on Rsc1**. D** – The chromatin structures of *MATalpha* and *MATa* differ prior to cleavage by HO. *MATalpha* has a large MNase resistant structure immediately flanking the HO site. The similar position at *MATa* has 3 positioned nucleosomes. In a *MATalpha Δrsc2* or *Δrsc7* strain the structure resembles that of *MATa* - the structure at *MATalpha* therefore is dependent on Rsc2 or Rsc7.

4 Rsc2 and Rsc7 set the chromatin structure surrounding the HO cleavage site in *MATalpha*

4.1 Aims of the chapter

1. To investigate the nature of the large MNase resistant chromatin structure at *MATalpha*

2. To determine the RSC subunit dependency in setting chromatin structure at the *MAT* locus

4.2 Rsc2 and Rsc7 maintain a specific chromatin structure at *MATalpha* but not *MATa*

The work presented in the previous chapter demonstrated a difference between *MATa* and *MATalpha* with respect to the chromatin structure surrounding the HO cleavage site prior to cleavage.

Close inspection of Figure 3.5 shows that in the absence of either *RSC2* or *RSC7* the large MNase resistant structure at *MATalpha* becomes more accessible to MNase and resolves to a similar pattern to that observed at *MATa.* Figure 4.1 shows a more direct comparison of the pre-HO cleavage *MATalpha* chromatin structure in RSC subunit mutants presented on the same indirect-end-label blot. These results are consistent with those reported by Kent *et al.* (2007) and confirm that RSC has dual functionality at the *MATalpha* locus in defining chromatin structure both before and after DSB formation with each distinct function mediated by different subunits within the complex. Kent *et al* (2007) were able to show in that in the absence of the large structure at *MATalpha* the efficiency of cleavage by HO endonuclease decreases slightly (Kent et al., 2007).

Figure 4.2 shows that this function of RSC does not apply to the *MATa* form of the *MAT* locus. MNase cleavage sites on the *MAT* side of the HO site are similar when compared with wild type in both *Δrsc2* and *Δrsc7* mutants. Thus it appears that Rsc2 and Rsc7 are involved in the formation of a

specific chromatin configuration at the *MATalpha* locus, whereas there is no function at *MATa*. It also appears that the wild-type chromatin structure at *MATa* is essentially identical to the *MATalpha* structure in a *Δrsc2* or *Δrsc7* mutant background. Therefore the chromatin surrounding the HO site at *MAT* is context dependent. Next, I examined whether HO sites placed into non-*MAT* chromatin contexts showed any dependence on Rsc2 or Rsc7 to set chromatin structure.

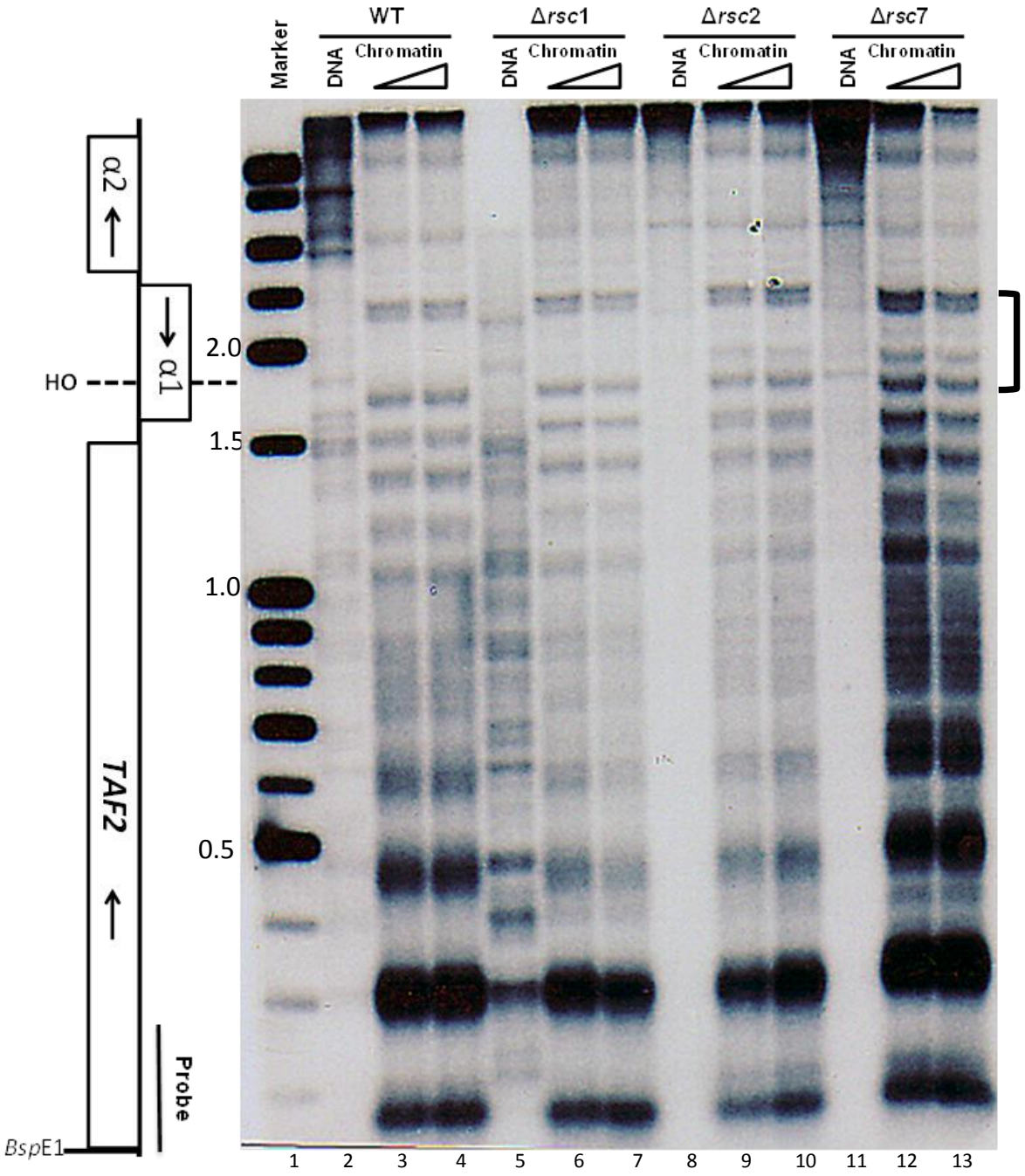

Figure 4.1 - Chromatin at *MATalpha* is dependent on Rsc2 and Rsc7
MATalpha has a chromatin structure that is dependent on Rsc2 and Rsc7. Chromatin was digested increasing concentrations of MNase (triangles) in permeabilised JKM179 spheroplasts at 37ºC for 2 minutes without the induction of *HO*. Deproteinized DNA was digested with 5u/ml MNase at 22ºC for 10 seconds. Similar analysis was performed in isogenic null mutants of *rsc1, rsc2* and *rsc7.* The Southern blot shows the indirect-end-labelling analysis, using the restriction enzyme and probe indicated. In the control a large MNase resistant structure is observed (bracket region) immediately on the *MAT* locus side to the HO cleavage site (lanes 3 and 4). This structure protects approximately 500bp of DNA indicating the presence of a non-canonical nucleosomal environment. The same structure is observed in *Δrsc1* (lanes 6 and 7). In *Δrsc2* and *Δrsc7* null mutants the chromatin pattern on the *MAT* locus side of the HO cleavage site resolves into separate cleavage sites consistent with the presence of three positioned canonical nucleosomes (lanes 9 and 10 and 12 and 13).

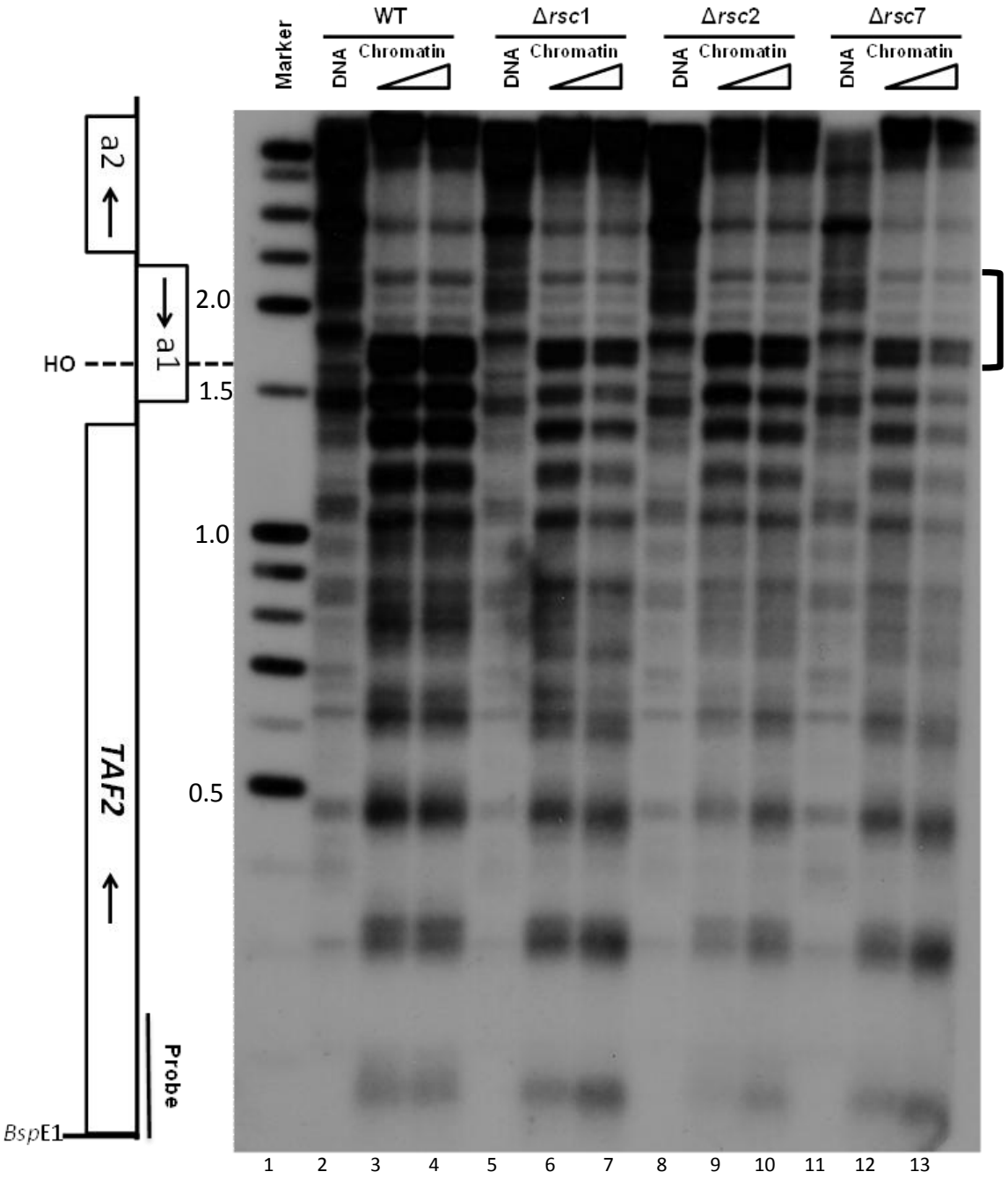

Figure 4.2 - *MATa* chromatin is not dependent on RSC

The chromatin environment surrounding the HO cleavage site at *MATa* is not dependent on Rsc1, Rsc2 or Rsc7. Chromatin was digested by increasing concentrations of MNase (triangles) in permeabilised JKM139 spheroplasts without the induction of HO as in Figure 4.1. Deproteinized DNA was digested with MNase as a control. Similar analysis was performed in isogenic null mutants of *rsc1*, *rsc2*, and *rsc7*. The Southern blot shows indirect-end-label analysis of the *MAT* locus. Lanes 3 and 4 show that there is a highly ordered nucleosome pattern at *MATa* but the area immediately to the *MAT* locus side of the HO cleavages site resolves as three nucleosomes. This pattern is similar to that observed in Δ*rsc2* and *Δrsc7* in Figure 4.1. Analysis of the RSC mutants show that the positioning of nucleosomes prior to cleavage by HO is independent of Rsc1, Rsc2, or Rsc7 (lanes 6,7, lanes 9, 10 and lanes 12 and 13 respectively).

4.3 RSC does not set pre-cleavage chromatin structure at HO cleavage sites engineered within non-*MAT* loci

Indirect-end-label analysis was performed on RSC mutant strains, isogenic with YFP17 and MK205a. YFP17 has an 117bp HO cleavage sequence inserted into the protein coding region of *LEU2* (as described in Chapter 3) and MK205a has a galactose-inducible 39bp HO cleavage site on chromosome V at +206 in the *URA3* protein coding region (Aylon et al., 2003). Figure 4.3 shows the indirect-end-label analysis of the chromatin structure in *LEU2* surrounding the engineered HO cleavage site. *LEU2* has positioned nucleosomes flanking either side of the HO cleavage site and these nucleosomes all protect 150bp of DNA indicating canonical nucleosomes. No dependency on Rsc2 or Rsc7 to set the nucleosome pattern surrounding the recognition site prior to cleavage is observed in this analysis. Similarly, Rsc1 is not required for the setting of chromatin structure around the HO cleavage site.

Figure 4.4 shows the indirect-end-label analysis of the basal chromatin in the yeast strain MK205a which contains an HO cleavage site in *URA3.* Indirect-end-label analysis of *URA3,* using the probe indicated, show that *URA3* has positioned nucleosomes flanking either side of the HO cleavage site. However, there is no large MNase resistant structure as indicated by the MNase cleavage pattern of chromatin associated DNA (compare lane 2 with lanes 3 and 4). Analysis of knock-out null mutants of *RSC1, RSC2* and *RSC7* shows that the nucleosome pattern surrounding the *URA3* HO cleavage site is not dependent on these RSC subunits. These analyses show that the chromatin structure surrounding the two HO sites chosen above both behave like those at *MATa* rather than *MATalpha* and are independent of Rsc2 and Rsc7.

In order to understand why the *MATalpha* HO chromatin behaves differently, I next examined the large MNase resistant structure to determine whether it is a large single protecting unit or a complex made up of smaller subunits such as nucleosomes.

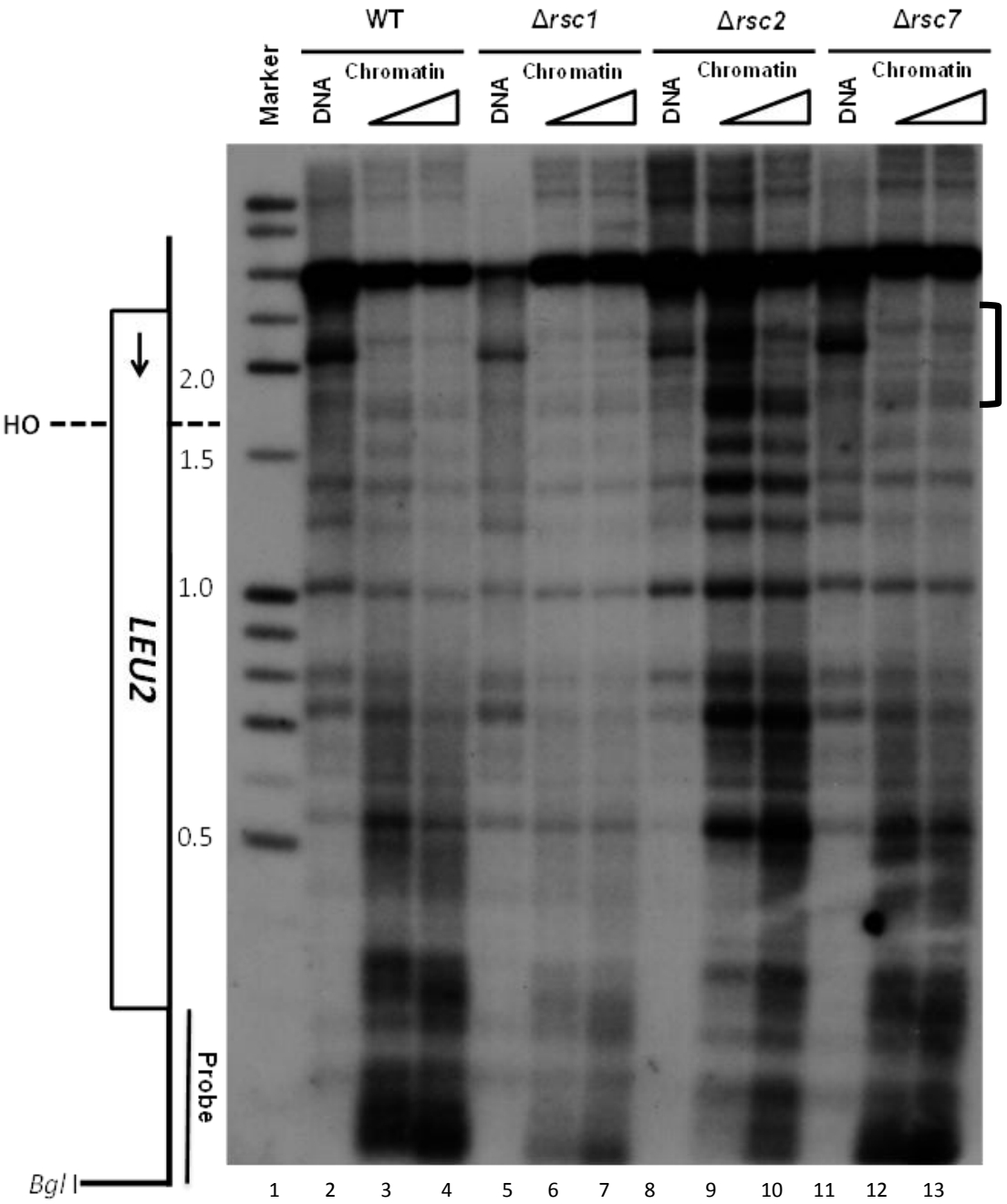

Figure 4.3 - RSC-independent nucleosome positioning at a non-*MAT* HO site in *LEU2*
LEU2::HOcs has a defined nucleosome structure which is not dependent on RSC. YFP17 contains an HO cleavage site in the open reading frame of *LEU2*. Cells were spheroplasted, permeabilised, and chromatin digested at 37ºC for 2 minutes with increasing concentrations of MNase (triangles). Deproteinized DNA was digested with 5u/ml MNase at 22ºC for 10 seconds as a control. The Southern blot shows the indirect-end-label analysis performed with the probe abutting the indicated restriction enzyme site. The HO cleavage site in *LEU2* is indicated and is flanked on both sides by positioned canonical nucleosomes as well as positioned nucleosomes within the coding region (lanes 3 and 4) Similar analysis was performed on isogenic null mutants of *rsc1, rsc2* and *rsc7* and the analyses show that there is no dependency on these subunits to set the chromatin structure prior to cleavage as the pattern does not change in comparison to the control (compare lanes 6-7, 9-10 and 12-13 respectively with lanes 2-3).

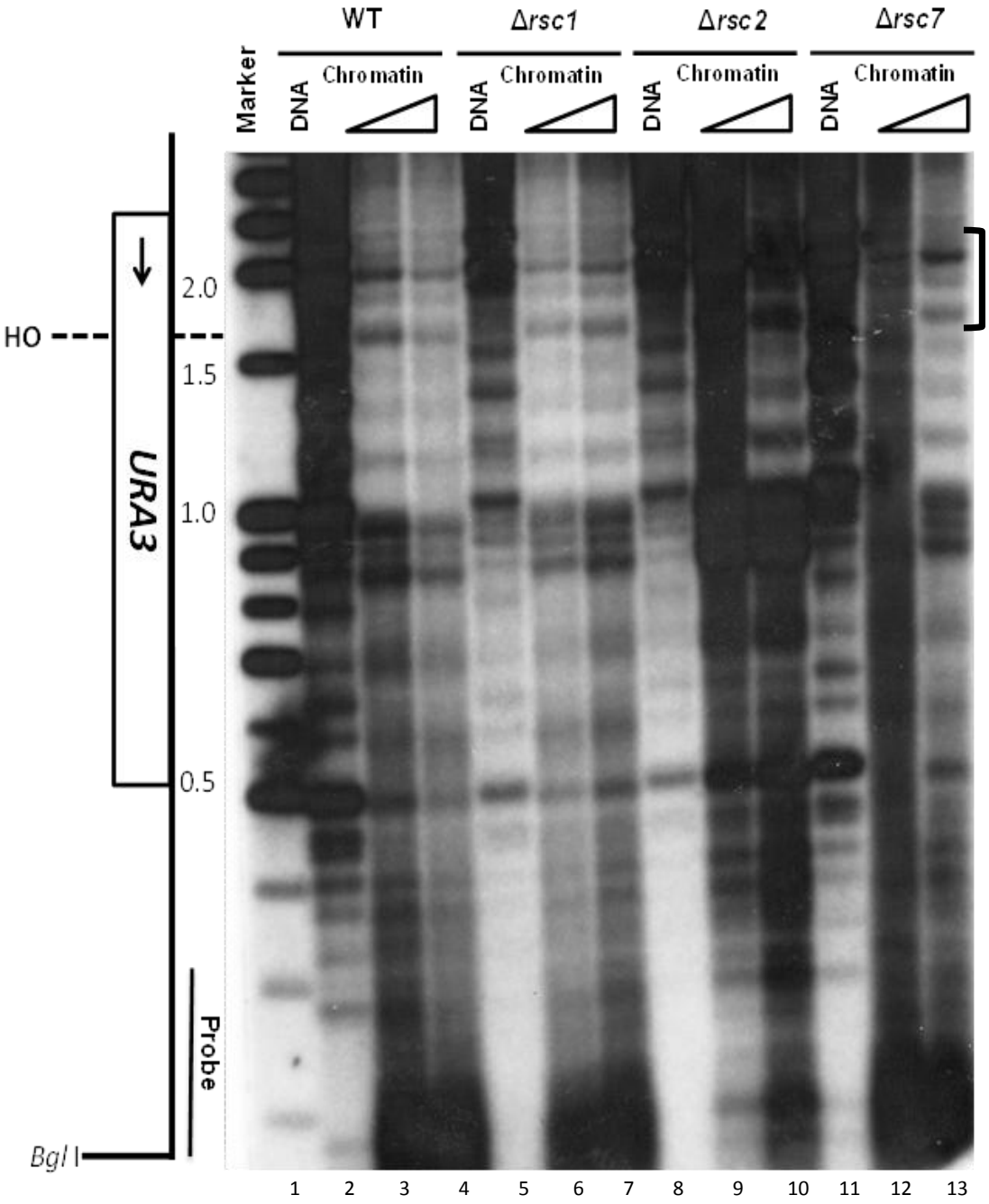

Figure 4.4 – RSC-independent nucleosome positioning at a non-*MAT* HO site in URA3
URA3::HOcs has a defined nucleosome structure which is not dependent on RSC. MK205a contains a HO cleavage site in the open reading frame of *URA3*. Cells were spheroplasted, permeabilised, and chromatin digested at 37ºC for 2 minutes with increasing concentrations of MNase (triangles). Deproteinized DNA was digested with 5u/ml MNase at 22ºC for 10 seconds as a control. The Southern blot shows the indirect-end-label analysis performed with the probe abutting the indicated restriction enzyme site. The HO cleavage site in *URA3* is indicated and is flanked on both sides by positioned canonical nucleosomes as well as positioned nucleosomes within the coding region (lanes 3 and 4) Similar analysis was performed on isogenic null mutants of *rsc1, rsc2* and *rsc7* and the analyses show that there is no dependency on these subunits to set the chromatin structure prior to cleavage as the pattern does not change in comparison to the control (compare lanes 6-7, 9-10 and 12-13 respectively with lanes 2-3).

4.4 The large MNase-resistant structure, the "alphasome", at *MATalpha* is consistent with being three aggregated nucleosomes

The analyses presented above show that a large chromatin particle protecting approximately 500bp of DNA, and abutting the HO cleavage site, is a unique feature of the *MATalpha* locus. Figure 4.1 shows that the MNase pattern in the absence of the RSC subunits Rsc2 and Rsc7 suggest the presence of three positioned nucleosomes occupying the similar position and suggesting that Rsc2 and Rsc7 may have a role in aggregating nucleosomes at the *MATalpha* locus. In order to test this model further, an alternative method of MNase-accessibility mapping of *in vivo* chromatin to indirect-end-labelling was employed. In this assay MNase-resistant DNA species created by nuclease digestion of yeast cell chromatin were directly visualized as "nucleosome ladders" after agarose gel electrophoresis, and then blotted and probed with small DNA fragments from specific regions of the *MAT* locus. Figure 4.5 shows MNase-resistant DNA species generated by digestion with a range of MNase concentrations in JKM179 and JKM139, *MATalpha* and *MATa* strains respectively. The DNA fragments were separated on a gel and probed with a fragment complementary to the *MAT* region abutting the HO site. Figure 4.5A shows that a MNase-resistant complex of approximately 500bp in size is observed at *MATalpha* as predicted from the previous indirect-end-label experiments. However, at increasing concentrations of MNase, this complex is broken down into three regions of 150bp protection suggesting that the alphasome comprises three separate nucleosomes but in close proximity and/or with relatively inaccessible linker regions. When a similar analysis is performed in JKM139, a *MATa* strain, three nucleosomes are observed with a low concentration of MNase indicating that these nucleosomes are not similarly aggregated.

Using this analytical approach to test RSC knock-out null mutants, it shows that in the absence of Rsc1, an MNase resistant structure similar to the wild-type is present at the *MATalpha* HO cleavage site again, which breaks down to a lesser extent with increasing concentrations of MNase when compared to the other RSC mutants. The structure of *MATa,* in

contrast, is not affected by the loss of Rsc1 (panel A4). In the absence of Rsc2 or Rsc7 the chromatin structure of *MATalpha* is digested to three separate nucleosomes with the lowest concentration of MNase but no change is observed at *MATa* (panels A2 and A3). This result supports the model that Rsc2 and Rsc7 have a role in the aggregation of nucleosomes at *MATalpha* but not at *MATa*. Since this aggregated structure appears to be unique to the *alpha* form of the *MAT* locus, it will be referred to below as the "alphasome".

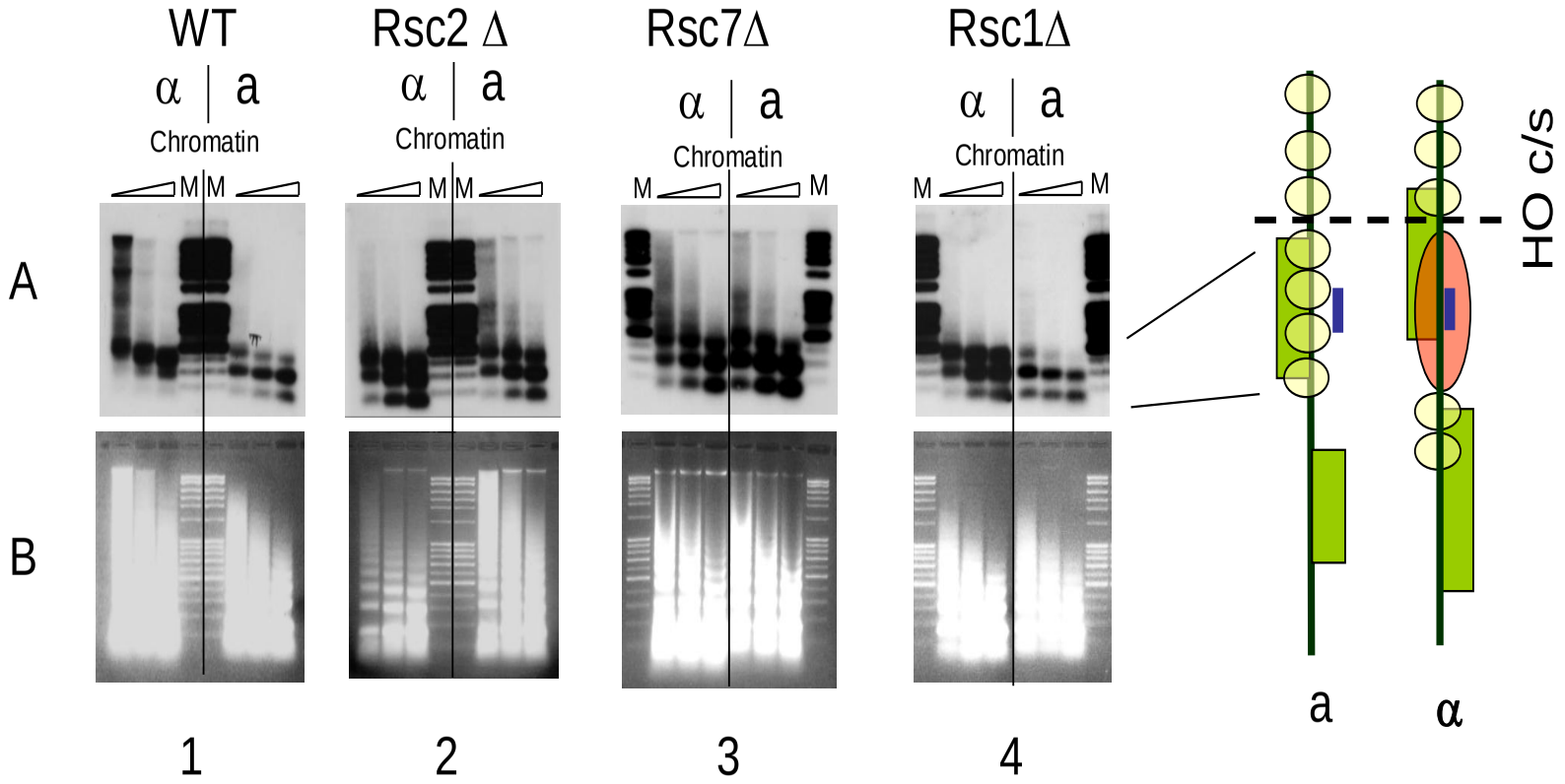

Figure 4.5 - The *MATalpha* locus contains three aggregated nucleosomes
Chromatin samples from *MATalpha* and *MATa* cells were subjected to MNase digestion (75u/ml, 150u/ml and 300u/ml – indicated by triangles) and the region on the *MAT* locus side of the HO cut site (HO c/s) was analysed by indirect labelling using the probe indicated (blue line). Images B 1- 4 show DNA separation prior to southern blotting. Images A 1-4 show the result of hybridisation with *MATalpha* or *MATa* specific probes designed to the approximate centre of the MNase resistant structure (384bp upstream of the HO cleavage site – red oval). A1 shows the presence of the MNase resistant structure in the *MATalpha* cells which only breaks down as the concentration of MNase increases. This structure is specific to the *MATalpha* locus, whereas the same region of DNA is wrapped around 3 separate nucleosomes in *MATa* cells. The MNase resistant structure at *MATalpha* is also observed in *Δrsc1* mutant yeast shown in A4 but also breaks down with increasing concentrations of MNase. The MNase resistant structure at *MATalpha* was found to be dependent on Rsc2 and Rsc7 as shown in A2 and A3. The loss of either of these nucleosome positioning factors results in a *MATa*-type chromatin structure occurring at *MATalpha* over this region.

4.5 Rsc7 has a direct function in alphasome formation at *MATalpha*

RSC exists in two isoforms defined by the presence of either Rsc1 or Rsc2 (see Section 1.6). The requirement of either Rsc2 or Rsc7 to create a normal chromatin structure at *MATalpha* is therefore intriguing as Rsc7 is present in both isoforms of RSC as part of the fungal specific module (Wilson et al., 2006). The fungal specific module contains the dimers of Rsc7/Rsc14, Rsc3/Rsc30 and Htl1 which interact with the main core of the RSC complex. Rsc3 and Rsc30 are zinc finger DNA binding proteins with a consensus sequence found at *MATalpha* but not in *MATa* (Figure 4.7). However, their incorporation into the complex is partially dependent on the Rsc7/Rsc14 dimer (Wilson et al., 2006). Therefore one hypothesis is that the *Δrsc7* null mutant phenocopies the *Δrsc2* null mutant due to the inability of the full RSC complex to form *i.e.* it therefore lacks the zinc-finger binding domains present in the Rsc3/Rsc30 dimer. This could prevent the RSC complex from being recruited to the *MATalpha* locus via the zinc-finger domains and therefore *RSC2* would not form the large nucleosome structure. This hypothesis was tested by analysing further RSC subunit mutants for the formation of the alphasome at the *MATalpha* locus.

Null mutants of *Δrsc7*, *Δrsc14, and Δhtl1* were made by replacing the entire coding region with the *kanMX* cassette. Due to repetitive DNA elements occurring downstream of *RSC30,* the region 216325 to 217884 on chromosome VIII (1500bp of coding region and 50bp upstream of TSS of *RSC30*) were replaced with the *kanMX* cassette. As *RSC3* is an essential gene it was not analysed.

Figure 4.6 shows the indirect-end-label analysis of the HO cleavage site of the *MATalpha* locus in different RSC subunit mutants, using the restriction enzyme and probe shown. Consistent with previous analysis the alphasome is digested with a pattern that suggests that it comprises three positioned nucleosomes in the *Δrsc7* mutant. However, the *Δrsc14, Δhtl1* and *Δrsc30* mutants exhibited the presence of an alphasome similar to that seen in the wild type. The loss of the Rsc7 binding partner Rsc14 therefore does not

disrupt the formation of the alphasome structure and neither does the loss of the zinc finger binding protein Rsc30 or Htl1 suggesting that Rsc7 has a specific function at *MATalpha*.

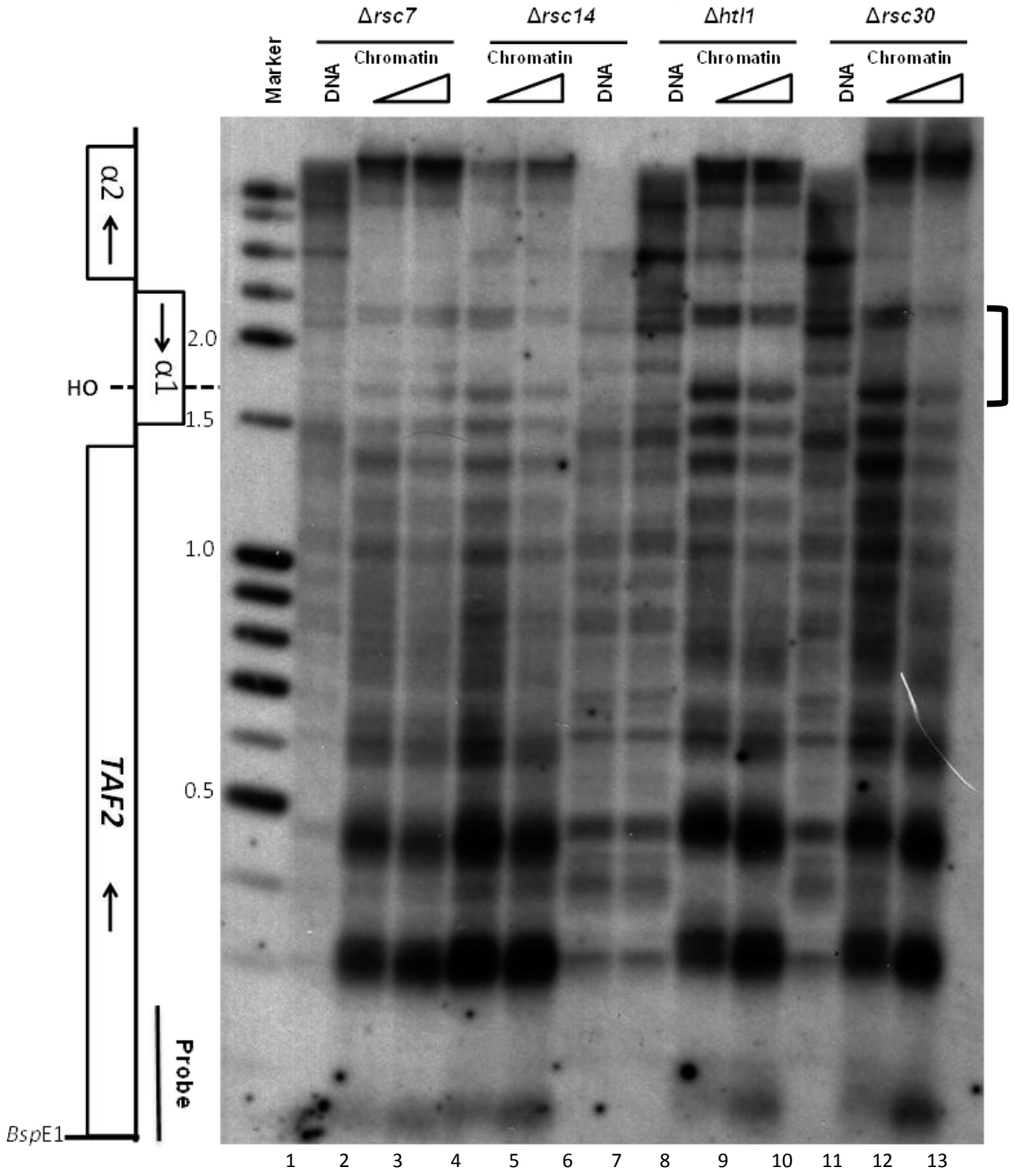

Figure 4.6 - Rsc7 has a specific function at *MATalpha*
Rsc7 functions independently of other fungal specific subunits of RSC. Chromatin analysis was performed in isogenic mutants in the JKM179 strain of the fungal specific subunit of the RSC complex; *Δrsc7, Δrsc14, Δrsc30, Δhtl1*. The Southern blot shows the indirect-end-label analysis performed with the probe abutting the indicated restriction enzyme site. In *Δrsc7* the DNA on the *MAT* locus side of the HO cleavage site is protected by three canonical nucleosomes, resembling the structure observed at the *MATa* locus. In the analysis of *Δrsc14*, *Δhtl1* and *Δrsc30* mutants the alphasome is observed protecting this region, similar to that seen at the WT *MATalpha* locus.

4.6 Summary

The results presented in this Chapter show that the asymmetrical chromatin structure at the *MAT* locus is unique to *MATalpha.* Nucleosomes are remodelled in a Rsc1-dependent manner from the site of a DSB exclusively on the *TAF2* side of the break both at *MATalpha* and in *MATa*. However this chapter demonstrates that Rsc2 and Rsc7 function to create a specific chromatin structure at *MATalpha* alone which has been termed the alphasome. This function is dependent on the presence of both the Rsc2 and Rsc7 subunits in the RSC complex and appears to involve the aggregation of three nucleosomes in a manner that reduces the MNase-sensitivity of the linker DNAs between them. The loss of alphasome forming activity observed in the *Δrsc7* mutant is not due to the loss of integrity of the RSC complex because mutants of the other fungal specific subunits do not lead to a loss of the activity even though more than one of these factors is required for efficient assembly of the RSC complex.

Previous mutant analysis (Kent *et* al., 2007) suggests that the presence of the alphasome is required for efficient cleavage by HO. Interestingly this structure is not required at *MATa* and there is no RSC dependency for chromatin remodelling suggesting that the chromatin structure should be less susceptible to cleavage by HO. Alphasome-like structures were not observed at HO cleavage sites that have been engineered into non-*MAT* loci. For example there is no RSC dependency for the nucleosome structure surrounding HO cleavage sites in *LEU2* or *URA3*. With regards to *LEU2*, there appears to be no decrease in efficiency of HO cleavage in either *Δrsc2* or *Δrsc7* null mutants since the level of HO site cleavage is the same in the experiments described in Chapter 3, suggesting that a RSC-dependent nucleosome structure is not a pre-requisite for efficient HO cleavage.

Interestingly, the DNA sequence of the Y/Z boundaries of *MATalpha* and *MATa* are quite different (Figure 4.7 and Chapter 1.2.2). The Y sequence is unique to each mating type whereas the Z sequences are conserved between the two mating types. Across the Y/Z boundary in

MATalpha is the sequence 5’ CGCGC 3’, the putative consensus binding sequence for the zinc finger DNA binding protein Rsc3 (Badis et al., 2008) suggesting that Rsc3 may be recruited at this binding sequence at *MATalpha*. This consensus sequence is not present in *MATa* suggesting that the RSC complex would not be recruited via Rsc3 to remodel chromatin at *MATa*.

Consistent with this hypothesis, the oligonucleotides that were inserted into the coding regions of *LEU2* and *URA3* were both originally obtained from the *MATa* locus (Paques et al., 1998; Sweetser et al., 1994). These HO cleavage sites do not contain the Rsc3 binding sequence and therefore the RSC complex would not be recruited to these sites via Rsc3. This would therefore preclude recruitment of RSC to these HO cleavage sites and remodelling of chromatin would not take place.

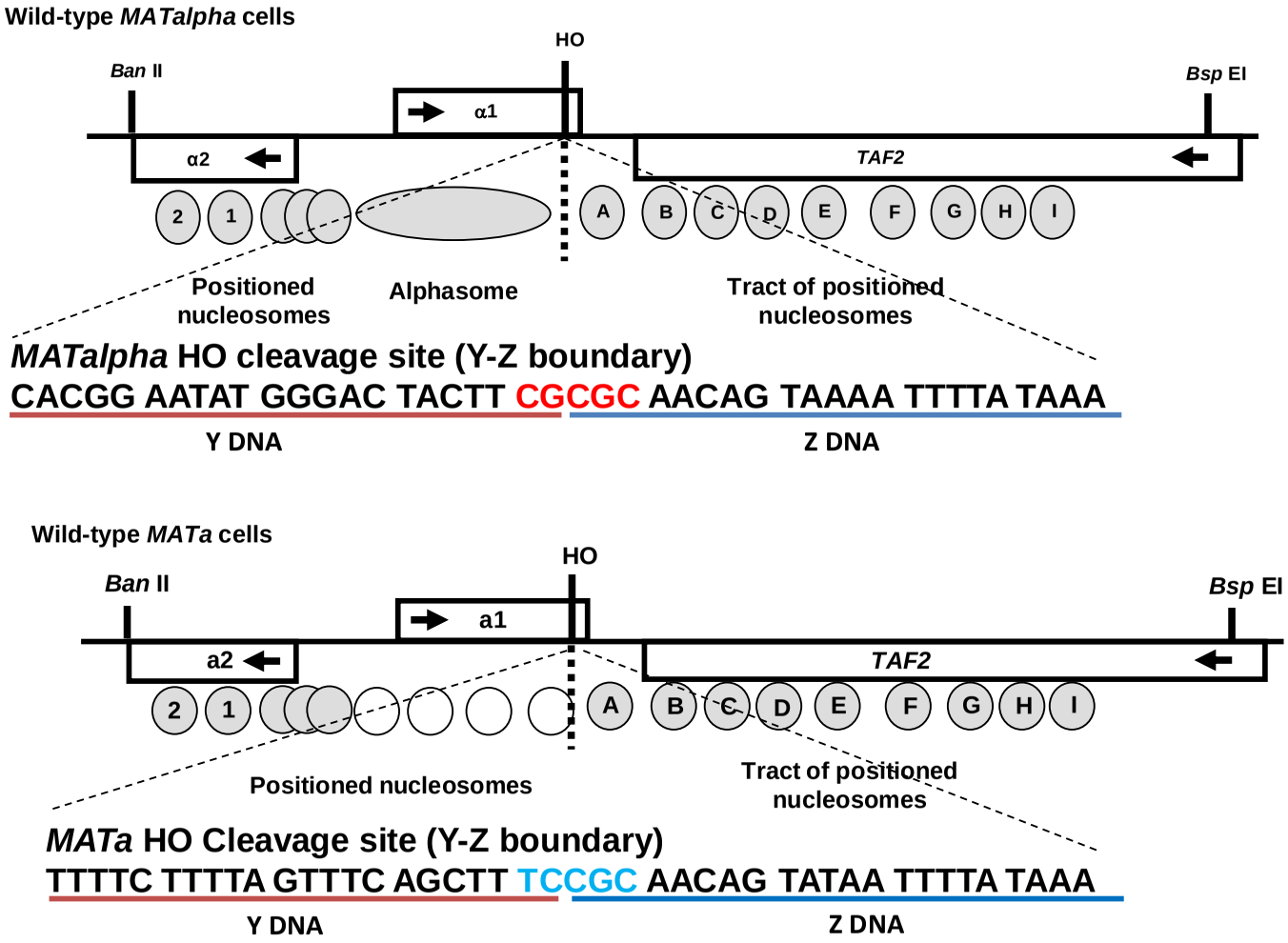

Figure 4.7 – The *MATalpha* Y/Z boundary contains an Rsc3 binding consensus sequence
The HO endonuclease cleaves at the Y/Z boundary, between bases Z3/Z4 on the Crick strand and Z7/Z8 on the Watson strand (Z bases are numbered upwards going away from the Y/Z boundary). The sequence overlapping the Y/Z boundary contains the putative Rsc3 binding sequence in *MATalpha* (in red) which is not present in the Y/Z boundary suggesting that the RSC complex may be able to bind to *MATalpha,* but not *MATa,* through the Rsc3 zinc-finger domain.

5 The Rsc1 BAH domain confers nucleosome sliding function in response to HO-induced DSBs at *MATalpha*

5.1 Aims of this chapter

1. To determine the domains required for Rsc1-dependent nucleosome remodelling at DSBs

2. To determine the domains required within Rsc2 for alphasome formation at *MATalpha*

5.2 Rsc1 and Rsc2 are homologous proteins

As previous chapters have shown, chromatin remodelling occurs in response to DNA damage induced by the endonuclease HO, both at the specialised *MAT* locus and at HO sites artificially placed in non-*MAT* locus chromosomal contexts. Previous research has shown that nucleosome remodelling surrounding a DSB is an essential prerequisite for efficient H2A phosphorylation and subsequent DNA repair (Kent et al., 2007). These analyses and those presented above have also shown that there is a specific chromatin structure at *MATalpha*, that is important for efficient cleavage of the locus by HO (Kent et al., 2007). Both of these functions are mediated through the RSC chromatin remodelling ATPase complex albeit through different subunits.

As described in Section 1.6, RSC is a 17 subunit SWI/SNF related complex (Figure 1.4). Seven of the RSC subunits are essential for cell viability including Sth1 that contains an ATPase motif, and this gene is homologous to *SNF2.* RSC however is unlikely to be a monolithic complex as evidence suggests that it exists in two isoforms, one containing Rsc1 and the other Rsc2. Rsc1 and Rsc2 are closely related; both contain two sequential bromodomains (BD), a bromo-adjacent homology (BAH) domain, and an AT hook (Figure 5.1). It has been shown that these domains do not play a role in

complex assembly but that they are essential for RSC function (Cairns et al., 1999).

Bromodomains bind directly to proteins, specifically to histone proteins and there is evidence that suggests that the bromodomains have some specificity for acetylated lysines (Section 1.6.1). It has been shown previously that the bromodomains of Rsc4, a subunit of the RSC complex, have a binding specificity for acetylated lysine residues (VanDemark et al., 2007). Therefore it is hypothesised that BDs recruit the RSC complex to specifically marked chromatin environments and that the different BDs present in Rsc1 and Rsc2 confer different binding activities and therefore have different functions. BAH domains were identified by their proximity to bromodomains but further investigation has revealed that this is not a universal definition of a BAH domain and little is known of BAH domain function (Goodwin and Nicolas, 2001). The AT hooks found in Rsc1 and Rsc2 potentially perform a function for the ATPase subunit, Sth1, as homologous ATPases in similar chromatin remodelling complexes contain an AT hook whereas Sth1 does not. Therefore it is predicted that the bromodomains or BAH domains confer the specific and distinct functions of Rsc1 and Rsc2. Null mutations of *RSC1* or *RSC2* are viable whereas and *Δrsc1 Δrsc2* double mutants are not, showing some functional redundancy of these proteins (Cairns et al., 1999; Goodwin and Nicolas, 2001). Single mutants are sensitive to genotoxic agents, have decreased telomere length, and show an altered cell cycle (Cairns et al., 1999). Rsc1 and Rsc2 are highly similar proteins and they share a highly similar domain organisation but analysis has shown they have distinct functions (Section 1.6).

The results presented in Chapters 3 and 4 show that Rsc1 is involved in RSC nucleosome remodelling activity in response to a DSB whereas the highly similar subunit Rsc2 is not. Conversely, Rsc2 is involved in alphasome formation at the *MATalpha* locus, whereas Rsc1 is not. Thus, even though the subunits are similar they have very distinct functions at the level of chromatin remodelling. Figure 5.1 shows an alignment of the Rsc1 and Rsc2 amino acid sequences as translated from the protein coding regions of their respective open reading frames. Identical and similar residues have been

highlighted which show a high degree of conservation between these two functionally distinct proteins. The domains common to both proteins are highlighted. Bromodomain 1 is highly conserved between Rsc1 and Rsc2; it is 77% similar and 60% identical, whereas bromodomain 2 is only 63% similar and 45% identical. The AT hook is conserved between the two proteins apart from a single conservative change in the amino acid sequence. The BAH domain is also highly conserved between these proteins, with 87% similar and 79% identical amino acid residues.

The presence of Rsc1 or Rsc2 defines the functionality of the RSC complex and the differences in the functional domains in these proteins are ideal targets for genetic studies to determine whether their function is defined by any of their domains. The work in this Chapter seeks to dissect the differences between Rsc1 and Rsc2 by swapping bromo and BAH domains and observing the resulting effects in terms of chromatin-remodelling at *MAT*.

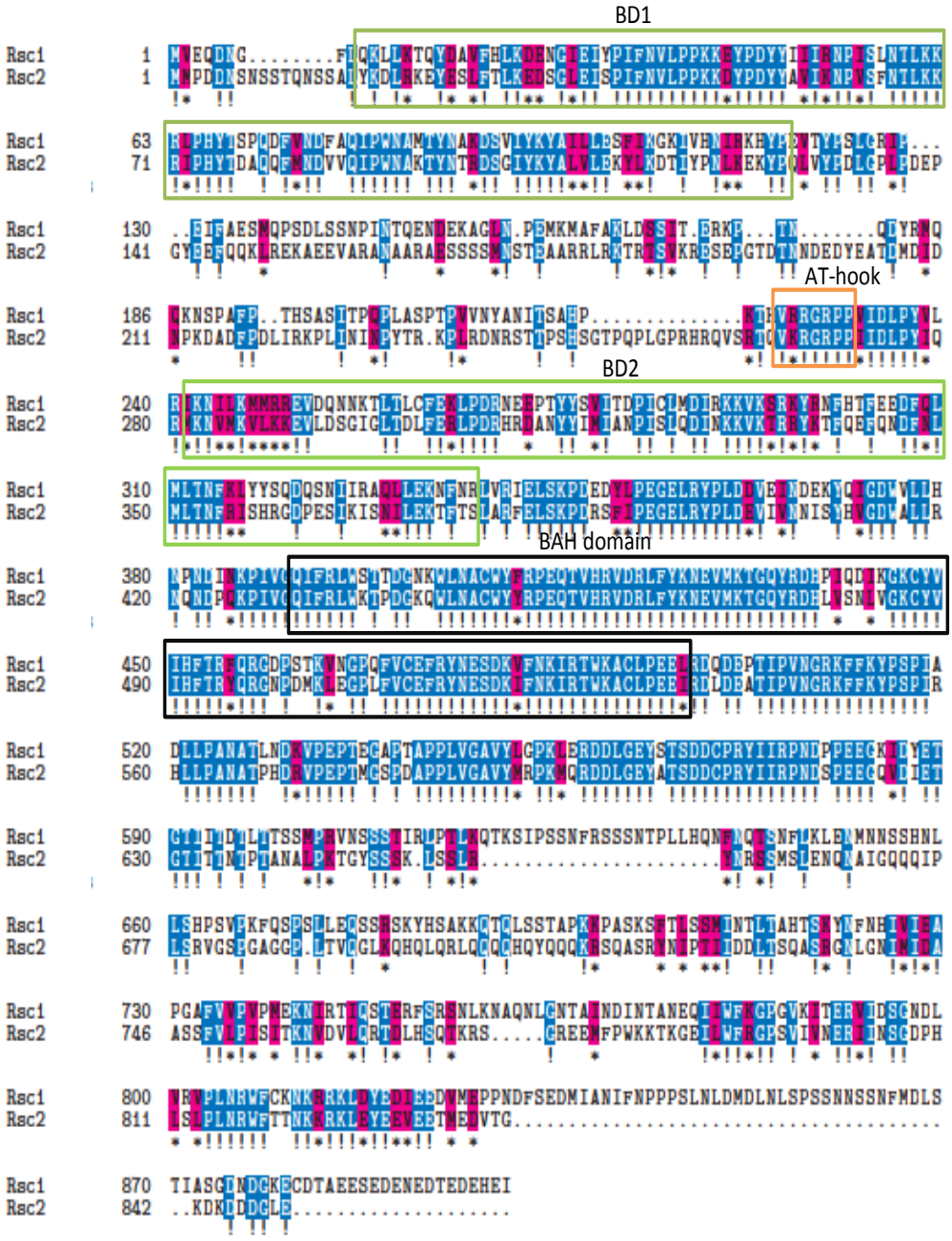

Figure 5.1 - Rsc1 and Rsc2 have a similar primary structure
The translated amino acid sequence of the coding regions of YGR056W (*RSC1*) and YLR357W (*RSC2*) were aligned using the ClustalW algorithm. Identical residues are in blue and labelled with "!", similar residues are in purple and labelled "*". Rsc1 and Rsc2 have a similar domain organisation and the four key functional domains are contained within open boxes; the bromodomains in green, the AT-hook in orange, and the BAH domain in black. The homologous region that is C – terminal of the BAH domain is required for incorporation into the RSC complex. The percentage of identical and similar amino acids for each domain was calculated; BD1 77% similar, 60% identical, BD2 60% similar and 43% identical, AT-hook 100% similar and 86% identical, and BAH domain 87% similar and 79% identical.

5.3 The Rsc1 BAH domain can confer DSB-dependent nucleosome sliding ability at the *MAT* locus to Rsc2

Plasmid constructs expressing Rsc1 or Rsc2 proteins in which bromodomains were swapped with the counterparts of the opposing protein were utilised to test whether or not specific domains could singularly confer nucleosome sliding activity at *MATalpha* after introduction of a DSB at the HO site. All strains were made in a *Δrsc1 Δrsc2* double null mutant rescued with *RSC2* expressed from a CEN/ARS yeast expression vector pRS415 as *Δrsc1 Δrsc2* double null mutants are inviable. These plasmids also contain a *URA3* marker. This plasmid was then shuffled out with either a plasmid containing *RSC1, RSC2,* or one of the following domain swap constructs: pRSC2^{BD1} has the Rsc2 BD1 coding sequence (amino acids 18-130) swapped with the Rsc1 BD1 coding sequence (amino acids 10-122); pRSC2^{BD2} has the Rsc2 BD2 coding sequence (amino acids 281-377) swapped with the Rsc1 BD2 coding sequence (amino acids 242-337); and pRSC2^{BAH} has the Rsc2 BAH coding sequence (amino acids 431-536) swapped with the Rsc1 BAH coding sequence (amino acids 391-496).

5.3.1 *RSC1* and *RSC2* expressed from a plasmid can rescue chromatin remodelling

As a control experiment, Figure 5.2A shows that DSB-dependent nucleosome remodelling after DSB induction at *MATalpha* occurs normally when a *Δrsc1 Δrsc2* double deletion mutant is rescued with a plasmid construct expressing *RSC1.* Consistent with the lack of Rsc2 activity in this strain, the alphasome region appears to dissociate into three nucleosomes. The converse control experiment shown in Figure 5.2B shows the analysis of a *Δrsc1 Δrsc2* double deletion mutant rescued with a plasmid construct expressing *RSC2* and shows that although chromatin remodelling in response to a DSB is not restored, the formation of the alphasome at the HO site is. Thus both Rsc1 and Rsc2 behave in this system exactly as expected and as described in the previous Chapters.

5.3.2 Bromodomains from Rsc1 cannot confer DSB-dependent nucleosome remodelling activity to Rsc2

Figures 5.3A and 5.3B shows analysis of chromatin surrounding the *MATalpha* locus, in *Δrsc1 Δrsc2* double deletion mutants harbouring a plasmid expressing Rsc2 but containing domain swaps of the Rsc1 BD1 or BD2 respectively. Both strains are unable to fully remodel chromatin in response to a DSB at *MATalpha* but correctly assemble the alphasome. Therefore both strains behave identically to a strain expressing an unmodified form of Rsc2 as shown in Figure 5.1B.

5.3.3 The Rsc1 BAH domain can confer DSB-dependent nucleosome remodelling activity to Rsc2

Figure 5.4 shows that the strain expressing Rsc2 with a Rsc1BAH domain swap has both normal alphasome structure immediately proximal to the HO cleavage site at *MATalpha* and interestingly, the ability to partially rescue Rsc1-dependent nucleosome sliding in response to formation of a DSB by HO endonuclease. This shows that the Rsc1 BAH domain confers some specificity to the Rsc1 protein and may define Rsc1-dependent chromatin remodelling in the RSC complex.

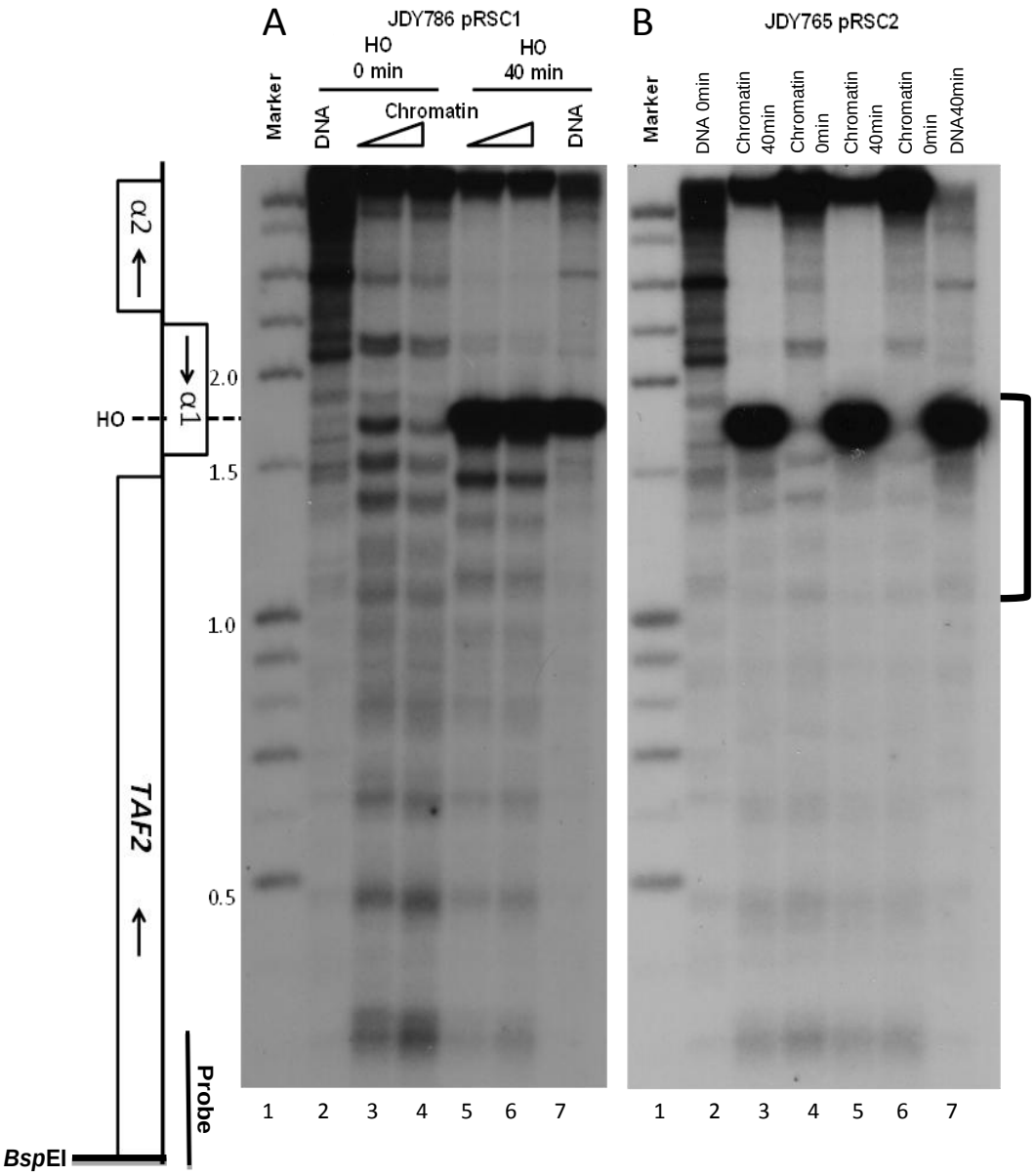

Figure 5.2 – p*RSC1* plasmid rescues DSB-dependent chromatin remodelling activity at *MATalpha*
Chromatin remodelling in response to an HO-induced DSB is rescued by p*RSC1* but not by p*RSC2*. Double Δrsc1/Δrsc2 mutants were created in JKM179 and rescued by shuffling a plasmid harbouring either *RSC1* or *RSC2*. Permeabilised spheroplasts were digested with increasing concentrations of MNase (triangles) for 2 minutes at 37ºC before (*t*=0) and after (*t-40*) induction of *HO* by addition of galactose to the media. DNA fragments were separated by electrophoresis, blotted onto nylon membrane and probed with a probe abutting the indicated restriction enzyme site. **A** - p*RSC1* rescues nucleosome remodelling in response to a HO-induced DSB at *MATalpha*. Nucleosomes are remodelled on the *TAF2* side of the DSB (bracketed region), similar to that seen in the wild type. Before the induction of the DSB, three positioned nucleosomes immediately flank the HO cleavage site on the *MAT* locus side. **B** - p*RSC2* does not rescue remodelling activity after the formation of a HO-induced DSB. p*RSC2* does restore the alphasome immediately on the *MAT* locus side of the HO cleavage.

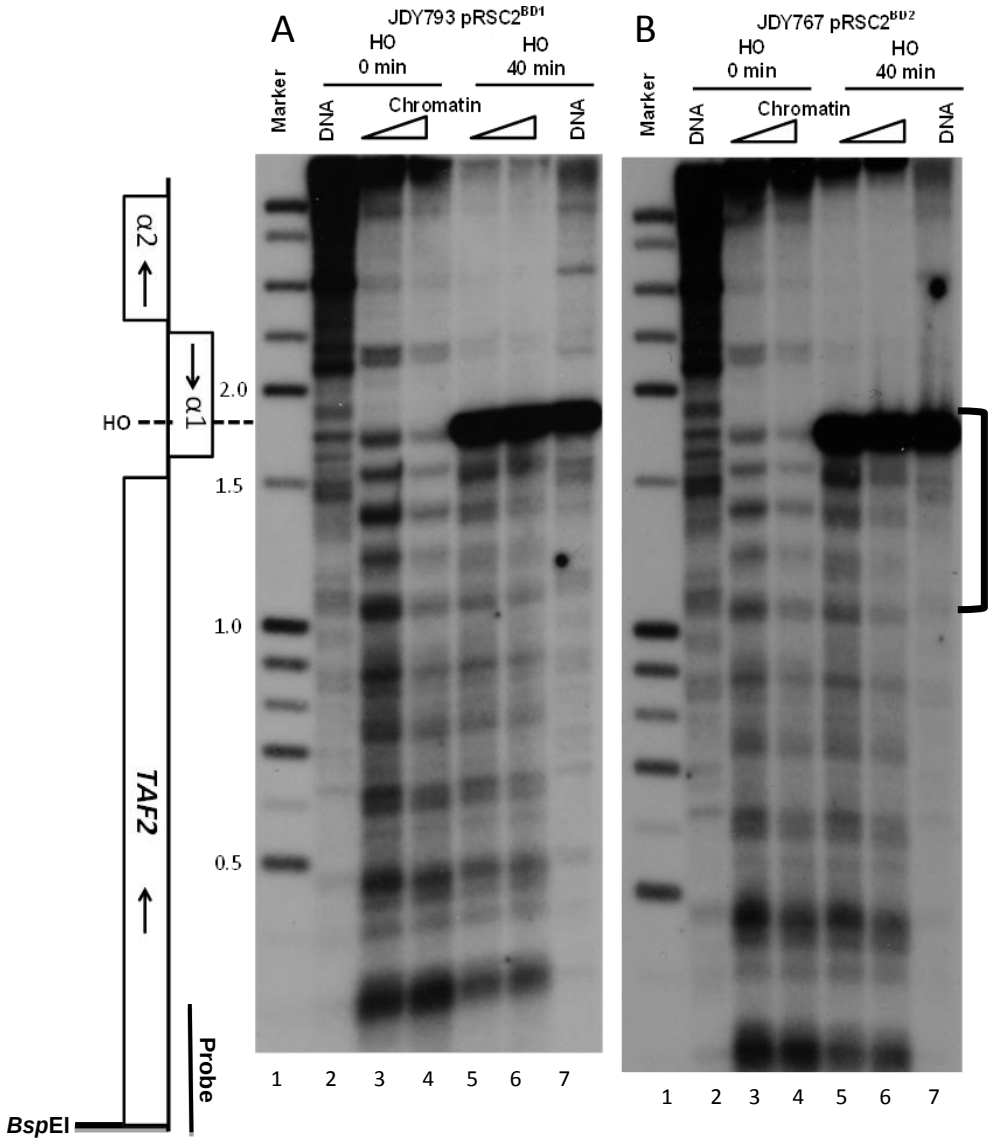

Figure 5.3 – Rsc1-bromodomains do not confer Rsc1 DSB-dependent remodelling activity at HO-induced DSBs at *MATalpha* to Rsc2

Swapping either of the Rsc1 BDs into Rsc2 does not rescue chromatin remodelling in response to an HO-induced DSBs. Double Δrsc1/Δrsc2 mutants were rescued by shuffling a plasmid harbouring *RSC2* containing a swapped BD1 or BD2 from *RSC1*. Indirect-end-label analysis of chromatin was performed before and after induction of HO as in Figure 5.2. **A** - Analysis shows that swapping BD1 of Rsc1 into *RSC2* does not confer nucleosome remodelling activity in response to an HO-induced DSB as the nucleosome pattern observed after 40 minutes of *HO* induction is very similar to that prior to induction (compare lanes 3-4 with lanes 5-6). The alphasome is present immediately to the *MAT* locus side of the HO cleavage site prior to induction **B -** similar observations are made when BD2 of Rsc1 is swapped into *RSC2*. Nucleosome remodelling in response to the formation of a DSB by HO at *MATalpha* does not occur however the alphasome immediately flanking the HO cleavage site, which is specific to *MATalpha*, is retained.

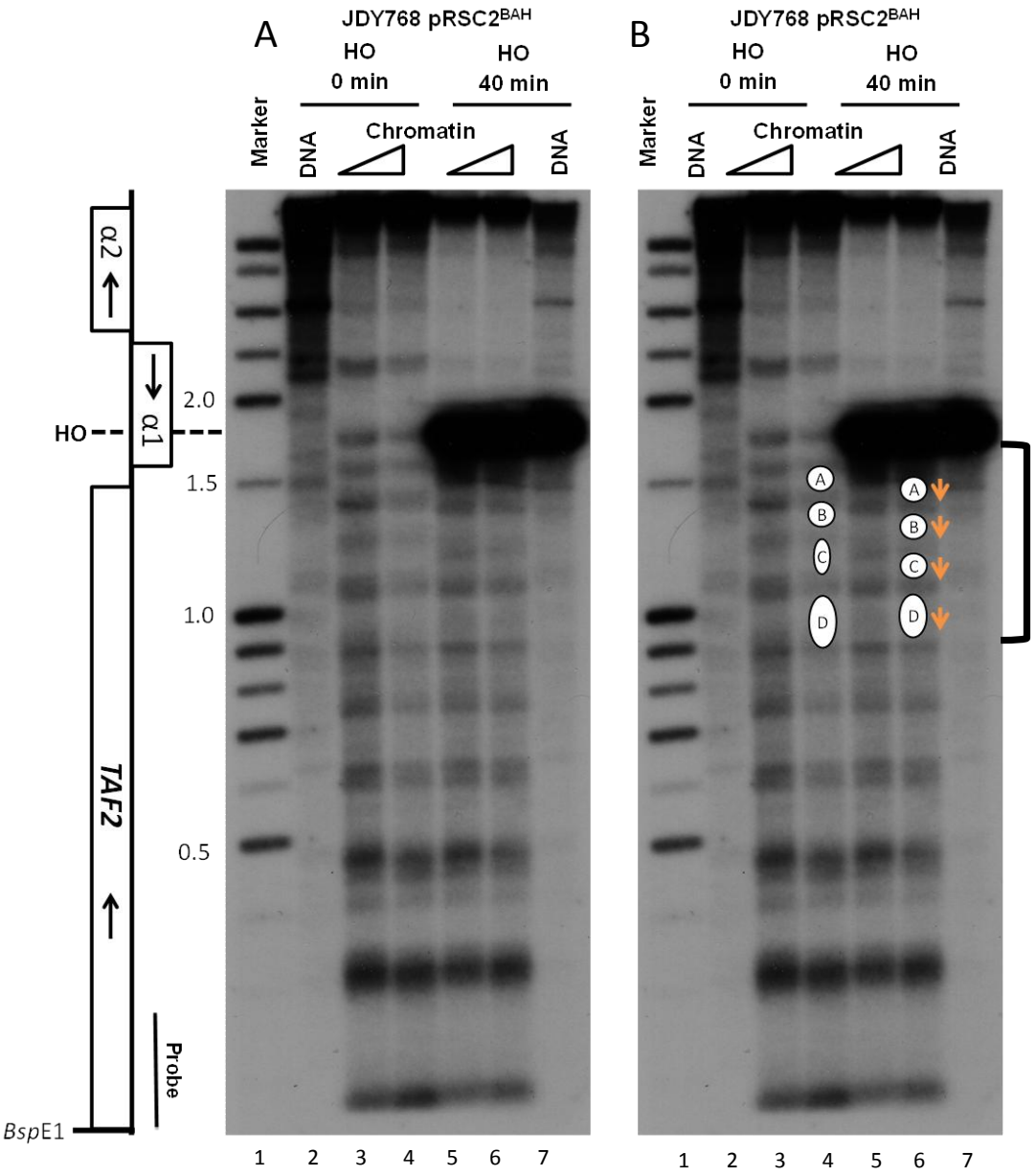

Figure 5.4 – The Rsc1-BAH domain confers nucleosome DSB-dependent chromatin remodelling at a HO-induced DSB at *MATalpha* to Rsc2

Swapping Rsc1 BAH domain into Rsc2 at least partially rescues nucleosome remodelling in response to an HO-induced DSB. Double Δrsc1/Δrsc2 mutants were rescued by shuffling a plasmid harbouring *RSC2* containing the BAH domain of *RSC1*. Indirect-end-label analysis was performed as described previously. **A –** Indirect-end-label analysis shows that there is nucleosome remodelling in response to the formation of a DSB by HO at *MATalpha* on the *TAF2* side of the break (compare lanes 3-4 with lanes 5-6). **B –** The inferred nucleosome pattern shows that nucleosome A – D are remodelled away the DSB, which is similar to what is observed in the wild type. The alphasome immediately flanking the HO cleavage site is retained.

5.4 Are bromodomain residues in the RSC complex required for alphasome maintenance?

Given that the experiments described above have identified the Rsc1-BAH domain as conferring DSB-dependent nucleosome remodelling activity to the RSC complex, I next tested whether or not bromodomains within the RSC complex were required for the remodelling activity specific for creating the alphasome structure at *MATalpha.* Figures 5.2 and 5.3 show that the Rsc2 activity can be complemented by either of the Rsc1 BDs inserted into Rsc2 suggesting that functional residues in the bromodomains must be common to Rsc1 and Rsc2. Interestingly RSC employs a third bromodomain-containing subunit, Rsc4, which specifically binds to acetylated lysine residues on nucleosomes (Kasten et al., 2004; VanDemark et al., 2007).

Figure 5.5 shows the sequence and predicted secondary structure of the Rsc1 (amino acids 1-380), Rsc2 (amino acids 1-420) and Rsc4 (amino acids 51-340), aligned according to their respective bromodomains. The bromodomains of Rsc1 and Rsc2 are shown in green boxes and the tandem bromodomains of Rsc4 are underlined in blue, predicted alpha helices are indicated in red and beta-sheets indicated in yellow.

The predicted secondary structure of Rsc4 is very similar to that of the previously published crystal structures (VanDemark et al., 2007). The resulting analysis shows that there is a high degree of amino acid sequence similarity between all three proteins and there is a striking similarity of the secondary structures. Rsc4 contains two tandem bromodomains whereas Rsc1 and Rsc2 contain intervening sequences that contain the AT hook. Previous analysis has shown that the bromodomains found in Rsc4 require two pairs of asparagine residues and two tyrosine residues (highlighted with red stars) to have binding specificity with acetylated lysine (VanDemark et al., 2007). The amino acids in Rsc4 that are required to bind to acetylated lysines of bromodomain-1 (BD1), Y92, Y93 and N134 are conserved in all three proteins. Similarly Y225 and Y226 of Rsc4 bromodomain-2 (BD2) are also conserved in all three proteins in both the primary and secondary structure. As these residues are conserved between Rsc1, Rsc2 and Rsc4 and are

essential for Rsc4 activity they were good candidates to study whether these residues are essential for Rsc2 chromatin remodelling activity.

Thus a number of plasmid constructs were made harbouring bromodomain mutations within *RSC2* at asparagine and tyrosine residues that are conserved between Rsc1, Rsc2 and Rsc4. Plasmids harbouring mutated bromodomains were shuffled into the *Δrsc1 Δrsc2* null mutant strain as described above. Figure 5.6 shows that a neither a single mutation of Rsc2 N96A in BD1 (lanes 6-7), a single mutation of Y315A in BD2 (lanes 9-10), nor a combination of both mutations (lanes 12-13) was able to abolish normal alphasome formation.

To investigate whether a mutated BD2 of *RSC2* could maintain the alphasome with the BD1 of Rsc1, a plasmid was made harbouring the Y315A *RSC2* BD2 mutation and the replacement of BD1 with the entire BD1 of *RSC1*. A plasmid harbouring a BD1 *RSC1* N88A mutation together with the Y315A *RSC2* mutation was also constructed. These plasmids were shuffled into *Δrsc1 Δrsc2* null mutants to determine the effect of these mutations on Rsc2-specific activity at *MATalpha*. Figure 5.7 shows that the alphasome is still formed by Rsc2 with the BD1 of *RSC1* and the BD2 Y315A mutation (lanes 6 and 7). Similarly the Rsc2-dependent formation of the alphasome is not abolished with when BD1 is replaced with Rsc1 BD1 with the N88A mutation of the *RSC1* bromodomain and the Y315A mutation of BD2 (lanes 9-10). Therefore the conserved residues essential for Rsc4 function are not required for the alphasome function of Rsc2.

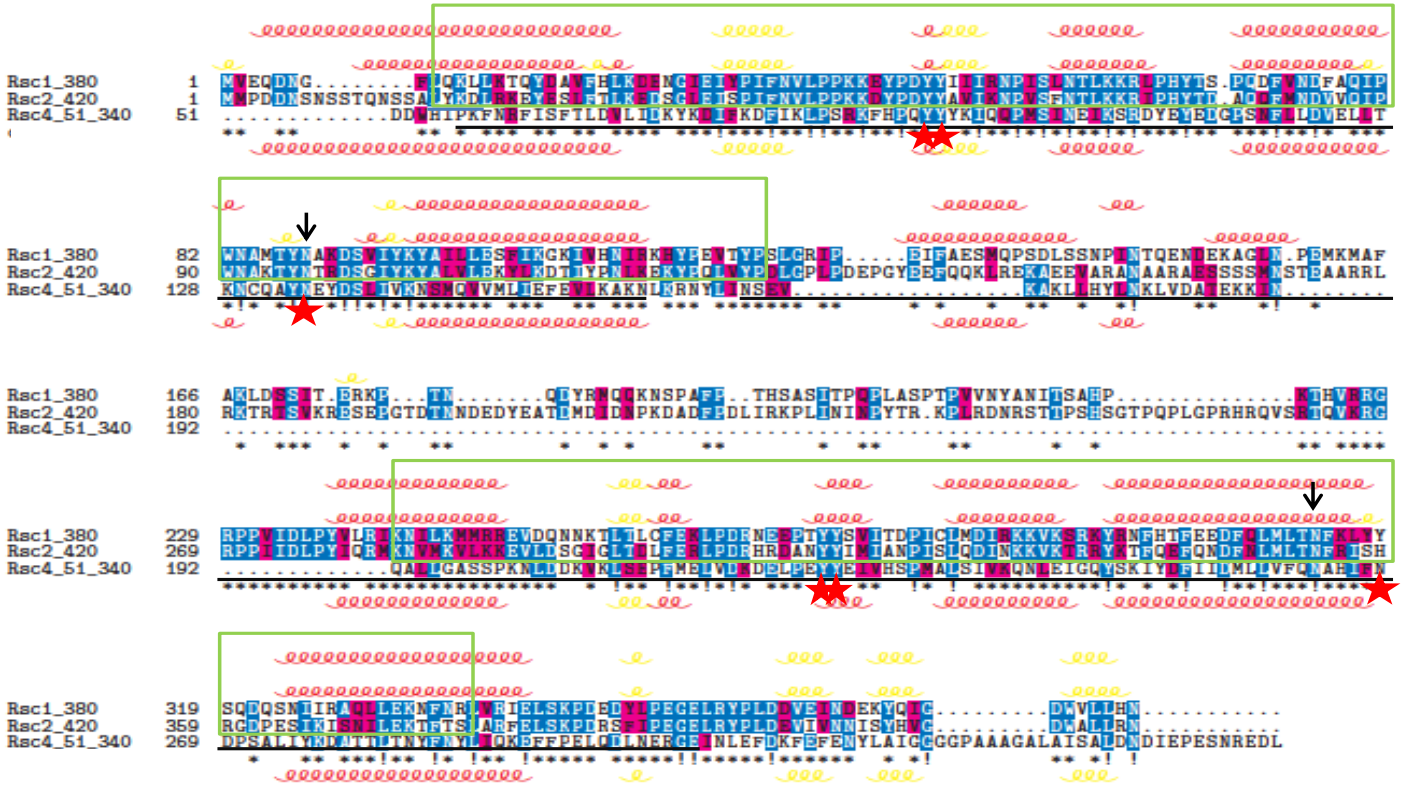

Figure 5.5 - Rsc1 and Rsc2 share primary and secondary structure homology with Rsc4
The three bromodomain-containing proteins in RSC share amino acid sequences and structural similarities. The amino acid sequences of YGR056W (*RSC1*), YLR357W (*RSC2*), and YKR008W (*RSC4*) of their respective bromodomains (*RSC1* aa1-380, *RSC2* aa1-420 and *RSC4* aa51-340) were aligned using the ClustalW method in the GUI Strap. Identical residues are shown in blue and labelled with "!" and similar residues are shown in purple and labelled with "*". Secondary structure was predicted using the SOPMA method and predicted alpha helices are shown in red and beta-sheets are shown in yellow. The residues within the bromodomains of Rsc1 and Rsc2 are enclosed within a green box and the residues of the bromodomains of Rsc4 are underlined in black. Residues that are essential for Rsc4 to bind to acetylated lysine residues are indicated with a red star. The residues that were mutated in BD1(*RSC1* N88, *RSC2* N96) and BD2 (*RSC2* Y315) are indicated with black arrows. Bromodomain 2 secondary predicted secondary is very similar in all three proteins and the mutated tyrosine occurs in conserved primary sequence. The mutated asparagine residue in BD1 (*RSC1* N88, *RSC2*, N96) are in a structurally similar regions as the essential N134 of Rsc4.

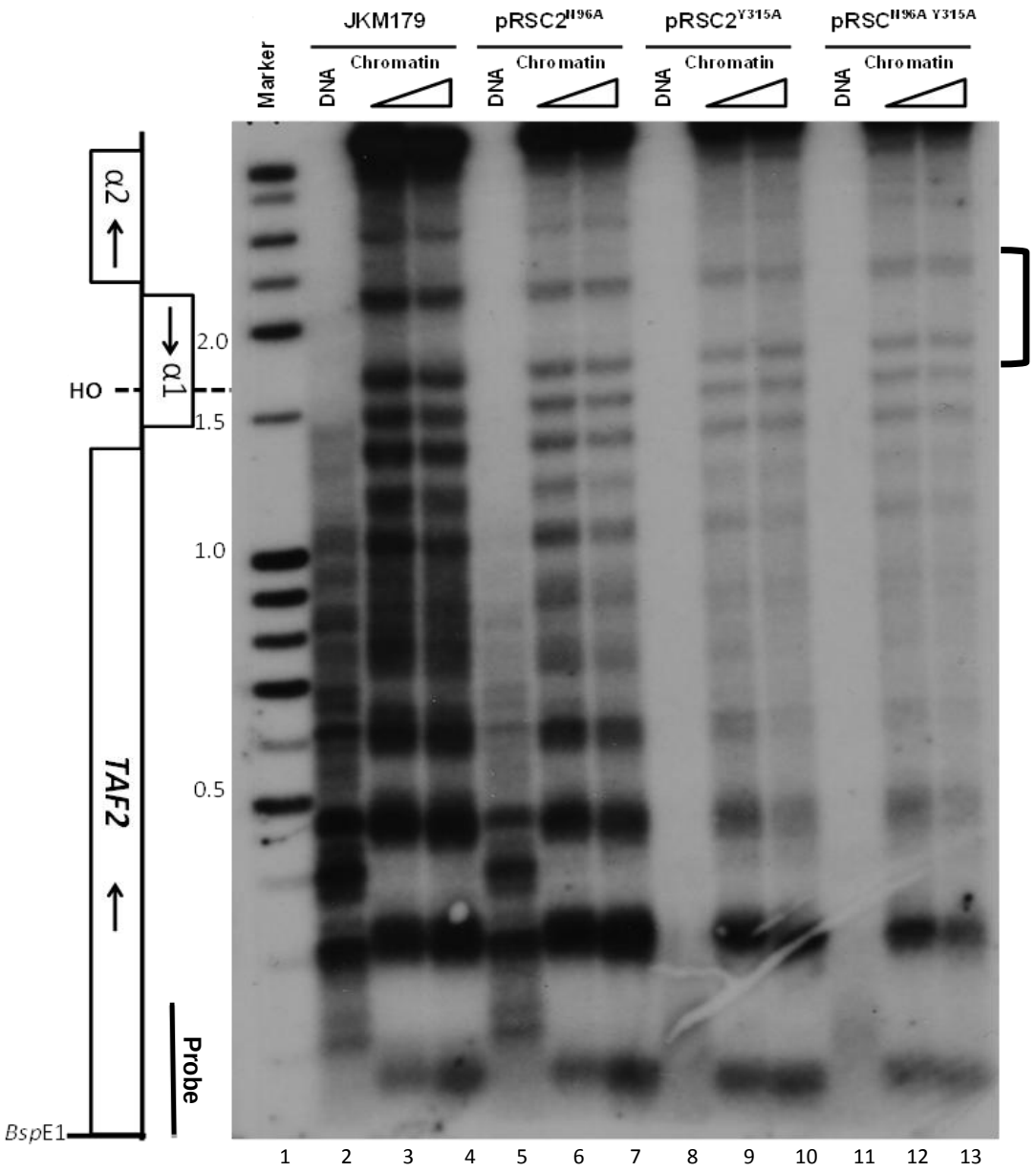

Figure 5.6 – Conserved bromodomain residues do not individually confer Rsc2-dependent alphasome formation at *MATalpha*

Mutating conserved residues found between Rsc2 and Rsc4 does not abolish alphasome formation. Double Δrsc1/Δrsc2 mutants were rescued by shuffling a plasmid harbouring *RSC2* containing mutations in conserved residues between Rsc2 and Rsc4; N96A, Y315A, or N96A/Y315A. Permeabilised spheroplasts were digested with 75u/ml and 150u/ml MNase for 2 minutes at 37ºC. DNA fragments were separated by electrophoresis, blotted onto nylon membrane and probed with a probe abutting the indicated restriction enzyme site. The analysis shows that mutation of the Rsc4-essential asparagine, N96, does not abolish formation of the *MATalpha* specific alphasome when compared to the wild-type control (compare lanes 3-4 with lanes 5-6 bracket region). Similar observations are made with the Y315A mutation (lanes 9-10) and in the double mutant N96A/Y315A (lanes 12-13).

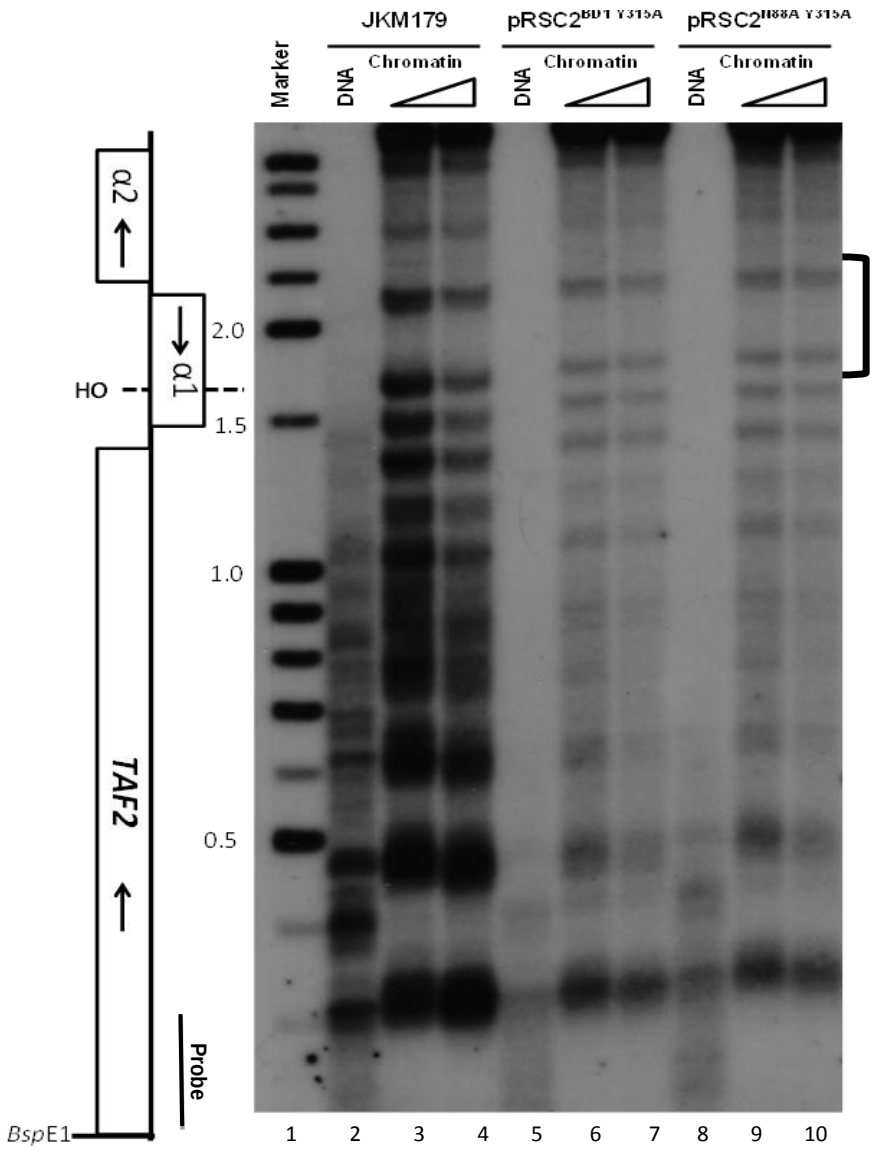

Figure 5.7 – The Rsc2-dependent alphasome formation is independent of Rsc2-BD1
Mutating conserved residues found between Rsc2 and Rsc4 in BD2 alongside replacement of Rsc2-BD1 with that of Rsc1 does not abolish alphasome formation. Double Δrsc1/Δrsc2 mutants were rescued by shuffling a plasmid harbouring *RSC2* containing a mutation in the conserved residues between Rsc2 and Rsc4; Y315A, alongside the replacement of BD1 with that of Rsc1. A second plasmid contains the same construct except that the BD1 from Rsc1 has a mutation at N88A, a conserved residue between Rsc1, Rsc2 and Rsc4. Indirect-end-label analysis was performed as described previously. Analysis shows that mutation of the Rsc4-essential Y315A alongside the replacement of the entire of BD1, does not abolish formation of the *MATalpha* specific alphasome when compared to the wild-type control (compare lanes 3-4 with lanes 5-6, bracketed region). The alphasome is present immediately to the *MAT* locus side of the HO cleavage site in both. Similar observations are made when the Y315A mutation is combined with a mutated BD1 from Rsc1 (lanes 9-10)

5.5 Summary

The data presented here and published previously (Kent et al., 2007; Shim et al., 2007) has shown that the ATPase-dependent chromatin remodelling complex RSC is required for both DSB-dependent chromatin remodelling and for setting the chromatin structure at *MATalpha* prior to efficient cleavage by HO. These activities are dependent on two different isoforms of RSC as defined by the presence of either Rsc1 or Rsc2 in the RSC complex. Rsc1 and Rsc2 are highly similar proteins that are likely to have occurred a result of the genome duplication event (Kellis et al., 2004). These proteins have an identical domain organisation; both proteins contain two bromodomains, an AT-hook, and a bromo-adjacent homology (BAH) domain. However, despite their similarity, it has been shown here that Rsc1 and Rsc2 have distinct and non-redundant functions.

Further investigation here showed that the bromodomains of Rsc1 and Rsc2 are very similar to Rsc4 both in primary and secondary structure. Previous work has shown that the bromodomains of Rsc4 have specificity for particular acetylated lysines which also confer specific function (VanDemark et al., 2007). This Chapter therefore tested the hypothesis that BDs or BAH domains within the RSC complex would confer distinct and specific chromatin-remodelling functions. Plasmid constructs were made in which the domains of Rsc1 and Rsc2 were interchanged and mutated. These plasmids were shuffled into *Δrsc1 Δrsc2* double mutants to see if they could rescue Rsc1- or Rsc2-dependent chromatin remodelling activity.

Neither BD1 nor BD2 inserted into Rsc2 conferred DSB-dependent nucleosome remodelling activity. However, the swapping of the BAH domains did partially confer Rsc1-specific activity onto Rsc2. A recent study has shown that the BAH domain of Rsc2 has a distinct structure in comparison to the BAH domain of Sir3 and that the Rsc2 BAH domain can, *in vitro*, bind recombinant histone H3 protein (Chambers et al., 2013). As the Rsc1- and Rsc2-BAH domains have very similar amino acid sequence it would be predicted they would have similar structure however the data presented here would suggest that only the Rsc1-BAH domain can interact with histones in the context of DNA damage.

Previous work on Rsc4 has revealed that there are a number of residues that are essential for the binding activity on particular acetylated lysine residues (VanDemark et al., 2007). An alignment of the Rsc1, Rsc2 and Rsc4 bromodomains reveals that the essential residues in Rsc4 are conserved between all three proteins. Plasmids were constructed containing Rsc2 with the Rsc4-essential residues mutated. Then, the chromatin surrounding the *MATalpha* locus was analysed to determine whether Rsc2-dependent formation of the alphasome was lost as a consequence of the mutations. The analysis presented here has shown that the mutations that should abolish Rsc4 binding activity, do not prevent formation of the alphasome.

These data suggest that the BAH domain of Rsc1 is required for chromatin remodelling activity. However, it is possible that the other domains of Rsc1 are required for the extensive remodelling observed in the wild type. The remodelling activity observed in Rsc2 is not dependent on a single domain of the protein as the swapping of a single domain of Rsc2 with that of Rsc1 does not abolish activity. Similarly, introducing mutations into the residues predicted to be required to bind to acetylated lysine does not abolish the Rsc2-dependent alphasome. This suggests that there may be some functional overlap in the bromodomains of Rsc2 or that the activity is independent of the domains tested above. The latter would support the hypothesis that Rsc7 has a distinct function to form the alphasome at *MATalpha* even though it bears little sequence homology with, and contains none of the domains found in, Rsc2.

6 Determination of genome wide Rsc1- and Rsc2-dependent sites of chromatin remodelling using Chromatin particle spectrum analysis (CPSA)

6.1 Aims of this chapter

1. To compare the chromatin landscape of the *S. cerevisiae* genome in wild type cells and *Δrsc1* and *Δrsc2* mutants.

2. To determine sites and modes of Rsc1 and Rsc2-dependent chromatin-remodelling in the yeast genome.

6.2 Chromatin Particle Spectrum Analysis of yeast chromatin

In the previous Chapters I have shown that the Rsc1 and Rsc2 bromo- and BAH domain containing subunits of the RSC ATPase complex conferred context dependent nucleosome remodelling functions to the *MAT* locus DSB formation and repair process. Both Rsc1 and Rsc2 have been implicated in a variety of other functional systems (Section 1.6.1); therefore this chapter aims to uncover whether chromatin remodelling is involved in these processes by extending the analysis of the Rsc1 and Rsc2 subunits to the wider genome. Here, I employed a method in which the entire MNase protected DNA ladder from chromatin is subjected to Illumina paired-end mode sequencing (Kent et al., 2011). This technique recovers the size of the nuclease protected particle as the map distance between the read-pairs in addition to mapping its absolute genomic position. This methodology, referred to as Chromatin Particle Spectrum Analysis (CPSA) can be used to map not only canonical nucleosome positions but both actively remodelled

nucleosomes and *trans*-activating factor bound DNA motifs (Kent et al., 2011).

CPSA was performed on the wild-type strain BY4741, as described in Methods 2.4 and the isogenic strains YO4686 and YO5266 that are *Δrsc1* and *Δrsc2* mutants respectively. Figure 6.1 shows the ladder of MNase resistant DNA species derived from chromatin digestion of each strain (each is a pooled triplicate sample), and the resulting paired-end sequence read frequencies plotted according to read-pair distance. Bands visible in the input DNA (present at 150bp, 300bp, and 450bp indicating protected regions corresponding to mono-, di- and tri- nucleosomes) are recapitulated as peaks in the sequence read frequency. The graph shows that the distribution of size particles between the wild type and mutant samples is very similar suggesting that direct comparison between the samples should be valid.

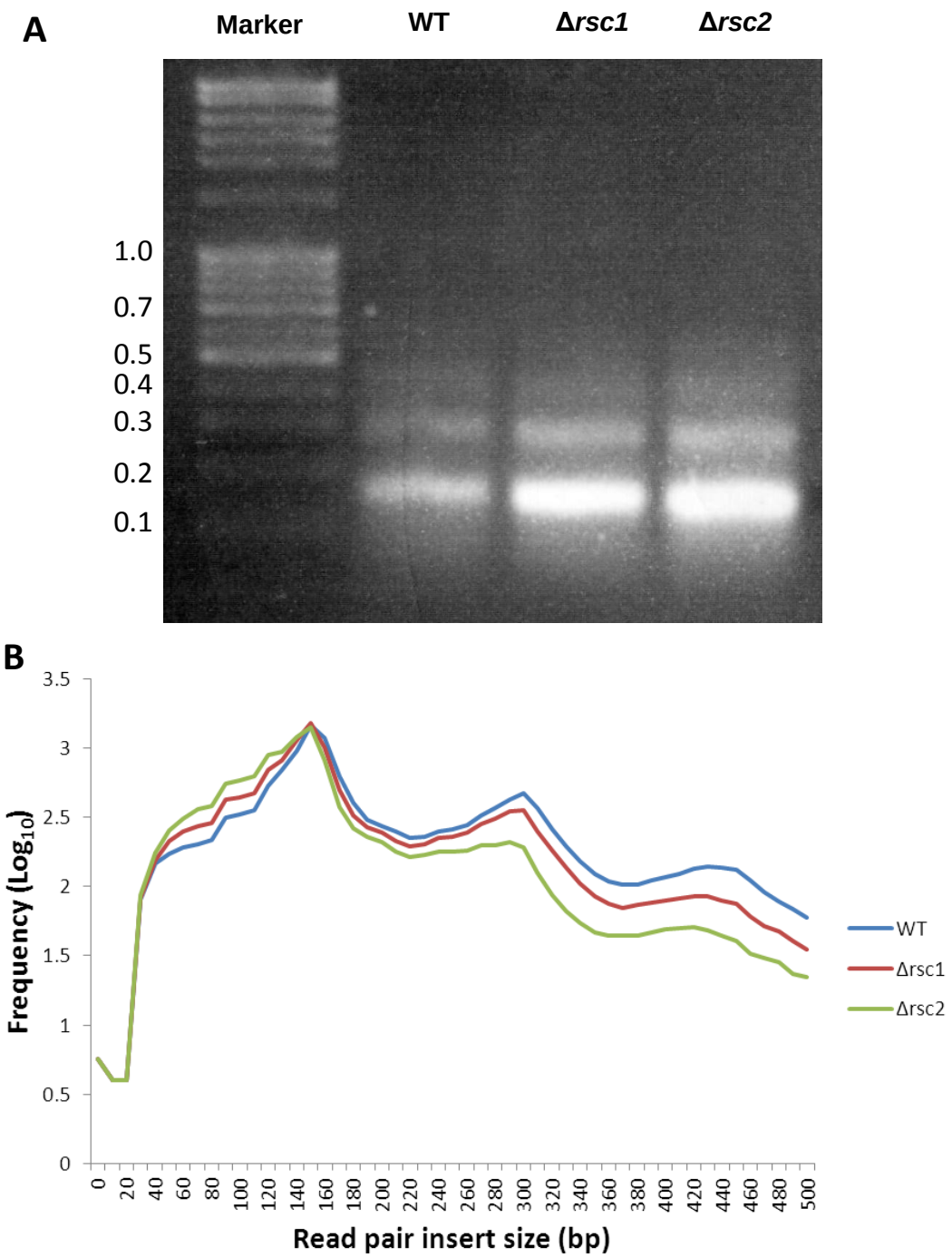

Figure 6.1 – Frequency of CPSA read-pair insert size reflects sizes of input DNA
A– Ethidium-stained agarose gel with 1µg of each CPSA input DNA shows intense bands at 150bp, 300bp, and 450bp indicating DNA protected from MNase cleavage by mono-, di-, and tri- nucleosomes. **B –** Graph of sequence read number versus the log of read-pair end-to-end distance/insert size for aligned sequences derived by CPSA of MNase –digested chromatin in wild-type, *Δrsc1, Δrsc2* yeast cells. Peaks at insert sizes of 150bp, 300bp, and, to a lesser extent, 450bp reflect the presence of mono-, di-, and tri-nucleosomes respectively. A shoulder on the 150bp peak indicates particles of a size less than 100bp potentially indicating the binding footprint of *trans*-activating factors or other chromatin particles.

6.3 Localised sequence read discrepancy in the CPSA dataset in Chromosome XII suggests a change in rDNA copy number in *Δrsc1* and *Δrsc2* strains

Rsc2 has been implicated in genomic stability with suggestions that *Δrsc2* mutants can exhibit aneuploidy or polyploidy (Baetz et al., 2004; Hsu et al., 2003). Aneuploidy in particular would complicate the analysis of the relative contribution of chromatin particle sequence reads between data sets described in this Chapter. Figure 6.2, therefore, shows an analysis of the number of reads obtained for each chromosome in each of the strains to test (with the assumption that each chromosome sequenced with comparable general efficiency) whether aneuploidy could be observed as regions of relative sequence read over- or under-representation. Figure 6.2A shows the total number of aligned reads obtained for each chromosome in the CPSA experiment and shows that approximately 3-fold more reads were obtained for the *Δrsc2* strain when compared to WT and *Δrsc1*. The gross difference is likely to represent variability in Ilumina sequencing performance (K. Paszkiewicz, personal communication) but a complete change in ploidy in the *Δrsc2* mutant cannot be ruled out. Ploidy could be further determined by FACS analysis.

Figure 6.2B shows the ratio of reads obtained for each chromosome compared to the whole genome against the relative length of the chromosome. For example, if a chromosome represents 10% of the total genome then 10% of read-pairs obtained from CPSA would be expected to align to the chromosome and would have a chromosome read-pair value of 1. This graph shows that all chromosomes in the three strains, with the exception of chromosome XII, exhibit a normalised relative sequence read frequency of 1. Interestingly the normalised relative sequence read frequencies observed for chromosome XII in the *Δrsc1* and *Δrsc2* mutants were both different from each other and by non-integer values with respect to the wild-type dataset. This result is not therefore compatible with a simple change in chromosome XII ploidy in the mutant strains. Chromosome XII has the unique feature of encoding the highly repetitive/high copy number rRNA genes; therefore I tested to see whether the presence of these repeats

contributed to the increased representation of read-pairs aligning to Chromosome XII in the wild-type and mutant datasets.

The ribosomal RNA gene is a large repeat of approximately 1.5MBp occupying 60% of chromosome XII. In wild type cells there are approximately 150 copies which produce 80% of the total RNA content of the cell. There are two populations of rDNA genes; those described as non-nucleosomal and transcriptionally active, and those described as nucleosomal and described as inactive. The ratio of active and inactive rDNA genes can change during the cell cycle and in different growth conditions (Fahy et al., 2005). Copies are lost by deleterious recombination events; the high copy number of rDNA is maintained in *S. cerevisiae* by gene amplification, a process that is dependent on the replication fork barrier protein Fob1and RNA Pol I (Kobayashi et al., 1998). The systematic sequencing of this region includes only two repeats of the rDNA so when the aligned read-pairs are rendered to this region in the integrated genome browser (IGB), as shown in Figure6.3A, the region is massively overrepresented in comparison to the non-rDNA region.

The normalised read frequency for aligned read-pairs for each of the three strains within the rDNA co-ordinates and read-pairs outside these coordinates are plotted in Figure 6.3B. The graph shows that the relative number of reads for the non-rDNA region of Chr XII is similar between the three samples. However, for the rDNA region, a 1.3 fold and 2.1 fold decreases is observed in the *Δrsc1* and *Δrsc2* strains respectively. The normalised read frequency compared to the relative length of the region in comparison to the whole genome suggests an rDNA copy of 113 for the WT, 85 for the *Δrsc1* strain and 52 for the *Δrsc2* strain. Taken together these results suggest that the main discrepancy in relative sequence-read depth between the three experiments is restricted to the rDNA repeat region. Although it cannot be determined from this analysis whether or not either of the mutants may have changed genome ploidy (e.g. become fully diploid), it can be concluded that aneuploidy was not likely to be present and analyses of the data sets was continued.

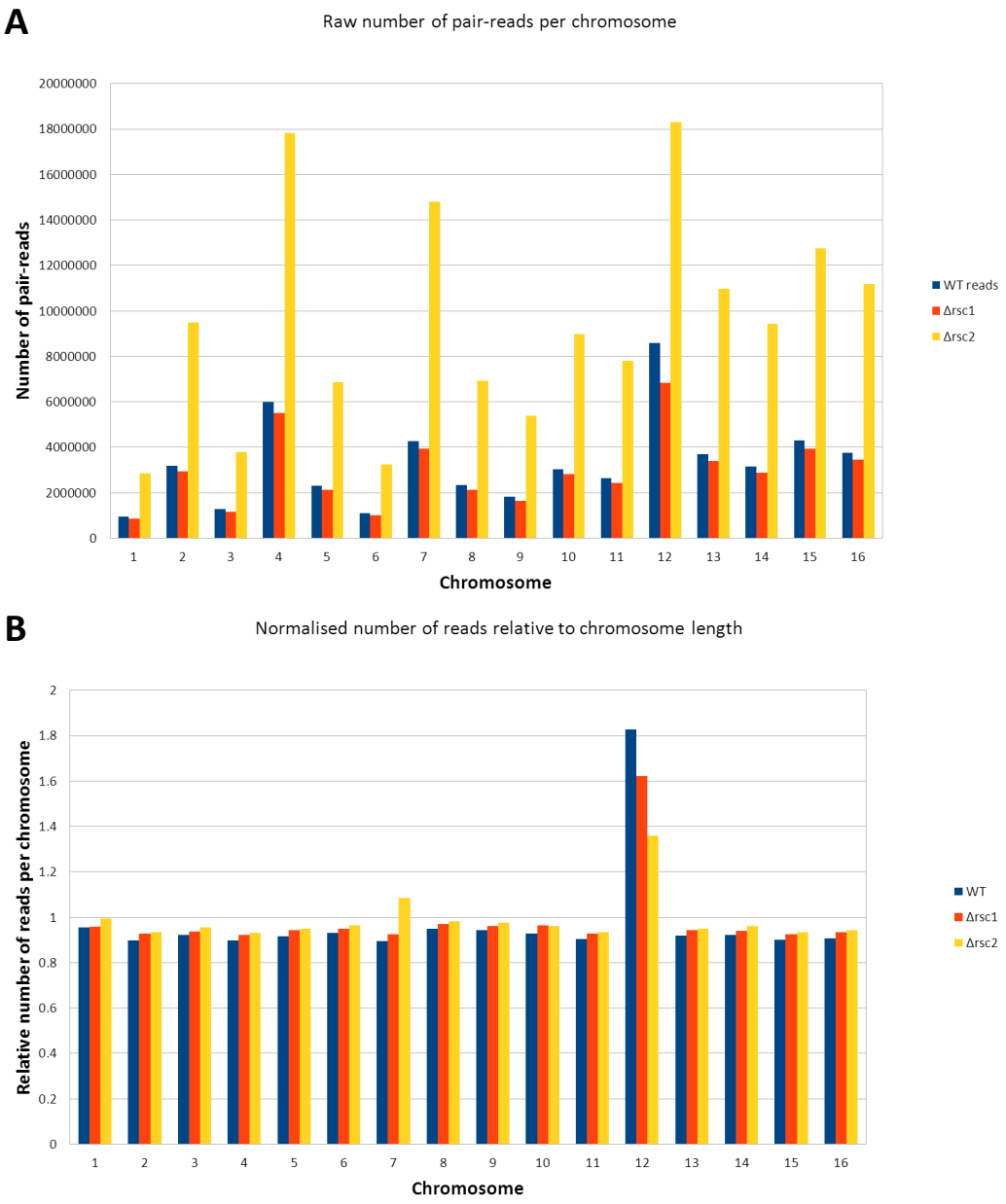

Figure 6.2 – The distributions of CPSA sequence reads from each chromosome in the wild-type and *rsc* mutant data-sets reveals a read depth discrepancy specific to chromosome XII
A - The total number of aligned paired end reads for the wild type (WT), Δ*rsc1* mutant, and Δ*rsc2* mutants were plotted for each chromosome showing that a similar number of reads were obtained for WT and Δ*rsc1* mutant. Approximately 3 fold more reads were obtained in the Δ*rsc2* strain. **B –** the relative number of reads per chromosome is the ratio of the relative number of reads per chromosome over the relative size of the chromosome. The expected value for each chromosome in a haploid genome would therefore be 1. The graph shows that, with the exception of chromosome XII, the relative read depth is equal for each chromosome in all three samples. Chromosome XII is relatively over-represented and is more so in the WT compared with the Δ*rsc1* and Δ*rsc2* mutants

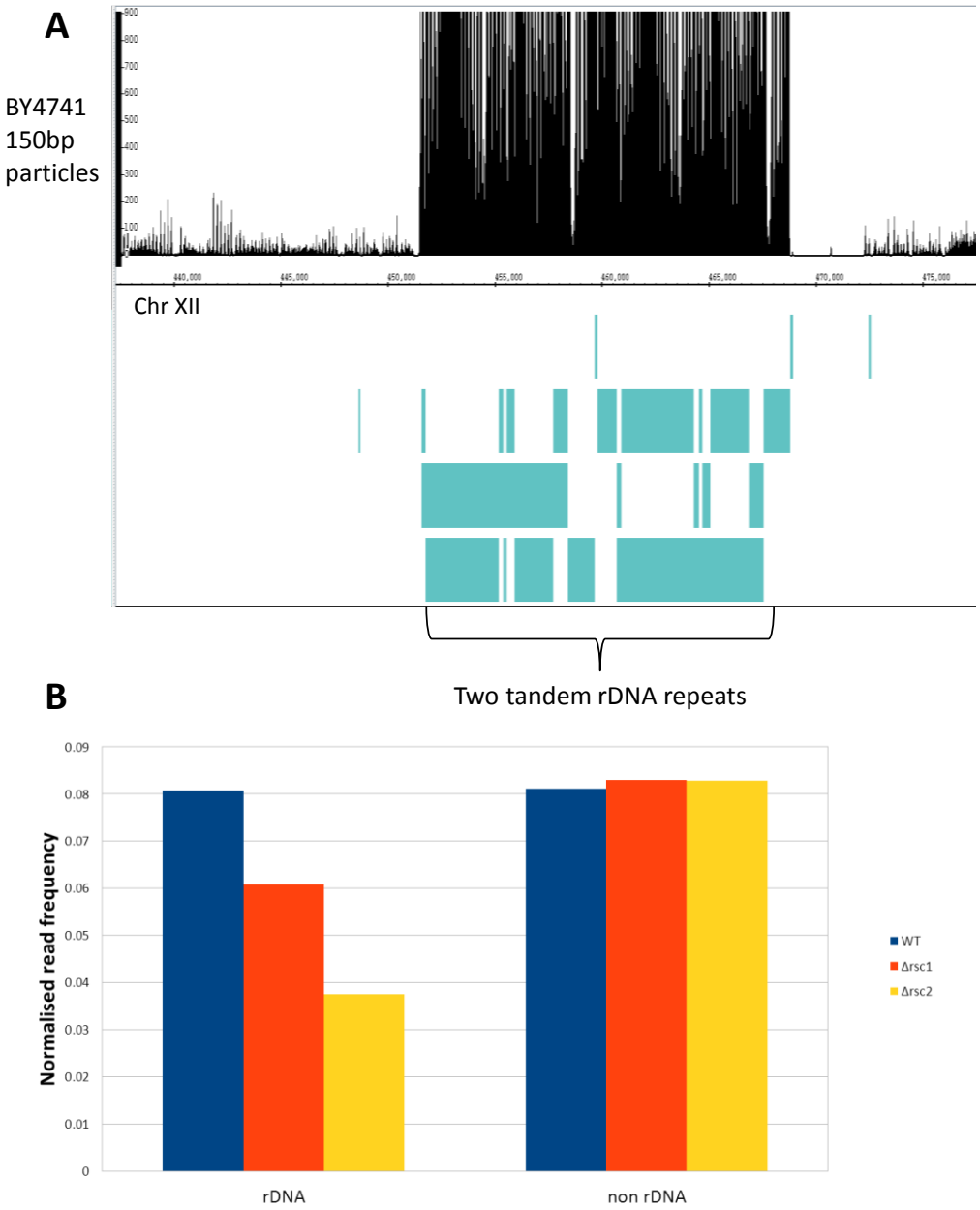

Figure 6.3 – The CPSA sequence read discrepancy at chromosome XII is RSC-dependent and associated with the rDNA repeat

Yeast rDNA is located on Chr XII and consists of tandem repeats to which all read-pairs from CPSA are aligned within the coordinates 451450 and 468780. **A –** Rendering the rDNA region of Chr XII shows that the rDNA is overrepresented as 100-200 copies of the region are aligned to two sequence copies in the reference genome **B** – The frequency of reads with a read-pair centre within 451450 and 468780 (rDNA) and reads with centres outside these coordinates (non-rDNA) were normalised by read depth and plotted for the WT, Δ*rsc1*, and Δ*rsc2* strains. This shows that the number of reads for non-rDNA is similar between WT and mutant however there is a decrease in rDNA reads of 1.3-fold decrease in Δ*rsc1* and 2.1-fold in Δ*rsc2* when compared to WT.

6.4 CPSA data successfully maps the highly defined chromatin structure surrounding transcriptional start sites in *Saccharomyces cerevisiae*

The read-pair datasets were separated into ranges of end-to-end distance (50bp to 450bp in 25bp steps) and the frequency distributions of the mid-points between read-pairs were determined across the yeast genome. This procedure treats all chromatin derived read-pairs as representing ends of DNA molecules protected from micrococcal nuclease digestion by putative chromatin particles. The mid-point of each read-pair describes a single genomic position equivalent to the eukaryotic nucleosome dyad (Luger et al., 1997). Peaks in the chromatin sequence read mid-point distributions therefore represent the presence of a positioned, nuclease-resistant chromatin particle at a specific location in the genome (Kent et al., 2011). For sake of simplicity, chromatin derived sequence read mid-point positions from the CPSA method will be referred to as “particle positions”, and the sequence read end-to-end distance as chromatin particle “size class”.

To test that the sequence data was correctly mapping nucleosomes and other MNase-resistant chromatin particles in the genome, particle position cumulative frequency – or “trend” – graphs at and surrounding yeast protein-coding gene transcriptional start sites (TSSs) were plotted. Using wild-type cell data, the normalised cumulative frequency of 150bp particle positions (nucleosome positions) surrounding all TSSs as defined by Xu *et al.* (2009) over a 2400bp window (1200bp upstream and downstream) in 10bp bins shows a defined nucleosome structure (Figure 6.4A). The characteristic nucleosome free region (NFR) between 0 and -200bp relative to the TSS is observed, together with positioned nucleosomes running into the coding region (Mavrich et al., 2008).

Plotting particle frequencies for all size classes describes the entire chromatin landscape surrounding a site (Kent et al., 2011; Maruyama et al., 2013). Figure 6.4B shows normalised cumulative particle position frequencies for size classes from 50-450bp in 25bp increments plotted against the distance relative to TSSs as described above. The landscape shows the NFR from 0 to -200bp relative to TSSs which can be visualised as

a deep “valley” in the landscape. Again positioned nucleosomes are observed both in the open reading frame and upstream from the TSS. Additionally, a large peak of approximately 100bp from the TSS in the 50-75bp size classes suggests the presence of small MNase-resistant particles within the NFR. Previously these species have been shown to represent DNA-bound transcription factors (Kent et al., 2011). It can therefore be concluded that the CPSA protocol employed here is mapping chromatin structure successfully and yielding results that are comparable with previously published studies.

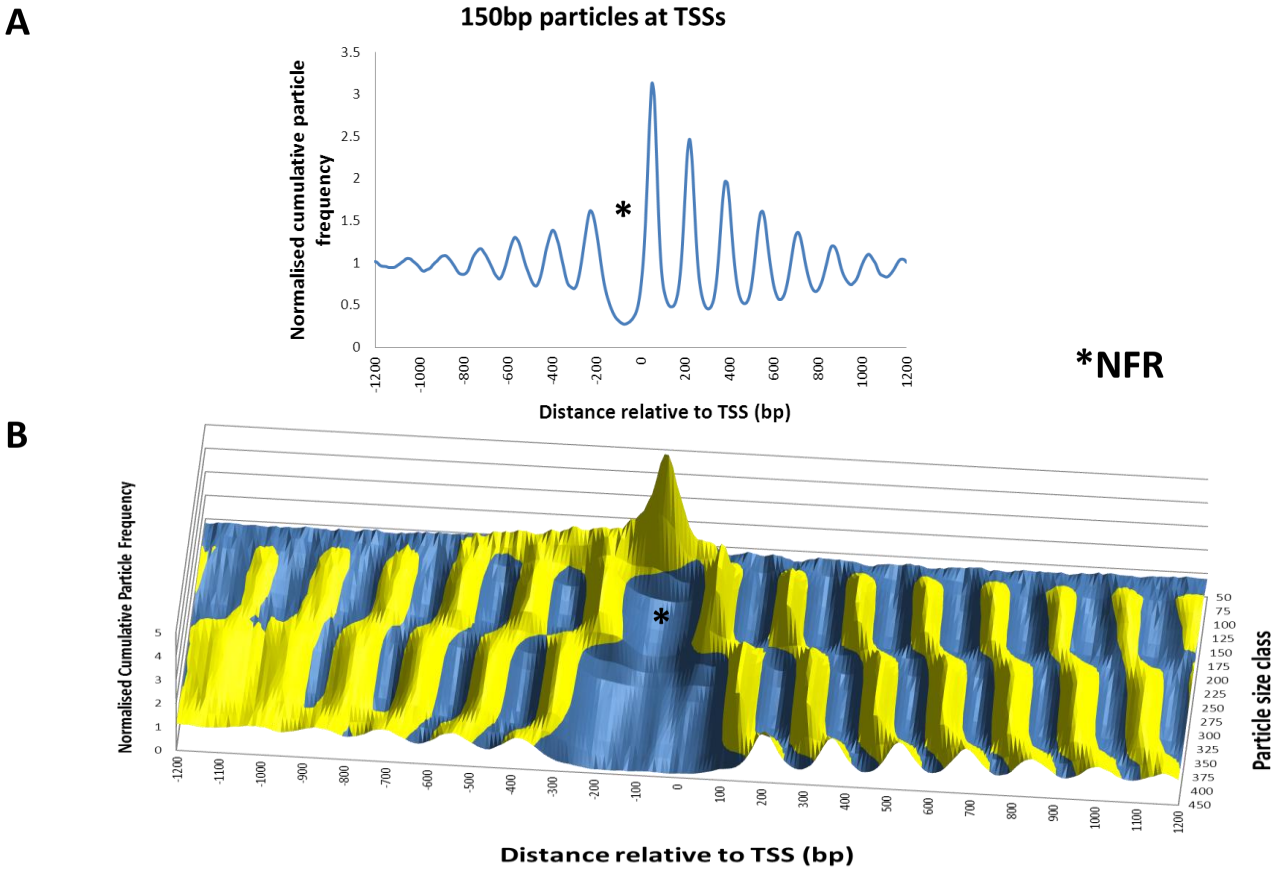

Figure 6.4 – Plots of cumulative chromatin particle frequency in various size classes from the wild-type CPSA data set, successfully reveal the characteristic chromatin architecture surrounding yeast TSSs

The cumulative frequencies of a particle size class surrounding all TSSs (n=5171; as described by Xu *et al* (2009)) in 2400bp window in 10bp bins were normalised by the cumulative particle frequency across the entire window and plotted against distance relative to the TSS to give a trend graph **A** – The cumulative frequency for 150bp particles surrounding TSSs show a nucleosome free region and position nucleosomes upstream and downstream of the NFR. **B –** Normalised cumulative frequencies for all particle size classes were rendered as a surface graph with frequencies of <1 coloured yellow and frequencies >1 blue. The graph shows TSSs have a nucleosome free region (NFR indicated by asterix) however this region is bound by particles that protect 50-75bp of DNA indicating *trans*-activating factors.

6.5 Chromatin particle landscapes surrounding protein-coding gene TSSs are altered in both *Δrsc1* and *Δrsc2* mutants

To gain a general overview of any Rsc1- or Rsc2-dependent changes in chromatin environment at yeast protein-coding genes, chromatin landscapes of the type described above (Figure 6.4) were plotted comparing the wild-type, *Δrsc1* and *Δrsc2* datasets. Figure 6.5 A-C shows that nucleosome structure at protein-coding gene TSSs is broadly similar between wild-type, *Δrsc1* and *Δrsc2* mutants. The chromatin structure for larger chromatin particles such di- and tri-nucleosomes remains similar between the three samples indicating that there is little change in the accessibility to linker regions. Strikingly there is a large apparent decrease in peak height in sub-nucleosome sized particles in the *Δrsc1* and *Δrsc2* samples when compared to wild-type. These results suggest that there may be a loss of DNA-bound transcription factors at TSSs in the absence of Rsc1 or Rsc2.

As described in the introduction (Section 1.6.2), RSC has been proposed to bind to DNA upstream of protein-coding TSSs via its Rsc3 subunit (Angus-Hill et al., 2001; Ng et al., 2002) Taking the most liberal definition of RSC binding, Badis *et al* (2008) defined 2325 of the protein coding genes to having a known TSS as having putative RSC binding potential through the CGCGC Rsc3-binding motif. Figure 6.5 D-I shows similar landscapes to those described above, but plotted for the 2325 genes identified by Badis *et al* (2008) as having putative Rsc3-binding motifs and for the remaining genes not containing the Rsc3-binding motif. These landscape plots show that the Rsc1- and Rsc2-dependent decrease in peak heights for sub-nucleosome sized particles does not appear to depend on the presence of a Rsc3-binding motif. In order to analyse these differences in more detail the datasets were broken down into individual chromatin particle size classes.

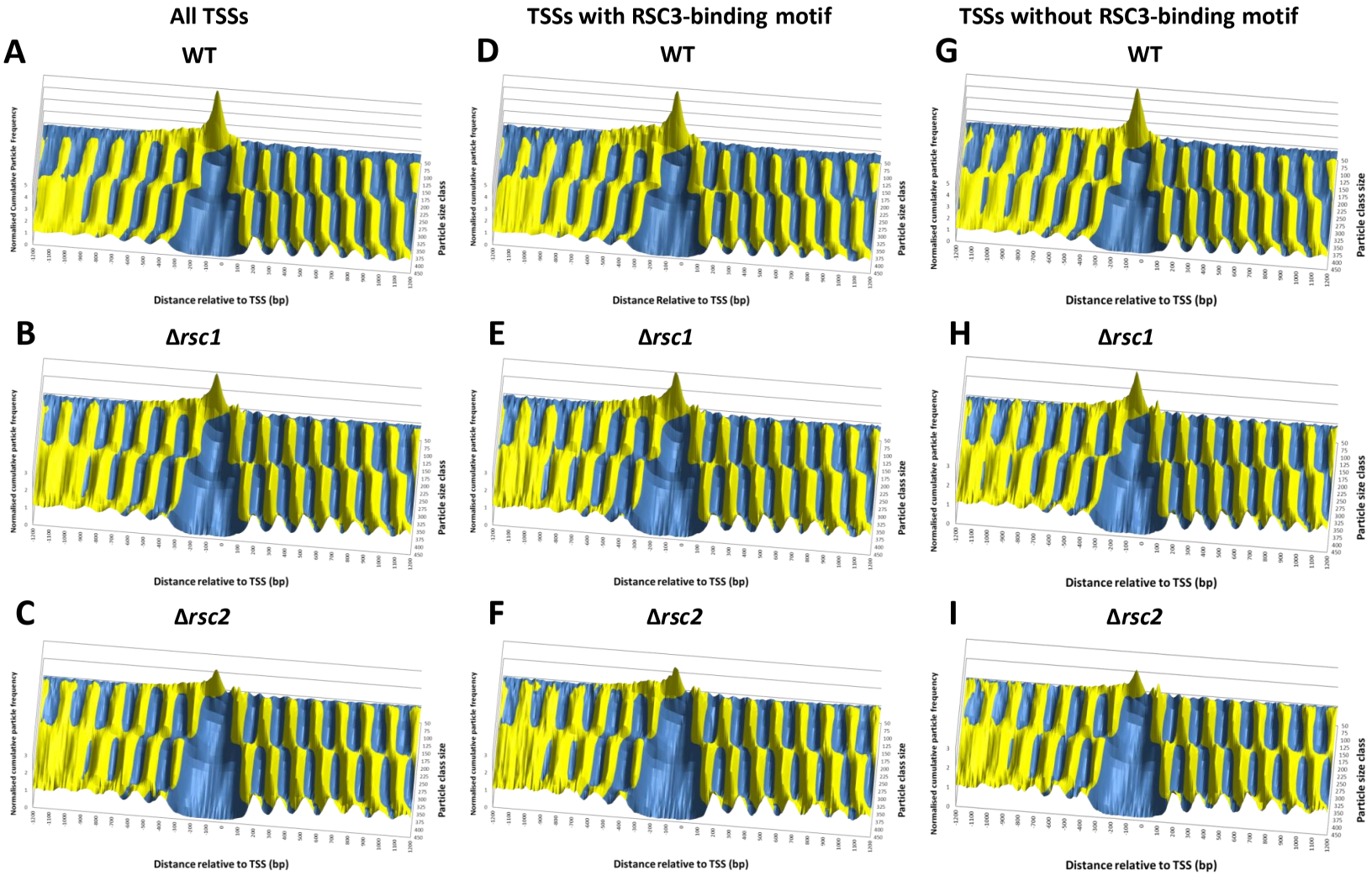

Figure 6.5 – The trend in the particle spectrum at TSSs shows a loss of particles <150bp in RSC subunit mutants
Normalised cumulative frequency for the entire spectrum of particles (50 - 450bp in 25bp intervals) were plotted in a 2400bp window centred on all TSSs (**A**), TSSs containing RSC3 binding motifs (**D**) and TSSs without a RSC3 binding motif (**G**). The similar trends are shown for Δ*rsc1* mutant **(B, E, H)** and Δ*rsc2* (**C, F, I)**. The trends show that particles of <100bp are generally lost independently of the presence of a RSC3-binding motif. The trends shown here and in Figures 6.6 and Figure 6.7 show there is little change in 150bp particles at TSSs.

6.6 Occupancy of the +1 and -1 nucleosomes surrounding TSSs is decreased in *Δrsc1* and *Δrsc2* mutants but is not dependent on the presence of the Rsc3 binding motif

To determine nucleosome-specific changes at yeast protein-coding genes in the *Δrsc1* and *Δrsc2* mutant strains, normalised cumulative frequency graphs of chromatin particle positions surrounding all protein-coding gene TSSs were compared using the 150bp size class CPSA data. Figure 6.6 A. confirms that the average positioning of nucleosomes at protein-coding gene TSSs is broadly similar in the absence of Rsc1 or Rsc2 compared to the wild-type. However, a modest, but significant ($p<0.001$, Wilcoxon Mann-Whitney test), decrease in median peak particle position frequency values comprising the +1 and -1 nucleosome cumulative frequency peaks suggests that there is some decrease in average nucleosome occupancy, or change in nucleosome position at these locations. Panel B shows the 150bp particles surrounding *ALG5* and *NEW1* rendered in the integrated genome browser (IGB) and illustrates the decrease in the peak height of the +1 and -1 nucleosome in the *Δrsc1* and *Δrsc2* samples when compared to the wild-type. This result is consistent with the average observation shown for TSSs in Panel A and suggests that the -1/+1 nucleosome occupancy rather than positioning is altered in the *rsc* mutants.

As described above, RSC has been proposed to bind to DNA upstream of protein-coding TSSs via its Rsc3 subunit and the CGCGC motif (Badis et al., 2008; Ng et al., 2002). Figure 6.7 shows the cumulative frequency graph of nucleosome positions surrounding TSSs both containing and lacking the Rsc3-binding motif as defined by Badis *et al* (2008). A significant Rsc1- and Rsc2-dependent decrease in the median peak particle position frequency values corresponding to the +1 and -1 nucleosome ($p<0.001$) occurs with both sets of genes suggesting that this effect of RSC is independent of the presence of the Rsc3-motif upstream of protein coding gene TSSs.

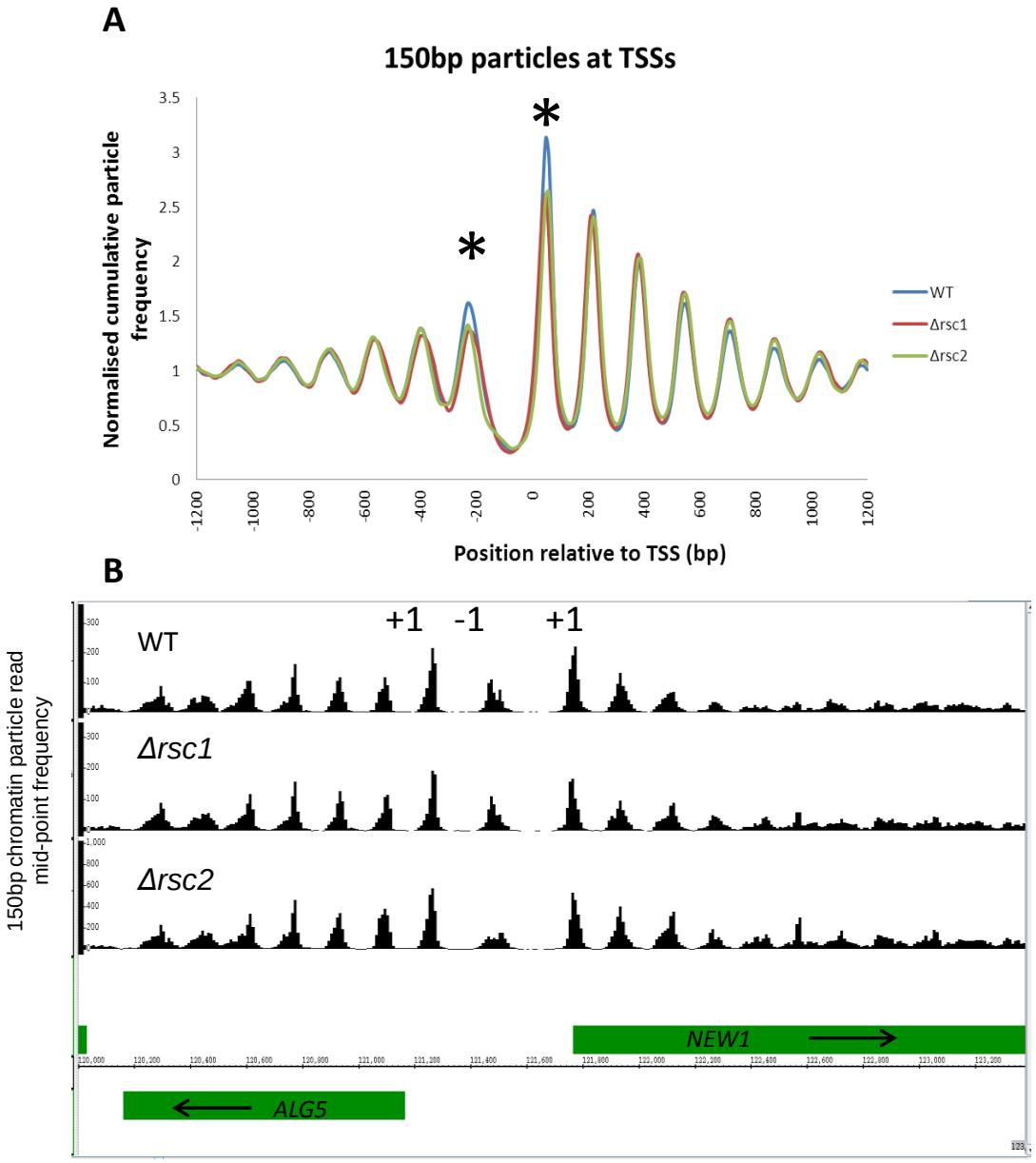

Figure 6.6 – Changes in the distribution of 150bp chromatin particles/nucleosomes surrounding protein-coding gene TSSs suggest a loss of occupancy at the +1 and -1 nucleosomes in *rsc* mutants
Normalised cumulative frequencies of 150bp particles at TSSs (n=5171) were plotted for the WT, Δ*rsc1*, and Δ*rsc2* mutants to compare nucleosome trends **A** – the cumulative frequency graphs show a significant (asterix - p<0.001 by WMW test) decrease in frequency for 150bp particles at the +1 and -1 nucleosome position surrounding TSS in both RSC subunit mutants **B** – rendering histograms of 150bp read-pairs in the integrated genome browser (IGB) shows a decrease in reads at the position of +1 and -1 nucleosomes at TSSs of protein coding regions indicating that the change in the average trend is also seen in the raw data at an individual loci

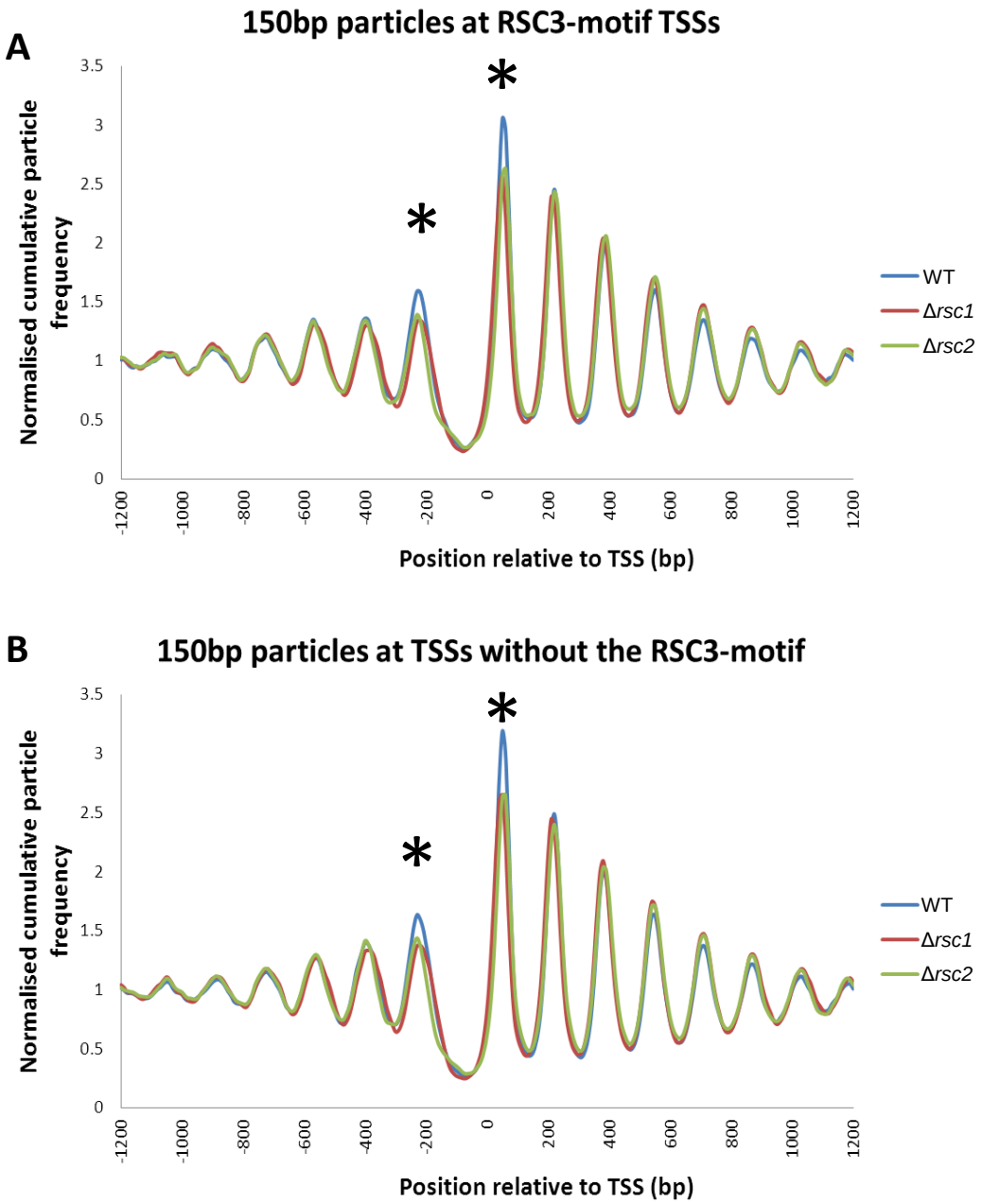

Figure 6.7 – Loss of occupancy of the +1 or -1 nucleosome at TSSs is independent of the presence of a RSC3 binding motif.
The normalised cumulative frequency of 150bp chromatin particles was plotted at (**A)** TSSs containing the RSC3 consensus binding motif (n=2325) and at (**B**) remaining TSSs that do not (n=2846). The trend graphs show that there is a significant drop ($p<0.001$) in the occupancy of the +1 and -1 nucleosome both at TSSs containing the RSC3 binding motif and those that that don not. The trend also shows subtle changes in the upstream nucleosomes in respect of the TSSs containing Rsc3-motifs.

6.7 Sub-nucleosomal MNase resistant particles associated with TSSs are dependent on Rsc1 and Rsc2

The results shown in Figure 6.5 suggest that the presence of MNase resistant chromatin particles that are smaller than nucleosomes show a change in distribution surrounding a protein-coding gene TSSs in the *Δrsc1* and *Δrsc2* mutants. Figure 6.8 shows normalised cumulative frequency graphs for the non-overlapping sub-nucleosome particle size classes, comparing wild-type to *Δrsc1* and *Δrsc2* mutants. Previously, the 50bp size class in CPSA data has been shown to represent DNA species protected from MNase digestion by the binding of sequence specific DNA binding proteins such as transcription factors (Kent et al., 2011). Figures 6.8 A-C show a decrease in peak height at a position approximately -150bp relative to the TSS which is more pronounced in the *Δrsc2* mutant than the *Δrsc1* mutant when compared to wild-type. This result would be consistent with a decrease in occupancy of transcription factors at motifs upstream of certain or all TSSs occurring in the *Δrsc1,* and to a greater extent the *Δrsc2* mutants. A similar decrease is seen at TSSs either containing or lacking a putative Rsc3-binding motif suggesting that the potential loss of DNA-bound transcription factors is independent of the presence of a Rsc3-binding motif at the TSS.

Previous CPSA studies have been able to resolve individual transcription factor bound motifs at specific genes (Kent et al., 2011). However, when the 50bp size class sequence read frequency data sets from this study were plotted at the single locus level it was found that read numbers were too low to achieve a comparison between individual loci (Figure 6.9). Therefore, it was not possible to take this part of the study any further. Nevertheless it can be concluded that loss of either Rsc1 or Rsc2 is likely to affect the transcription factor binding profiles upstream of protein-coding gene TSSs.

Although the CPSA dataset did not provide sufficient sequence read coverage to map individual 50bp MNase-resistant chromatin particles, there were sufficient reads to plot positions of 100bp particles. Figure 6.8 shows that a change is observed in the 100bp particle cumulative frequency profile

in the *Δrsc1* and *Δrsc2* mutants, and is dependent on the presence of a Rsc3-binding motif. This change is further explored at the individual locus level below.

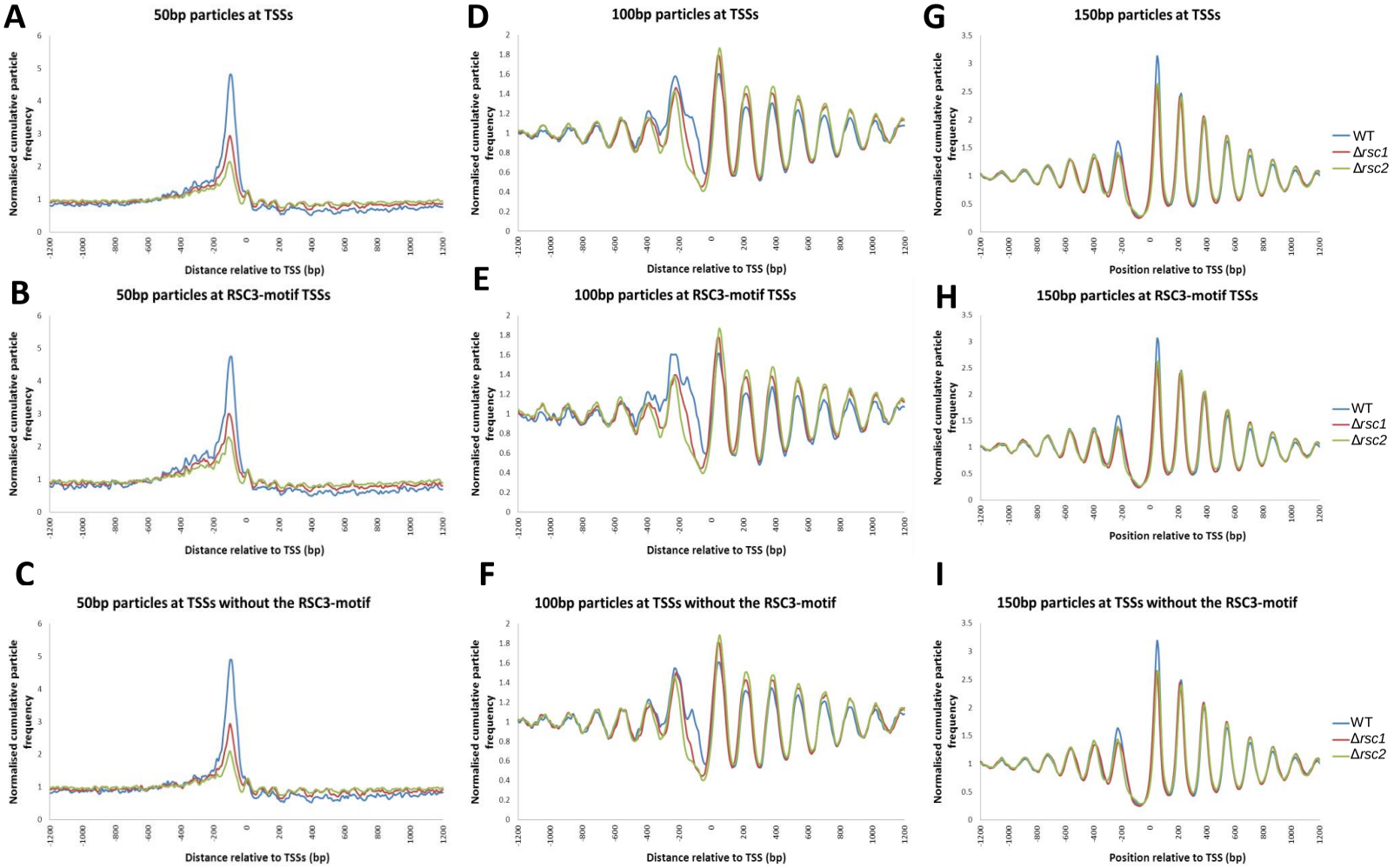

Figure 6.8 – Changes in the distribution of sub-nucleosomal chromatin particles are observed associated with protein-coding gene TSSs in both *Δrsc1* and *Δrsc2* mutants are dependent on the presence of the RSC3 binding motif

The normalised cumulative frequency graphs for 50bp, 100bp, and 150bp particles were plotted relative to TSSs (**A, D, G**), TSSs with RSC3 motifs (**B, E, F**) and TSSs without the RSC3 motif **(C, F, I)** respectively**.** WT trend is shown in blue, Δ*rsc1* trend in red and Δ*rsc2* trend in green. A loss of 50bp particles at -150bp relative to TSSs is independent of RSC3-binding motifs and is greater Δ*rsc2* compared to Δ*rsc1*. A similar loss of 100bp chromatin particles at -250bp is observed in Δ*rsc1* and Δ*rsc2* datasets at all TSSs and TSSs containing RSC3 binding motifs. This is not observed at TSSs without the RSC3 binding site.

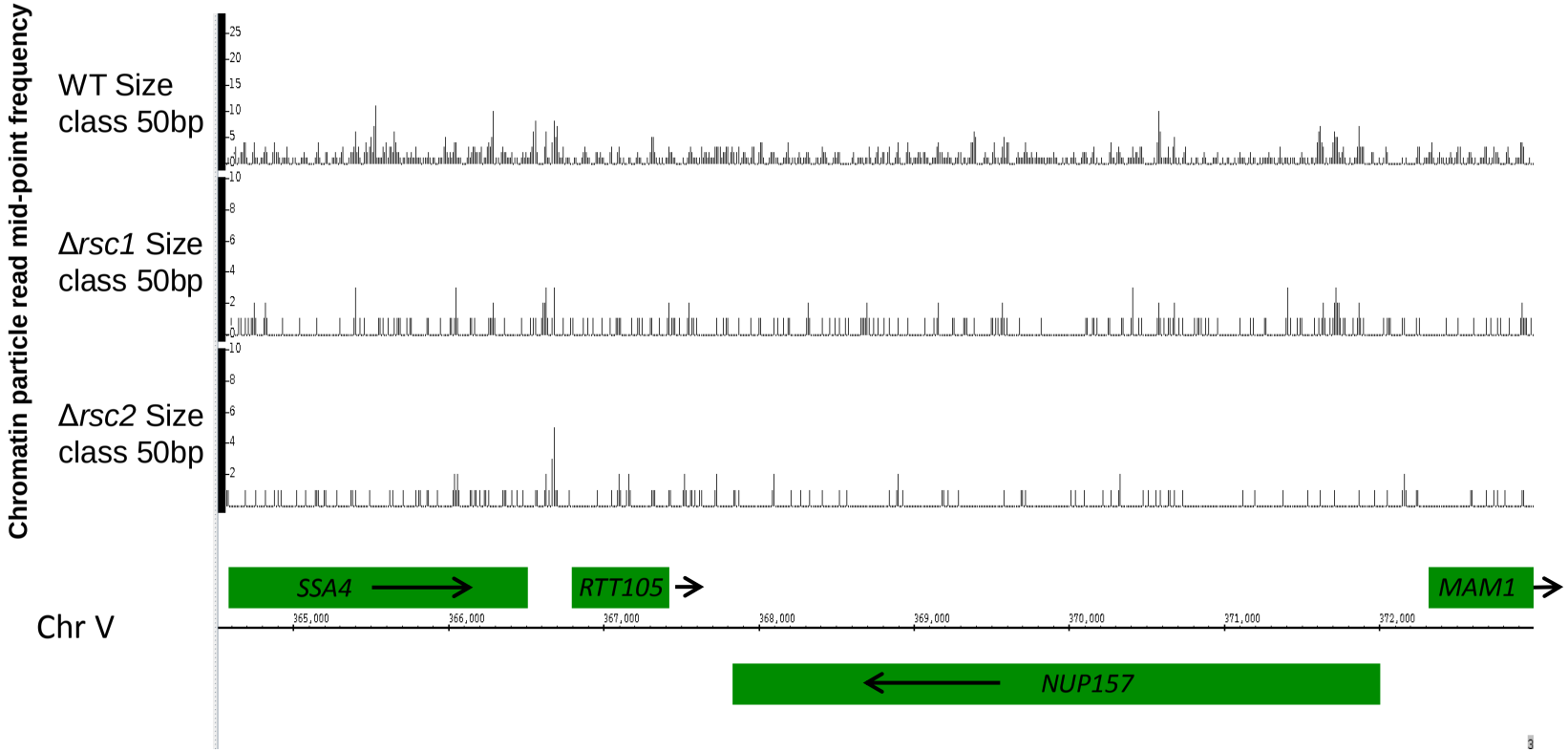

Figure 6.9 - Insufficient read depth for 50bp particle size class prevents single locus analysis and comparison
Histograms of 50bp pair reads were plotted in 10bp bins along each chromosome for wild-type, Δ*rsc1* and Δ*rsc2* datasets and rendered in the IGB to show these reads relative to the positions of open reading frames. Shown is a region of chromosome V showing that the read depth of 50bp particles in intergenic regions is very similar to that of the reads obtained across the chromosome i.e. noise, and therefore precludes analysis of the 50bp particle class size at the single locus level.

6.8 An RSC-dependent 100bp chromatin particle is observed at the *GAL1/10* UAS

Floer et al., (2010) have previously described an apparent non-canonical nucleosome associated with the upstream activation sequence (UAS) of *GAL1/GAL10* that is dependent on the RSC complex. In a r*sc3-ts* mutant a canonical nucleosome was observed to replace this structure, encroaching over the UAS to compete with Gal4 for binding (Floer et al., 2010). The DNA within the implied non-canonical RSC-remodelled nucleosome appeared to be more extensively cleaved by MNase *in vivo* to create fragments smaller than 150bp, and more typically in the region of 100-120bp.

Figure 6.10 shows a genome browser trace of the *GAL1/10* promoter with both 150bp (canonical nucleosome) and 100bp chromatin particle frequencies derived from wild-type, *Δrsc1* and *Δrsc2* data sets. Consistent with the observation of Floer et al (2010), a peak of sequence reads in the 100bp size class data is observed within the UAS region in the wild-type dataset. A similar sized peak is observed in the *rsc2* data set, but a smaller peak is observed in the *Δrsc1* dataset. One interpretation of this observation might be that the RSC-dependent non-canonical nucleosome, that this peak of reads might represent, specifically requires the activity of the Rsc1 subunit in the RSC complex. However, it should be noted that a concomitant increase in sequence reads at this location in the 150bp size class data is *not* observed in the *Δrsc1* mutant dataset. This result is therefore not consistent with the idea that this MNase-resistant region of DNA is a remodelled nucleosome, and may be more consistent with the presence of a Rsc1-dependent transcription factor complex that specifically protects 100bp of DNA from MNase cleavage. A similar result was observed at the *DNF2* locus, shown in Figure 6.11, except that in this UAS region the large 100bp peak observed in the wild-type data set is lost in both *Δrsc1* and *Δrsc2* mutants.

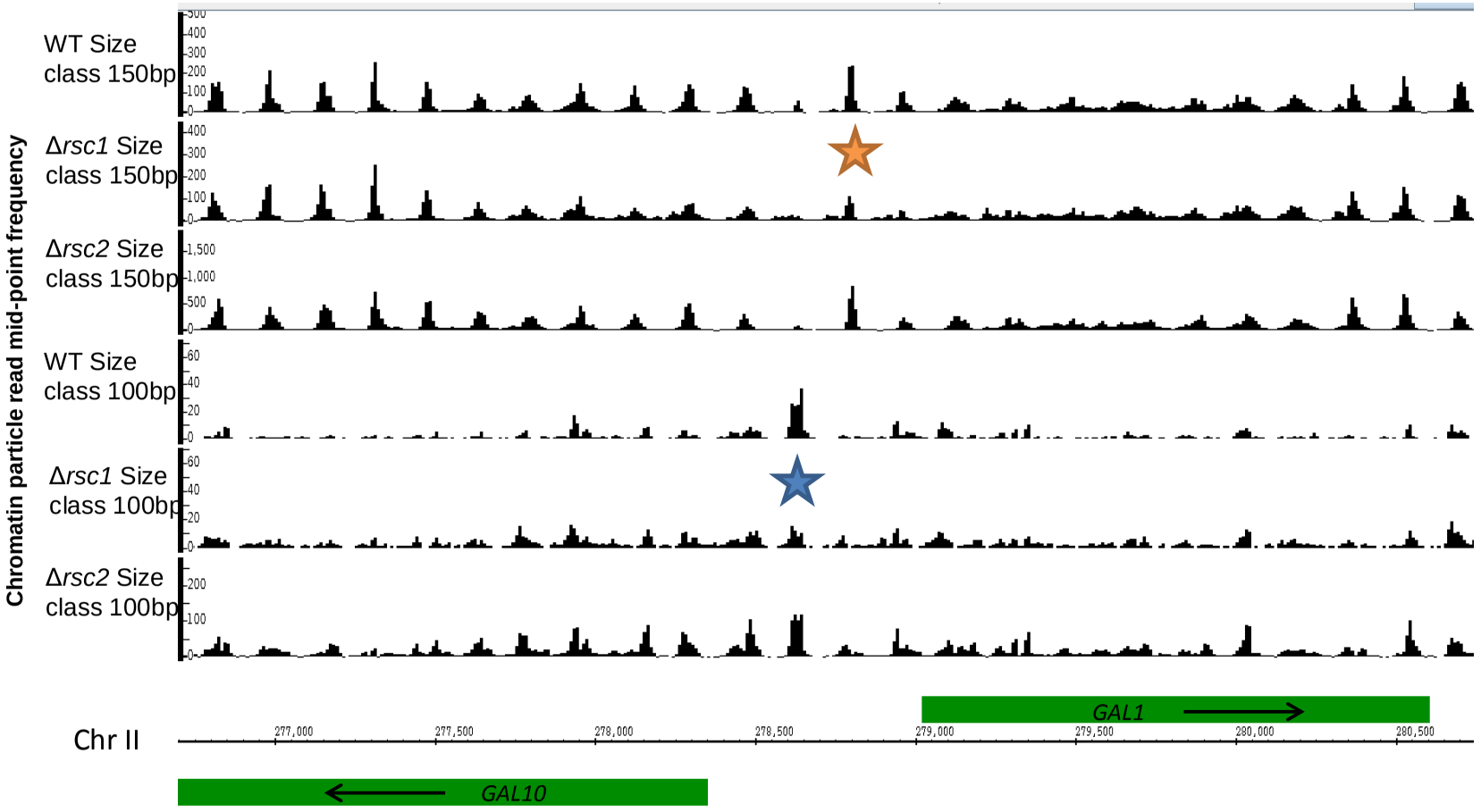

Figure 6.10 - A 100bp MNase-resistant chromatin particle within the *GAL1/GAL10* intergenic region is dependent on Rsc1
Histograms of 150bp (nucleosome) and 100bp pair reads were plotted in 10bp bins along each chromosome for wild-type, Δ*rsc1* and Δ*rsc2* datasets and rendered in the IGB to show these reads relative to the positions of open reading frames. Shown are the *GAL1* and *GAL10* loci on chromosome II with the nucleosome (150bp) and 100bp particle distributions shown in the three datasets. There is a canonical nucleosome pattern in both loci with a decrease in the height of the *GAL1* +1 nucleosome (orange asterix) in Δ*rsc1*. There is a large peak in the 100bp particle size class at the *GAL1* "-1 nucleosome" position (blue asterix) which is not present in Δ*rsc1* data set.

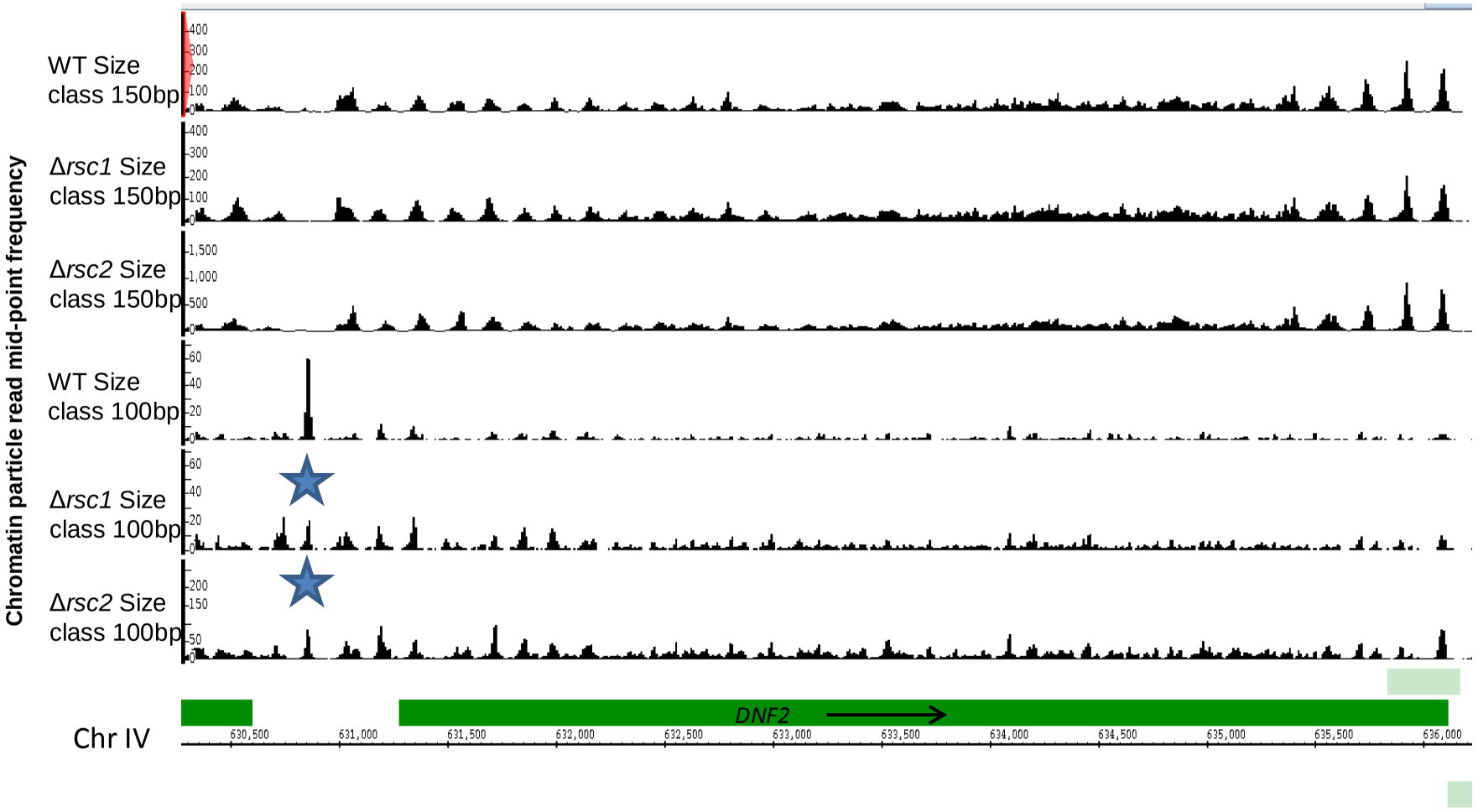

Figure 6.11 –A 100bp particle downstream of the *DNF2* TSS is dependent on Rsc1 or Rsc2
Histograms of 150bp (nucleosome) and 100bp pair reads were plotted for wild-type, Δ*rsc1* and Δ*rsc2* datasets and rendered in IGB. Shown is the *DNF2* locus on chromosome IV with the nucleosome and 100bp particle distributions shown in the three datasets. There is a little change in the canonical nucleosome pattern between the three datasets however there is a large peak in the 100bp particle size class at the *DNF2* "-1 nucleosome" position which is not present in the Δ*rsc1* or Δ*rsc2* data set (blue asterix).

6.9 100bp chromatin particles show a variable dependency on Rsc1 and Rsc2

Figure 6.8 D-F show the particle cumulative frequency surrounding protein-coding gene TSSs for the 100bp CPSA data size class. The trend of 100bp particles surrounding all protein coding gene TSSs is largely similar in distribution to that of the 150bp particles with similarly positioned particles both upstream and downstream relative to the TSS and an intervening particle free region. This result suggests that the *in vivo* MNase digestion of nucleosomes also produces DNA fragments of 100bp±20bp where MNase has accessed the histone-bound DNA of the nucleosome-DNA complex. Figure 6.8D also shows that DNA bound to nucleosomes downstream of protein coding gene TSSs are more accessible to MNase in a *Δrsc1* or *Δrsc2* mutant and therefore relatively more 100bp particles are seen compared to wild-type. In contrast, the DNA bound to the particle in the "-1" position relative to the TSS is less accessible to MNase in the mutant strains. A similar pattern is observed at TSSs containing a Rsc3-motif; DNA bound to the -1 particle is less accessible in the mutant strains compared to wild-type, however Rsc1- or Rsc2-depedent MNase accessibility is not observed at the -1 particle of TSSs lacking a Rsc3-motif. This result shows that the Rsc1- or Rsc2-dependent increase in MNase accessibility of nucleosomes downstream of the TSS is independent of the Rsc3-motif whereas the Rsc1- or Rsc2-dependent MNase accessibility of the -1 particle is dependent on the Rsc3-motif. This suggests that there are a number of protein-coding genes with a Rsc3-motif that have a Rsc1- or Rsc2-dependent particle upstream from the TSS that produces a 100bp DNA fragments after MNase digestion in the wild-type, similar to *GAL1/10* and *DNF2* shown above.

In order to determine the precise distribution of 100bp particles in the genome and their dependency on Rsc1 or Rsc2 a peak marking and comparison procedure (described in Methods 2.4.9) was applied to the 100bp particle size class datasets. The process, implemented by using a Perl script PeakMarkCompare.plx outputs three lists from a pair-wise comparison of two datasets A and B: an A_AND_B list; an A_NOT_B list; a B_NOT_A

list. An example of the output of the process is shown graphically in Figure 6.12A for the *GAL1/GAL10* locus showing the expected marking of the positions of the 100bp particle present in the wild-type dataset but not the *Δrsc1* mutant dataset. A second example (Figure 6.12B) shows a section of chromosome II where 100bp particles are present between the open reading frames of *RAD18* and *CYC8* in the wild-type but not in *Δrsc2* and a 100bp particle between the open reading frames of *TLK2* and *LYS2* that is seen in both datasets.

Table 6.1 presents the total number of 100bp-particle-peaks that were identified using this approach when comparing wild-type to *Δrsc1* or to *Δrsc2* in each of the three categories; those in wild-type and mutant, those in wild-type but not mutant, and those in mutant but not wild-type. The number of 100bp particles located in proximity to an open reading frame is also shown. The definition for “Near ORF” was defined as an intergenic particle within 400bp of the ‘ATG’ coordinates of a Rsc3-motif associated open reading frame, protein-coding or non-coding. A distance of 400bp was chosen as the Rsc1- or Rsc2-dependent 100bp particle at TSSs with Rsc3-motifs is -200bp relative to the TSS (Figure 6.8) with an additional 200bp added to account for the difference between the TSS and the ‘ATG’ codon of a gene (Xu et al., 2009; Zhang and Dietrich, 2005). For example the ATG of the *GAL1* ORF has the coordinates of 279021 however the TSS is mapped to 278856, a difference of 165bp.

There are fewer 100bp particles which are located upstream of open reading frames that match between the wild-type and *Δrsc2* datasets in comparison to wild-type and *Δrsc1* datasets. In compliment to this, the table shows that there are more 100bp particles only found in the wild-type in the absence of Rsc2 when compared to an absence of Rsc1 suggesting more 100bp particles upstream of ORFs are dependent on Rsc2 in comparison to Rsc1. The analysis has shown a total of 713 100bp particles upstream of ORFs when comparing wild-type to *Δrsc1* and 717 when comparing wild-type to *Δrsc2* showing consistency in the analysis. These data suggest that there are approximately 566 Rsc2-dependent 100bp particles compared to 357 Rsc1-dependent particles that are upstream of ORFs, however it will further

be examined how many of these 100bp particles overlap. Previous studies have estimated that RSC has approximately 700 physiological targets in the yeast genome (Ng et al., 2002) which is similar to the 566 Rsc2-dependent 100bp particles shown here.

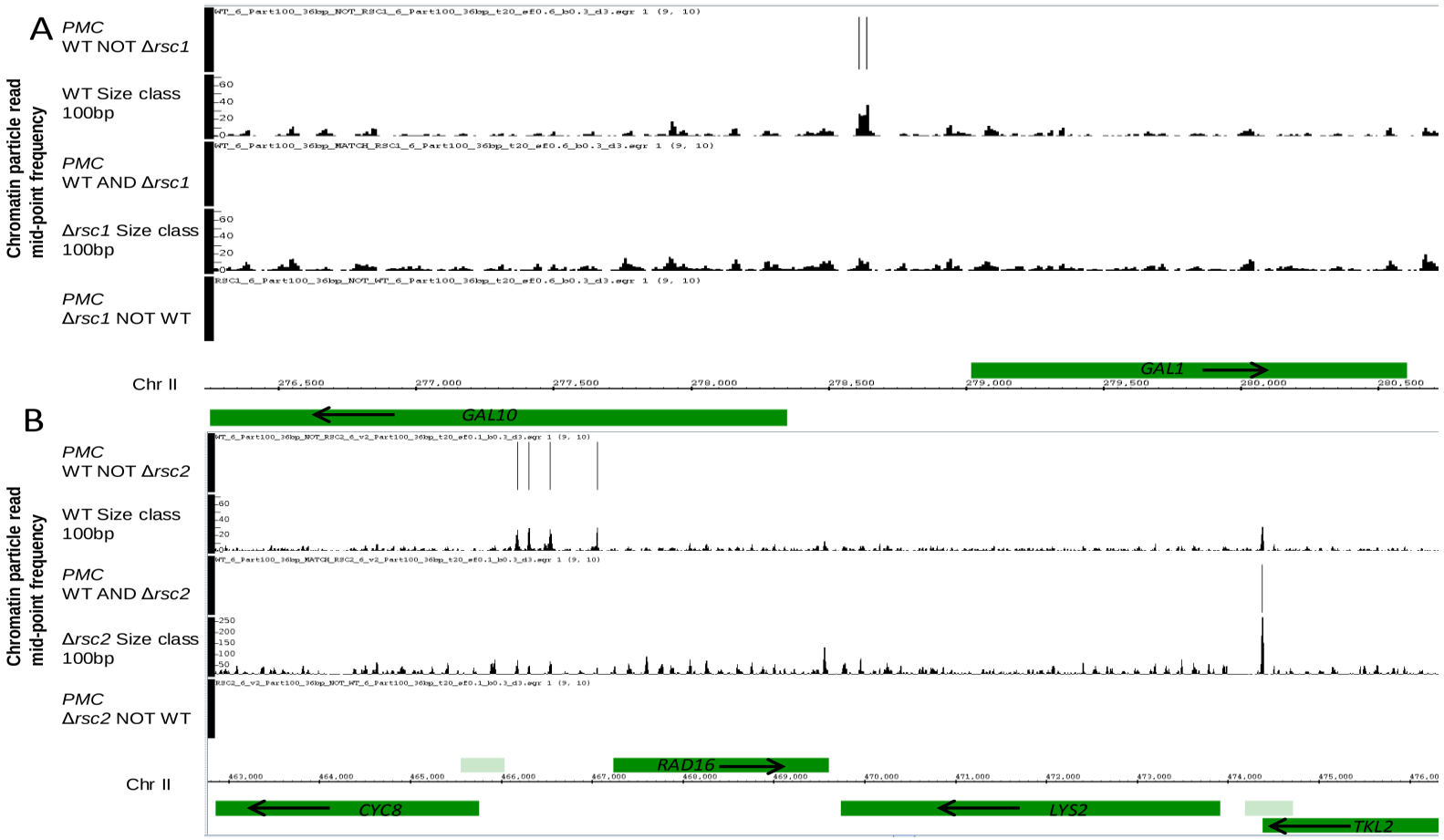

Figure 6.12 – Use of a simple differential peak marking algorithm identifies the sites of RSC-dependent 100bp MNase-resistant chromatin particles in the genome. The procedure marks chromatin particle positions as peak summits in sequence read mid-point frequency above a user-defined noise threshold in wild-type and mutant datasets that have been scaled to each other according to experimental read depth. The positions are then classified according to those that match (AND) or differ (NOT) between the two datasets. The NOT datasets include differences in position of peaks, and > two-fold differences in peak summit frequency. The procedure ignores NOT calls in frequency difference close to the noise threshold boundary to avoid simple threshold call artefacts. The screenshots show 100bp particles alongside open reading frames with peaks in one or both datasets marked with a vertical line.

	WT AND mutant		WT NOT mutant		Mutant NOT WT	
	Total	Near ORF	Total	Near ORF	Total	Near ORF
Δrsc1	930	356	740	357	152	45
Δrsc2	661	151	1096	566	183	43

Table 6.1 – A summary of 100bp particle position marking shows a number of Rsc1 and Rsc2 dependent 100bp particles positioned within 400bp of a Rsc3-motif ORF

WT AND Mutant – The number of peaks summits of greater than 20 reads (allowing for a 30% boundary window) that match between wild-type and Δ*rsc1* or Δ*rsc2* datasets and the number of those peaks within 400bp of a Rsc3-motif open reading frame. WT NOT Mutant – the number of peaks different by 2-fold between WT and mutant and the number of those peaks within 350bp of a Rsc3-motif open reading frame. Mutant NOT WT – the number of peaks different by 2-fold between mutant and WT and the number of those peaks within 350bp of a Rsc3-motif open reading frame.

6.10 Rsc1- and Rsc2-dependent 100bp chromatin particles occur upstream of ribosomal protein genes and tRNA genes

Rsc1- and Rsc2-dependent 100bp particles were identified in Table 6.1 at a number of open reading frames in the genome. Figure 6.13 shows the number of identified Rsc1- or Rsc2-dependent open reading frames that have a 100bp particle which overlap or are unique to one dataset. Nearly all Rsc1-dependent 100bp particles at open reading frames are also found in the Rsc2-dependent 100bp particle dataset with a further 223 which are unique to the Rsc2-dependent dataset. This result suggests that Rsc1 and Rsc2 have a highly similar function in setting the chromatin structure for a similar group of genes.

To determine whether these genes could be grouped functionally, GO Term analysis was performed on the open reading frames that have Rsc1- or Rsc2-dependent particles. The GO Term analysis for similar functional ontology is summarised in Table 6.2 and shows that a significant number of Rsc1- or Rsc2-dependent 100bp particles are adjacent to genes grouped by triplet codon-amino acid adaptor activity and structural components of the ribosome. These groups of genes consist of tRNA and ribosomal protein genes. These targets are consistent with previously published studies that identify ribosomal protein genes and tRNA genes as targets of the RSC complex (Angus-Hill et al., 2001; Damelin et al., 2002; Ng et al., 2002; Parnell et al., 2008).

Figure 6.13 shows that there are 223 uniquely Rsc2-dependent 100bp particles suggesting that there may be a subset of tRNA or protein coding genes that are only dependent on Rsc2. Figure 6.14 shows the normalised cumulative frequency graph of 100bp particles surrounding the 223 Rsc2-depedent sites split into tRNA genes and protein coding genes. The graphs show that even though there is a greater dependency on Rsc2 to set the chromatin structure at these loci, there is also a dependency on Rsc1. This suggests that Rsc1 or Rsc2 have overlapping functions at the 580 unique genes identified in Figure 6.12 which include tRNA and ribosomal protein

genes. Next I examined the role of Rsc1 and Rsc2 in setting the chromatin structure specifically at tRNA and ribosomal protein genes.

	GO Term Function ontology
Rsc1-dependent	Triplet codon-amino acid adaptor activity (75 of 357 p<0.001) Structural component of ribosome (44 of 357 p<0.001)
Rsc2-dependent	Triplet codon-amino acid adaptor activity (162 of 566 p<0.001) Structural component of ribosome (73 of 566 p<0.001)

Table 6.2 – 100bp particles are found within 350bp of tRNAs and ribosomal protein genes
The gene IDs of ORFs with Rsc1- or Rsc2- dependent 100bp particles were searched for similar Function GO Terms using the Sacchromyces Genome Database. Rsc1- and Rsc2- dependent 100bp particles are significantly associated with structural components of the ribosome and genes with triplet codon-amino acid adaptor activity.

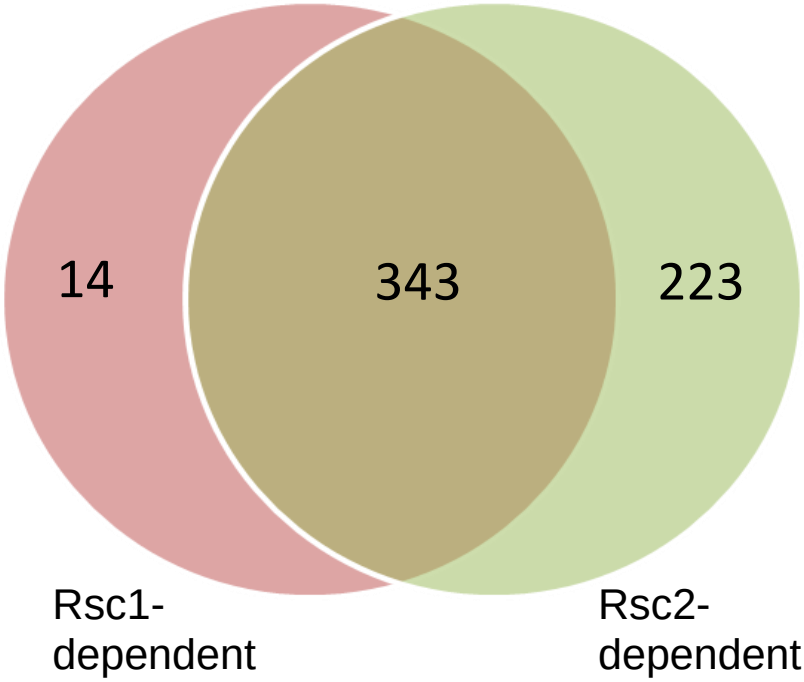

Figure 6.13– Rsc1- and Rsc2-dependent 100bp particles overlap
Open reading frames which have a Rsc1- or Rsc2- dependent 100bp particle within 400bp of the 'ATG' were compared to show genes that overlap and those that are unique to one dataset. Most of the Rsc1-dependent 100bp particles are also Rsc2-dependent and a number of particles are uniquely Rsc2-depedent.

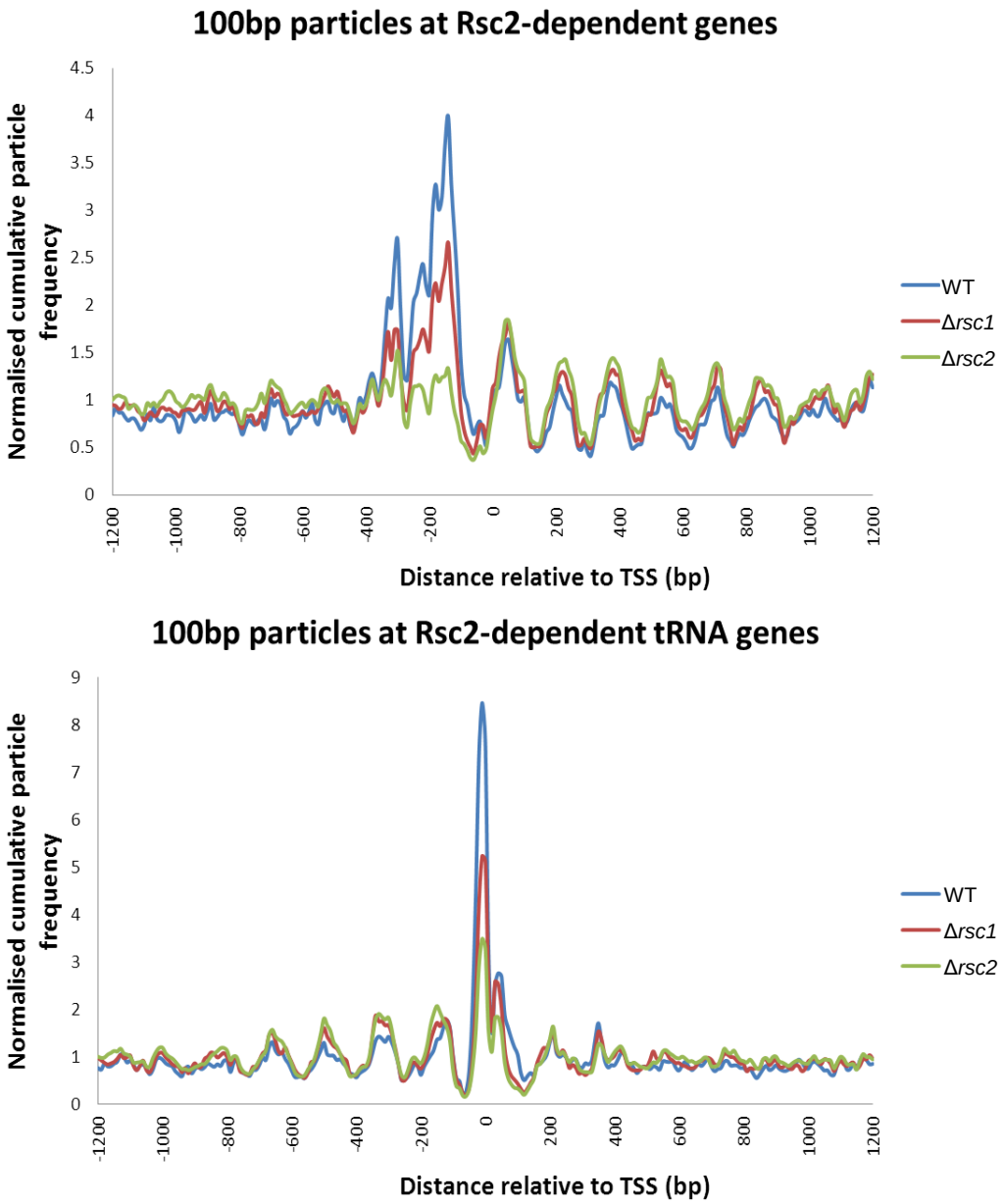

Figure 6.14 – Rsc1 and Rsc2 have similar function at 100bp particles at TSSs and at tRNA genes
Rsc1- and Rsc2-dependent 100bp chromatin particles are found at a number of overlapping genes however 223 are shown to be dependent on Rsc2. The trend of 100bp particles is shown for the protein-coding and tRNA genes with an Rsc2-dependent 100bp particle. The trends show that, even though there is a larger decrease in the peak height in the absence of Rsc2, there is still a decrease in peak height in the absence of Rsc1 suggesting overlapping function.

6.11 tRNA gene chromatin structure is Rsc1- and Rsc2-dependent

S. cerevisiae has 274 intact tRNA genes which are approximately 73-95 nucleotides in length (Hani and Feldmann, 1998).The chromatin structure of tRNA genes is regulated by three chromatin remodelling complexes ISWI1, ISWI2, and RSC; ISWI2 positions upstream nucleosomes, ISWI1 maintains the gene body as a nucleosome free regions and RSC targets the downstream nucleosomes (Kumar and Bhargava, 2013). Furthermore, Valenzuela *et al.* (2009) have presented data that suggest that in the absence of Rsc2 there is a decrease in RNA pol III transcription factors. This may also interplay with the tRNA-*HMR* barrier which prevents Sir2-mediated chromatin silencing from spreading (Valenzuela et al., 2009). Alongside these observations, the data presented above suggest that the RSC complex targets tRNA genes in order to modify the chromatin structure.

Figure 6.15 shows normalised cumulative frequency graphs for 100bp and 150bp particles in a 1200bp window centred on the TSS of yeast tRNA genes that have a Rsc1 or Rsc2-dependent 100bp particle as determined in Section 6.9. It is important to note that the tRNA gene body will lie between 0 and +100 relative to the TSS due to the short nature of the coding region. A significant decrease in the peak height of 100bp particles over the TSS of the tRNA between the wild-type and mutant strain suggests that there is a decrease in the binding of a particle at the TSS in the *Δrsc1* and *Δrsc2*. A significant decrease in 100bp particles over the gene body was only observed in the absence of Rsc2. In the nucleosome size class data there is no change in the pattern of ISWI2-dependent upstream nucleosomes between the wild-type and mutant strains however there is a slight, but significant, shift of the RSC-dependent downstream nucleosomes towards the TSS in the *Δrsc1* mutant. No significant change is observed in the *Δrsc2* mutant. The small 150bp peak that lies across the tRNA gene body may be attributed to a combined cleavage product of the two 100bp complexes that border the TSS and sit across the gene body.

Figure 6.16 shows the 100bp and 150bp size class particle histograms rendered in IGB showing a decrease in 100bp particle peak heights upstream

and over the body of the tRNA gene in the *Δrsc1* and *Δrsc2* datasets. This shows that the loss of 100bp chromatin particles is observed at the individual locus level. In the absence of Rsc1, the downstream nucleosome at tT(AGU)N1 (Figure 6.16A) is closer to the tRNA gene in comparison to wild-type (indicated by arrow).

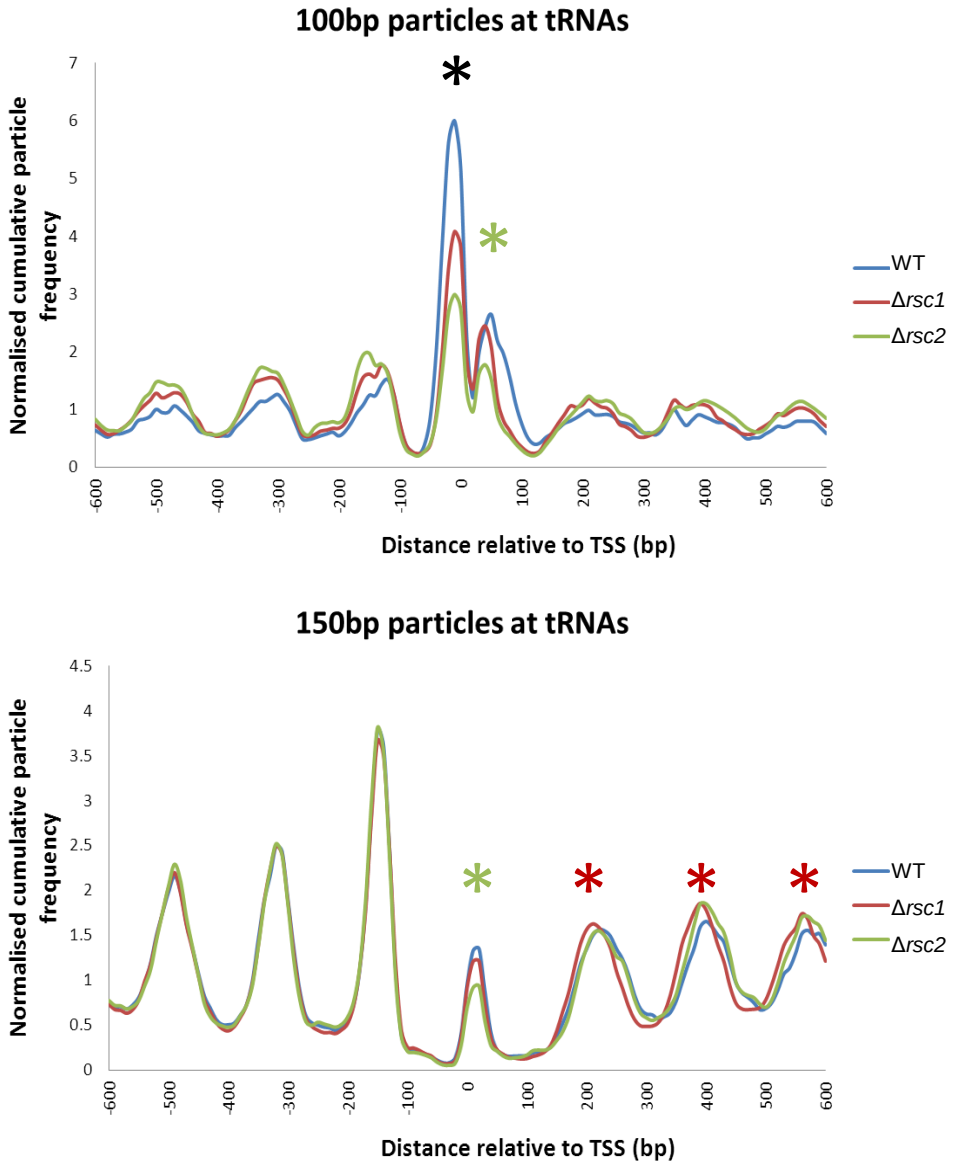

Figure 6.15 – Rsc1 and Rsc2-dependent 100bp particles are found at the TSS of tRNAs
Trend graphs of normalised cumulative frequency of 100bp and 150bp were plotted in a 600bp surrounding the TSS of yeast tRNAs (n=274) for wild-type (blue), *Δrsc1* (red) and *Δrsc2* (green) datasets. The trends show a significant change in peak heights for 100bp particles upstream of the body of tRNAs (black asterix) and a significant in the peak height of 100bp particles in the body of tRNAs in the Δ*rsc2* datasets (green asterix). A significant loss of 150bp particles is seen in the *Δrsc2* dataset (green asterix) and a significant shift in nucleosomes towards the tRNA gene body is seen in the *Δrsc1* dataset (red asterix).

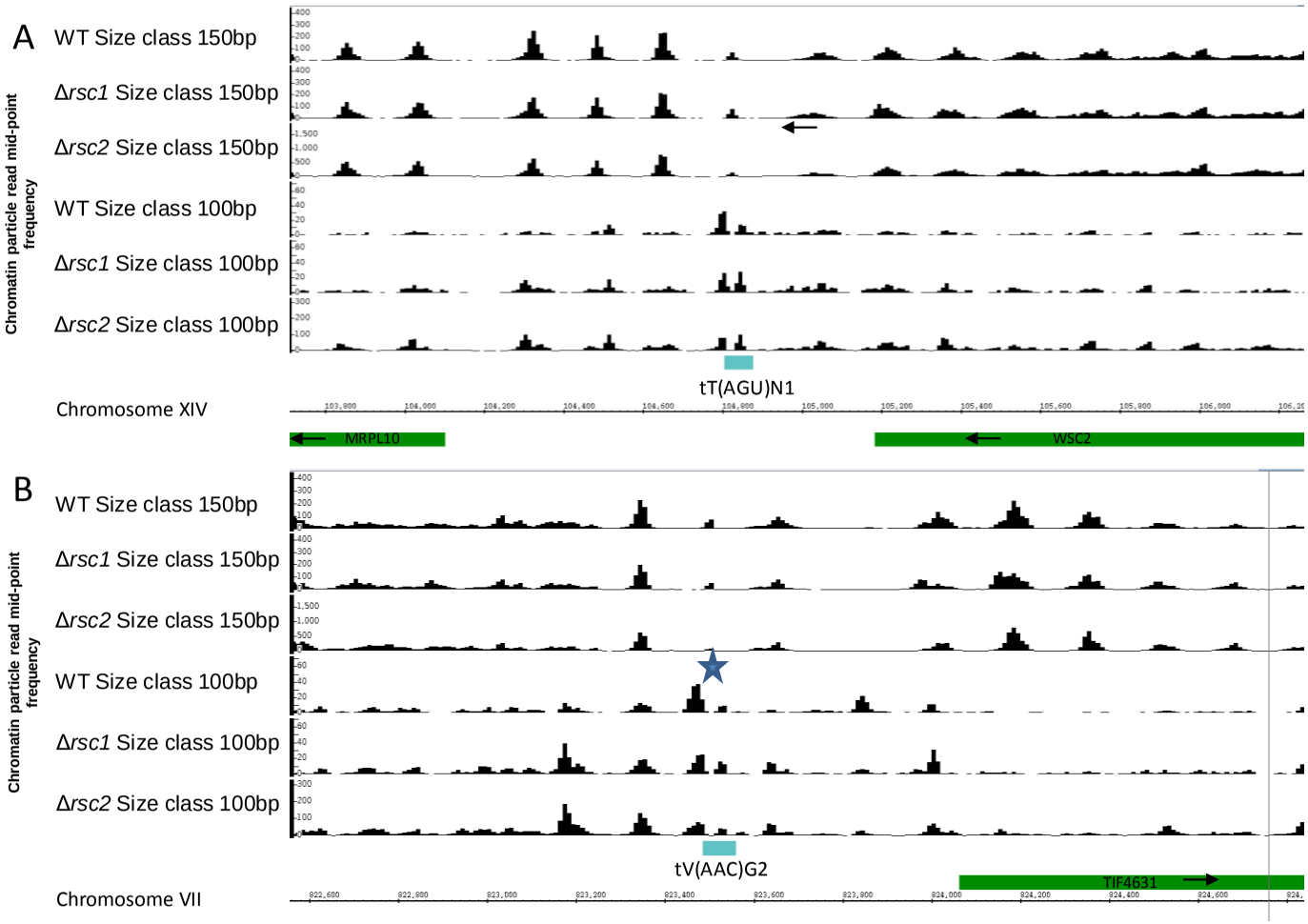

Figure 6.16 – Particle histograms show a decrease in 100bp at tRNA gene border in Δ*rsc1* and Δ*rsc2* datasets
Two examples of tRNA genes with the respective 150bp and 100bp particle data for the wild-type and mutants. tRNA reading frames are shown in blue boxes. A decrease of 100bp particles is observed at the tRNA border in both the absence of Rsc1 or Rsc2 (blue asterix). In the example of tT(AGU)N1 there is a slight shift of the first downstream nucleosome in the absence of Rsc1 (indicated by arrow) but not in the absence of Rsc2. The small 150bp particle that sits in the otherwise NFR over the tRNA body is likely to be a digest product of the tandem smaller particles that border and are within the tRNA.

6.12 A 100bp particle associated with Fhl1 binding sites is dependent on Rsc1 or Rsc2

Using the *S. cerevisiae* GO database to search for proteins of similar function, it is evident that Rsc1 and Rsc2 have an overlapping function in setting a 100bp chromatin particle upstream of the TSS of ribosomal protein genes. Many studies have identified the RSC complex as being bound at ribosomal protein genes but little is understood of the function of the RSC complex in this environment (Angus-Hill et al., 2001; Ng et al., 2002; Parnell et al., 2008). Fhl1 is a transcription factor that regulates expression of ribosomal protein genes, and Leinschmidt et al (2006) have suggested that Fhl1 binding is dependent on the RSC complex (Kasahara et al., 2007; Kleinschmidt et al., 2006).

Figure 6.17 shows the normalised cumulative frequency graphs of 100bp, and 150bp particles in a 2400bp window centred on Fhl1 binding sites comparing wild-type, *Δrsc1*, and *Δrsc2* datasets. The peak height in the 100bp particle size class is lower over the Fhl1 binding site in both *Δrsc1* and *Δrsc2* dataset with a larger, and significant, decrease only seen in the latter. A significant decrease is also seen in the 100bp particles from +100 to +250 relative to the Fhl1 binding site in both mutant datasets compared to wild-type. The trend of nucleosomes downstream of Fhl1 binding sites is similar to that of the average trend of TSSs shown in Figure 6.4. This suggests that Fhl1-bound ribosomal protein genes generally have a similar chromatin environment to canonical transcriptional start sites with positioned nucleosomes downstream of the binding region and a nucleosome free region over the Fhl1 binding site.

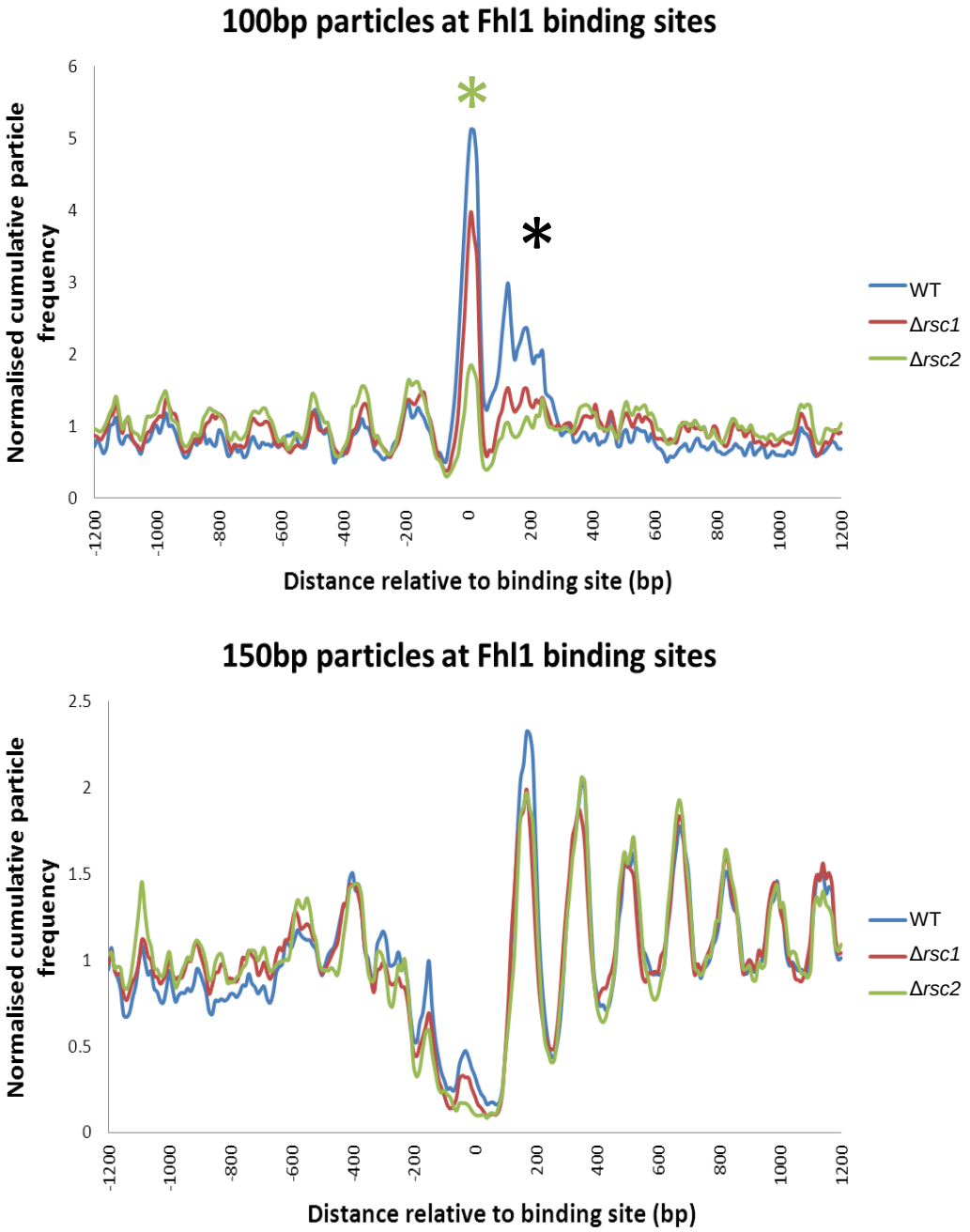

Figure 6.17 –Rsc1 and Rsc2-dependent 100bp particles are found at Fhl1 binding sites
Normalised cumulative frequency graphs of 100bp and 150bp were plotted in a 2400bp window surrounding the Fhl1 binding sites as determined by MacIsaac *et al* (2006) (n=78) for wild-type (blue), Δ*rsc1* (red) and Δ*rsc2* (green) datasets. The graphs show a large decrease in peak height in 100bp particles over the Fhl1 binding site with a larger and significant decrease observed in the Δ*rsc2* dataset in comparison to a small and insignificant decrease in Δ*rsc1* (green asterix). There is a further significant decrease in 100bp particles +100bp to +250bp relative to the Fhl1 binding site in both mutant strains (black asterix). The trend of 150bp particles shows that the nucleosomes at Fhl1 sites are positioned downstream relative to the Fhl1 binding site but a disorganised chromatin structure upstream of the binding site.

6.13 Underlying DNA sequence shows a number of transcription factors associated with Rsc1 or Rsc2-dependent 100bp particles

Figure 6.17 shows that Rsc1 and Rsc2 are necessary to assemble 100bp chromatin particles at Fhl1 binding sites. To determine whether 100bp particles are located at other transcription factor binding motifs throughout the genome, DNA sequences surrounding the locations of Rsc1- or Rsc2-dependent 100bp chromatin particles were extracted and common motifs within them determined using the motif discovery software DREME (Bailey, 2011). Table 6.3 shows conserved motifs (Enrichment pvalue <0.001) that were determined using the motif discovery software, occurring within the surrounding 200bp underlying DNA sequence of Rsc1- and Rsc2-depedent 100bp chromatin particles. The conserved DNA motifs were compared to conserved binding motifs for transcription factors (allowing for one substitution) using **Yea**st **S**earch for **T**ranscriptional **R**egulators **A**nd **C**onsensus **T**racking (Abdulrehman et al., 2011) and the results are shown in Table 6.3. There are 3 associated motifs with Rsc1-dependent 100bp particles compared with 11 with Rsc2-dependent 100bp particles. However a number of transcription factors overlap between the two, for example Rsc1- and Rsc2-dependent 100bp chromatin particles are found at Fkh1 and Fhk2 binding sites. This suggests that Rsc1 and Rsc2 may have functional redundancy at setting chromatin structure at these transcription factor binding motifs.

To investigate this possibility further, I examined the trend in genome-wide chromatin structure at, and surrounding, the TF binding sites that were generated in the previous analysis. Figure 6.18 shows the normalised cumulative frequency of 100bp particles comparing wild-type to *Δrsc1* and wild-type to *Δrsc2* in a 2400bp window centred on the binding sites of transcription factors that are potentially associated with Rsc1- and Rsc2-dependent chromatin particles (Figure 6.18 - Gcr1, Mot3, Msn4 and Xbp1, Appendix A.2 and A.3 Ash1, Azf1, Fkh1, Fkh2, Msn2, Pho4, Rtg3, Stb5, and Swi4). A pronounced peak in the trend of 100bp particles at the transcription

factors binding sites of Gcr1, Msn4 and Swi4 (Appendix A.3) is lost in the *Δrsc1* and *Δrsc2* datasets. 100bp particles surrounding transcription factors which are not associated with Rsc1- or Rsc2-dependent 100bp particles according to the analysis above only show a modest decrease in 100bp particles in the absence of Rsc1 or Rsc2 (Figure 6.19). These results suggest that some transcription factor binding sites have strongly positioned 100bp particles which are dependent on Rsc1 or Rsc2.

Rsc1-dependent		Rsc2-dependent	
MOTIF	**Transcription Factors**	**MOTIF**	**Transcription Factors**
DTATATAW	Fkh1, Fkh2	GGWTCGA	Ash1, Gcr1, Rtg1, Rtg3, Stb5, Xbp1
GGWTCGA	Ash1, Gcr1, Rtg1, Rtg3, Stb5, Xbp1	MAARAAA	Swi4
RAAAAAGA	Cup2	ACTBGGCC	Hac1, Skn7, Stb5, Xbp1, Rim101
		DATATA	none
		ACCACKA	Fkh1, Fkh2, Gis1, Msn2, Msn4, Nrg1, Rph1, Stb5, Xbp1
		BTAAGGCG	Gcr1, Gis1, Msn2, Msn4, Nrg1, Rph1, Stb5
		AAGARA	Mot3
		CGMGCTAC	Hac1, Rtg1, Rtg3, Stb5
		TGGCGYAA	Gcn4, Stb5
		CCATCGTK	Gcr1, Hac1, Mot3, Nrg1, Pho4, Stb5, Xbp1
		ATACTGAM	Ash1, Fkh1, Fkh2, Rtg1, Rtg3, Stb5

Table 6.3 – Rsc1- and Rsc2-dependent 100bp chromatin particles are associated with similar transcription factors
The 200bp underlying DNA sequence surrounding Rsc1- or Rsc2-dependent 100bp particles was extracted and common motifs were searched for using DREME as described by Bailey (2011). Those with an Expected pvalue <0.001 are shown. Transcription factors with similar binding motifs (allowing one substitution) are shown alongside each conserved motif.

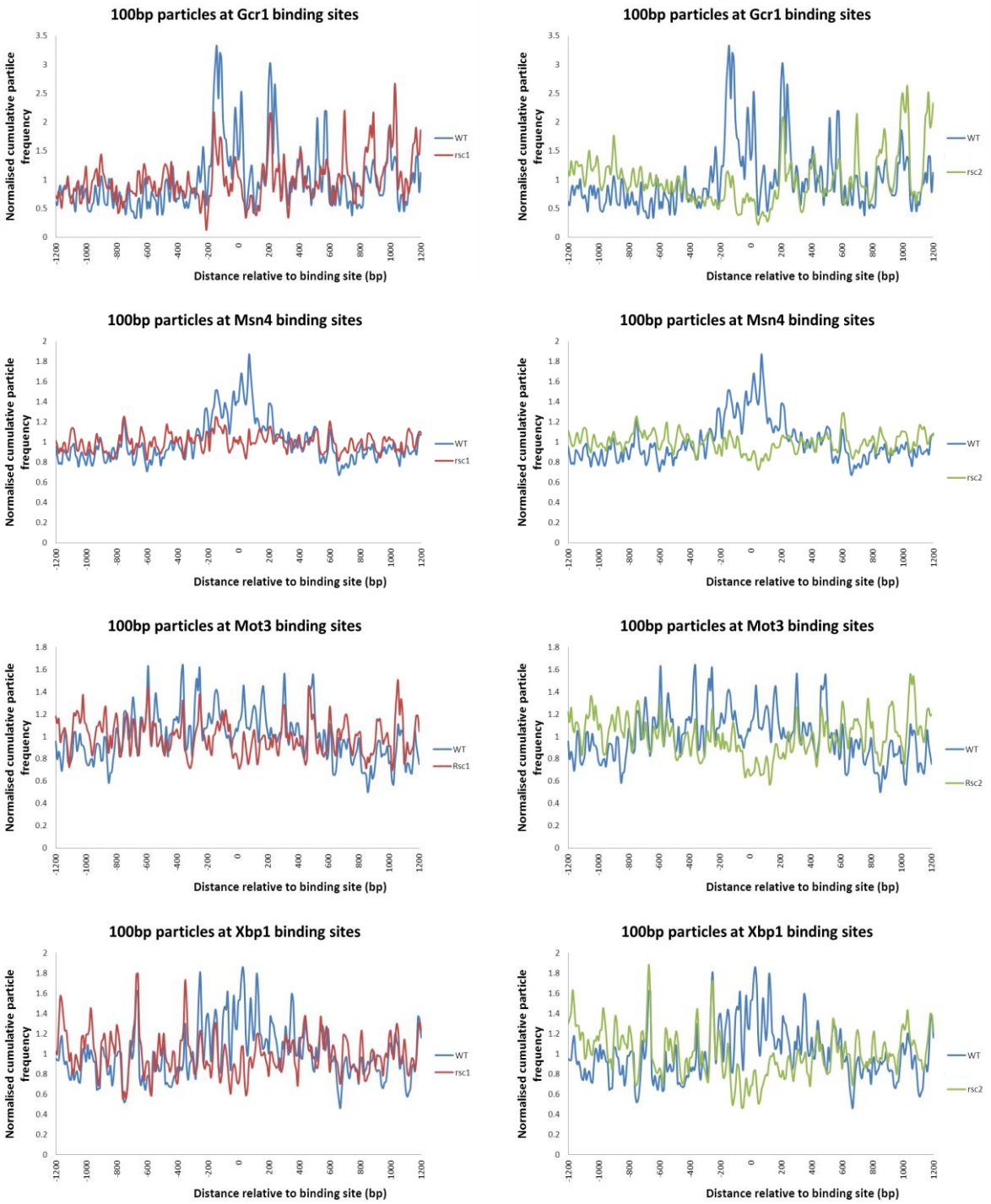

Figure 6.18 – 100bp particles are generally lost at TF binding sites in the absence of Rsc1 or Rsc2
The trend graphs for 100bp particles surrounding a 2400bp window centred on the transcription factor binding site (Gcr1 n=10, Msn4 n=161, Mot3 n=63, Xbp1 n=37) that are associated with Rsc1- and Rsc2-dependent 100bp particles show that in the wild-type a strongly positioned 100bp particle is found over (i.e. Msn4) or bordering (i.e. Gcr1) the binding site. The trends show that this peak height decrease in the absence of Rsc1 (red) or Rsc2 (green) with a greater decrease seen in the latter. A decrease of 100bp particles is generally seen at all transcription factor binding sites.

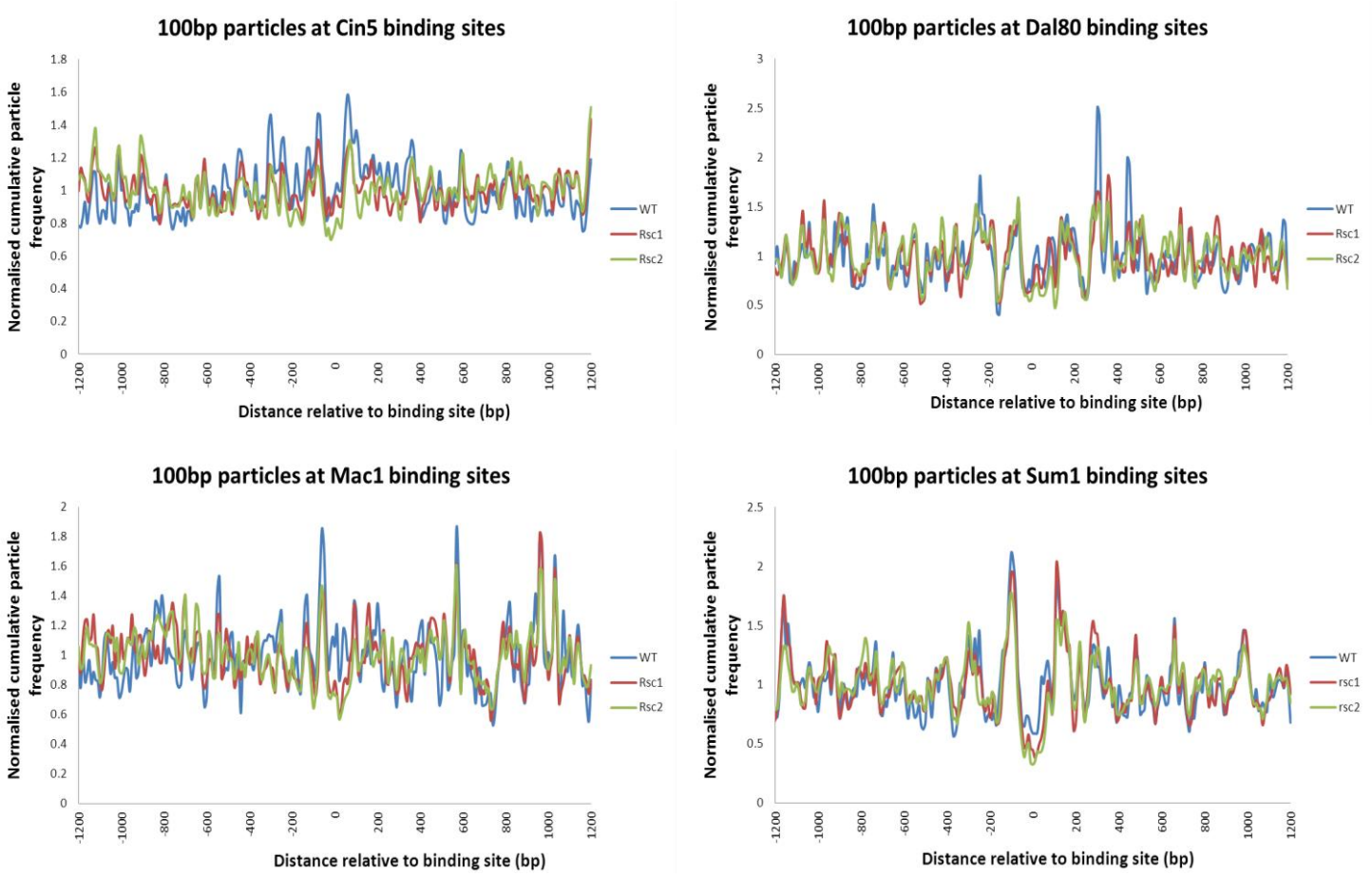

Figure 6.19 –Rsc1 and Rsc2-dependent 100bp particles are not associated with transcription factors that do not have a conserved motif in the underlying DNA surrounding 100bp particles

Normalised cumulative frequency graphs of 100bp particles were plotted in a 2400bp surrounding the binding sites of Cin5 (n=113), Dal80 (n=24), Mac1 (n=37) and Sum1 (n=49) as determined by MacIsaac *et al* (2006) for wild-type (blue), Δ*rsc1* (red) and Δ*rsc2* (green) datasets. The trends show that these transcription factor binding sites have some dependency on Rsc1 or Rsc2 to set 100bp chromatin structure but there is no loss of strongly positioned particles

6.14 Summary

In this chapter I have used CPSA (Kent *et al.,* 2011) to map the chromatin landscape in *Δrsc1* and *Δrsc2* mutants. The RSC complex has been shown previously to be associated with many sites in the genome, preferentially in intergenic regions and in close proximity to protein coding regions (Parnell et al., 2008). Rsc3 is a subunit of the RSC complex and contains a zinc-finger domain with a predicted DNA binding motif which also occurs preferentially in intergenic regions and in close proximity to protein coding regions. Therefore the RSC complex may be recruited to the genome through the Rsc3 subunit (Badis et al., 2008). Analysis shown in this Chapter indicates that the landscape of nucleosomes at genes with a predicted Rsc3 binding site within the promoter region is not distinctly different in comparison with the average chromatin landscape around a TSS with the exception of a decrease in +1 and -1 nucleosome occupancy. However, there is a loss of sub-nucleosome sized particles at Rsc3-motif-associated TSSs and the presence of 100bp chromatin particles is dependent on the presence of the Rsc3-motif.

In Sections 6.9 and onwards, 100bp MNase-resistant particles were shown to occur throughout the genome in intergenic regions and at certain locations within 400bp of open reading frames that have a Rsc3-motif. Normalised cumulative frequency graphs show that there is a dependency on Rsc1 or Rsc2 to set the chromatin structure at these loci however individual loci may show a greater dependency on Rsc1 or Rsc2 as shown with the *GAL1* and *DNF2* examples. Extraction of the underlying DNA sequence at Rsc1- or Rsc2-dependent 100bp chromatin particles reveals a set of transcription factor binding motifs that associate with Rsc1 or Rsc2 function in creating 100bp chromatin particles. However it was not possible to identify a specific transcription factor of sub-set of such factors that would uniquely define whether a Rsc1- or Rsc2-dependent chromatin structure would arise in the genome.

7 Discussion

7.1 RSC remodels nucleosomes at HO-induced double stranded DNA break in a Rsc1-dependent manner

RSC is an abundant and essential complex in *S. cerevisiae* for maintaining genomic stability when presented with genotoxic agents such as MMS (methylmethane sulphate) and ionizing radiation (Bennett et al., 2001; Cairns et al., 1996). In this respect RSC is similar to INO80, another ATPase-dependent chromatin remodelling complex found in budding yeast. INO80 is required to promote the removal of UV lesions by the nucleotide excision repair pathway by remodelling chromatin (Jiang et al., 2010) and is recruited to double stranded DNA breaks (DSBs) within 1-2 hours of their formation by HO endonuclease at the MAT locus (Conaway and Conaway, 2009). INO80 is required to remodel chromatin in the region surrounding the DSB to allow the Mre11-Rad50-Xrs2 (MRX) complex to perform 5' strand resection to facilitate the formation of single-stranded DNA which signals to activate DNA damage checkpoint pathways (Bao and Shen, 2007a).

RSC has also been identified as facilitating end joining repair of DSBs and RSC also interacts at least with Mre11 of the MRX complex (Kent et al., 2007; Shim et al., 2005). Investigations at the highly specialised *MAT* locus show that nucleosomes are rapidly remodelled away from the site of DNA damage after the induction of the DSB by the HO endonuclease (Kent et al., 2007; Shim et al., 2007). These independent studies show that the formation of a histone depleted region is required for the efficient phosphorylation of the histone protein H2A and the loading of the MRX complex to complete strand resection (Downs et al., 2004). Data presented by Kent *et al.* suggests that this remodelling event requires the RSC subunit Rsc1 whilst Shim *et al*. and Liang *et al* (2007) present contradictory data that suggest that Rsc2 is required for this DSB-dependent remodelling activity (Kent et al., 2007; Liang et al., 2007; Shim et al., 2007).

Chapter 5 shows that Rsc1 and Rsc2 are highly similar proteins as they have very similar amino acid sequences and a conserved domain profile. Data obtained from co-immunoprecipitation and mass spectrometry has

shown that Rsc1 and Rsc2 are present in two separate isoforms of the RSC complex (Cairns et al., 1999; Chambers et al., 2012a). A *Δrsc1* or *Δrsc2* mutant show growth defects and sensitivity to genotoxic agents suggesting they are required in DNA repair pathways and double *Δrsc1 Δrsc2* mutants are inviable suggesting that there is some functional overlap (Bao and Shen, 2007a; Bennett et al., 2001; Cairns et al., 1999; Chambers et al., 2012a)

Data presented in Chapter 3 and Chapter 5 show indirect end-label analysis of MNase digested chromatin of both wild type and RSC subunit mutants. These analyses show that the loss of the Rsc1 subunit results in the loss of DSB-dependent chromatin remodelling on the *TAF2* side of the HO cleavage site at the *MAT* locus in both the *MATalpha* and *MATa* locus. This remodelling activity is rescued by plasmid-borne *RSC1* but not by plasmid-borne *RSC2.* Data presented in Chapter 3 also shows that nucleosomes are remodelled at a HO-induced DSB at *LEU2* and that this remodelling event also requires Rsc1 and is independent of Rsc2 or Rsc7.

The data presented in Chapter 3 leads to three conclusions; firstly, chromatin remodelling observed at the *MAT* locus within 30-40 minutes after the induction of a DSB precedes remodelling which is dependent on INO80 (Morrison et al., 2004; van Attikum et al., 2004). Secondly it can be concluded that the remodelling of nucleosomes that is seen exclusively on the *TAF2* side of the HO-induced DSB at *MATalpha* is dependent on Rsc1 and independent of Rsc2. Thirdly, nucleosome remodelling is observed at both *MATa* and non-*MAT* HO cleavage sites, such as *LEU2,* and that the remodelling at both types of loci is Rsc1-dependent. These results contrast those of previous observations by Liang *et al* and Shim *et al* who concluded nucleosome remodelling at DSBs is Rsc2-dependent. Shim *et al.* used qPCR to determine the presence of positioned nucleosomes at *MAT* before and after induction of HO. However, they do show that 1 hour after HO induction a reduction of nucleosome is seen in a *Δrsc2* mutant compared to wild-type though this reduction is delayed (Shim et al., 2007). Liang *et al.* used indirect-end-label analysis to determine nucleosome positions before and after HO-induction at the *MAT* locus. However chromatin was digested for 5 to 15 minutes with MNase resulting blots that do not even show the large band that

wold represent a DSB or any remodelling in the wild-type strain (Liang et al., 2007). Therefore the work presented here suggests that the Rsc1-isoform of the RSC complex has a functional role distinct from the Rsc2-isoform of RSC in the repair pathway for DSBs in the context of the genome. Data showing that Rsc1 mutants are generally sensitive to genotoxic agents that cause double strand DNA breaks (Bennett et al., 2001; Oum et al., 2011), suggests that the interaction of RSC with HO-induced DSBs is independent of HO endonuclease or the underlying HO cleavage site sequence. Similar data also shows that *rsc2* mutants, and other non-essential subunit mutants, are sensitive to genotoxic agents but this may be due to mis-regulation of stress-induced genes (see below) or that *rsc2* mutants are defective in later stages of repair pathways (Chai et al., 2005; Oum et al., 2011)

Little is understood about how RSC is recruited to a DSB, though it has been suggested that RSC directly interacts with the MRX complex through an interaction with the Rsc1 and Mre11 subunits (Papamichos-Chronakis and Peterson, 2013; Shim et al., 2005). However, wild-type nucleosome remodelling at *MATalpha* is observed in *mre11* and *rad50* mutants suggesting recruitment of RSC is independent of the MRX complex (Kent et al., 2007). Both Tel1 and Mec1 are also recruited to HO-induced DSBs and repair of DSBs is defective in *mec1* mutants. (Chai et al., 2005; Lisby et al., 2004). Mec1 and Tel1 phosphorylate H2A in order to recruit further repair proteins however this phosphorylation is a process downstream of RSC complex recruitment (Downs et al., 2004; Liang et al., 2007). Therefore, the recruitment mechanism of RSC to DSBs is still elusive, though a number of hypotheses remain to be tested: RSC may be recruited to the *MAT* locus DSB via the HO endonuclease. A yeast two-hybrid screen could be used to determine whether the RSC complex and HO endonuclease physically interact; RSC may bind directly to broken DNA ends. Electrophoretic mobility shift assays (gel shift assays) could test whether RSC binds to DNA ends produced by HO endonuclease cleavage.

7.2 The BAH domain of Rsc1 confers DSB-dependent nucleosome remodelling to the RSC complex

Both Rsc1 and Rsc2 contain two bromodomains and a domain named a bromo-adjacent homology domain as it was first identified as an adjacent domain to bromodomains, though this has been shown to be not the only definition of this domain (Cairns et al., 1999; Goodwin and Nicolas, 2001). Bromodomains bind acetylated lysines as a way of recruiting complexes to other proteins or to promote or antagonise enzyme activity whereas little is currently known on the function of BAH domains (VanDemark et al., 2007). For the budding yeast cell to be viable it must contain two of the four bromodomains found in Rsc1 and Rsc2 but none are essential on their own suggesting that the bromodomains have overlapping function (Cairns et al., 1999).

The data presented in Chapter 3 shows that, despite their similarity, Rsc1 is required for DSB-dependent nucleosome remodelling, a function that cannot be complemented by Rsc2. The analysis presented in Chapter 5 shows the results of swapping the bromodomains and BAH domains of Rsc1 with the equivalent domains in Rsc2 and determining whether DSB-dependent nucleosome remodelling occurs at the *MATalpha* locus. The data shows that swapping either of the two bromodomains of Rsc1 into the similar positions of Rsc2 does not confer remodelling activity to Rsc2. Interestingly, swapping the BAH domain of Rsc1 into Rsc2 does restore DSB-dependent nucleosome remodelling as observed at the *MAT alpha.* These results provide further evidence that remodelling of nucleosomes at DSBs is Rsc1-dependent.

The importance of the BAH domain has recently been highlighted by observations of the human pBAF (polybromo) complex which contains a subunit BAF180 that contains six bromodomains and two BAH domain. There is a high prevalence of mutations in these domains in cancer demonstrating the importance of these domains in genome stability (Xue et al., 2000). BAF180 protein has been likened to an amalgamation of the three RSC subunits Rsc1, Rsc2, and Rsc4 suggesting functionality of these domains may be conserved (Brownlee et al., 2012; Goodwin and Nicolas,

2001). The BAH domain of metazoans Orc1 (origin of replication) binds histone H4 dimethylated lysine showing the BAH domain can specifically bind to proteins (Kuo et al., 2012a). However, a recent study has elucidated the 3-dimensional structure of the Rsc2–BAH domain and has shown that, *in vitro*, both Rsc1 and Rsc2 BAH domains are capable of binding histone H3 (Chambers et al., 2013). The Rsc2 structure is different to the Sir3-like BAH domain structure and interacts with histone proteins with distinct structural differences. Though the structure of the Rsc1-BAH domain has not been examined, it has been shown that, *in* vitro, the Rsc1-BAH domain is also capable of binding histone H3 (Chambers et al., 2013). After recruitment to the site of DNA damage, the RSC complex may interact with the local nucleosomes through interaction with histone H3 proteins in the nucleosome core through the Rsc1-BAH domain. Even though the Rsc1 and Rsc2 BAH domains have very similar amino acid sequence and the H3 binding residues appear to be conserved (Chambers et al., 2013), the evidence in Chapter 5 would suggest that the Rsc2 BAH domain is unable to perform the same function as the Rsc1-BAH domain. This may suggest that, *in vivo*, the Rsc1-BAH domain has a stronger binding affinity for histone proteins and allows Rsc1-RSC to interact with histones in the context of DNA damage whilst in competition with many other histone modifying enzymes. This could be investigated using gel shift assays and the prediction would be that the Rsc1-BAH can compete with the Rsc2-BAH domain for histone H3 binding.

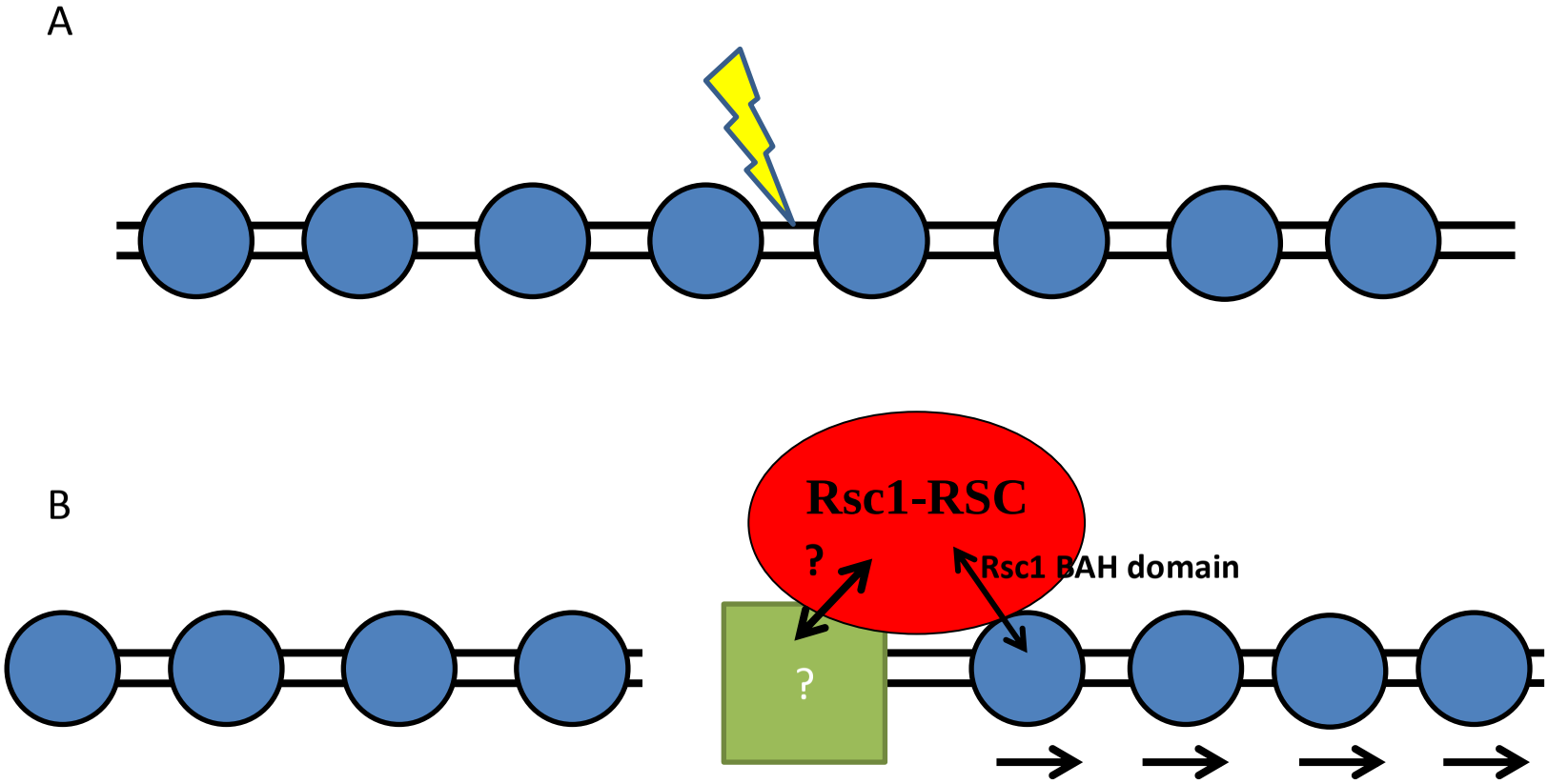

Figure 7.1 – Rsc1-dependent nucleosome remodelling at double-strand breaks
A – Genotoxic agents (yellow bolt) cause DNA damage such as double-strand breaks **B** – The RSC complex is one of the very first proteins recruited to the DSB through an as yet unknown mechanism. The Rsc1 BAH domain has DSB-dependent chromatin remodelling activity and the BAH domain has been shown to directly interact with histone proteins leading to the hypothesis that the RSC complex interacts with nucleosomes through the BAH domain. The RSC complex, using its ATPase dependent activity, translocates nucleosomes along the DNA strand away from the broken DNA ends.

7.3 Rsc2 remodels nucleosomes to form the alphasome at *MAT alpha*

The *MATing* (*MAT*) type locus is a highly specialised region of the *S. cerevisiae* genome which allows the cell to change mating type by a specialised form of homologous recombination called gene conversion (Haber, 2012). The process is initiated by the highly regulated *homothallic* (HO) endonuclease which creates a double-strand DNA break within the *MAT* locus at the boundary of the mating type specific Y region and the mating type conserved Z region (Wang et al., 1997). This chromosome lesion is then repaired using the silenced mating type cassette as a donor by homologous recombination involving both leading and lagging strand synthesis resulting in an intrachromosomal gene conversion event. Preference to use the opposing mating type cassette as a donor is achieved in 90% of mating type switching events by the alteration of the chromatin structure of chromosome III to make the opposite mating type the preferred donor (Haber, 1998; Haber, 2012).

As shown in Chapter 4, the *MATalpha* locus contains a chromatin particle that has a much larger DNA footprint than a canonical nucleosome. In a *Δrsc2* or *Δrsc7* mutant the large chromatin particle immediately flanking the HO cleavage site at *MATalpha* becomes less resistant to micrococcal nuclease. As shown in Chapter 4, the chromatin structure of *MATalpha* in a *Δrsc2* or *Δrsc7* strain becomes very similar to that observed at the similar position in *MATa*. Kent *et al*. (2007) demonstrated that this *MATalpha* chromatin particle is required for efficient cleavage of the *MATalpha* locus by HO endonuclease and consequently efficient mating type switching. Chapter 4 however shows that this large chromatin particle is not observed at *MATa* or the engineered *LEU2::HOcs* or the *URA3::HOcs* and therefore this particle is unique to the *MATalpha* locus. Hence, this large chromatin particle has been named the alphasome.

Further analysis of the chromatin particle shows that in the absence of Rsc2 or Rsc7 this region in *MATalpha* is occupied by three nucleosomes in contrast to the wild-type or *Δrsc1* mutant where the alphasome is observed. This suggests either that the RSC complex remodels three nucleosomes into

a MNase-resistant structure that protects 450bp of DNA or that an unknown MNase resistant structure binds to this region to protect DNA from MNase cleavage.

From the data presented in Chapter 4 showing that there is no dependency on RSC subunits to set the chromatin structure at *MATa* prior to cleavage by HO, it can be suggested that the chromatin structure of the *MATa* does not antagonise the cleavage of the DNA strand by HO. The HO site occurs in both *MAT* loci within a linker region suggesting that the nucleosome remodelling observed at *MATalpha* is not required to promote accessibility. HO cleaves at the same relative position in *MATalpha* and *MATa* even though the Y-regions of the different loci have no sequence similarity, and *MATalpha* has a much higher GC content than *MATa* (Wang et al., 1997). The increased GC content of *MATalpha* may alter the local persistence length of the HO cleavage site at *MATalpha* and the alphasome is required to alter this persistence length to increase the cleavage by HO (Hormeno et al., 2011). A small increase in DNA tension can completely inhibit cleavage by two-site endonucleases (Gemmen et al., 2006) thus the alphasome may function to reduce DNA tension and increase DNA looping to increase cleavage efficiency by HO. This hypothesis could be tested by treating a *MATalpha Δrsc2* mutant strain with hydrogen peroxide to reduce negative DNA supercoiling to see if HO cleavage returns to wild-type levels

As discussed below, a binding motif has been identified for the RSC subunit Rsc3 which contains a zinc-finger DNA binding domain. The motif, CGCGC is found at the HO cleavage site in *MATalpha* but not in *MATa.* Of note, the cleavage sites in the strains containing *LEU2::HOcs* or *URA3::HOcs* were originally obtained from *MATa* sequence. Consequently the potential Rsc3-binding site is not present at these non-*MAT* cleavage sites and consistent with this hypothesis, the alphasome is not observed at these loci. Wang *et al.* (1997) have shown that a large protein specifically binds to the *MAT alpha* cleavage sequence but not to *MATa* (Wang et al., 1997). One hypothesis is therefore that RSC is recruited to *MATalpha* via Rsc3 to remodel chromatin to ensure efficient cleavage (Weinstein-Fischer et al., 2000).

As shown in Chapter 4, this remodelling is dependent on both Rsc2 and Rsc7, RSC subunit proteins that neither share sequence similarity nor similar domains. Previous research has shown that the loss of Rsc7 results in RSC from being improperly assembled and Rsc3/Rsc30 are not present in the complex (Wilson et al., 2006). Despite using all viable RSC subunit knockouts of the fungal specific module, a phenocopy for the *Δrsc7* mutant was not found. Despite this, and alongside the evidence that Rsc2 can interact with histones through the BAH or bromodomains, there is little evidence that Rsc7 would interact directly with a nucleosome. An alternative explanation is that the loss of Rsc7 results in the loss of Rsc3 from the RSC complex and therefore precludes binding to the *MATalpha* locus. This hypothesis may be tested by electromobility shift assays to test whether a purified RSC complex without Rsc2 can bind the *MATalpha* DNA sequence in comparison to a RSC complex lacking Rsc7. Similarly, a system could be used to tether a RSC complex lacking the Rsc7 subunit to the *MATalpha* locus to test whether alphasome formation is restored in a *Δrsc7* mutant strain.

In conclusion these data shows that there is a *MATalpha* specific chromatin structure, the alphasome, likely to represent three aggregated nucleosomes that is required for efficient cleavage by HO endonuclease. This remodelling may be required to ensure the DNA strand is in the correct conformation for cleavage by HO endonuclease but is not required at *MATa* due to a different GC content and therefore not at the other HO cleavage sites investigated. The loss of Rsc7 is likely to result in Rsc3/Rsc30 not being assembled into the RSC complex and therefore the loss of remodelling at *MATalpha* prior to HO cleavage.

7.4 The bromodomains of Rsc2 do not confer alphasome formation at MAT alpha

Rsc2, like Rsc1 and Rsc4, contains two bromodomains but specific binding targets for the bromodomains of Rsc1 and Rsc2 have yet to be found. The tandem bromodomains of Rsc4 however have been shown to specifically target Gcn5 and itself in an autoregulation process showing that bromodomains have an important *in vivo* function in recruiting the RSC complex to functional targets (VanDemark et al., 2007). The binding of the bromodomains of Rsc4 to their targets depends on pairs of tyrosine residues, Y92/Y93 and Y225/Y226, and asparagine residues, N134 and N268 which are conserved in the Rsc1 and Rsc2 proteins (VanDemark et al., 2007). This suggests that the bromodomains of Rsc2 may be involved in specific protein-protein interactions to facilitate the Rsc2-specific chromatin remodelling observed at *MATalpha.*

Chapter 5 presents the indirect end-label analysis of bromodomain mutants of the Rsc2 protein to determine alphasome formation at *MATalpha*. None of the mutants tested affected the formation of the alphasome at *MATalpha* suggesting that, individually, these residues within the bromodomains are not required for alphasome formation. Further investigation is required to determine whether the bromodomains of Rsc2 are functioning to facilitate nucleosome remodelling at *MATalpha* or indeed that Rsc2, like Rsc1, functionally interacts with nucleosomes through the BAH domain. Further analysis would use Rsc2 bromodomain and BAH domain mutants to determine non-functional mutants.

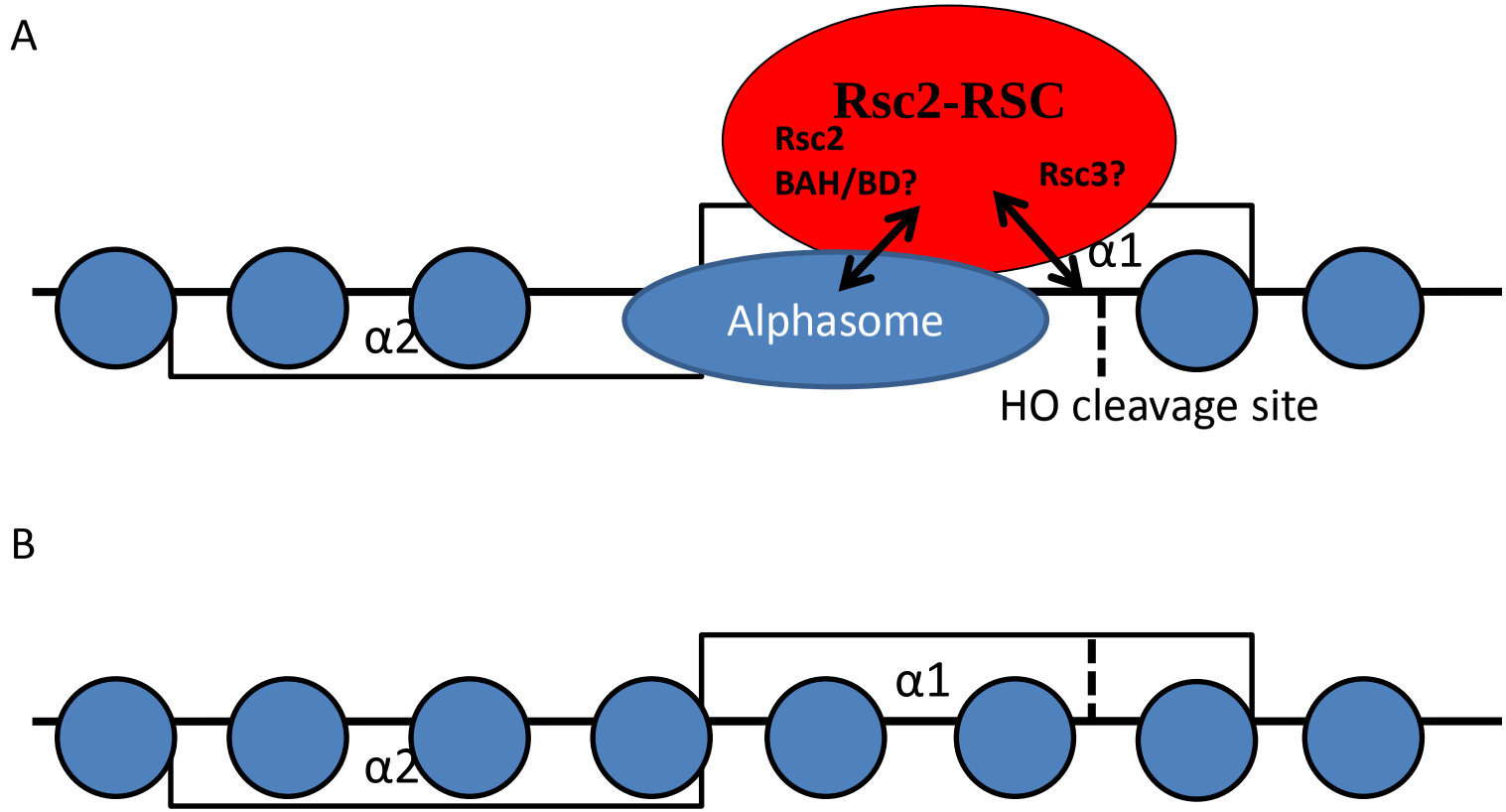

Figure 7.2 – Rsc2-dependent alphasome at the *MATalpha* locus
A cartoon representation of the chromatin structure at the *MATalpha* locus. **A** – Wild-type chromatin shows that the Rsc2-RSC complex associates via the Rsc3 subunit and the Rsc3-motif in the underlying DNA sequence. RSC interacts with the chromatin on the *MAT* locus side of the HO cleavage site, possibly through the BAH or bromodomains of the Rsc2 subunit, and in an ATP-dependent manner, remodels three nucleosomes into the alphasome. **B** – in *Δrsc2 MATalpha* strains the Rsc2-dependent remodelling activity is absent and in *Δrsc7 MATalpha* strains the RSC complex is unable to associate through the Rsc3-specific binding activity resulting in a chromatin structure of three spaced nucleosomes.

7.5 Deletion of *rsc1* and *rsc2* genes reveal both specific and overlapping sites of chromatin-remodelling function in the wider genome

Chromatin particle spectrum analysis was first described by Kent *et al.* (2011) as a technique to map a range of chromatin particles, with a range of DNA footprint sizes, back to the genome. This allows for base pair accurate positions of nucleosomes and transcription factors and allows the chromatin landscape of particular genomic features such as transcriptional start sites and centromeres to be determined and compared between wild type and mutant cell samples. (Durand-Dubief et al., 2012; Kent et al., 2011).

Chapter 6 describes CPSA analysis of the whole *S. cerevisiae* genome comparing a wild type reference strain BY4741 and two RSC subunit mutant strains YO4686 (*Δrsc1*) and YO5266 (*Δrsc2*). One initial surprise in Chapter 6 was that in the absence of Rsc1 or Rsc2, a decrease in the number of CPSA read-pairs that align to the rDNA repeats was observed on chromosome XII. This result can be interpreted to suggest that there is a decrease in the copy number of the rDNA repeats in the absence of Rsc1 or Rsc2. It has previously been shown that the loss of Rsc2 results in the loss of rDNA silencing and that Rsc2 is significantly enriched in chromatin across the rDNA repeats through direct interaction with histone H3 through the BAH domain (Chambers et al., 2013). It has been suggested that the yeast cell keeps a fraction of the 35S rRNA genes in a transcriptionally inactive state in order to maintain rDNA copy number and genomic stability (Ide et al., 2010). As shown in this thesis, and discussed below, RSC is required for chromatin structure at tRNA genes (Kumar and Bhargava, 2013) and the chromatin structure of tRNA genes has been shown to be a barrier to heterochromatin (Donze and Kamakaka, 2001). This tRNA gene chromatin structure restricts Sir-mediated heterochromatin silencing at the silent mating-type *HMR* locus and this heterochromatin-barriers function has shown to be dependent on Rsc2 (Jambunathan et al., 2005; Simms et al., 2008). The rDNA silencing chromatin is dependent on Sir2 only and a tRNA ($tRNA^{GLN}$) prevents the spreading of silencing along chromosome XII (Biswas et al., 2009). Taken

together it can be suggested that the loss of Rsc1 or Rsc2 results in a change in both the heterochromatin barriers and chromatin structure of the rDNA repeats of chromosome XII. This would result in an open chromatin state that leads to the loss of silencing and the direct destabilisation of the rDNA repeats or selection pressure for rRNA down-regulation, both of which might result in a decrease in rDNA copy number. To analyse this further I would use pulse field gel analysis and Southern Blotting, as in previous studies (Houseley and Tollervey, 2011), to determine rDNA copy number in a *Δrsc2* strain compared to wild-type. I would also analyse if there is a change in ratio of active to inactive rDNA genes in an *rsc* mutant compared to WT which would suggest a change in the chromatin structure in this region and therefore may lead to instability. If copy number does decrease it would be predicted that this phenotype would not be rescued by plasmid borne *RSC2* containing the *RSC1* BAH domain but would be rescued by normal *RSC2*, unless Rsc1-BAH and Rsc2-BAH have similar histone H3 binding affinities (See Section 7.2).

The CPSA procedure allows a landscape of chromatin particle size to be plotted relative to classes of genomic features. Chapter 6.6 showed that the average chromatin landscape surrounding TSSs of genes containing a Rsc3-binding motif in their promoter region was similar to that observed generally. However, a significant decrease in +1 and -1 nucleosome occupancy is observed in the absence of Rsc1 or Rsc2, and was independent of the presence of an Rsc3-motif at the TSS. A decrease in the transcription factor size class (50bp) was observed in *Δrsc1* and *Δrsc2* mutants, a loss which, like the loss of +1 and -1 nucleosomes, does appear to be dependent on Rsc3-binding motifs. It has previously been shown that the RSC complex is associated with nucleosome positioning and nucleosome density at RNA Pol II and Pol III promoters respectively (Parnell et al., 2008). The data presented here suggest that the RSC complex is required for maintaining a stable +1 and -1 nucleosome at promoter regions throughout the genome and the consequence of a loss of +1 and -1 nucleosome occupancy is a decrease of transcription factor binding. Due to the relatively low depth of read-pairs in the 50bp size class obtained in this experiment it is

difficult to draw conclusions from this dataset. Therefore, I would repeat the experiment in Chapter 6 to obtain more 50bp read-pair depth in a wild-type, *Δrsc1* and *Δrsc2* mutant. To further demonstrate that there is a decrease in +1 and -1 nucleosome occupancy I would use MNase digestion of cross-linked chromatin and qPCR of regions that are protected by a +1 or -1 nucleosome in a wild-type strain (Bryant, 2012). In a *Δrsc1* or *Δrsc2* strain it would be expected that there would be less +1 and -1 nucleosome-DNA protection.

Floer *et al*. (2010) suggested that the RSC complex has a novel role in remodelling nucleosomes in the promoter regions of open reading frames to facilitate the binding of transcriptional activators. The RSC complex was suggested to binds to a nucleosome to partially unwind the DNA thereby facilitating access to the sequence for activator proteins. In the absence of core RSC complex proteins such as Sth1 and Rsc3 then the partially unwound nucleosome is lost and canonical nucleosomes encroach over the region. Chromatin-seq data to support this idea showed an MNase-resistant chromatin particle of smaller size than a canonical nucleosome in the divergent promoter region of *GAL1/GAL10* which also contains Rsc3 binding motifs suggesting a recruitment mechanism for RSC (Floer et al., 2010). A chromatin particle in the 100bp CPSA size class was observed at GAL1/10. However, the CPSA in Chapter 6 shows that the loss of Rsc1 or Rsc2 results in the loss of this particle but does not result in the encroachment of canonical nucleosomes over the region. The study by Floer *et al* utilised *sth1* and *rsc3* mutants which prevent the formation of the RSC complex or remove the zinc-finger DNA-binding domain respectively. One hypothesis is that the loss of Rsc1 or Rsc2 results in the loss RSC function to maintain a non-canonical nucleosome but does not prevent the RSC complex from binding to the locus. RSC bound at the locus may prevent nucleosomes from encroaching over this region correlating with the function of RSC to maintain NFRs (Parnell et al., 2008). This hypothesis could be tested using EMSA to see if a *Δrsc1* or *Δrsc2* RSC complex can bind the underlying DNA sequence at the *GAL1/10* locus.

Further 100bp particles were shown to be present within 400bp of open reading frames which contain an Rsc3-binding motif in the promoter region. These 100bp particles show variable dependency on Rsc1 and Rsc2. The underlying DNA sequence shows that these 100bp particles are associated with certain transcription factors and trends of these sites show a loss of 100bp particles in *Δrsc1* and *Δrsc2* mutants. The 100bp particles observed at some transcription factor binding sites may be RSC-remodelled nucleosomes required to promote transcription factor binding similar to the example shown previously at *GAL1/10*. RSC may be recruited to the site via Rsc3 to the Rsc3-binding motif and RSC interact with the nucleosome to disrupt histone/DNA interactions to promote transcription factor binding (Figure 7.4). Previous studies of the transcriptome of *rsc3, rsc30* and *sth1* mutants have shown varying effects on the level of transcription of individual groups of genes, such as ribosomal protein genes, with almost an equal number up-regulated and down-regulated (Angus-Hill et al., 2001; Parnell et al., 2008). A key observation is that these studies have utilised mutants of essential RSC subunits, therefore potentially ablating essential RSC activity in transcription elongation rather than a change in chromatin structure (Section 1.6). Therefore, key and necessary further work would be to complete transcriptome analysis in a *rsc1* or *rsc2* mutant. It would be very interesting to see how Rsc1- and Rsc2-dependent 100bp chromatin particles correlate with levels of transcription.

Previous studies have identified RSC as maintaining chromatin at RNA Pol III dependent genes including tRNAs in order for expression of tRNA genes and maintaining silencing boundaries (Dubey and Gartenberg, 2007; Good et al., 2013; Kumar and Bhargava, 2013; Parnell et al., 2008). RSC functions to position nucleosomes downstream of the tRNA coding region in order to maintain the nucleosome free region over the coding region (Kumar and Bhargava, 2013). Chapter 6 shows that tRNA coding regions are associated with the presence of 100bp chromatin particles. However, the loss of Rsc1 or Rsc2 results in the loss of MNase-protected 100bp regions at tRNA genes. The loss of Rsc1 results in a significant shift of downstream nucleosomes towards the coding region, a shift is seen in the *Δrsc2* data but

this is not significant. As the coding region of tRNA is a nucleosome free region it is unlikely that this 100bp particle is a remodelled nucleosome, rather this 100bp particle may represent the footprint of the transcriptional machinery at the tRNA coding region. Assembly of RNA polymerase III (Pol III) is initiated by the binding of two units of the TFIIIC transcription factor which in turns recruits TFIIIB and Pol III (Bartholomew et al., 1993; Schramm and Hernandez, 2002). The TFIIIB-TFIIIC complex has been shown to protect approximately 150bp DNA from MNase cleavage but MNase can also cleave between TFIIIB and TFIIIC to leave shorter MNase fragments which are the approximate size of the tRNA gene i.e. 75-95 base pairs (Kassavetis et al., 1990; Nagarajavel et al., 2013) The loss of either Rsc1 or Rsc2 may result in the mis-remodelling of downstream nucleosomes that antagonises the binding of TFIIIC and precludes the assembly of the transcriptional machinery at tRNAs (Figure 7.3). This would be consistent with the observations in Chapter 6 of the loss of 100bp particles at tRNA genes in *Δrsc1* and *Δrsc2* datasets and previous data that show a general decrease in transcription of tRNA genes in essential RSC subunit mutants (Kumar and Bhargava, 2013; Parnell et al., 2008). To test whether the loss of Rsc1 or Rsc2 prevents TFIIIC from binding tRNA genes I would use chromatin immunopreciptation to determine which DNA sequences TFIIIC is bound. The prediction would be to expect that the interaction of TFIIIC with tRNA genes to be lost in *Δrsc1* or *Δrsc2* mutants.

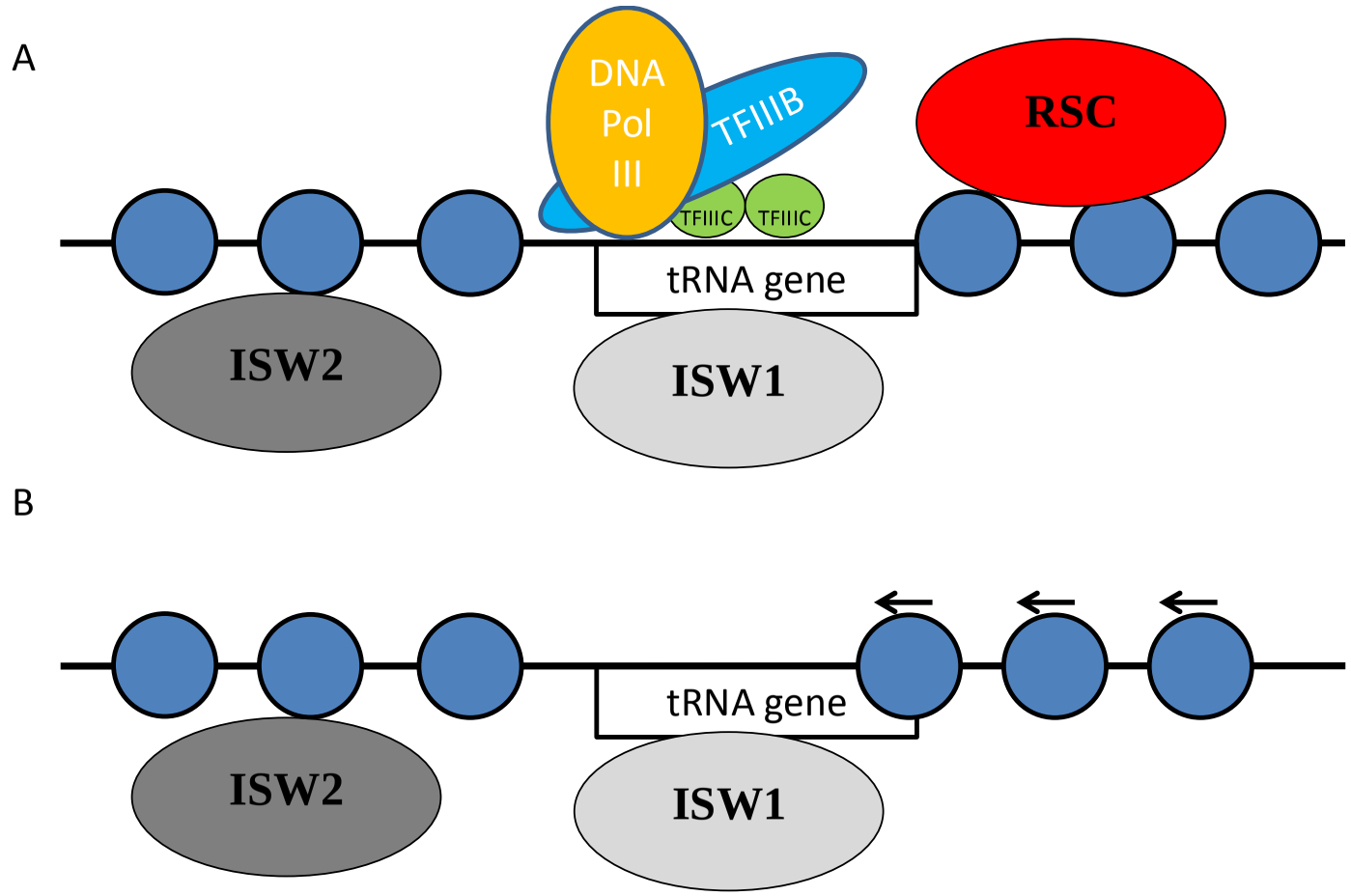

Figure 7.3– Chromatin structure of tRNA genes is dependent on multiple chromatin remodellors including RSC
The cartoon represents the chromatin structure of a tRNA gene. **A** – Wild-type cells; upstream nucleosome periodicity is maintained by ISW2 whereas the nucleosome free region is maintained by ISW1. The RSC complex remodels upstream nucleosomes away from the gene body allowing the Pol III-associated transcription factors to bind and recruit Pol III for transcription. This complex has a MNase footprint of 100bp. **B** - *Δrsc1* and *Δrsc2* strains; in the absence of Rsc1 or Rsc2 the upstream nucleosomes encroach over the tRNA gene body competing with TFIIC binding and resulting in a loss of the RNA Pol III transcription initiation complex. This coincides with the loss of a particle with a 100bp MNase footprint in this region in *Δrsc1* and *Δrsc2* strains.

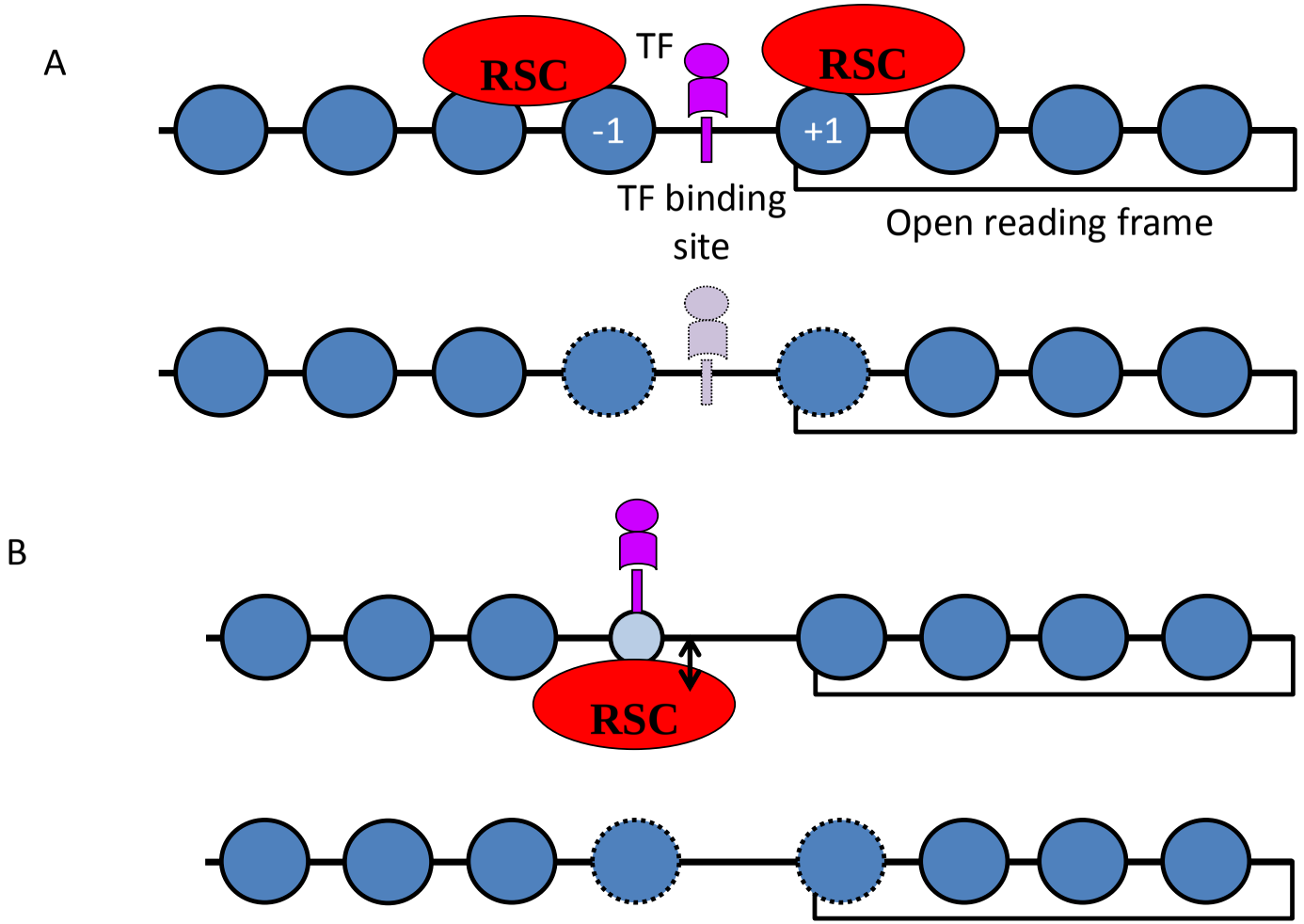

Figure 7.4 – RSC dependent remodelling at gene promoter regions acts to promote access to transcription factors
A - Generally RSC (either Rsc1-RSC or Rsc2-RSC) maintains the stabile positioning of the +1 and -1 nucleosomes at promoter regions which function to allow transcription factors to bind in the nucleosome free region. In the absence of Rsc1 or Rsc2 the +1 and -1 nucleosomes are less well positioned and antagonise the binding of transcription factors. **B** – at a subset of promoter regions, the transcription factor is in competition for the DNA-binding motif with a nucleosome. RSC (either Rsc1-RSC or Rsc2-RSC) remodels the nucleosome to disrupt histone/DNA contacts allowing the transcription factor to bind. This RSC-remodelled nucleosome protects approximately 100bp from MNase digestion. RSC is recruited to the gene via the Rsc3 subunit and a Rsc3-binding motif in the underlying DNA sequence.

7.6 Concluding remarks

This thesis has analysed the abundant ATPase-dependent chromatin remodelling complex RSC in *S. cerevisiae*. I have identified four distinct outcomes of remodelling by the RSC complex in different genomic contexts which answer some of the key questions in Chapter 1: firstly the RSC complex remodels nucleosomes away (nucleosome sliding) from DSBs a process that is dependent on the BAH domain of RSC; secondly the Rsc2 and Rsc7 subunits of RSC complex can aggregate nucleosomes in order to change the metabolism of DNA at the *MATalpha* locus, showing distinct chromatin structures of the two forms of the *MAT* locus; thirdly genome wide analysis of *Δrsc1* and *Δrsc2* mutants has shown that the RSC complex generally remodels chromatin in promoter regions throughout the genome in an Rsc1- and Rsc2- dependent manner. This activity remodels chromatin in the promoter region, potentially to promote transcription factor binding but whether this remodelling activity affects transcriptional activity is a question that will require further investigation; fourthly RSC sets the chromatin structure at tRNA genes in an Rsc1- and Rsc2-dependent manner, potentially to facilitate the binding of transcriptional machinery.

As described in Chapter 1, *S. cerevisiae* contains a host of ATPase-dependent chromatin remodelling factors of which RSC is just one. These complexes have redundant, opposing and synergistic functions showing that chromatin is both highly dynamic and tightly controlled. This thesis demonstrates that RSC has unique and important functions in ensuring processes involving DNA and contributes to both genome stability and cell regulation.

References

Abdulrehman, D., Monteiro, P.T., Teixeira, M.C., Mira, N.P., Lourenco, A.B., dos Santos, S.C., Cabrito, T.R., Francisco, A.P., Madeira, S.C., Aires, R.S.*, et al.* (2011). YEASTRACT: providing a programmatic access to curated transcriptional regulatory associations in Saccharomyces cerevisiae through a web services interface. Nucleic Acids Res *39*, D136-140.

Agmon, N., Yovel, M., Harari, Y., Liefshitz, B., and Kupiec, M. (2011). The role of Holliday junction resolvases in the repair of spontaneous and induced DNA damage. Nucleic Acids Res *39*, 7009-7019.

Ahmad, K., and Henikoff, S. (2002). The histone variant H3.3 marks active chromatin by replication-independent nucleosome assembly. Mol Cell *9*, 1191-1200.

Allard, S., Utley, R.T., Savard, J., Clarke, A., Grant, P., Brandl, C.J., Pillus, L., Workman, J.L., and Cote, J. (1999). NuA4, an essential transcription adaptor/histone H4 acetyltransferase complex containing Esa1p and the ATM-related cofactor Tra1p. EMBO J *18*, 5108-5119.

Amodeo, G.A., Momcilovic, M., Carlson, M., and Tong, L. (2010). Biochemical and functional studies on the regulation of the Saccharomyces cerevisiae AMPK homolog SNF1. Biochemical and biophysical research communications *397*, 197-201.

Angus-Hill, M.L., Schlichter, A., Roberts, D., Erdjument-Bromage, H., Tempst, P., and Cairns, B.R. (2001). A Rsc3/Rsc30 Zinc Cluster Dimer Reveals Novel Roles for the Chromatin Remodeler RSC in Gene Expression and Cell Cycle Control. Molecular Cell *7*, 741-751.

Armache, K.J., Garlick, J.D., Canzio, D., Narlikar, G.J., and Kingston, R.E. (2011). Structural Basis of Silencing: Sir3 BAH Domain in Complex with a Nucleosome at 3.0 angstrom Resolution. Science *334*, 977-982.

Aylon, Y., and Kupiec, M. (2004). DSB repair: the yeast paradigm. DNA repair *3*, 797-815.

Aylon, Y., Liefshitz, B., Bitan-Banin, G., and Kupiec, M. (2003). Molecular Dissection of Mitotic Recombination in the Yeast Saccharomyces cerevisiae. Mol Cell Biol *23*, 1403-1417.

Badis, G., Chan, E.T., van Bakel, H., Pena-Castillo, L., Tillo, D., Tsui, K., Carlson, C.D., Gossett, A.J., Hasinoff, M.J., Warren, C.L., *et al.* (2008). A Library of Yeast Transcription Factor Motifs Reveals a Widespread Function for Rsc3 in Targeting Nucleosome Exclusion at Promoters. Molecular Cell *32*, 878-887.

Baetz, K.K., Krogan, N.J., Emili, A., Greenblatt, J., and Hieter, P. (2004). The ctf13-30/CTF13 genomic haploinsufficiency modifier screen identifies the yeast chromatin remodeling complex RSC, which is required for the establishment of sister chromatid cohesion. Mol Cell Biol *24*, 1232-1244.

Bailey, T.L. (2011). DREME: motif discovery in transcription factor ChIP-seq data. Bioinformatics *27*, 1653-1659.

Bannister, A.J., and Kouzarides, T. (2011). Regulation of chromatin by histone modifications. Cell Res *21*, 381-395.

Bao, Y., and Shen, X. (2007a). Chromatin remodeling in DNA double-strand break repair. Curr Opin Genet Dev *17*, 126-131.

Bao, Y., and Shen, X. (2007b). INO80 subfamily of chromatin remodeling complexes. Mutation research *618*, 18-29.

Bartholomew, B., Durkovich, D., Kassavetis, G.A., and Geiduschek, E.P. (1993). Orientation and Topography of Rna Polymerase-Iii in Transcription Complexes. Molecular and Cellular Biology *13*, 942-952.

Bazan, J.F. (2008). An old HAT in human p300/CBP and yeast Rtt109. Cell cycle *7*, 1884-1886.

Beitz, E. (2000). TEXshade: shading and labeling of multiple sequence alignments using LATEX2 epsilon. Bioinformatics *16*, 135-139.

Ben-Aroya, S., Pan, X., Boeke, J.D., and Hieter, P. (2010). Making temperature-sensitive mutants. Methods in enzymology *470*, 181-204.

Bennett, C.B., Lewis, L.K., Karthikeyan, G., Lobachev, K.S., Jin, Y.H., Sterling, J.F., Snipe, J.R., and Resnick, M.A. (2001). Genes required for ionizing radiation resistance in yeast. Nat Genet *29*, 426-434.

Beranek, D.T. (1990). Distribution of methyl and ethyl adducts following alkylation with monofunctional alkylating agents. Mutation research *231*, 11-30.

Berger, S.L. (2007). The complex language of chromatin regulation during transcription. Nature *447*, 407-412.

Biswas, M., Maqani, N., Rai, R., Kumaran, S.P., Iyer, K.R., Sendinc, E., Smith, J.S., and Laloraya, S. (2009). Limiting the extent of the RDN1 heterochromatin domain by a silencing barrier and Sir2 protein levels in Saccharomyces cerevisiae. Mol Cell Biol *29*, 2889-2898.

Boiteux, S., Gellon, L., and Guibourt, N. (2002). Repair of 8-oxoguanine in Saccharomyces cerevisiae: interplay of DNA repair and replication mechanisms. Free radical biology & medicine *32*, 1244-1253.

Boiteux, S., and Guillet, M. (2004). Abasic sites in DNA: repair and biological consequences in Saccharomyces cerevisiae. DNA repair *3*, 1-12.

Boiteux, S., and Jinks-Robertson, S. (2013). DNA repair mechanisms and the bypass of DNA damage in Saccharomyces cerevisiae. Genetics *193*, 1025-1064.

Bonazzi, V., Medjkane, S., Quignon, F., and Delattre, O. (2005). Complementation analyses suggest species-specific functions of the SNF5 homology domain. Biochemical and biophysical research communications *336*, 634-638.

Botstein, D., and Fink, G.R. (2011). Yeast: an experimental organism for 21st Century biology. Genetics *189*, 695-704.

Brachmann, C.B., Davies, A., Cost, G.J., Caputo, E., Li, J., Hieter, P., and Boeke, J.D. (1998). Designer deletion strains derived from Saccharomyces cerevisiae S288C: a useful set of strains and plasmids for PCR-mediated gene disruption and other applications. Yeast *14*, 115-132.

Brand, A.H., Breeden, L., Abraham, J., Sternglanz, R., and Nasmyth, K. (1985). Characterization of a "silencer" in yeast: a DNA sequence with properties opposite to those of a transcriptional enhancer. Cell *41*, 41-48.

Brogaard, K., Xi, L., Wang, J.P., and Widom, J. (2012). A map of nucleosome positions in yeast at base-pair resolution. Nature *486*, 496-501.

Brown, J.A., Holmes, S.G., and Smith, M.M. (1991). The chromatin structure of Saccharomyces cerevisiae autonomously replicating sequences changes during the cell division cycle. Mol Cell Biol *11*, 5301-5311.

Brownlee, P.M., Chambers, A.L., Oliver, A.W., and Downs, J.A. (2012). Cancer and the bromodomains of BAF180. Biochemical Society transactions *40*, 364-369.

Bruno, M., Flaus, A., Stockdale, C., Rencurel, C., Ferreira, H., and Owen-Hughes, T. (2003). Histone H2A/H2B dimer exchange by ATP-dependent chromatin remodeling activities. Mol Cell *12*, 1599-1606.

Bryant, G.O. (2012). Measuring nucleosome occupancy in vivo by micrococcal nuclease. Methods in molecular biology *833*, 47-61.

Bungard, D., Reed, M., and Winter, E. (2004). RSC1 and RSC2 are required for expression of mid-late sporulation-specific genes in Saccharomyces cerevisiae. Eukaryotic cell *3*, 910-918.

Burns, L.G., and Peterson, C.L. (1997). The yeast SWI-SNF complex facilitates binding of a transcriptional activator to nucleosomal sites in vivo. Mol Cell Biol *17*, 4811-4819.

Byeon, B., Wang, W., Barski, A., Ranallo, R.T., Bao, K., Schones, D.E., Zhao, K., Wu, C., and Wu, W.H. (2013). The ATP-dependent Chromatin Remodeling Enzyme Fun30 Represses Transcription by Sliding Promoter-proximal Nucleosomes. The Journal of biological chemistry *288*, 23182-23193.

C. Guthrie, G.R.F. (1991). Guide to Yeast Genetics and Molecular Biology. Academic Press, San Diego.

Cairns, B.R., Lorch, Y., Li, Y., Zhang, M., Lacomis, L., Erdjument-Bromage, H., Tempst, P., Du, J., Laurent, B., and Kornberg, R.D. (1996). RSC, an Essential, Abundant Chromatin-Remodeling Complex. Cell *87*, 1249-1260.

Cairns, B.R., Schlichter, A., Erdjument-Bromage, H., Tempst, P., Kornberg, R.D., and Winston, F. (1999). Two Functionally Distinct Forms of the RSC Nucleosome-Remodeling Complex, Containing Essential AT Hook, BAH, and Bromodomains. Molecular Cell *4*, 715-723.

Caldecott, K.W. (2008). Single-strand break repair and genetic disease. Nat Rev Genet *9*, 619-631.

Callebaut, I., Courvalin, J.C., and Mornon, J.P. (1999). The BAH (bromo-adjacent homology) domain: a link between DNA methylation, replication and transcriptional regulation. FEBS letters *446*, 189-193.

Cao, Y., Cairns, B.R., Kornberg, R.D., and Laurent, B.C. (1997). Sfh1p, a component of a novel chromatin-remodeling complex, is required for cell cycle progression. Mol Cell Biol *17*, 3323-3334.

Carey, M., Li, B., and Workman, J.L. (2006). RSC exploits histone acetylation to abrogate the nucleosomal block to RNA polymerase II elongation. Mol Cell *24*, 481-487.

Cariello, N.F., Keohavong, P., Sanderson, B.J., and Thilly, W.G. (1988). DNA damage produced by ethidium bromide staining and exposure to ultraviolet light. Nucleic Acids Res *16*, 4157.

Carr, A.M. (1997). Control of cell cycle arrest by the Mec1sc/Rad3sp DNA structure checkpoint pathway. Curr Opin Genet Dev *7*, 93-98.

Chaban, Y., Ezeokonkwo, C., Chung, W.H., Zhang, F., Kornberg, R.D., Maier-Davis, B., Lorch, Y., and Asturias, F.J. (2008). Structure of a RSC-nucleosome complex and insights into chromatin remodeling. Nat Struct Mol Biol *15*, 1272-1277.

Chai, B., Huang, J., Cairns, B.R., and Laurent, B.C. (2005). Distinct roles for the RSC and Swi/Snf ATP-dependent chromatin remodelers in DNA double-strand break repair. Genes & Development *19*, 1656-1661.

Chakravarthy, S., Park, Y.J., Chodaparambil, J., Edayathumangalam, R.S., and Luger, K. (2005). Structure and dynamic properties of nucleosome core particles. FEBS letters *579*, 895-898.

Chambers, A.L., Brownlee, P.M., Durley, S.C., Beacham, T., Kent, N.A., and Downs, J.A. (2012a). The two different isoforms of the RSC chromatin remodeling complex play distinct roles in DNA damage responses. PLoS One *7*, e32016.

Chambers, A.L., Ormerod, G., Durley, S.C., Sing, T.L., Brown, G.W., Kent, N.A., and Downs, J.A. (2012b). The INO80 chromatin remodeling complex prevents

polyploidy and maintains normal chromatin structure at centromeres. Genes Dev *26*, 2590-2603.

Chambers, A.L., Pearl, L.H., Oliver, A.W., and Downs, J.A. (2013). The BAH domain of Rsc2 is a histone H3 binding domain. Nucleic Acids Res.

Chatterjee, N., Sinha, D., Lemma-Dechassa, M., Tan, S., Shogren-Knaak, M.A., and Bartholomew, B. (2011). Histone H3 tail acetylation modulates ATP-dependent remodeling through multiple mechanisms. Nucleic Acids Res *39*, 8378-8391.

Chen, X., Cui, D., Papusha, A., Zhang, X., Chu, C.D., Tang, J., Chen, K., Pan, X., and Ira, G. (2012). The Fun30 nucleosome remodeller promotes resection of DNA double-strand break ends. Nature *489*, 576-580.

Cheung, W.L., Turner, F.B., Krishnamoorthy, T., Wolner, B., Ahn, S.H., Foley, M., Dorsey, J.A., Peterson, C.L., Berger, S.L., and Allis, C.D. (2005). Phosphorylation of histone H4 serine 1 during DNA damage requires casein kinase II in S. cerevisiae. Current biology : CB *15*, 656-660.

Chodaparambil, J.V., Edayathumangalam, R.S., Bao, Y., Park, Y.J., and Luger, K. (2006). Nucleosome structure and function. Ernst Schering Research Foundation workshop, 29-46.

Choi, J.K., Grimes, D.E., Rowe, K.M., and Howe, L.J. (2008). Acetylation of Rsc4p by Gcn5p is essential in the absence of histone H3 acetylation. Mol Cell Biol *28*, 6967-6972.

Clapier, C.R., and Cairns, B.R. (2009). The biology of chromatin remodeling complexes. Annu Rev Biochem *78*, 273-304.

Cleaver, J.E., and Bootsma, D. (1975). Xeroderma pigmentosum: biochemical and genetic characteristics. Annu Rev Genet *9*, 19-38.

Coic, E., Martin, J., Ryu, T., Tay, S.Y., Kondev, J., and Haber, J.E. (2011). Dynamics of Homology Searching During Gene Conversion in Saccharomyces cerevisiae Revealed by Donor Competition. Genetics *189*, 1225-1233.

Colis, L.C., Raychaudhury, P., and Basu, A.K. (2008). Mutational specificity of gamma-radiation-induced guanine-thymine and thymine-guanine intrastrand cross-

links in mammalian cells and translesion synthesis past the guanine-thymine lesion by human DNA polymerase eta. Biochemistry *47*, 8070-8079.

Conaway, R.C., and Conaway, J.W. (2009). The INO80 chromatin remodeling complex in transcription, replication and repair. Trends in biochemical sciences *34*, 71-77.

Conde, R., Cueva, R., and Larriba, G. (2007). Rsc14-controlled expression of MNN6, MNN4 and MNN1 regulates mannosylphosphorylation of Saccharomyces cerevisiae cell wall mannoproteins. FEMS Yeast Research *7*, 1248-1255.

Connolly, B., White, C.I., and Haber, J.E. (1988). Physical monitoring of mating type switching in Saccharomyces cerevisiae. Mol Cell Biol *8*, 2342-2349.

Corona, D.F., and Tamkun, J.W. (2004). Multiple roles for ISWI in transcription, chromosome organization and DNA replication. Biochimica et biophysica acta *1677*, 113-119.

Cuthbert, G.L., Daujat, S., Snowden, A.W., Erdjument-Bromage, H., Hagiwara, T., Yamada, M., Schneider, R., Gregory, P.D., Tempst, P., Bannister, A.J.*, et al.* (2004). Histone deimination antagonizes arginine methylation. Cell *118*, 545-553.

Daley, J.M., Palmbos, P.L., Wu, D., and Wilson, T.E. (2005). Nonhomologous end joining in yeast. Annu Rev Genet *39*, 431-451.

Damelin, M., Simon, I., Moy, T.I., Wilson, B., Komili, S., Tempst, P., Roth, F.P., Young, R.A., Cairns, B.R., and Silver, P.A. (2002). The genome-wide localization of Rsc9, a component of the RSC chromatin-remodeling complex, changes in response to stress. Mol Cell *9*, 563-573.

Denny, W.A., Turner, P.M., Atwell, G.J., Rewcastle, G.W., and Ferguson, L.R. (1990). Structure-activity relationships for the mutagenic activity of tricyclic intercalating agents in Salmonella typhimurium. Mutation research *232*, 233-241.

Donze, D., Adams, C.R., Rine, J., and Kamakaka, R.T. (1999). The boundaries of the silenced HMR domain in Saccharomyces cerevisiae. Genes Dev *13*, 698-708.

Donze, D., and Kamakaka, R.T. (2001). RNA polymerase III and RNA polymerase II promoter complexes are heterochromatin barriers in Saccharomyces cerevisiae. EMBO J *20*, 520-531.

Downs, J.A., Allard, S., Jobin-Robitaille, O., Javaheri, A., Auger, A., Bouchard, N., Kron, S.J., Jackson, S.P., and Côté, J. (2004). Binding of Chromatin-Modifying Activities to Phosphorylated Histone H2A at DNA Damage Sites. Molecular Cell *16*, 979-990.

Downs, J.A., Lowndes, N.F., and Jackson, S.P. (2000). A role for Saccharomyces cerevisiae histone H2A in DNA repair. Nature *408*, 1001-1004.

Doyon, Y., and Cote, J. (2004). The highly conserved and multifunctional NuA4 HAT complex. Curr Opin Genet Dev *14*, 147-154.

Du, J., Nasir, I., Benton, B.K., Kladde, M.P., and Laurent, B.C. (1998). Sth1p, a Saccharomyces cerevisiae Snf2p/Swi2p Homolog, Is an Essential ATPase in RSC and Differs From Snf/Swi in Its Interactions With Histones and Chromatin-Associated Proteins. Genetics *150*, 987-1005.

Dubey, R.N., and Gartenberg, M.R. (2007). A tDNA establishes cohesion of a neighboring silent chromatin domain. Genes & Development *21*, 2150-2160.

Durand-Dubief, M., Will, W.R., Petrini, E., Theodorou, D., Harris, R.R., Crawford, M.R., Paszkiewicz, K., Krueger, F., Correra, R.M., Vetter, A.T.*, et al.* (2012). SWI/SNF-like chromatin remodeling factor Fun30 supports point centromere function in S. cerevisiae. PLoS genetics *8*, e1002974.

Durocher, D., and Jackson, S.P. (2001). DNA-PK, ATM and ATR as sensors of DNA damage: variations on a theme? Current opinion in cell biology *13*, 225-231.

Durr, H., Flaus, A., Owen-Hughes, T., and Hopfner, K.P. (2006). Snf2 family ATPases and DExx box helicases: differences and unifying concepts from high-resolution crystal structures. Nucleic Acids Res *34*, 4160-4167.

Ebbert, R., Birkmann, A., and Schuller, H.J. (1999). The product of the SNF2/SWI2 paralogue INO80 of Saccharomyces cerevisiae required for efficient expression of various yeast structural genes is part of a high-molecular-weight protein complex. Molecular microbiology *32*, 741-751.

Eberharter, A., and Becker, P.B. (2004). ATP-dependent nucleosome remodelling: factors and functions. Journal of cell science *117*, 3707-3711.

Emili, A. (1998). MEC1-dependent phosphorylation of Rad9p in response to DNA damage. Mol Cell *2*, 183-189.

Eriksson, P.R., Ganguli, D., Nagarajavel, V., and Clark, D.J. (2012). Regulation of histone gene expression in budding yeast. Genetics *191*, 7-20.

Ewing, B., and Green, P. (1998). Base-calling of automated sequencer traces using phred. II. Error probabilities. Genome Res *8*, 186-194.

Ewing, B., Hillier, L., Wendl, M.C., and Green, P. (1998). Base-calling of automated sequencer traces using phred. I. Accuracy assessment. Genome Res *8*, 175-185.

Fahy, D., Conconi, A., and Smerdon, M.J. (2005). Rapid changes in transcription and chromatin structure of ribosomal genes in yeast during growth phase transitions. Experimental cell research *305*, 365-373.

Falnes, P.O., Johansen, R.F., and Seeberg, E. (2002). AlkB-mediated oxidative demethylation reverses DNA damage in Escherichia coli. Nature *419*, 178-182.

Ferguson, L.R., and Denny, W.A. (1991). The genetic toxicology of acridines. Mutation research *258*, 123-160.

Ferguson, L.R., and Denny, W.A. (2007). Genotoxicity of non-covalent interactions: DNA intercalators. Mutation research *623*, 14-23.

Fischer, C.J., Saha, A., and Cairns, B.R. (2007). Kinetic model for the ATP-dependent translocation of Saccharomyces cerevisiae RSC along double-stranded DNA. Biochemistry *46*, 12416-12426.

Flanagan, J.F., and Peterson, C.L. (1999). A role for the yeast SWI/SNF complex in DNA replication. Nucleic Acids Res *27*, 2022-2028.

Flaus, A., and Owen-Hughes, T. (2011). Mechanisms for ATP-dependent chromatin remodelling: the means to the end. The FEBS journal *278*, 3579-3595.

Fleck, O., and Nielsen, O. (2004). DNA repair. Journal of cell science *117*, 515-517.

Floer, M., Wang, X., Prabhu, V., Berrozpe, G., Narayan, S., Spagna, D., Alvarez, D., Kendall, J., Krasnitz, A., Stepansky, A.*, et al.* (2010). A RSC/nucleosome complex determines chromatin architecture and facilitates activator binding. Cell *141*, 407-418.

Florio, C., Moscariello, M., Ederle, S., Fasano, R., Lanzuolo, C., and Pulitzer, J.F. (2007). A study of biochemical and functional interactions of Htl1p, a putative component of the Saccharomyces cerevisiae, Rsc chromatin-remodeling complex. Gene *395*, 72-85.

Forsburg, S.L. (2001). The art and design of genetic screens: yeast. Nat Rev Genet *2*, 659-668.

Fu, Y., Zhu, Y., Zhang, K., Yeung, M., Durocher, D., and Xiao, W. (2008). Rad6-Rad18 mediates a eukaryotic SOS response by ubiquitinating the 9-1-1 checkpoint clamp. Cell *133*, 601-611.

Futcher, A.B. (1988). The 2 micron circle plasmid of Saccharomyces cerevisiae. Yeast *4*, 27-40.

Gemmen, G.J., Millin, R., and Smith, D.E. (2006). Tension-dependent DNA cleavage by restriction endonucleases: two-site enzymes are "switched off" at low force. Proc Natl Acad Sci U S A *103*, 11555-11560.

Geourjon, C., and Deleage, G. (1995). SOPMA: significant improvements in protein secondary structure prediction by consensus prediction from multiple alignments. Computer applications in the biosciences : CABIOS *11*, 681-684.

Giaever, G., Chu, A.M., Ni, L., Connelly, C., Riles, L., Veronneau, S., Dow, S., Lucau-Danila, A., Anderson, K., Andre, B.*, et al.* (2002). Functional profiling of the Saccharomyces cerevisiae genome. Nature *418*, 387-391.

Gille, C., and Frommel, C. (2001). STRAP: editor for STRuctural Alignments of Proteins. Bioinformatics *17*, 377-378.

Ginsburg, D.S., Govind, C.K., and Hinnebusch, A.G. (2009). NuA4 lysine acetyltransferase Esa1 is targeted to coding regions and stimulates transcription elongation with Gcn5. Mol Cell Biol *29*, 6473-6487.

Gkikopoulos, T., Schofield, P., Singh, V., Pinskaya, M., Mellor, J., Smolle, M., Workman, J.L., Barton, G.J., and Owen-Hughes, T. (2011). A role for Snf2-related nucleosome-spacing enzymes in genome-wide nucleosome organization. Science *333*, 1758-1760.

Goldmark, J.P., Fazzio, T.G., Estep, P.W., Church, G.M., and Tsukiyama, T. (2000). The Isw2 chromatin remodeling complex represses early meiotic genes upon recruitment by Ume6p. Cell *103*, 423-433.

Good, P.D., Kendall, A., Ignatz-Hoover, J., Miller, E.L., Pai, D.A., Rivera, S.R., Carrick, B., and Engelke, D.R. (2013). Silencing near tRNA genes is nucleosome-mediated and distinct from boundary element function. Gene *526*, 7-15.

Goodwin, G.H., and Nicolas, R.H. (2001). The BAH domain, polybromo and the RSC chromatin remodelling complex. Gene *268*, 1-7.

Gothel, S.F., and Marahiel, M.A. (1999). Peptidyl-prolyl cis-trans isomerases, a superfamily of ubiquitous folding catalysts. Cellular and molecular life sciences : CMLS *55*, 423-436.

Grollman, A.P., and Moriya, M. (1993). Mutagenesis by 8-oxoguanine: an enemy within. Trends in genetics : TIG *9*, 246-249.

Guldener, U., Heck, S., Fielder, T., Beinhauer, J., and Hegemann, J.H. (1996). A new efficient gene disruption cassette for repeated use in budding yeast. Nucleic Acids Res *24*, 2519-2524.

Gunjan, A., Paik, J., and Verreault, A. (2005). Regulation of histone synthesis and nucleosome assembly. Biochimie *87*, 625-635.

Haber, J.E. (1998). Mating-type gene switching in Saccharomyces *cerevisiae*. Annual Review of Genetics *32*, 561-599.

Haber, J.E. (2012). Mating-type genes and MAT switching in Saccharomyces cerevisiae. Genetics *191*, 33-64.

Hani, J., and Feldmann, H. (1998). tRNA genes and retroelements in the yeast genome. Nucleic Acids Res *26*, 689-696.

Hargreaves, D.C., and Crabtree, G.R. (2011). ATP-dependent chromatin remodeling: genetics, genomics and mechanisms. Cell Res *21*, 396-420.

Hargreaves, V.V., Shell, S.S., Mazur, D.J., Hess, M.T., and Kolodner, R.D. (2010). Interaction between the Msh2 and Msh6 nucleotide-binding sites in the

Saccharomyces cerevisiae Msh2-Msh6 complex. The Journal of biological chemistry *285*, 9301-9310.

Hartley, P.D., and Madhani, H.D. (2009). Mechanisms that specify promoter nucleosome location and identity. Cell *137*, 445-458.

Hartwell, L.H. (1967). Macromolecule synthesis in temperature-sensitive mutants of yeast. Journal of bacteriology *93*, 1662-1670.

Hartwell, L.H., and Weinert, T.A. (1989). Checkpoints: controls that ensure the order of cell cycle events. Science *246*, 629-634.

Harvey, A.C., Jackson, S.P., and Downs, J.A. (2005). Saccharomyces cerevisiae histone H2A Ser122 facilitates DNA repair. Genetics *170*, 543-553.

Hassa, P.O., Haenni, S.S., Elser, M., and Hottiger, M.O. (2006). Nuclear ADP-ribosylation reactions in mammalian cells: where are we today and where are we going? Microbiology and molecular biology reviews : MMBR *70*, 789-829.

Hecht, A., Laroche, T., Strahlbolsinger, S., Gasser, S.M., and Grunstein, M. (1995). Histone H3 and H4 N-Termini Interact with Sir3 and Sir4 Proteins - a Molecular-Model for the Formation of Heterochromatin in Yeast. Cell *80*, 583-592.

Hefferin, M.L., and Tomkinson, A.E. (2005). Mechanism of DNA double-strand break repair by non-homologous end joining. DNA repair *4*, 639-648.

Hershko, A., and Ciechanover, A. (1998). The ubiquitin system. Annu Rev Biochem *67*, 425-479.

Herskowitz, I. (1988). Life cycle of the budding yeast Saccharomyces cerevisiae. Microbiological reviews *52*, 536-553.

Hickman, M.A., and Rusche, L.N. (2010). Transcriptional silencing functions of the yeast protein Orc1/Sir3 subfunctionalized after gene duplication. Proceedings of the National Academy of Sciences of the United States of America *107*, 19384-19389.

Hicks, W.M., Kim, M., and Haber, J.E. (2010). Increased Mutagenesis and Unique Mutation Signature Associated with Mitotic Gene Conversion. Science *329*, 82-85.

Hoffman, C.S., and Winston, F. (1987). A ten-minute DNA preparation from yeast efficiently releases autonomous plasmids for transformation of Escherichia coli. Gene *57*, 267-272.

Hong, H., Cao, H., and Wang, Y. (2007). Formation and genotoxicity of a guanine-cytosine intrastrand cross-link lesion in vivo. Nucleic Acids Res *35*, 7118-7127.

Hormeno, S., Ibarra, B., Carrascosa, J.L., Valpuesta, J.M., Moreno-Herrero, F., and Arias-Gonzalez, J.R. (2011). Mechanical properties of high-G.C content DNA with a-type base-stacking. Biophysical journal *100*, 1996-2005.

Houseley, J., and Tollervey, D. (2011). Repeat expansion in the budding yeast ribosomal DNA can occur independently of the canonical homologous recombination machinery. Nucleic Acids Res *39*, 8778-8791.

Houtgraaf, J.H., Versmissen, J., and van der Giessen, W.J. (2006). A concise review of DNA damage checkpoints and repair in mammalian cells. Cardiovascular revascularization medicine : including molecular interventions *7*, 165-172.

Hsu, J.M., Huang, J., Meluh, P.B., and Laurent, B.C. (2003). The yeast RSC chromatin-remodeling complex is required for kinetochore function in chromosome segregation. Mol Cell Biol *23*, 3202-3215.

Hubscher, U., Maga, G., and Spadari, S. (2002). Eukaryotic DNA polymerases. Annu Rev Biochem *71*, 133-163.

Hughes, T.R., Marton, M.J., Jones, A.R., Roberts, C.J., Stoughton, R., Armour, C.D., Bennett, H.A., Coffey, E., Dai, H., He, Y.D.*, et al.* (2000). Functional discovery via a compendium of expression profiles. Cell *102*, 109-126.

Huth, J.R., Bewley, C.A., Nissen, M.S., Evans, J.N., Reeves, R., Gronenborn, A.M., and Clore, G.M. (1997). The solution structure of an HMG-I(Y)-DNA complex defines a new architectural minor groove binding motif. Nature structural biology *4*, 657-665.

Ide, S., Miyazaki, T., Maki, H., and Kobayashi, T. (2010). Abundance of ribosomal RNA gene copies maintains genome integrity. Science *327*, 693-696.

Imai, S., Armstrong, C.M., Kaeberlein, M., and Guarente, L. (2000). Transcriptional silencing and longevity protein Sir2 is an NAD-dependent histone deacetylase. Nature *403*, 795-800.

Ira, G., Malkova, A., Liberi, G., Foiani, M., and Haber, J.E. (2003). Srs2 and Sgs1-Top3 suppress crossovers during double-strand break repair in yeast. Cell *115*, 401-411.

Ira, G., Satory, D., and Haber, J.E. (2006). Conservative inheritance of newly synthesized DNA in double-strand break-induced gene conversion. Molecular and Cellular Biology *26*, 9424-9429.

Iyer, R.R., Pluciennik, A., Burdett, V., and Modrich, P.L. (2006). DNA mismatch repair: functions and mechanisms. Chemical reviews *106*, 302-323.

Jackson, S.P. (2002). Sensing and repairing DNA double-strand breaks. Carcinogenesis *23*, 687-696.

Jambunathan, N., Martinez, A.W., Robert, E.C., Agochukwu, N.B., Ibos, M.E., Dugas, S.L., and Donze, D. (2005). Multiple bromodomain genes are involved in restricting the spread of heterochromatic silencing at the Saccharomyces cerevisiae HMR-tRNA boundary. Genetics *171*, 913-922.

Jaskelioff, M., Van Komen, S., Krebs, J.E., Sung, P., and Peterson, C.L. (2003). Rad54p is a chromatin remodeling enzyme required for heteroduplex DNA joint formation with chromatin. Journal of Biological Chemistry *278*, 9212-9218.

Jiang, Y., Wang, X., Bao, S., Guo, R., Johnson, D.G., Shen, X., and Li, L. (2010). INO80 chromatin remodeling complex promotes the removal of UV lesions by the nucleotide excision repair pathway. Proc Natl Acad Sci U S A *107*, 17274-17279.

Johnson, S.M., Tan, F.J., McCullough, H.L., Riordan, D.P., and Fire, A.Z. (2006). Flexibility and constraint in the nucleosome core landscape of Caenorhabditis elegans chromatin. Genome Res *16*, 1505-1516.

Jun, S.H., Kim, T.G., and Ban, C. (2006). DNA mismatch repair system. Classical and fresh roles. The FEBS journal *273*, 1609-1619.

Kamakaka, R.T., and Biggins, S. (2005). Histone variants: deviants? Genes Dev *19*, 295-310.

Kaplun, L., Ivantsiv, Y., Bakhrat, A., Tzirkin, R., Baranes, K., Shabek, N., and Raveh, D. (2006). The F-box protein, Ufo1, maintains genome stability by recruiting the yeast mating switch endonuclease, Ho, for rapid proteasome degradation. The Israel Medical Association journal : IMAJ *8*, 246-248.

Karpenshif, Y., and Bernstein, K.A. (2012). From yeast to mammals: recent advances in genetic control of homologous recombination. DNA repair *11*, 781-788.

Kasahara, K., Ohtsuki, K., Ki, S., Aoyama, K., Takahashi, H., Kobayashi, T., Shirahige, K., and Kokubo, T. (2007). Assembly of regulatory factors on rRNA and ribosomal protein genes in Saccharomyces cerevisiae. Mol Cell Biol *27*, 6686-6705.

Kassabov, S.R., Henry, N.M., Zofall, M., Tsukiyama, T., and Bartholomew, B. (2002). High-resolution mapping of changes in histone-DNA contacts of nucleosomes remodeled by ISW2. Mol Cell Biol *22*, 7524-7534.

Kassavetis, G.A., Braun, B.R., Nguyen, L.H., and Geiduschek, E.P. (1990). S. cerevisiae TFIIIB is the transcription initiation factor proper of RNA polymerase III, while TFIIIA and TFIIIC are assembly factors. Cell *60*, 235-245.

Kasten, M., Szerlong, H., Erdjument-Bromage, H., Tempst, P., Werner, M., and Cairns, B.R. (2004). Tandem bromodomains in the chromatin remodeler RSC recognize acetylated histone H3 Lys14. EMBO J *23*, 1348-1359.

Kellis, M., Birren, B.W., and Lander, E.S. (2004). Proof and evolutionary analysis of ancient genome duplication in the yeast Saccharomyces cerevisiae. Nature *428*, 617-624.

Kelly, D.E., Lamb, D.C., and Kelly, S.L. (2001). Genome-wide generation of yeast gene deletion strains. Comparative and functional genomics *2*, 236-242.

Kent, N.A., Adams, S., Moorhouse, A., and Paszkiewicz, K. (2011). Chromatin particle spectrum analysis: a method for comparative chromatin structure analysis using paired-end mode next-generation DNA sequencing. Nucleic Acids Res *39*, e26.

Kent, N.A., Bird, L.E., and Mellor, J. (1993). Chromatin analysis in yeast using NP-40 permeabilised sphaeroplasts. Nucl Acids Res *21*, 4653-4654.

Kent, N.A., Chambers, A.L., and Downs, J.A. (2007). Dual Chromatin Remodeling Roles for RSC during DNA Double Strand Break Induction and Repair at the Yeast MAT Locus. Journal of Biological Chemistry *282*, 27693-27701.

Kent, N.A., Karabetsou, N., Politis, P.K., and Mellor, J. (2001). In vivo chromatin remodeling by yeast ISWI homologs Isw1p and Isw2p. Genes Dev *15*, 619-626.

Kent, N.A., and Mellor, J. (1995). Chromatin structure snap-shots: rapid nuclease digestion of chromatin in yeast. Nucleic Acids Res *23*, 3786-3787.

Khanna, K.K., and Jackson, S.P. (2001). DNA double-strand breaks: signaling, repair and the cancer connection. Nat Genet *27*, 247-254.

Kleinschmidt, M., Schulz, R., and Braus, G.H. (2006). The yeast CPC2/ASC1 gene is regulated by the transcription factors Fhl1p and Ifh1p. Current genetics *49*, 218-228.

Kobayashi, T., Heck, D.J., Nomura, M., and Horiuchi, T. (1998). Expansion and contraction of ribosomal DNA repeats in Saccharomyces cerevisiae: requirement of replication fork blocking (Fob1) protein and the role of RNA polymerase I. Genes Dev *12*, 3821-3830.

Kolodner, R.D., Putnam, C.D., and Myung, K. (2002). Maintenance of genome stability in Saccharomyces cerevisiae. Science *297*, 552-557.

Kornberg, R.D. (1977). Structure of chromatin. Annu Rev Biochem *46*, 931-954.

Kostriken, R., Strathern, J.N., Klar, A.J., Hicks, J.B., and Heffron, F. (1983). A site-specific endonuclease essential for mating-type switching in Saccharomyces cerevisiae. Cell *35*, 167-174.

Kouzarides, T. (2007). Chromatin modifications and their function. Cell *128*, 693-705.

Krogan, N.J., Keogh, M.C., Datta, N., Sawa, C., Ryan, O.W., Ding, H., Haw, R.A., Pootoolal, J., Tong, A., Canadien, V.*, et al.* (2003a). A Snf2 family ATPase complex required for recruitment of the histone H2A variant Htz1. Mol Cell *12*, 1565-1576.

Krogan, N.J., Kim, M., Tong, A., Golshani, A., Cagney, G., Canadien, V., Richards, D.P., Beattie, B.K., Emili, A., Boone, C.*, et al.* (2003b). Methylation of histone H3 by

Set2 in Saccharomyces cerevisiae is linked to transcriptional elongation by RNA polymerase II. Mol Cell Biol *23*, 4207-4218.

Kumar, Y., and Bhargava, P. (2013). A unique nucleosome arrangement, maintained actively by chromatin remodelers facilitates transcription of yeast tRNA genes. BMC genomics *14*, 402.

Kunkel, T.A. (2004). DNA replication fidelity. The Journal of biological chemistry *279*, 16895-16898.

Kuo, A.J., Song, J., Cheung, P., Ishibe-Murakami, S., Yamazoe, S., Chen, J.K., Patel, D.J., and Gozani, O. (2012a). The BAH domain of ORC1 links H4K20me2 to DNA replication licensing and Meier-Gorlin syndrome. Nature *484*, 115-119.

Kuo, A.J., Song, J.K., Cheung, P., Ishibe-Murakami, S., Yamazoe, S., Chen, J.K., Patel, D.J., and Gozani, O. (2012b). The BAH domain of ORC1 links H4K20me2 to DNA replication licensing and Meier-Gorlin syndrome. Nature *484*, 115-+.

Langmead, B., Trapnell, C., Pop, M., and Salzberg, S.L. (2009). Ultrafast and memory-efficient alignment of short DNA sequences to the human genome. Genome biology *10*, R25.

Laurent, B.C., Yang, X., and Carlson, M. (1992). An essential Saccharomyces cerevisiae gene homologous to SNF2 encodes a helicase-related protein in a new family. Mol Cell Biol *12*, 1893-1902.

Lawley, P.D., and Phillips, D.H. (1996). DNA adducts from chemotherapeutic agents. Mutation research *355*, 13-40.

Lee, J.S., and Shilatifard, A. (2007). A site to remember: H3K36 methylation a mark for histone deacetylation. Mutation research *618*, 130-134.

Lee, K.K., Prochasson, P., Florens, L., Swanson, S.K., Washburn, M.P., and Workman, J.L. (2004). Proteomic analysis of chromatin-modifying complexes in Saccharomyces cerevisiae identifies novel subunits. Biochemical Society transactions *32*, 899-903.

Lhomme, J., Constant, J.F., and Demeunynck, M. (1999). Abasic DNA structure, reactivity, and recognition. Biopolymers *52*, 65-83.

Li, B., Carey, M., and Workman, J.L. (2007). The role of chromatin during transcription. Cell *128*, 707-719.

Li, B., Pattenden, S.G., Lee, D., Gutierrez, J., Chen, J., Seidel, C., Gerton, J., and Workman, J.L. (2005). Preferential occupancy of histone variant H2AZ at inactive promoters influences local histone modifications and chromatin remodeling. Proc Natl Acad Sci U S A *102*, 18385-18390.

Li, G., and Reinberg, D. (2011). Chromatin higher-order structures and gene regulation. Curr Opin Genet Dev *21*, 175-186.

Li, G.M. (2008). Mechanisms and functions of DNA mismatch repair. Cell Res *18*, 85-98.

Li, H., Handsaker, B., Wysoker, A., Fennell, T., Ruan, J., Homer, N., Marth, G., Abecasis, G., Durbin, R., and Genome Project Data Processing, S. (2009). The Sequence Alignment/Map format and SAMtools. Bioinformatics *25*, 2078-2079.

Liang, B., Qiu, J., Ratnakumar, K., and Laurent, B.C. (2007). RSC Functions as an Early Double-Strand-Break Sensor in the Cell's Response to DNA Damage. Current Biology *17*, 1432-1437.

Lindahl, T. (1993a). Instability and decay of the primary structure of DNA. Nature *362*, 709-715.

Lindahl, T. (1993b). Instability and decay of the primary structure of DNA. Nature *362*, 709-715.

Linger, J., and Tyler, J.K. (2006). Global replication-independent histone H4 exchange in budding yeast. Eukaryotic cell *5*, 1780-1787.

Lisby, M., Barlow, J.H., Burgess, R.C., and Rothstein, R. (2004). Choreography of the DNA damage response: spatiotemporal relationships among checkpoint and repair proteins. Cell *118*, 699-713.

Liu, C.L., Kaplan, T., Kim, M., Buratowski, S., Schreiber, S.L., Friedman, N., and Rando, O.J. (2005). Single-nucleosome mapping of histone modifications in S. cerevisiae. PLoS biology *3*, e328.

Liu, N., Peterson, C.L., and Hayes, J.J. (2011). SWI/SNF- and RSC-catalyzed nucleosome mobilization requires internal DNA loop translocation within nucleosomes. Mol Cell Biol *31*, 4165-4175.

Lo, W.S., Duggan, L., Emre, N.C., Belotserkovskya, R., Lane, W.S., Shiekhattar, R., and Berger, S.L. (2001). Snf1--a histone kinase that works in concert with the histone acetyltransferase Gcn5 to regulate transcription. Science *293*, 1142-1146.

Longhese, M.P., Foiani, M., Muzi-Falconi, M., Lucchini, G., and Plevani, P. (1998). DNA damage checkpoint in budding yeast. EMBO J *17*, 5525-5528.

Lorch, Y., Maier-Davis, B., and Kornberg, R.D. (2010). Mechanism of chromatin remodeling. Proc Natl Acad Sci U S A *107*, 3458-3462.

Low, J.K., and Wilkins, M.R. (2012). Protein arginine methylation in Saccharomyces cerevisiae. The FEBS journal *279*, 4423-4443.

Luger, K., Dechassa, M.L., and Tremethick, D.J. (2012). New insights into nucleosome and chromatin structure: an ordered state or a disordered affair? Nature reviews Molecular cell biology *13*, 436-447.

Luger, K., Mader, A.W., Richmond, R.K., Sargent, D.F., and Richmond, T.J. (1997). Crystal structure of the nucleosome core particle at 2.8 A resolution. Nature *389*, 251-260.

Lydeard, J.R., Lipkin-Moore, Z., Sheu, Y.J., Stillman, B., Burgers, P.M., and Haber, J.E. (2010). Break-induced replication requires all essential DNA replication factors except those specific for pre-RC assembly. Genes & Development *24*, 1133-1144.

Lyndaker, A.M., Goldfarb, T., and Alani, E. (2008). Mutants defective in Rad1-Rad10-Slx4 exhibit a unique pattern of viability during mating-type switching in Saccharomyces cerevisiae. Genetics *179*, 1807-1821.

Malik, H.S., and Henikoff, S. (2003). Phylogenomics of the nucleosome. Nature structural biology *10*, 882-891.

Marfella, C.G., and Imbalzano, A.N. (2007). The Chd family of chromatin remodelers. Mutation research *618*, 30-40.

Maruyama, H., Harwood, J.C., Moore, K.M., Paszkiewicz, K., Durley, S.C., Fukushima, H., Atomi, H., Takeyasu, K., and Kent, N.A. (2013). An alternative beads-on-a-string chromatin architecture in Thermococcus kodakarensis. EMBO reports *14*, 711-717.

Mavrich, T.N., Ioshikhes, I.P., Venters, B.J., Jiang, C., Tomsho, L.P., Qi, J., Schuster, S.C., Albert, I., and Pugh, B.F. (2008). A barrier nucleosome model for statistical positioning of nucleosomes throughout the yeast genome. Genome Res *18*, 1073-1083.

McCullough, A.K., Dodson, M.L., and Lloyd, R.S. (1999). Initiation of base excision repair: glycosylase mechanisms and structures. Annu Rev Biochem *68*, 255-285.

Mcgill, C., Shafer, B., and Strathern, J. (1989). Coconversion of Flanking Sequences with Homothallic Switching. Cell *57*, 459-467.

McKnight, J.N., Jenkins, K.R., Nodelman, I.M., Escobar, T., and Bowman, G.D. (2011). Extranucleosomal DNA binding directs nucleosome sliding by Chd1. Mol Cell Biol *31*, 4746-4759.

Mellor, J., and Morillon, A. (2004). ISWI complexes in Saccharomyces cerevisiae. Biochimica et biophysica acta *1677*, 100-112.

Memisoglu, A., and Samson, L. (2000). Base excision repair in yeast and mammals. Mutation research *451*, 39-51.

Meneghini, M.D., Wu, M., and Madhani, H.D. (2003). Conserved histone variant H2A.Z protects euchromatin from the ectopic spread of silent heterochromatin. Cell *112*, 725-736.

Minca, E.C., and Kowalski, D. (2011). Replication fork stalling by bulky DNA damage: localization at active origins and checkpoint modulation. Nucleic Acids Res *39*, 2610-2623.

Minucci, S., and Pelicci, P.G. (2006). Histone deacetylase inhibitors and the promise of epigenetic (and more) treatments for cancer. Nature reviews Cancer *6*, 38-51.

Mizuguchi, G., Shen, X., Landry, J., Wu, W.H., Sen, S., and Wu, C. (2004). ATP-driven exchange of histone H2AZ variant catalyzed by SWR1 chromatin remodeling complex. Science *303*, 343-348.

Moazed, D., Kistler, A., Axelrod, A., Rine, J., and Johnson, A.D. (1997). Silent information regulator protein complexes in Saccharomyces cerevisiae: A SIR2/SIR4 complex and evidence for a regulatory domain in SIR4 that inhibits its interaction with SIR3. Proceedings of the National Academy of Sciences of the United States of America *94*, 2186-2191.

Modrich, P., and Lahue, R. (1996). Mismatch repair in replication fidelity, genetic recombination, and cancer biology. Annu Rev Biochem *65*, 101-133.

Mohrmann, L., and Verrijzer, C.P. (2005). Composition and functional specificity of SWI2/SNF2 class chromatin remodeling complexes. Biochimica et biophysica acta *1681*, 59-73.

Monneau, Y.R., Soufari, H., Nelson, C.J., and Mackereth, C.D. (2013). Structure and activity of the peptidyl-prolyl isomerase domain from the histone chaperone Fpr4 towards histone H3 proline isomerization. The Journal of biological chemistry.

Moore, J.K., and Haber, J.E. (1996). Cell cycle and genetic requirements of two pathways of nonhomologous end-joining repair of double-strand breaks in Saccharomyces cerevisiae. Mol Cell Biol *16*, 2164-2173.

Moreira, J.M.A., and Holmberg, S. (1999). Transcriptional repression of the yeast CHA1 gene requires the chromatin-remodeling complex RSC. EMBO J *18*, 2836-2844.

Moretti, P., Freeman, K., Coodly, L., and Shore, D. (1994). Evidence That a Complex of Sir Proteins Interacts with the Silencer and Telomere Binding-Protein Rap1. Genes & Development *8*, 2257-2269.

Morrison, A.J., Highland, J., Krogan, N.J., Arbel-Eden, A., Greenblatt, J.F., Haber, J.E., and Shen, X. (2004). INO80 and gamma-H2AX interaction links ATP-dependent chromatin remodeling to DNA damage repair. Cell *119*, 767-775.

Mouret, S., Baudouin, C., Charveron, M., Favier, A., Cadet, J., and Douki, T. (2006). Cyclobutane pyrimidine dimers are predominant DNA lesions in whole human skin exposed to UVA radiation. Proc Natl Acad Sci U S A *103*, 13765-13770.

Nagarajavel, V., Iben, J.R., Howard, B.H., Maraia, R.J., and Clark, D.J. (2013). Global 'bootprinting' reveals the elastic architecture of the yeast TFIIIB-TFIIIC transcription complex in vivo. Nucleic Acids Res.

Narlikar, G.J., Sundaramoorthy, R., and Owen-Hughes, T. (2013). Mechanisms and Functions of ATP-Dependent Chromatin-Remodeling Enzymes. Cell *154*, 490-503.

Nasmyth, K., Stillman, D., and Kipling, D. (1987). Both positive and negative regulators of HO transcription are required for mother-cell-specific mating-type switching in yeast. Cell *48*, 579-587.

Nasmyth, K.A. (1982). Molecular genetics of yeast mating type. Annu Rev Genet *16*, 439-500.

Nathan, D., Ingvarsdottir, K., Sterner, D.E., Bylebyl, G.R., Dokmanovic, M., Dorsey, J.A., Whelan, K.A., Krsmanovic, M., Lane, W.S., Meluh, P.B.*, et al.* (2006). Histone sumoylation is a negative regulator in Saccharomyces cerevisiae and shows dynamic interplay with positive-acting histone modifications. Genes Dev *20*, 966-976.

Nelson, C.J., Santos-Rosa, H., and Kouzarides, T. (2006). Proline isomerization of histone H3 regulates lysine methylation and gene expression. Cell *126*, 905-916.

Ng, H.H., Robert, F., Young, R.A., and Struhl, K. (2002). Genome-wide location and regulated recruitment of the RSC nucleosome-remodeling complex. Genes & Development *16*, 806-819.

Nickoloff, J.A., Chen, E.Y., and Heffron, F. (1986). A 24-base-pair DNA sequence from the MAT locus stimulates intergenic recombination in yeast. Proc Natl Acad Sci U S A *83*, 7831-7835.

Nickoloff, J.A., Singer, J.D., and Heffron, F. (1990). In vivo analysis of the Saccharomyces cerevisiae HO nuclease recognition site by site-directed mutagenesis. Mol Cell Biol *10*, 1174-1179.

Nicol, J.W., Helt, G.A., Blanchard, S.G., Jr., Raja, A., and Loraine, A.E. (2009). The Integrated Genome Browser: free software for distribution and exploration of genome-scale datasets. Bioinformatics *25*, 2730-2731.

Nicolette, M.L., Lee, K., Guo, Z., Rani, M., Chow, J.M., Lee, S.E., and Paull, T.T. (2010). Mre11-Rad50-Xrs2 and Sae2 promote 5' strand resection of DNA double-strand breaks. Nat Struct Mol Biol *17*, 1478-1485.

Noll, D.M., Mason, T.M., and Miller, P.S. (2006). Formation and repair of interstrand cross-links in DNA. Chemical reviews *106*, 277-301.

Norris, A., Bianchet, M.A., and Boeke, J.D. (2008). Compensatory Interactions between Sir3p and the Nucleosomal LRS Surface Imply Their Direct Interaction. PLoS genetics *4*.

Norris, A., and Boeke, J.D. (2010). Silent information regulator 3: the Goldilocks of the silencing complex. Genes & Development *24*, 115-122.

Nyberg, K.A., Michelson, R.J., Putnam, C.W., and Weinert, T.A. (2002). Toward maintaining the genome: DNA damage and replication checkpoints. Annu Rev Genet *36*, 617-656.

Obeid, S., Blatter, N., Kranaster, R., Schnur, A., Diederichs, K., Welte, W., and Marx, A. (2010). Replication through an abasic DNA lesion: structural basis for adenine selectivity. EMBO J *29*, 1738-1747.

Oliver, S.G., Winson, M.K., Kell, D.B., and Baganz, F. (1998). Systematic functional analysis of the yeast genome. Trends in biotechnology *16*, 373-378.

Oum, J.H., Seong, C., Kwon, Y., Ji, J.H., Sid, A., Ramakrishnan, S., Ira, G., Malkova, A., Sung, P., Lee, S.E.*, et al.* (2011). RSC facilitates Rad59-dependent homologous recombination between sister chromatids by promoting cohesin loading at DNA double-strand breaks. Mol Cell Biol *31*, 3924-3937.

Papamichos-Chronakis, M., and Peterson, C.L. (2013). Chromatin and the genome integrity network. Nat Rev Genet *14*, 62-75.

Papamichos-Chronakis, M., Watanabe, S., Rando, O.J., and Peterson, C.L. (2011). Global regulation of H2A.Z localization by the INO80 chromatin-remodeling enzyme is essential for genome integrity. Cell *144*, 200-213.

Paques, F., Leung, W.-Y., and Haber, J.E. (1998). Expansions and Contractions in a Tandem Repeat Induced by Double-Strand Break Repair. Mol Cell Biol *18*, 2045-2054.

Parnell, T.J., Huff, J.T., and Cairns, B.R. (2008). RSC regulates nucleosome positioning at Pol II genes and density at Pol III genes. EMBO J *27*, 100-110.

Paulovich, A.G., Armour, C.D., and Hartwell, L.H. (1998). The Saccharomyces cerevisiae RAD9, RAD17, RAD24 and MEC3 genes are required for tolerating irreparable, ultraviolet-induced DNA damage. Genetics *150*, 75-93.

Peterson, C.L., and Cote, J. (2004). Cellular machineries for chromosomal DNA repair. Genes Dev *18*, 602-616.

Peterson, C.L., and Laniel, M.A. (2004). Histones and histone modifications. Current biology : CB *14*, R546-551.

Pokholok, D.K., Harbison, C.T., Levine, S., Cole, M., Hannett, N.M., Lee, T.I., Bell, G.W., Walker, K., Rolfe, P.A., Herbolsheimer, E.*, et al.* (2005). Genome-wide map of nucleosome acetylation and methylation in yeast. Cell *122*, 517-527.

Poklar, N., Pilch, D.S., Lippard, S.J., Redding, E.A., Dunham, S.U., and Breslauer, K.J. (1996). Influence of cisplatin intrastrand crosslinking on the conformation, thermal stability, and energetics of a 20-mer DNA duplex. Proc Natl Acad Sci U S A *93*, 7606-7611.

Polo, S.E., and Jackson, S.P. (2011). Dynamics of DNA damage response proteins at DNA breaks: a focus on protein modifications. Genes Dev *25*, 409-433.

Pommier, Y., Redon, C., Rao, V.A., Seiler, J.A., Sordet, O., Takemura, H., Antony, S., Meng, L., Liao, Z., Kohlhagen, G.*, et al.* (2003). Repair of and checkpoint response to topoisomerase I-mediated DNA damage. Mutation research *532*, 173-203.

Prakash, S., and Prakash, L. (2000). Nucleotide excision repair in yeast. Mutation research *451*, 13-24.

Raisner, R.M., and Madhani, H.D. (2006). Patterning chromatin: form and function for H2A.Z variant nucleosomes. Curr Opin Genet Dev *16*, 119-124.

Rando, O.J., and Winston, F. (2012). Chromatin and transcription in yeast. Genetics *190*, 351-387.

Ravindra, A., Weiss, K., and Simpson, R.T. (1999). High-resolution structural analysis of chromatin at specific loci: Saccharomyces cerevisiae silent mating-type locus HMRa. Molecular and Cellular Biology *19*, 7944-7950.

Richmond, T.J., and Davey, C.A. (2003). The structure of DNA in the nucleosome core. Nature *423*, 145-150.

Robert, F., Pokholok, D.K., Hannett, N.M., Rinaldi, N.J., Chandy, M., Rolfe, A., Workman, J.L., Gifford, D.K., and Young, R.A. (2004). Global position and recruitment of HATs and HDACs in the yeast genome. Mol Cell *16*, 199-209.

Robzyk, K., Recht, J., and Osley, M.A. (2000). Rad6-dependent ubiquitination of histone H2B in yeast. Science *287*, 501-504.

Roh, T.Y., Ngau, W.C., Cui, K., Landsman, D., and Zhao, K. (2004). High-resolution genome-wide mapping of histone modifications. Nature biotechnology *22*, 1013-1016.

Romeo, M.J., Angus-Hill, M.L., Sobering, A.K., Kamada, Y., Cairns, B.R., and Levin, D.E. (2002). HTL1 Encodes a Novel Factor That Interacts with the RSC Chromatin Remodeling Complex in Saccharomyces cerevisiae. Mol Cell Biol *22*, 8165-8174.

Russell, D.W., Jensen, R., Zoller, M.J., Burke, J., Errede, B., Smith, M., and Herskowitz, I. (1986). Structure of the Saccharomyces cerevisiae HO gene and analysis of its upstream regulatory region. Molecular and Cellular Biology *6*, 4281-4294.

Saha, A., Wittmeyer, J., and Cairns, B.R. (2002). Chromatin remodeling by RSC involves ATP-dependent DNA translocation. Genes Dev *16*, 2120-2134.

Saha, A., Wittmeyer, J., and Cairns, B.R. (2005). Chromatin remodeling through directional DNA translocation from an internal nucleosomal site. Nat Struct Mol Biol *12*, 747-755.

Sancar, A., Lindsey-Boltz, L.A., Unsal-Kacmaz, K., and Linn, S. (2004). Molecular mechanisms of mammalian DNA repair and the DNA damage checkpoints. Annu Rev Biochem *73*, 39-85.

Sanders, S.L., Portoso, M., Mata, J., Bahler, J., Allshire, R.C., and Kouzarides, T. (2004). Methylation of histone H4 lysine 20 controls recruitment of Crb2 to sites of DNA damage. Cell *119*, 603-614.

Sarma, K., and Reinberg, D. (2005). Histone variants meet their match. Nature reviews Molecular cell biology *6*, 139-149.

Schaaper, R.M., and Dunn, R.L. (1987). Spectra of spontaneous mutations in Escherichia coli strains defective in mismatch correction: the nature of in vivo DNA replication errors. Proc Natl Acad Sci U S A *84*, 6220-6224.

Schmid, F.X. (1995). Protein folding. Prolyl isomerases join the fold. Current biology : CB *5*, 993-994.

Schotta, G., Lachner, M., Sarma, K., Ebert, A., Sengupta, R., Reuter, G., Reinberg, D., and Jenuwein, T. (2004). A silencing pathway to induce H3-K9 and H4-K20 trimethylation at constitutive heterochromatin. Genes Dev *18*, 1251-1262.

Schramm, L., and Hernandez, N. (2002). Recruitment of RNA polymerase III to its target promoters. Genes & Development *16*, 2593-2620.

Schwabish, M.A., and Struhl, K. (2007). The Swi/Snf complex is important for histone eviction during transcriptional activation and RNA polymerase II elongation in vivo. Mol Cell Biol *27*, 6987-6995.

Seeler, J.S., and Dejean, A. (2003). Nuclear and unclear functions of SUMO. Nature reviews Molecular cell biology *4*, 690-699.

Shen, X., Mizuguchi, G., Hamiche, A., and Wu, C. (2000). A chromatin remodelling complex involved in transcription and DNA processing. Nature *406*, 541-544.

Shen, X., Ranallo, R., Choi, E., and Wu, C. (2003). Involvement of actin-related proteins in ATP-dependent chromatin remodeling. Mol Cell *12*, 147-155.

Shia, W.J., Osada, S., Florens, L., Swanson, S.K., Washburn, M.P., and Workman, J.L. (2005). Characterization of the yeast trimeric-SAS acetyltransferase complex. The Journal of biological chemistry *280*, 11987-11994.

Shim, E.Y., Hong, S.J., Oum, J.-H., Yanez, Y., Zhang, Y., and Lee, S.E. (2007). RSC Mobilizes Nucleosomes To Improve Accessibility of Repair Machinery to the Damaged Chromatin. Mol Cell Biol *27*, 1602-1613.

Shim, E.Y., Ma, J.-L., Oum, J.-H., Yanez, Y., and Lee, S.E. (2005). The Yeast Chromatin Remodeler RSC Complex Facilitates End Joining Repair of DNA Double-Strand Breaks. Mol Cell Biol *25*, 3934-3944.

Shogren-Knaak, M., Ishii, H., Sun, J.M., Pazin, M.J., Davie, J.R., and Peterson, C.L. (2006). Histone H4-K16 acetylation controls chromatin structure and protein interactions. Science *311*, 844-847.

Siede, W., Friedberg, A.S., Dianova, I., and Friedberg, E.C. (1994). Characterization of G1 checkpoint control in the yeast Saccharomyces cerevisiae following exposure to DNA-damaging agents. Genetics *138*, 271-281.

Simic, R., Lindstrom, D.L., Tran, H.G., Roinick, K.L., Costa, P.J., Johnson, A.D., Hartzog, G.A., and Arndt, K.M. (2003). Chromatin remodeling protein Chd1 interacts with transcription elongation factors and localizes to transcribed genes. EMBO J *22*, 1846-1856.

Simms, T.A., Dugas, S.L., Gremillion, J.C., Ibos, M.E., Dandurand, M.N., Toliver, T.T., Edwards, D.J., and Donze, D. (2008). TFIIIC binding sites function as both heterochromatin barriers and chromatin insulators in Saccharomyces cerevisiae. Eukaryotic cell *7*, 2078-2086.

Smolle, M., Venkatesh, S., Gogol, M.M., Li, H., Zhang, Y., Florens, L., Washburn, M.P., and Workman, J.L. (2012). Chromatin remodelers Isw1 and Chd1 maintain chromatin structure during transcription by preventing histone exchange. Nat Struct Mol Biol *19*, 884-892.

Southall, S.M., Cronin, N.B., and Wilson, J.R. (2014). A novel route to product specificity in the Suv4-20 family of histone H4K20 methyltransferases. Nucleic Acids Res *42*, 661-671.

Soutourina, J., Bordas-Le Floch, V., Gendrel, G., Flores, A., Ducrot, C., Dumay-Odelot, H., Soularue, P., Navarro, F., Cairns, B.R., Lefebvre, O.*, et al.* (2006). Rsc4 Connects the Chromatin Remodeler RSC to RNA Polymerases. Mol Cell Biol *26*, 4920-4933.

Sternglanz, R., and Schindelin, H. (1999). Structure and mechanism of action of the histone acetyltransferase Gcn5 and similarity to other N-acetyltransferases. Proc Natl Acad Sci U S A *96*, 8807-8808.

Stockdale, C., Flaus, A., Ferreira, H., and Owen-Hughes, T. (2006). Analysis of nucleosome repositioning by yeast ISWI and Chd1 chromatin remodeling complexes. The Journal of biological chemistry *281*, 16279-16288.

Strahl, B.D., and Allis, C.D. (2000). The language of covalent histone modifications. Nature *403*, 41-45.

Sugawara, N., Wang, X., and Haber, J.E. (2003). In vivo roles of Rad52, Rad54, and Rad55 proteins in Rad51-mediated recombination. Mol Cell *12*, 209-219.

Sugiyama, T., Zaitseva, E.M., and Kowalczykowski, S.C. (1997). A single-stranded DNA-binding protein is needed for efficient presynaptic complex formation by the Saccharomyces cerevisiae Rad51 protein. The Journal of biological chemistry *272*, 7940-7945.

Sutton, A., Shia, W.J., Band, D., Kaufman, P.D., Osada, S., Workman, J.L., and Sternglanz, R. (2003). Sas4 and Sas5 are required for the histone acetyltransferase activity of Sas2 in the SAS complex. The Journal of biological chemistry *278*, 16887-16892.

Sweetser, D.B., Hough, H., Whelden, J.F., Arbuckle, M., and Nickoloff, J.A. (1994). Fine-resolution mapping of spontaneous and double-strand break-induced gene conversion tracts in Saccharomyces cerevisiae reveals reversible mitotic conversion polarity. Mol Cell Biol *14*, 3863-3875.

Szerlong, H., Saha, A., and Cairns, B.R. (2003). The nuclear actin-related proteins Arp7 and Arp9: a dimeric module that cooperates with architectural proteins for chromatin remodeling. EMBO J *22*, 3175-3187.

Szeto, L., and Broach, J.R. (1997). Role of alpha 2 protein in donor locus selection during mating type interconversion. Molecular and Cellular Biology *17*, 751-759.

Takahara, H., Okamoto, H., and Sugawara, K. (1985). Specific Modification of the Functional Arginine Residue in Soybean Trypsin-Inhibitor (Kunitz) by Peptidylarginine Deiminase. Journal of Biological Chemistry *260*, 8378-8383.

Tan, M., Luo, H., Lee, S., Jin, F., Yang, J.S., Montellier, E., Buchou, T., Cheng, Z., Rousseaux, S., Rajagopal, N.*, et al.* (2011). Identification of 67 histone marks and histone lysine crotonylation as a new type of histone modification. Cell *146*, 1016-1028.

Taneda, T., and Kikuchi, A. (2004). Genetic analysis of RSC58, which encodes a component of a yeast chromatin remodeling complex, and interacts with the transcription factor Swi6. Molecular genetics and genomics : MGG *271*, 479-489.

Tang, L., Nogales, E., and Ciferri, C. (2010). Structure and function of SWI/SNF chromatin remodeling complexes and mechanistic implications for transcription. Progress in biophysics and molecular biology *102*, 122-128.

Thompson, J.D., Gibson, T.J., and Higgins, D.G. (2002). Multiple sequence alignment using ClustalW and ClustalX. Current protocols in bioinformatics / editoral board, Andreas D Baxevanis [et al] *Chapter 2*, Unit 2 3.

Tirosh, I., Sigal, N., and Barkai, N. (2010). Widespread remodeling of mid-coding sequence nucleosomes by Isw1. Genome biology *11*, R49.

Treich, I., and Carlson, M. (1997). Interaction of a Swi3 homolog with Sth1 provides evidence for a Swi/Snf-related complex with an essential function in Saccharomyces cerevisiae. Mol Cell Biol *17*, 1768-1775.

Treich, I., Ho, L., and Carlson, M. (1998a). Direct interaction between Rsc6 and Rsc8/Swh3, two proteins that are conserved in SWI/SNF-related complexes. Nucleic Acids Research *26*, 3739-3745.

Treich, I., Ho, L., and Carlson, M. (1998b). Direct interaction between Rsc6 and Rsc8/Swh3,two proteins that are conserved in SWI/SNF-related complexes. Nucleic Acids Res *26*, 3739-3745.

Tsuchiya, E., Hosotani, T., and Miyakawa, T. (1998). A mutation in NPS1/STH1, an essential gene encoding a component of a novel chromatin-remodeling complex RSC, alters the chromatin structure of Saccharomyces cerevisiae centromeres. Nucleic Acids Res *26*, 3286-3292.

Tsukuda, T., Fleming, A.B., Nickoloff, J.A., and Osley, M.A. (2005). Chromatin remodelling at a DNA double-strand break site in Saccharomyces cerevisiae. Nature *438*, 379-383.

Tsukuda, T., Trujillo, K.M., Martini, E., and Osley, M.A. (2009). Analysis of chromatin remodeling during formation of a DNA double-strand break at the yeast mating type locus. Methods *48*, 40-45.

Turner, S.D., Ricci, A.R., Petropoulos, H., Genereaux, J., Skerjanc, I.S., and Brandl, C.J. (2002). The E2 ubiquitin conjugase Rad6 is required for the ArgR/Mcm1 repression of ARG1 transcription. Mol Cell Biol *22*, 4011-4019.

Udugama, M., Sabri, A., and Bartholomew, B. (2011). The INO80 ATP-dependent chromatin remodeling complex is a nucleosome spacing factor. Mol Cell Biol *31*, 662-673.

Valenzuela, L., Dhillon, N., and Kamakaka, R.T. (2009). Transcription independent insulation at TFIIIC-dependent insulators. Genetics *183*, 131-148.

van Attikum, H., Fritsch, O., Hohn, B., and Gasser, S.M. (2004). Recruitment of the INO80 Complex by H2A Phosphorylation Links ATP-Dependent Chromatin Remodeling with DNA Double-Strand Break Repair. Cell *119*, 777-788.

van Bakel, H., Tsui, K., Gebbia, M., Mnaimneh, S., Hughes, T.R., and Nislow, C. (2013). A Compendium of Nucleosome and Transcript Profiles Reveals Determinants of Chromatin Architecture and Transcription. PLoS genetics *9*.

van der Kemp, P.A., de Padula, M., Burguiere-Slezak, G., Ulrich, H.D., and Boiteux, S. (2009). PCNA monoubiquitylation and DNA polymerase eta ubiquitin-binding domain are required to prevent 8-oxoguanine-induced mutagenesis in Saccharomyces cerevisiae. Nucleic Acids Res *37*, 2549-2559.

VanDemark, A.P., Kasten, M.M., Ferris, E., Heroux, A., Hill, C.P., and Cairns, B.R. (2007). Autoregulation of the rsc4 tandem bromodomain by gcn5 acetylation. Mol Cell *27*, 817-828.

Varela, I., Tarpey, P., Raine, K., Huang, D., Ong, C.K., Stephens, P., Davies, H., Jones, D., Lin, M.L., Teague, J.*, et al.* (2011). Exome sequencing identifies frequent mutation of the SWI/SNF complex gene PBRM1 in renal carcinoma. Nature *469*, 539-542.

Vignali, M., Hassan, A.H., Neely, K.E., and Workman, J.L. (2000). ATP-dependent chromatin-remodeling complexes. Mol Cell Biol *20*, 1899-1910.

Wang, R., Jin, Y., and Norris, D. (1997). Identification of a protein that binds to the Ho endonuclease recognition sequence at the yeast mating type locus. Mol Cell Biol *17*, 770-777.

Wang, S.L., and Cheng, M.Y. (2012). The defects in cell wall integrity and G2-M transition of the htl1 mutant are interconnected. Yeast *29*, 45-57.

Wang, W. (2003). The SWI/SNF family of ATP-dependent chromatin remodelers: similar mechanisms for diverse functions. Current topics in microbiology and immunology *274*, 143-169.

Wang, X., and Haber, J.E. (2004). Role of Saccharomyces single-stranded DNA-binding protein RPA in the strand invasion step of double-strand break repair. PLoS biology *2*, E21.

Weiler, K.S., and Broach, J.R. (1992). Donor Locus Selection during Saccharomyces-Cerevisiae Mating Type Interconversion Responds to Distant Regulatory Signals. Genetics *132*, 929-942.

Weinert, T.A., Kiser, G.L., and Hartwell, L.H. (1994). Mitotic checkpoint genes in budding yeast and the dependence of mitosis on DNA replication and repair. Genes Dev *8*, 652-665.

Weinstein-Fischer, D., Elgrably-Weiss, M., and Altuvia, S. (2000). Escherichia coli response to hydrogen peroxide: a role for DNA supercoiling, topoisomerase I and Fis. Molecular microbiology *35*, 1413-1420.

Weiss, K., and Simpson, R.T. (1997). Cell type-specific chromatin organization of the region that governs directionality of yeast mating type switching. EMBO J *16*, 4352-4360.

Weiss, K., and Simpson, R.T. (1998). High-resolution structural analysis of chromatin at specific loci: Saccharomyces cerevisiae silent mating type locus HML alpha. Molecular and Cellular Biology *18*, 5392-5403.

White, C.I., and Haber, J.E. (1990). Intermediates of recombination during mating type switching in Saccharomyces cerevisiae. EMBO J *9*, 663-673.

Wilson, B., Erdjument-Bromage, H., Tempst, P., and Cairns, B.R. (2006). The RSC Chromatin Remodeling Complex Bears an Essential Fungal-Specific Protein Module With Broad Functional Roles. Genetics *172*, 795-809.

Winzeler, E.A., Shoemaker, D.D., Astromoff, A., Liang, H., Anderson, K., Andre, B., Bangham, R., Benito, R., Boeke, J.D., Bussey, H.*, et al.* (1999). Functional characterization of the S. cerevisiae genome by gene deletion and parallel analysis. Science *285*, 901-906.

Wippo, C.J., Israel, L., Watanabe, S., Hochheimer, A., Peterson, C.L., and Korber, P. (2011). The RSC chromatin remodelling enzyme has a unique role in directing the accurate positioning of nucleosomes. EMBO J *30*, 1277-1288.

Wood, R.D. (1996). DNA repair in eukaryotes. Annu Rev Biochem *65*, 135-167.

Xiao, H., Jackson, V., and Lei, M. (2006). The FK506-binding protein, Fpr4, is an acidic histone chaperone. FEBS letters *580*, 4357-4364.

Xu, Z., Wei, W., Gagneur, J., Perocchi, F., Clauder-Munster, S., Camblong, J., Guffanti, E., Stutz, F., Huber, W., and Steinmetz, L.M. (2009). Bidirectional promoters generate pervasive transcription in yeast. Nature *457*, 1033-1037.

Xue, Y., Canman, J.C., Lee, C.S., Nie, Z., Yang, D., Moreno, G.T., Young, M.K., Salmon, E.D., and Wang, W. (2000). The human SWI/SNF-B chromatin-remodeling complex is related to yeast rsc and localizes at kinetochores of mitotic chromosomes. Proc Natl Acad Sci U S A *97*, 13015-13020.

Yu, S., Smirnova, J.B., Friedberg, E.C., Stillman, B., Akiyama, M., Owen-Hughes, T., Waters, R., and Reed, S.H. (2009). ABF1-binding sites promote efficient global genome nucleotide excision repair. The Journal of biological chemistry *284*, 966-973.

Yukawa, M., Katoh, S., Miyakawa, T., and Tsuchiya, E. (1999). Nps1/Sth1p, a component of an essential chromatin-remodeling complex of Saccharomyces cerevisiae, is required for the maximal expression of early meiotic genes. Genes to cells : devoted to molecular & cellular mechanisms *4*, 99-110.

Yukawa, M., Koyama, H., Miyahara, K., and Tsuchiya, E. (2002). Functional differences between RSC1 and RSC2, components of a for growth essential chromatin-remodeling complex of Saccharomyces cerevisiae, during the sporulation process. Fems Yeast Research *2*, 87-91.

Zakian, V.A., Brewer, B.J., and Fangman, W.L. (1979). Replication of each copy of the yeast 2 micron DNA plasmid occurs during the S phase. Cell *17*, 923-934.

Zentner, G.E., and Henikoff, S. (2013). Regulation of nucleosome dynamics by histone modifications. Nat Struct Mol Biol *20*, 259-266.

Zhang, H., Roberts, D.N., and Cairns, B.R. (2005). Genome-wide dynamics of Htz1, a histone H2A variant that poises repressed/basal promoters for activation through histone loss. Cell *123*, 219-231.

Zhang, Q., Chakravarty, S., Ghersi, D., Zeng, L., Plotnikov, A.N., Sanchez, R., and Zhou, M.M. (2010). Biochemical profiling of histone binding selectivity of the yeast bromodomain family. PLoS One *5*, e8903.

Zhang, Y., Smith, C.L., Saha, A., Grill, S.W., Mihardja, S., Smith, S.B., Cairns, B.R., Peterson, C.L., and Bustamante, C. (2006). DNA translocation and loop formation mechanism of chromatin remodeling by SWI/SNF and RSC. Mol Cell *24*, 559-568.

Zhang, Z., and Dietrich, F.S. (2005). Mapping of transcription start sites in Saccharomyces cerevisiae using 5' SAGE. Nucleic Acids Res *33*, 2838-2851.

Zhou, W., and Doetsch, P.W. (1993). Effects of abasic sites and DNA single-strand breaks on prokaryotic RNA polymerases. Proc Natl Acad Sci U S A *90*, 6601-6605.

Appendix

Frag size	Log frag	Distance migrated
2000	3.301029996	42.8
1500	3.176091259	60.5
1000	3	89.5
900	2.954242509	97.5
800	2.903089987	105.5
700	2.84509804	115
600	2.77815125	125.5
500	2.698970004	136.6

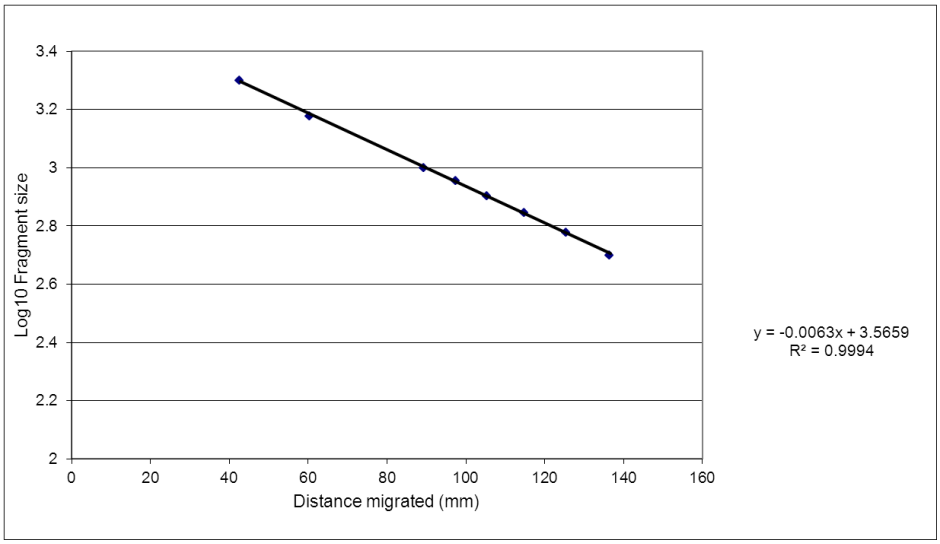

Fragment	Distance migrated	Calculated size
1	52.5	168.8845432
2	59.5	162.4759233
3	67.1	167.7156077
4	76.1	157.7650253
5	86	238.998826
6	105	166.5447463
7	123	
	Average size	177.0641119

Appendix A.1 – Calibration curve to calculate size of MNase protected regions
The distance migrated by the marker fragments was plotted against the log size of the fragment to produce a calibration curve. By applying the formula of y=mx+c, the size of the fragments was calculated and the difference between neighbouring fragments calculated to give a size of the MNase protected region. For the MNase protected regions in Figure 3.1, there is an average size of 177bp,, approximately the size of a nucleosome.

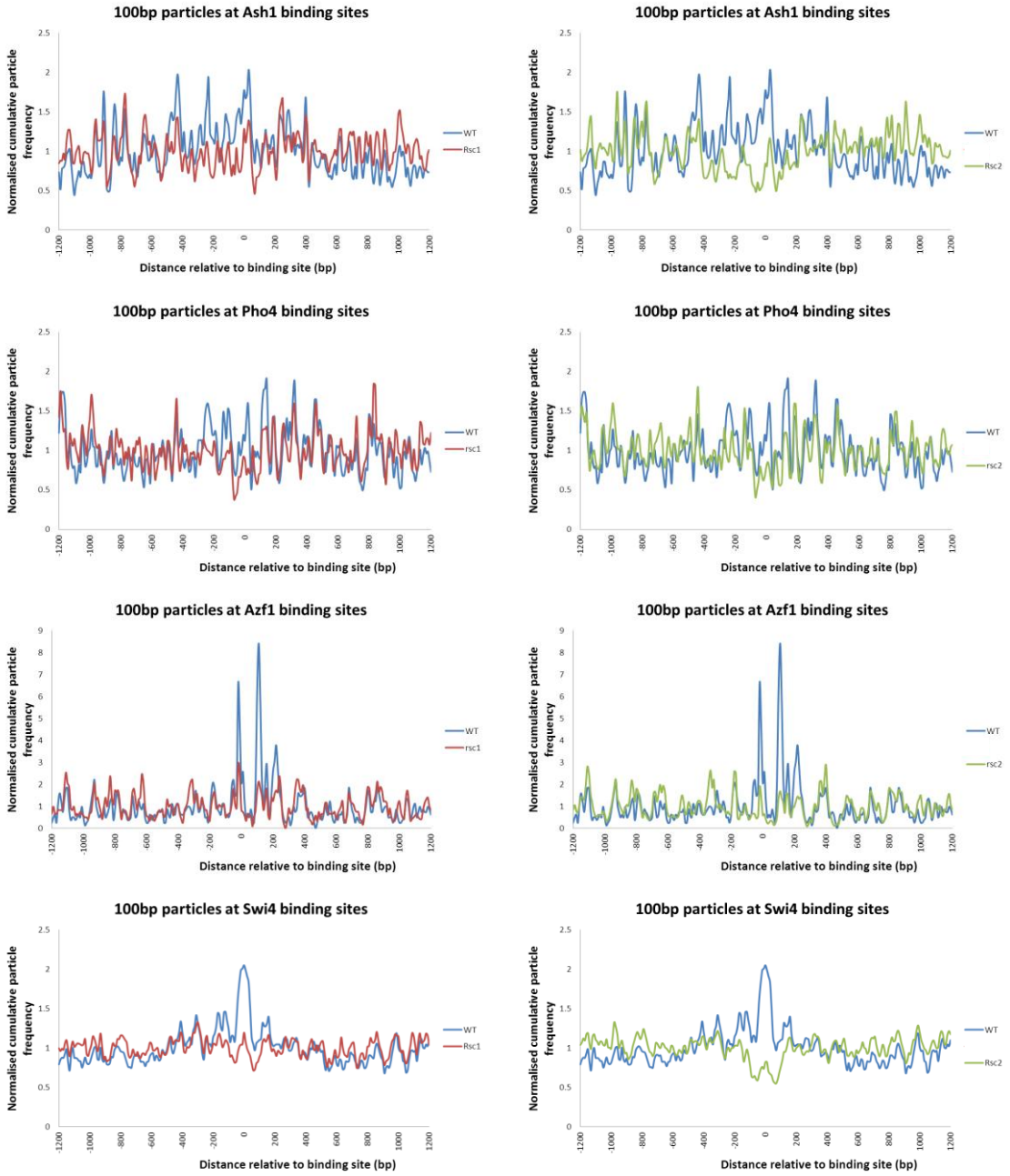

Appendix A.2 – Rsc1 and Rsc2 dependent 100bp particles at TF binding sites

Trend graphs of normalised cumulative frequency of 100bp were plotted in a 2400bp surrounding the binding sites of TFs Ash1 (n=30), Pho4 (n=24), Azf1 (n=4), and Swi4 (n=166) as determined by MacIsaac *et al* (2006) for wild-type (blue), Δ*rsc1* (red) and Δ*rsc2* (green) datasets. The trends show that these transcription factor binding sites do not have a dependency on Rsc1 or Rsc2 to set chromatin structure to the same extent as transcription factors with an associated conserved binding motif.

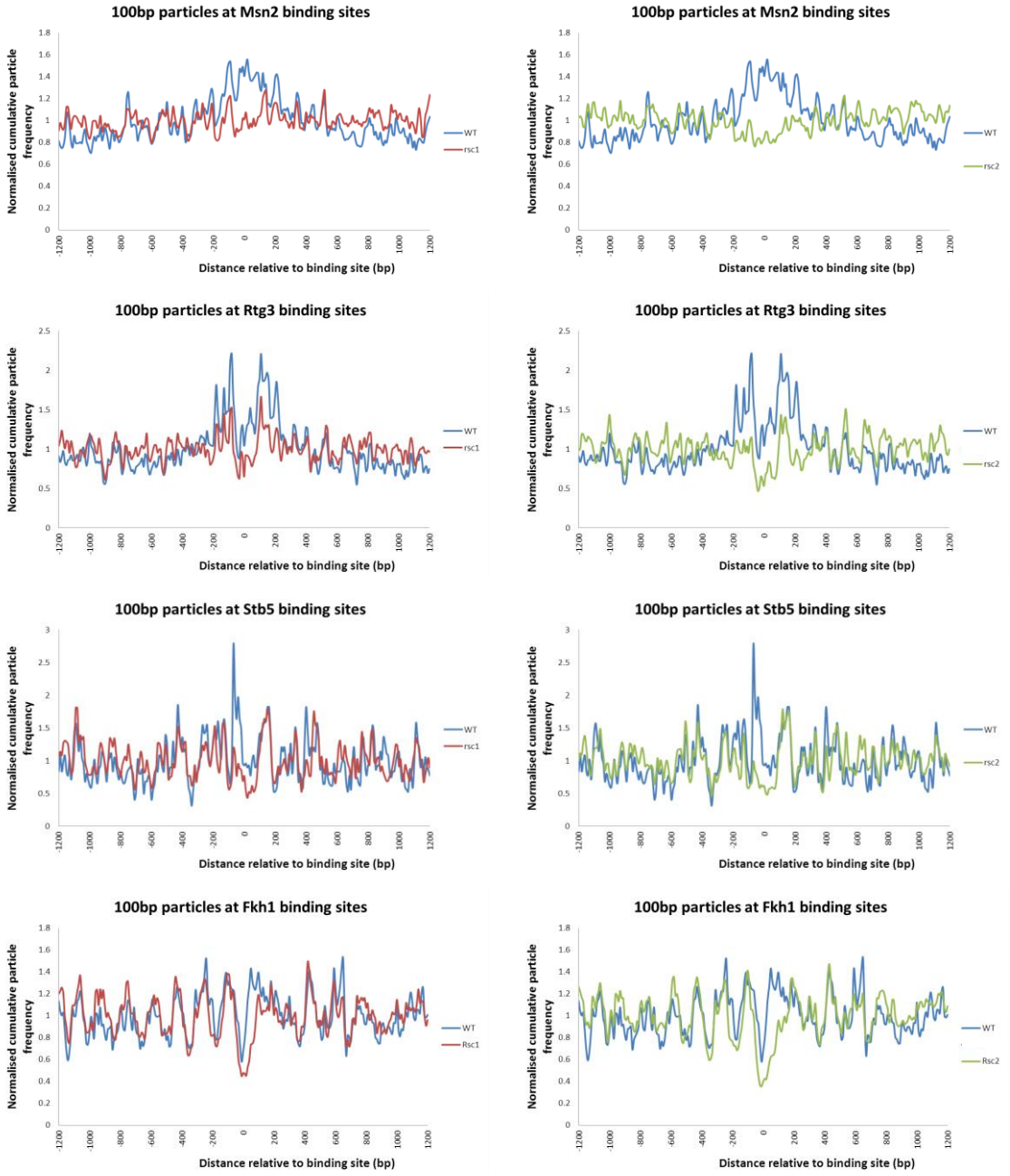

Appendix A.3 – Rsc1 and Rsc2 dependent 100bp particles at TF binding sites

Trend graphs of normalised cumulative frequency of 100bp were plotted in a 2400bp surrounding the binding sites of TFs Msn2 (n=183), Rtg3 (n=74), Stb5 (n=19) and Fkh1 (n=88) as determined by MacIsaac *et al* (2006) for wild-type (blue), Δ*rsc1* (red) and Δ*rsc2* (green) datasets. The trends show that these transcription factor binding sites do not have a dependency on Rsc1 or Rsc2 to set chromatin structure to the same extent as transcription factors with an associated conserved binding motif.